University of Sheffield

Investigating Host Responses to the Typhoid Toxin of *Salmonella Enterica*

Michelle King
Department of Biosciences
University of Sheffield

A thesis submitted in partial fulfilment of the requirements for the degree of Doctor of Philosophy

October 2024

Declaration

I, Michelle King, confirm that this thesis is my own work. I am aware of the University's Guidance on the Use of Unfair Means (*www.sheffield.ac.uk/ssid/unfair-means*). This work has not previously been presented for an award at this, or any other, university.

Michelle King, October 2024

Acknowledgements

First and foremost, I would like to thank my supervisor, Dan Humphreys. Thank you for all your support and for finding the positives in even the most questionable data. You never quite gave up on me even when you easily could have. I couldn't have done this without you. I would also like to thank the past and present members of the Humphreys Lab: Salma, Mohammed, Dan, Nadia, Nataya, Francesca, and Zhou. Thank you for answering all my stupid questions and for keeping me going when I didn't think I could.

Outside of the lab, I would like to thank my supervisors Tom Darton and Mark Bass for their helpful advice throughout my project. Thank you to Weronika, Mark and Laura, and the other members of DiMeN Cohort 5. We started together, we finish together.

I would also like to thank Sharks and everyone else in Tag Rugby Sheffield for helping make Sheffield a home. Thank you to Kayleigh for listening to me rant and for the Kipper Kuddles. Thank you to Lily for being a friend during a really tough time and for all the internet cat content. Big thanks to Mike and Monty, it really is the other two people in the three-person group chat.

Finally, thank you to my mum. You have no idea what it is I do, but your support and belief in me has never wavered.

Abstract

The typhoid toxin is an important virulence factor secreted by *S*. Typhi and is believed to play a role in promoting infection (Miller et al., 2018). The toxin induces DNA damages and triggers the innate immune response (Ibler et al., 2019). Part of this is activation of type I interferon signalling which induces hundreds of ISGs, including ISG15. This protein plays an important role in combatting viral infection (Alphonse et al., 2021), and has an emerging role in defending against bacterial infections (Radoshevich and Cossart., 2018, Wu et al., 2024).

This thesis shows that the typhoid toxin caused DNA damage, cell cycle arrest and cell death in different cell types. Toxin-induced DNA damage led to increased expression of ISG15 in HT1080 human fibroblasts. Further investigation found ISG15 played no role in toxin-induced DNA damage as both wild-type and ISG15-deficient A549 cells underwent cell cycle arrest and senescence. In parallel however, marked ISG15-deficient A549 cells treated with IFNα resulted in apparent cell death. This was supported by RNA sequencing of IFNα-treated ISG15-deficient A549 cells, which revealed expression of the tumour necrosis factor pathway implicated in apoptosis. In contrast, wild-type A549 cells exhibited increased expression of interferon-stimulated gene (ISGs) pathways associated with defence against viral infections. IFNα induced apoptosis in ISG15 deficient cells due to loss of USP18, which was shown to be driven by ISG15 in a IFNα-dependent manner. Finally, ISG15 was found to be important in containing intracellular *Salmonella*. In the absence of ISG15, IFNα-treated cells underwent cell death thereby releasing the *Salmonella* into the extracellular environment. This could increase dissemination and *Salmonella* invasion of sterile sites such as the bloodstream in ISG15-deficient humans. The thesis supports the view that ISG15 plays a role in defending the host against intracellular bacterial pathogens, which now includes *Salmonella*.

List of Figures

List of Tables

Abbreviations

APH Aphidicolin
ATM Ataxia telangiectasia mutated
ATR Ataxia telangiectasia and Rad 3 related gene
BAK Bcl-2 antagonist/killer 1
BAX Bcl- 2 associated X protein
BCL-2 B-cell lymphoma-2
BER Base Excision Repair
BIM Bcl-2-like 11
BMDM Bone marrow derived macrophage
CDT Cytolethal distending toxin
CPT camptothecin
CMAH Cytidine monophospho-N-acetylneuraminic acid hydroxylase
CtIP C-terminal interacting protein
CDK Cyclin-dependent kinase inhibitor
CHK Checkpoint kinase
CXCL8 CXC ligand 8
DAMPs Damage-associated molecular patterns
dCTP Deoxycytidine triphosphate
DDRs DNA damage responses
DAPI 4',6-diamidino-2-phenylindole
DMEM Dulbecco's Modified Eagle's Medium
DMSO Dimethyl sulfoxide
DSB Double strand break
E. coli *Escherichia coli*
EdU 5-Ethynyl-2′-deoxyuridine
EHEC Enterohaemorrhagic *E. coli*
ERAD Endoplasmic reticulum-associated degradation
ETP Etoposide
EXO1 Exonuclease 1
FADD Fas-associated death domain
FasL Fas ligand
FBS Foetal bovine serum
Gag Group specific antigen
IFNα Interferon alpha
HR Homologous recombination
HRK Harakiri, BCL2 Interacting Protein
IL-6 Interleukin-6
iNTS Invasive non-typhoidal
IR Ionising radiation
IRF Interferon regulatory protein
ISGs Interferon stimulated genes
ISG15 Interferon stimulated gene 15
ISRE Interferon-stimulated response element
JAK Janus kinase
KAN Kanamycin

LPS Liposaccharides
MDM2 Mouse double minute 2
MEF Mouse embryonic fibroblast
MCP1 Monocyte chemoattractant protein 1
NEDD4 Neural precursor cell expressed developmentally down-regulated 4
NHEJ non-homologous end joining
NLPR3 NOD-, LRR-, and pyrin domain–containing protein 3
NTS Non-typhoidal
PAMPs Pathogen-associated molecular patterns
PAR Poly[ADP-ribose]
PARP1 Poly [ADP-ribose] polymerase 1
PRRs Pattern recognition receptors
PBS Phosphate buffered saline
PDAC Pancreatic ductal carcinoma
p-pRB Phosphorylated retinoblastoma protein
P.S Penicillin Streptomycin
PUMA p53 upregulated modulator of apoptosis
RPA Replication protein A
SASP Senescence-associated secretory phenotype
SCV Salmonella containing vacuole
SSB Single strand break
SSBR Single Strand Break Repair
SPI Salmonella pathogenicity island
ST19 *Salmonella* typhimurium sequence type 19
ST313 *Salmonella* typhimurium sequence type 313
STAT Signal transducer and activator of transcription
STING (Stimulator of interferon genes
tAIF Truncated AIF
TBK Tank binding kinase
TCV Typhoid conjugate vaccine
TLR4 Toll-like receptor 4
TNFα Tumour necrotising factor alpha
TNFR1 Type 1 TNF receptor
TRADD TNF receptor-associated death domain
Tsg101 Tumour susceptibility gene 101
TtsA Typhoid toxin secretion A
TYK2 Tyrosine-protein kinase 2
TX^{HQ} H160 mutant toxin
TX^{WT} Wild type typhoid toxin
USP18 Ubiquitin-specific protease 18
ViPS Vi polysaccharide
WHO World Health Organisation
WT Wild type
XRRC1 X-ray repair cross complementing 1

Part 1: Literature Review

Chapter 1: Salmonella Enterica Infection

1.1 Introduction

Serovars of *Salmonella enterica* are major causes of human morbidity and mortality, causing either self-limiting infection of the intestinal mucosa or more lethal invasive infections of the bloodstream (bacteraemia) and organs of the reticuloendothelial system. Globally it is estimated that that non-typhoidal *Salmonella* (NTS) is responsible for 93 million intestinal infections annually and 155,000 associated deaths (Balasubramanian et al., 2019). Invasive infections account for a further 535,000 deaths from invasive serovars of non-typhoidal *Salmonella* (iNTS) and 136,000 deaths result from *Salmonella* Typhi and Paratyphi which cause typhoid (enteric) fever (Stanaway et al., 2019). This represents a serious disease burden. The problem is compounded further by growing antimicrobial resistance, the need for more effective typhoid vaccines, and the emergence of new iNTS strains in sub-Saharan Africa (Feasey et al. 2012, Haselbeck et al., 2017). Research into novel therapeutics is ongoing, but to prevent and treat infection we must first fully understand the mechanisms of *Salmonella* infection and the underlying molecular factors that may promote or inhibit its success.

1.2 *Salmonella Enterica* Infection is a Global Health Burden

More than 2600 serovars of *Salmonella enterica* have been identified and is a leading cause of gastroenteritis. Over 95% of infections are thought to occur through the consumption of contaminated food and water and the World Health Organisation (WHO) has listed *Salmonella* infection as one of the top 4 causes of diarrhea worldwide (Acheson and Hohmann, 2001, Balasubramanian et al., 2019). This also represents a significant economic burden through illness related absences from the workplace (Hoffman, Batz and Morris, 2012). Infections by non-typhoidal serovars such as *Salmonella* Typhimurium cause symptoms such as stomach cramps, acute onset diarrhea and fever. However, infection is usually self-limiting and will resolve without treatment in 1-7 days in an otherwise healthy host (Feasey et al. 2012, Lamichane et al., 2024). NTS is a worldwide problem causing disease in low-, middle- and high-income countries, e.g. in Europe, USA, where *S.* Typhiumurium sequence type 19 (ST19) is a common agent of self-limiting gastroenteritis but rarely causes invasive blood-borne infections. Complications may arise when infection occurs high risk populations such as infants, the elderly and individuals suffering from malnutrition, HIV infection, malaria, sickle-cell anaemia or other conditions resulting in a compromised immune system (Acheson and Hoffman, 2001, Feasey et al., 2012). This is a particularly problematic in sub-Saharan African where the emergence of invasive NTS (iNTS) serovars such as *S.* Typhimurium sequence type 13 (ST313) has stretched often already under resourced health facilities. Not only is iNTS infection a leading cause of bacteraemia in both African adults and children, it has an associated mortality rate of 20-25% (Feasey et al., 2012, Phu Huong Lan et al., 2016). It has been theorised that ST313 may have capitalised on antimicrobial resistance and genome degradation to take advantage of the ecological niche provided by high rates of HIV, malnutrition and other diseases (Feasey et al. 2012, Pulford et al., 2021). A global systematic review by Marchello et al. in 2022 reported

45 different complications from iNTS infection with the most prevalent being septicaemia.

Unlike NTS and iNTS that cause disease in humans and animals, typhoid fever is human-specific disease caused by *Salmonella* Typhi (*S*. Typhi) and Paratyphi, and remains a significant health challenge in many low-income countries with a reported 11-21 million cases of typhoid fever annually with 5 million cases of paratyphoid fever. This results in an estimated 135,000 – 230,000 deaths a year (Lamichane et al., 2024). Although the global burden has decreased since the 1990s and has been largely eradicated in high-income countries, typhoid fever remains endemic in South and South East Asia, and sub-Saharan Africa (Als et al., 2018, Masuet-Aumatell and Atouguia, 2021). Whereas other iNTS serovars such as ST313 have emerged and seen increasing rates of infection in the last 40 years (Van Puyvelde et al., 2019), typhoid fever is an ancient disease. It was proposed by Papagrigorakis et al. (2006) that typhoid fever was the cause of the Athens plague in 430BC however this was disputed by Shapiro, Rambaut and Gilbert (2006) that same year. The bacillus of typhoid fever was allegedly discovered in the 1880s (Rec, L.M., 1883, Andrews and Ryan, 2016) during a time when typhoid fever became widespread and an important cause of illness and death with the overcrowded and unsanitary urban environments of Europe and the USA allowing the disease to run rampant (Parry et al., 2012). The name “typhoid fever” originated with the physician, Pierre Charles Alexander Louis, who recognised the similarity of the symptoms to typhus and described them as ‘typhoidal” (Ajiboula et al., 2018). Following an incubation period of 7-14 days (Parry et al., 2012) patients present with symptoms including vomiting, malaise, abdominal discomfort and relative bradycardia in some instances. One of the key clinical signs is a persistent fever beginning with a low-grade fever (>37.5^{o}C to 38.2^{o}C) and progressing to a high-grade fever (>38.2^{o}C to 41.5^{o}C) by the second week. Without treatment or management, the fever may persist for a month or longer (Lamichane et al., 2024). Additionally, a small number of patients who contract typhoid fever become chronic carriers after symptoms resolve, still shedding bacteria 12 months after the initial infection. This maintains the presence of *S*. Typhi in human populations and allows for further infection (Parry et al., 2012, Masuet-Aumatell and

Atouguia, 2020, Lamichane et al., 2024). Chronic *S*. Typhi infection has also been linked to a 9-fold higher prevalence of gallbladder carcinoma creating a further health burden (Tewari, Mishra and Shukla, 2010, Koshiol et al., 2016).

1.3 Diagnosing *Salmonella Enterica* Infection

The gastroenteritis symptoms resulting from non-typhoidal *Salmonella* infection are usually self-resolving and can be managed by the patient at home, therefore no clinical diagnosis is required. For more serious iNTS and typhoidal infections, diagnosis begins with assessment of clinical signs and symptoms. Unfortunately, in areas of the world where these types of infections are endemic this is often where diagnosis ends due to limited medical resources (Andrews and Ryan, 2016). Where medical microbiology is available it is possible to identify *Salmonella* species in the lab through recovery of bacteria from faecal samples or rectal swabs if the former is not available (Acheson and Hohmann, 2001).

The diagnosis of typhoid fever is difficult due to a lack of specific symptoms. Many of the symptoms such as fever, diarrhea and malaise are common to other enteric bacterial pathogens, although the presentation of bloody diarrhea is not a common symptom of typhoid fever and may instead indicate *Shigella* or enterohaemorrhagic *E. coli* (EHEC) infection instead (Acheson and Hohmann, 2001). The gold standard for diagnosis is a bone marrow culture where bacteria are isolated after the bone marrow is harvested from the sternum or iliac crest. This method gives 90% specificity after culturing for 4 days, however is less commonly used due to the highly invasive nature of the procedure (Mahmoud et al. 2023). Instead, blood culture is usually performed but, although considered a routine procedure, it is expensive and often not readily available in the developing world (Sapkota et al., 2023). The facilities that are available frequently have a limited capacity and may have to send positive cultures to a central laboratory to confirm identification

This situation could be eased by the development of a rapid diagnostic test for typhoid fever that could be used at the point of diagnosis. Such serological tests are available which are less expensive than blood culture, can be used with minimal training and deliver results quickly. These include the Widal test, TUBEX and Typhi dot tests (Lim et al., 1998, Baker, Favorov and Dougan, 2010, Mahmoud et al., 2023). However, in order for this type of test to become the gold standard diagnostic tool, the WHO has set a target of 100% for sensitivity, specificity and positive/negative result. Currently, none of the available tests come close to attaining this rigorous standard (Baker, Favorov and Dougan, 2010, Ajibola et al., 2018). At present the standard protocol for diagnosing typhoid fever in Sierra Leone and Malawi is clinical assessment followed by two Widal tests performed by different technicians. The presence of other enteric bacterial infections in the area must also be considered and ruled out (Mahmoud et al., 2023).

Research is ongoing to identifying unique serological markers for typhoid fever. The markers currently available show low levels of sensitivity and specificity, but data emerging from areas of endemic typhoid fever have identified IgA to *S.* Typhi LPS and IgG to HlyE as potential biomarkers for use in rapid diagnostic tests (Ajibola et al., 2018).

1.4 Treatment of Typhoid Fever

The management of non-typhoidal *Salmonella* infection does not usually require medical treatment and any intervention usually centres around preventing dehydration (Oracz et al., 2003). Management of typhoid fever begins with prevention. Reporting of individual cases and disease surveillance can help identify areas of outbreaks, allowing intervention and preventing further spread (Mahmoud et al., 2023). Controlling infection numbers relies on the provision of clean water, adequate disposal of sewage, hygienic food handling and immunisation programs (Parry et al., 2002, Lamichane et al., 2024).

Treatment of individual patients does not usually require hospitalisation unless presenting with warning symptoms, such as altered state of consciousness or persistent vomiting (Parry et al., 2023). Most patients can be treated as outpatients and can be administered an antibiotic. Chloramphenicol was one of the first antibiotics to be used for the treatment of typhoid fever, however its use declined due to adverse effects, primarily suppression of the bone marrow (Wiest, Cochran and Tecklenburg, 2012). Other antibiotics were commonly used such as ampicillin and trimethoprim-sulfamethoxazole and were found to be effective until the 1990s (Parry et al., 2023). These in turn were replaced by fluoroquinolones, a class of antimicrobials that includes ciprofloxacin and ofloxacin, and are still used despite an increase in resistance. Should a patient fail to respond to fluoroquinolones, a combination of azithromycin and cephalosporins, such as ceftriaxone, can be used as an alternative (Mahmoud et al., 2023). The WHO conducted a review of the efficacy of the different antimicrobials available and recommends ciprofloxacin, ceftriaxone, and azithromycin as the first-choice treatments for enteric fever, however any data available on antimicrobial resistance in the local area should be considered when choosing an antibiotic (Parry et al., 2023).

Treatment of typhoid fever using antimicrobials is an ongoing race between finding effective treatments and the ability of the bacteria to develop resistance. Due to a lack of reliable and quick diagnostics in areas where typhoid fever is endemic, the disease may be over-diagnosed, leading to excessive and inappropriate use of antibiotics (Andrews and Ryan, 2016). This has led to *S*. Typhi developing resistance to all of the commonly used antimicrobials and can lead to complications for sufferers of typhoid fever such a failure to respond to treatment, prolonged carriage and the development of more serious medical conditions such as intestinal perforation, anaemia and haemorrhage (Marchello, Birkhold and Crump, 2020, Parry et al., 2023)

1.5 Vaccinations for Typhoid Fever

Although the main strategies for preventing the spread of typhoid fever revolve around access to clean water and hygienic food preparation practices, immunisation has also been used to limit disease spread and is recommended for travellers heading to areas when typhoid fever is endemic (Masuet-Aumatell and Atouguia, 2021). Three vaccinations for typhoid fever are currently recommended by the WHO:

- **typhoid conjugate vaccine (TCV)** (children from 6 months of age, adults up to either 45 or 65 years depending on the specific vaccine administered)
- **unconjugated Vi polysaccharide (ViPS)** (for all persons over 2 years of age)
- **live attenuated Ty21a vaccines** (for all persons over 6 years of age).

(World Health Organisation, 2018)

Of the three vaccines, the TCV vaccine is recommended by the WHO due to its suitability for use across all age groups, including young children and the long-term protection it is believed to offer (World Health Organisation, 2018). The TCV vaccine induces an immune response against the Vi polysaccharide antigen found on the outside of the bacterial capsule of *S*. Typhi (Jin et al., 2017). Completion of a 4-year randomised control trial assessing the efficacy of a TCV vaccine (Vi-TT) in Malawian children found that the overall efficacy was 78.3% after 4 years. Incidences of typhoid fever were confirmed by blood culture and found that of the 14069 children vaccinated, efficacy was determined to be 70.6% in children under 2 years rising to 79.3% in children aged 5-12 years (Patel et al., 2024).

ViPS consists solely of the polysaccharide antigen and has so far found to offer less protection than TCV. A 2020 study showed efficacy of the vaccine to be 61% two years post vaccination. This study was conducted using typhoid surveillance 66,458 individuals living in an urban slum area of Kolkata city, India (Islam et al., 2020). However, an earlier study in the same area found that efficacy varied depending on age group. Children aged 5-15 years displayed 56% efficacy, but this greatly increased to 80% in children aged 2-4 years. This higher level of protection in younger children may be attributed to mass vaccination programs for 2-year-olds

with herd immunity developing as a result (Sur et al., 2009, World Health Organisation, 2018).

The Ty21a vaccine is orally administered and is based on a live attenuated Ty2 strain of *S*. Typhi and lacks the Vi antigen. Large scale field trials of children in Chile, Egypt and Indonesia found that protection against typhoid fever was in the range of 33-67%. Long term surveillance found that efficacy was 67% after 3 years, falling to 62% after 7 years (Simanjuntak et al., 1991, World Health Organisation, 2018)

A systematic review of the efficacy of all types of typhoid fever vaccines in areas of endemic infection. TCV offered the highest degree of protection, with a single shot offering 83% efficacy two years post immunisation. ViPS and Ty21a trailed with 58% and 45% pooled efficacy respectively. For this reason, TCV is the preferred vaccine for large scale immunisation programs as well as its suitability for use in young children with Ty21a or ViPS vaccines used for travellers to areas where typhoid fever is endemic, especially in parts of the world where TCV is not yet licenced (Gloeck et al., 2023). The WHO recommends that TCV immunisations should be introduced as part of a preventative strategy alongside health education and improved training for health care professionals in diagnosing typhoid fever (Hancuh et al., 2023).

Chapter 2: *Salmonella* Typhi

2.1 Pathogenesis of *Salmonella* Infection

Initially both typhoidal and non-typhoidal serovars of *S*. enterica invade host cells in the same manner. The first hurdle the *Salmonella* must overcome is crossing the intestinal epithelium. Only a small number will succeed with the rest remaining in the intestinal lumen (Hume et al., 2017, Gal-Mor, 2019). *Salmonella* preferentially adheres to microfold (M) cells of Peyer's patches which transport the bacteria from the intestinal lumen to the lymphoid tissue. Uptake can also occur through the invasion of non-phagocytic enterocytes (Fàbrega and Vila, 2013, Gal-Mor, 2019).

Salmonella possesses the ability to gain entry to the host cell by inducing its own phagocytosis (Eng et al., 2015). This relies on a type-3 secretion system (T3SS). *Salmonellae* have two types of T3SS coded on *Salmonella* pathogenicity islands (SPI) 1 or 2 (SPI-1 or SPI-2). The first T3SS, encoded on SPI-1 is responsible for translocating virulence effector proteins during invasion into host cells in order to establish the *Salmonella* containing vacuole (SCV) and preventing the host cell from undergoing apoptosis. The second found on SPI-2 is dedicated to intracellular pathogenesis promoting intracellular survival and replication by delivering virulence effector proteins in response to conditions within the SCV (Deng et al., 2017, Sibinell-Sousa et al., 2021). *Salmonella* is a Gram-negative organism with an inner and outer membrane separated by the periplasm containing peptidoglycan. The structure of the T3SS resembles a "molecular needle" comprising of three major components – an inner membrane export apparatus, a hollowed body spanning the inner to the outer membranes (basal body) and an extracellular needle with a translocon, the "needle tip" that provides a hollowed conduit into host cells (Burkinshaw and Strynadka, 2014, Deng et al., 2017).

Salmonella and other pathogens use effectors delivered by their SPI-1 T3SS to induce host plasma membrane ruffling. This is driven by a rearrangement of the cytoskeleton and interferes with epithelial barrier integrity and is achieved through the release of effectors such as SopE, SopE2 and SopB that remodel the actin cytoskeleton via activating Rho GTPases (Deng et al., 2017, Hume et al., 2017, Sibinell-Sousa et al., 2021). Invading *Salmonella* become enclosed in the SCV, the only vesicle-bound compartment where the bacteria can replicate (McGhie et al., 2009, Lorkowski et al., 2014). However, this also activates the MAPK and NF-κB pathways triggering the release of pro-inflammatory cytokines (Sibinell-Sousa et al., 2021).

This is where the similarities between NTS and typhoidal *Salmonella* infection ends. NTS infection of the underlying lamina propria and the expression of pathogen-associated molecular patterns (PAMPs) induces a strong immune response leading to activation of neutrophils, macrophages and other immune cells. This leads to

professional phagocytosis of free *Salmonella* in the lamina propria, and restricts the infection to the intestine, usually self-resolving within a few days (Gal-Mor, 2019). *S.* Typhi infection, on the other hand, does not induce such an immune response. Typhoid fever resulting from infection is not usually characterised by intestinal inflammation or diarrhea commonly found with NTS infection (Dougan and Baker, 2014, Gal-Mor, 2019). This enables *S.* Typhi to disseminate out of the intestinal epithelium and establish a systemic infection (Johnson, Mylona and Frankel, 2018).

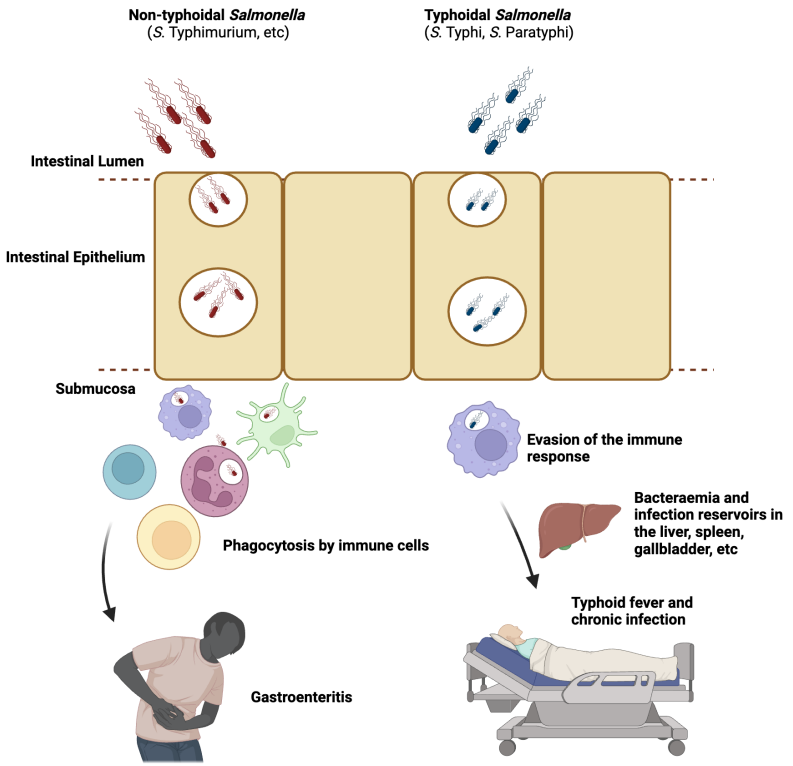

Fig 1.1 **Pathogenesis of Salmonella Enterica Infection.** Non-typhoidal *Salmonella* trigger an immune response resulting in gastroenteritis symptoms and a self-resolving infection. Typhoidal Salmonella evade the immune response resulting in typhoid fever and chronic infection.

2.2 Genetic Adaptions of *Salmonella* Typhi

Whereas NTS serovars of *S.* enterica are generalists due to their ability to infect a wide range of host species, *S.* Typhi is a human specific pathogen (Gonzalez-

Escobedo et al., 2011, Dougan and Baker, 2014, Johnson, Mylona and Frankel, 2018). However, it has been found that *S*. Typhi is able to replicate in chimpanzees, but did not illicit any typhoid-like symptoms suggesting that factors other than inability to replicate in non-human hosts contributes to its specificity (Deng et al., 2014, Chong et al., 2017). Surprisingly, despite the differences in immune responses and clinical symptoms, analysis of the genomes between *S*. Typhi and NTS serovars show more than 80% of genes are shared (Schultz et al., 2021). However, the *S*. Typhi genome contains a high number of pseudogenes with approximately 200 genes showing inactivity or functional disruption when compared to their *S*. Typhimurium homologues (Baker and Dougan, 2014, Deng et al., 2014, Gal-Mor, Boyle and Grassi, 2014). Furthermore, 30 genes linked to gastroenteritis were found to be degraded in both *S*. Typhi and *S*. Paratyphi providing a genomic reason for the lack of these symptoms in typhoid fever (McClelland et al., 2004). Many of the other degraded genes are related to the T3SS and known pathogenicity islands. *S*. Typhi has lost genes associated with SPI-1 to SPI-5 while SPI-14 (present in *S*. Typhimurium) is completely absent (Baker and Dougan, 2014). Conversely, SPI-7 (which encodes the Vi antigen discussed below), SPI-15, SPI-17 and SPI-18 are found in *S*. Typhi, but not in S. Typhimurium (Gal-mor et al., 2014). This indicated that the evolutionary history of *S*. Typhi has favoured gene loss that has promoted intracellular survival and immune evasion at the cost of restricted host-tropism (Sabbagh et al., 2010, Gal-Mor et al., 2014). In sub-Saharan Africa genome analysis suggests that ST313 has undergone similar genome degradation resulting in evolutionary convergence with *S*. Typhi and causing a shift towards evolving into a human-specific pathogen (Okoro et al., 2015, Panzenhagen et al., 2018).

2.3 The Vi Antigen

The production of some bacterial products is common to all *S*. enterica serovars, however some are unique to *S*. Typhi. The Vi antigen is one of them (Dougan and Baker, 2014). This is a polysaccharide capsule that works to inhibit phagocytosis and reduces the secretion of TNFα (tumour necrotising factor alpha) by preventing TLR4 (Toll-like receptor 4) signalling and inhibiting neutrophil recruitment (Hirose et al., 1997, Wain et al., 2005, Tischler and McKinney, 2010). Early experiments found the Vi capsule enhanced infection of *S*. Typhi (Hone et al., 1988) as well as increase in the severity of symptoms (Hornick et al., 1970). However, these studies also discovered that the Vi capsule is not essential for pathogenicity of *S*. Typhi as infection was established by Vi-negative mutants with patients developing typhoid-like symptoms. A review of the field effectiveness of the ViPS vaccine in China found outbreaks of typhoid fever caused by Vi-negative *S*. Typhi (Arya, S., 2002).

2.4 The Typhoid Toxin

Another distinguishing characteristic of *S*. Typhi and *S*. Paratyphi is production of the typhoid toxin. This is a bacterial genotoxin, part of a unique class of bacterial toxins that target DNA upon infection causing DNA damage which, if it becomes too extensive and cannot be repaired drives cell cycle arrest or cell death (Jindasa et al., 2011, Grasso and Frisan, 2015). Currently three members of the bacterial genotoxin family have been identified: colibactin, a peptide-polyketide genotoxin produced by polyketide synthetase (pks^+) *Escherichia coli* (*E. coli*), cytolethal distending toxin (CDT) produced by several Gram-negative bacteria, and finally the typhoid toxin produced by *S*. Typhi (Grasso and Frisan, 2015).

However, although bacterial toxins are important virulence factors for a number of pathogens with many similarities, there are also key differences. Although the typhoid toxin and the shiga toxin, produced by some strains of *E. coli,* are both classified as AB toxins they differ in terms of structure and function. Both are

composed structurally of an active subunit (A) and a binding site (B). However, Shiga toxin follows the typical AB structure comprising of one active subunit (A) and five binding subunits (B) whereas the typhoid toxin is comprised of a more unusual A2B5 structure with 5 binding subunits (PltB) but *two* active subunits (PltA and CdtB). The CdtB subunit is not found in the Shiga toxin (Melton-Celsa, 2014, Liu et al., 2022). They also differ in terms of their mechanism of action. The Shiga toxin primarily targets the ribosomes to inhibit protein synthesis, whereas the Typhoid toxin causes DNA damage through it's CdtB subunit. Essentially, despite both being AB toxins the Shiga toxin and Typhoid toxin target different cellular mechanisms and cause distinct diseases (Melton-Celsa, 2014, Galan, 2016, Liu et al., 2022).

However the Typhoid toxin does share similarities with other CDTs. Internalisation of the A subunit is dependent on the action of the B component. CDTs are AB_2 trimers with CdtA and CdtC comprising the binding structure and CdtB acting as the active subunit with all three required for maximum toxic effect (Chen et al., 2023). The homology between *cdtA*, *cdtB* and *cdtC* can vary greatly, even within the same species, with *cdtb* being the most conserved of the three (Grasso and Frisan, 2015). The typhoid toxin is instead structured into a A_2B_5 complex where a pentameric ring called PltB is the binding component and CdtB and PltA form the active subunit **(Fig 1.2)**. PltA acts as a link to PltB, which binds to specifically to Neu5Ac (*N*-acetylneuraminic acid) terminated glycans on the cell surface-membrane receptors, and covalently linked to CdtB by a disulphide bond (Liu et al., 2022).

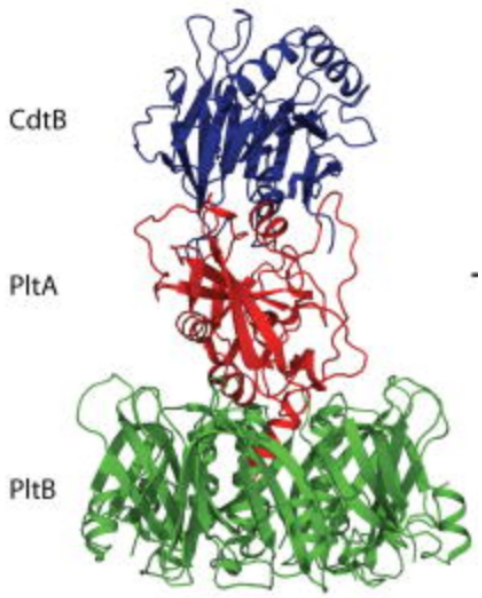

Fig 1.2 **Structure of the Typhoid Toxin (Song et al., 2013).** The typhoid toxin is an AB toxin comprising of a CdtB active subunit, a PltB binding site and a PltA linker protein.

The structure of the typhoid toxin is unusual in that the PltA and CdtB subunits of the typhoid toxin are very similar in structure to that of the pertussis toxin S1. The CdtB subunit of the typhoid toxin is also structurally similar to that of the CDT, giving the typhoid toxin a hybrid structure. Studies have shown that like CDT the three components are functionally intertwined with *pltA* and *pltB* a requirement for *cdtb*-dependent toxin activity (Spano, Ugalde and Galan, 2008, Galan, 2016).

The CdtB subunit is a common characteristic across as these toxins and possesses DNA catalytic ability. It is both functionally and structurally homologous to mammalian DNase I (Nesic, Hsu and Stebbins, 2004). However, the DNase capabilities of CdtB are far less potent that DNase I. *In vitro* studies found that the catalytic ability of CdtB to be 100 times less than that of bovine DNase I. CdtB shares two conserved histidine residues in common with DNase I (H160 and H1274). Introducing a simple mutation into H160 resulted in a complete loss of toxicity despite complete assembly of the ternary complex suggesting that it is essential for CdtB catalytic activity (Nesic, Hsu and Stebbins, 2004).

The harmful effects of CDTs on host cells have been well documented (Guidi et al., 2013, Chileoches, Bergonzini and Frisan, 2021, Mathiason et al., 2021, Jurenas et al., 2022). CDT and the typhoid toxin both need to be transported to the nucleus for them to act upon their molecular target, DNA (Grasso and Frisan, 2015). Much of our knowledge for typhoid toxin has been gathered through studies on CDTs. The CdtB subunit is delivered into the host cell nucleus by the CdtA and CdtC subunits where it can undertake its catalytic activity, triggering a DNA damage response (DDR) and eventual cell cycle arrest and death (Lara-Tejero and Galan, 2000, Guerra et al., 2011). There was some debate regarding the model of DNA damage with some researchers favouring a direct double strand break (DSB) theory and others believing that cell cycle arrest and cell death lead to DNA fragmentation (Elwell and Dreyfus, 2000, Frisan et al., 2002). Evidence of a delay between entry of CdtB into the nucleus (Nishikubo et al., 2003) and the first detection of DSBs (Frisan et al. 2003) gave support to the latter. The debate was settled by Fedor et al. (2012) who found that CDT initially causes single strands breaks (SSBs) which then progress to DSBs during S-phase. Prolonged exposure to CDT has been shown to lead to apoptosis (O' Hara et al., 2008, Jindasa et al. 2011, Marquardt et al., 2021) and genomic instability (Guidi et al., 2012, Tremblay et al., 2021).

Intriguingly, 40 NTS *Salmonella* serovars out of ~2500 serovars also carry genes that encode for CDT-toxins and are also capable of eliciting DNA damage (Miller et al., 2018). Among these is *Salmonella* Javiana (*S*. Javiana), a gastroenteritis causing NTS serovar of *S. enterica* encoding *pltB, pltA* and *cdtB* that assemble into the typhoid toxin (Lee et al., 2020). This non-typhoidal ortholog of the typhoid toxin displays some genetic differences from the *S*. Typhi toxin variant. Inactivation of pltB did not result in loss of toxin activity as it does in S. Typhi, however the *S*. Javiana toxin induced a similar DDR to the *S*. Typhi toxin, suggesting it may also play an important role in *S*. Javiana pathogenesis (Mezal, Bae and Khan, 2014, Miller et al., 2018).

2.5 Secretion and Transport of the Typhoid Toxin

Other AB toxins are produced by extracellular bacteria, suggesting that the toxin is taken up by host cells via receptor-mediated processes. The Typhoid toxin, however, is expressed only by intracellular bacteria suggesting that *S*. Typhi is able to circumvent cellular uptake and instead directly intoxicate the cell from within. Surprisingly this is not the case (Fowler et al. 2017). Spano, Ugalde and Galan (2007) instead showed that the Typhoid toxin must first be exposed to the extracellular environment before it can intoxicate the cell. This provides the S. Typhi with a safe harbour to establish a persistent infection whilst acting as a source of toxin that can intoxicate other cells.

The typhoid toxin is secreted by intracellular bacteria into the lumen of SCV through a dedicated secretion system which facilitates its transport through the peptidoglycan layer (Spano et al., 2008, Geiger et al., 2020). This allows it to be trafficked out of the infected cell and cause further intoxication of bystander cells (Chong et al., 2017). The toxin is first secreted when favourable conditions within the SCV are detected by the *Salmonella*'s PhoP/PhoQ sensory system (Chemello and Fowler, 2024). Expression of the typhoid toxin is mediated by IgeR, preventing its secretion when the *Samonella* are still in the extracellular environment by binding to the *cdtB* promoter (Haghjoo and Galan, 2007, Rodriguez-Rivera et al., 2015).

The toxin is then packaged within vesicle carriers ready for transportation. The journey across the peptidoglycan is mediated by TtsA (typhoid toxin secretion A) although so far there is no information on how TtsA recognises its substrate (Geiger et al., 2020). TtsA breaks down the peptidoglycan layer of the bacterial cell wall, allowing the toxin to pass through. The cell wall is then remodelled without causing the bacteria to lyse (Geiger et al., 2020). Although essential for transportation of the *S*. Typhi toxin, it does not appear to be vital for toxin activity in *S*. Javiana (Miller et al., 2018).

Once released binding of the toxin onto the surface of the target cell is mediated by PtlB which preferentially binds to Neu5Ac-terminated glycans (Song et al., 2003, Deng et al., 2014, Chong et al., 2017). The toxin is then internalised through receptor-mediated endocytosis (Chang et al., 2022). The preferential binding to Neu5Ac points towards the human specificity of *S*. Typhi. Most mammals produce CMAH (Cytidine monophospho-N-acetylneuraminic acid hydroxylase), an enzyme that converts Neu5Ac to Neu5Gc, however it is not produced in humans. This means that human sialoglycans do not undergo this conversion process and remain in the Neu5Ac form (Buchlis et al., 2013). The typhoid toxin does not bind to Neu5Gc and therefore in species that display a greater ratio of Neu5GC, such as chimpanzees (mentioned previously), will not induce symptoms of typhoid fever even if the bacteria are able to replicate. Mice do possess Neu5Ac binding sites, but engineered mouse mutants who have Neu5Gc become resistant to the typhoid toxin and therefore offer a potential experimental model (Deng et al., 2015).

Once internalised into the host cell the toxin is transported to the Golgi apparatus and the endoplasmic reticulum via retrograde trafficking (Chang et al., 2019, 2022) Here the toxin is disassembled by the endoplasmic reticulum-associated degradation (ERAD) pathway which transports the enzymatic subunits to the cytosol. The CdtB subunit posseses a nuclear localisation signal that directs it to the nucleus where it can carry out it's catalytic function (Chang et al., 2016, 2019, 2022). The Humphreys lab has shown that the Typhoid toxin causes SSBs which cause replication stress and overwhelms the RPA pathway, leading to RPA exhaustion and cellular senescence.

2.6 The Effects of *Salmonella* Typhi *In Vivo*

S. Typhi has evolved a number of adaptations that allow it to avoid detection by the immune system, but long-term persistence requires the *Salmonella* to establish infection in a privileged niche. This is a state of equilibrium where the bacteria are not cleared, but the infection is contained within parts of the body such as the liver or gallbladder (Gal-Mor, 2019). It was not clear at first what role the typhoid toxin

played in *S*. Typhi played. A 2013 study by Song et al. found that injecting mice with purified typhoid toxin induced typhoid-like symptoms such as neutrophil depletion, malaise, weight loss and eventual death, but not fever. Mice injected with a catalytically inactive H160 mutant version of the toxin did not develop any symptoms. This led the authors to believe that the toxin and specifically the CdtB subunit was involved in the manifestation of typhoid symptoms.

More recent studies have instead indicated that instead the typhoid toxin may be more involved in promoting cell survival and chronic infection (Del Bel Belluz et al., 2016, Miller et al., 2018). When mice were infected with *S*. Typhimurium expressing typhoid toxin genes, not only were gastroenteritis symptoms found to be lessened, but the toxin also promoted survival of the mouse host. 40% of mice infected with wild-type *S*. Typhimurium became severely ill and had to be euthanised before the experiment was concluded (2 months) whereas all mice injected with the toxin expressing engineered strain survived until the end of the experiment (6 months). Bacteria was recovered from the liver and cecum of mice injected with the toxin expressing *S*. Typhimurium after 180 days, with the liver seemingly the preferred location for infection. No bacteria were recovered from mice injected with the control strain suggesting that the typhoid toxin promotes persistent infection (Del Bel Belluz et al., 2016). Miller et al (2018) infected mice with *S.* Javiana, which exhibited increased systemic spread and decreased levels of pathology relative to *ΔcdtB S.* Javiana (Millet al 2018). Both studies provide examples by which typhoid toxin promotes systemic and persistent *Salmonella* infections in a mouse model.

Ethical concerns make it difficult to conduct similar experiments in humans. However, a randomised, double-blind human challenge study in 2019 by Gibani et al challenged 40 volunteers who were infected with either wild-type or a toxin-negative (TN) strain of *S*. Typhi. Participants were monitored for 14 days and were administered the antibiotic Ciprofloxacin upon typhoid fever (~75% of cases) or at 14 days if no symptoms were apparent. Clinical symptoms were monitored and blood cultures taken daily, but surprisingly there was no difference in the rate of infection or clinical symptoms was observed between the two groups other than bacteraemia

endured significantly longer in the TN group (WT 48h; TN 96h). This shows that the typhoid toxin does not cause typhoid symptoms and is not required for infection.

Finally, the health implications of *S*. Typhi infection may be long lasting. Chronic infection established in the gallbladder has been linked to increased incidences of gallbladder carcinoma (Dutta et al., 2000, Koshiol et al., 2016, Shukla et al., 2021). Chronic carriage of *S*. Typhi is associated with gallstones in 80-90% of cases (Di Domenico et al., 2017). This is thought to be down to a combined effect of the DNA damage induced by the typhoid toxin and the biofilm production by *S*. Typhi which aids in establishing a persistent infection. This results in chronic inflammation and exposure of the epithelial cells to ongoing damage by the toxin (Koshiol, et al., 2016, Di Domenico et al. 2017). Once chronic colonisation has been established it is no longer treatable with antibiotics and the only option left is resection of the gallbladder (Jahan et al., 2022).

The first part of this project will focus on host responses to the typhoid toxin *in vitro* in both human and mouse cells.

Chapter 3: The DNA Damage Response

3.1 Introduction

DNA contains all the genetic information needed for life, but considering its importance it is a surprisingly delicate molecule undergoing tens of thousands of lesions which must be repaired (Jackson and Bartek, 2009, Milano et al., 2024). Failure to do so has been linked to a number of human diseases and disorders (Nelson and Dizdaroglu, 2020). The origin of such damage can originate from both endogenous and exogenous sources such as replication errors, UV radiation and inflammation. DNA lesions can lead to replication stress and mutations which in turn can lead to carcinogenesis (Nelson and Dizdaroglu, 2020).

DNA damage triggers activation of the DNA damage response. This first aims to stabilise lesion sites and initiate repair. If the damage is too extensive then cell cycle arrest or cell death may occur (Jackson and Bartek, 2009).

3.2 Causes of DNA Damage

Ionising radiation (IR) (alpha, beta, gamma, neutrons and x-rays) is prevalent in our environment causing both direct and indirect damage. Damage takes the form of either double strand breaks formed by multiple lesions positioned closely together or single strand breaks which are identifiable by signature base end modifications (Chatterjee and Walker, 2018). Ultraviolet (UV) radiation from the sun is a leading cause of skin cancer and like IR can induce damage through either direct or indirect means. Our cells easily absorb UV with maximal absorption occurring at 260nm (Sinha and Häder, 2002, Chatterjee and Walker, 2018). Finally, as well as UV rays we are exposed to many DNA damage causing agents in our natural environment such as chemicals and extremes of heat and cold. Often the replication machinery is the target of chemical agents such as camptothecin (CPT) and aphidicolin (APH). CPT traps topoisomerase and blocks DNA re-ligation, introducing stress at replication forks by forming abnormal replication intermediates (Shao et al., 1991, Mei et al., 2020). APH blocks dCTP (deoxycytidine triphosphate) incorporation by binding to the active site of DNA polymerase a, resulting in the formation of long strands of single stranded DNA which is fragile and vulnerable to breakage if not stabilised (Snyder and Regan, 1981, Vesela et al., 2017).

Sources of DNA may also come from cellular metabolic processes such as hydrolysis, oxidation, alkylation and replication errors (Hakem, 2008). DNA replication is a smooth-running machine, but can unravel when it encounters obstacles such as mismatched base insertions, substitutions, deletions or R-loops (Tubbs and Nussenzweig, 2019). The effects can be devastating on the cell resulting in stalled or collapsed replication forks, further DNA breakage, genetic mutations or cell death (Toledo et al., 2017). In order to try and maintain genomic stability and cell

viability the DDR is activated, a complex network of genes responsible for repairing DNA damage Coon and Benarroch et al., 2018, Pile et al., 2018, Verni, 2022)

3.3 Cellular Outcomes to DNA Damage

Once DNA damage is detected within the cell the DDR orchestrates the activation of pathways and genes that initiate repair, but ultimately determine the fate of the cell. The possible outcomes to DNA damage can be boiled down to survival, senescence, or death. The first strategy is to protect the cell from further damage and reverse the damage that has already occurred. When damage is extensive the cell may instead undergo cell cycle arrest or programmed cell death (Nathans et al., 2021, Visser and Thomas, 2021)

3.3.1 DNA Repair Mechanisms

DNA repair can be conducted in one of two ways; either through direct reversal of DNA damage or by removal of damaged bases and synthesis of a new DNA strand (Cooper, 2000). Direct reversal of DNA damage can only be used on a few specific types of DNA damage and is only suitable when a few based have been damaged However, it is possible to reverse the damage caused by UV light by this mechanism, one of the most common forms of DNA damage. It has an added advantage of being energy efficient and any repairs are error free as no new DNA synthesis is required making it suitable for frequently occurring damage (Cooper, 2000, Gutierrez and O'Connor, 2021, Lecca and Ihekwaba-Ndibe, 2022).
More serious forms of damage such as DSBs require repair through a different mechanism. (Shrivastav, De Haro and Nickoloff, 2007, Willers, Pfäffle and Zou, 2012). This is a serious cytotoxic lesion that requires careful management. Failure to repair this type of break leads to genomic instability and cell death and mis-repair leading to further errors such as inappropriate end-joining and chromosomal translocation (Ceccaldi, Rondinelli and D'Andrea, 2015). DSBs are characterised by a break in the phosphorus sugar backbone where both DNA strands are broken in the same location or at least in close enough proximity to cause the double helix to separate into two separate entities (Cannan and Pederson, 2017). DSBs are

repaired through either non-homologous end joining (NHEJ) or homologous recombination (HR).

NHEJ is the predominant mechanism used, repairing ~80% of all DSBs in human cells. The first protein on the scene is Ku70/80 which binds and stabilises the ends of the break and recruits other repair proteins. Next the strands are brought together in a process called “synapsis” which is mediated by the LIG4 (XRCC4–DNA ligase 4) complex which directly ligates the two DNA ends. Synapsis can be enhanced by the action of XLF (XRCC4-like factor) (Cannan and Pederson, 2017, Zhao et al., 2020). If required, end processing is carried out by polymerases (Polμ, Polλ, TdT (terminal deoxynucleotidyl transferase)) to form a complimentary ligand with excess single stranded DNA cleaved by the nuclease Artemis (Cannan and Pederson, 2017, Zhao et al., 2021, Stinson and Loparo, 2022). As NHEJ does not rely on strand invasion it is the only repair mechanism able to repair DSBs during the G0 and G1 phases of the cell cycle. This comes at a cost as direct ligation of the two DNA is error-prone, unlike HR which relies on alignment of a homologous template and is error free in comparison (Zhao et al., 2021, Stinson and Loparo, 2022).

If NHEJ is considered the fast mechanism, then HR is the slow. HR will be chosen over NHEJ if there are sister chromatids nearby which can provide a homologous template for repair (Ensminger and Löbrich, 2020). The defining characteristic of HR is the strand invasion by a 3’ single stranded (ss)DNA into a homologous duplex. Before this can begin, resectioning of the 5’ end is carried out by the MRN complex. This is comprised of MRE11 (Meiotic Recombination 11 Homolog A), Rad50 and NBS1 (Nijmegen Breakage Syndrome 1). MRE11 possesses both endonuclease and exonuclease activity and in conjunction with mammalian CtIP (C-terminal interacting protein) to cleave at the 5’ end in 50-100 nucleotide sections. Further resectioning is carried out by EXO1 (Exonuclease 1) (Cannan and Pederson, 2017). Once this is completed RPA (Replication protein 1) binds to the processed 3’ ssDNA end, stabilising and protecting the vulnerable ssDNA (Dueva and Iliakis, 2020). This is replaced by RAD51 initiating formation of the RAD51 filament. This mediates strand invasion and homology search resulting in homology directed repair (Cannan and

Pederson, 2017, Carver and Zhang, 2021). Once it has annealed to its complementary sequence a D loop is formed, displacing the opposing strand and initiating synthesis of a new DNA strand. Leading strand synthesis on the opposing strand is primed by extension of the D loop allowing annealing to the 3' ssDNA on the other side of the break and changing the structure of the D loop to a cross-structure called a "double Holliday junction". These are resolved by cleaving a single nucleotide which is then repaired by DNA ligase. Unlike NHEJ which can operated throughout the entire cell cycle, HR is restricted to the S/G2 phase (Chapman et al., 2012, Jasin and Rothstein, 2013, Cannan and Pederson, 2017) However, utilising complementary strand repair is relatively without error and so, depending on the extent of the DNA damage, may be preferential over NHEJ (Chapman, Taylor and Boulton, 2012).

Single strand breaks (SSBs) are the most common form of DNA damage where damage occurs only to one DNA strand, often occurring due to oxidative stress. If left unrepaired they can cause replication stress, genome instability and may progress to a full DSB (Hossain, Lin, Yan, 2018, Caldecott, 2024). The mechanism of repair for SSBs varies depending on the source of the damage but are generally repaired using a global pathway known as Single Strand Break Repair (SSBR) which permits rapid repair of SSBs. This is generally considered to be a sub-pathway of Base Excision Repair (BER) and consists of four steps: detection, DNA end processing, gap-filling repair synthesis and DNA ligation (Abbots and Wilson, 2016). Detection is policed by PARP1 (Poly [ADP-ribose] polymerase 1) which quickly detects and binds to the break. This in turn is bound by PAR (poly[ADP-ribose]) which triggers its own activation and recruits XRRC1 (X-ray repair cross complementing 1) to the break site (Chaudhuri and Nussenweig, 2019). This protein plays a role in break resealing and in DNA end processing (Brem and Hall, 2005, Wei et al., 2013). The next step is gap filling which usually only requires replacement of a single nucleotide, but in some circumstances may require insertion of two or more nucleotides. The final step is DNA ligation which involves three DNA ligase genes (LIG1, LIG3, LIG4). LIG3 encodes three polypeptides (LIG3α, LIG3β and mtLIG3) with LIG3α requiring

stabilisation by XRRC1 with some evidence that LIG1 may also have some dependency for stability and accumulation (Caldecott, 2008)

3.3.2 Senescence

When DNA is severe and repair is not possible then cells may enter a state of senescence that prevents the passage of damaged DNA to daughter cells and is therefore considered a tumour suppressor mechanism. Senescence is a state of irreversible, stable cell cycle arrest characterised by resistance to apoptosis and significantly altered morphology. Cells become flattened, distended and vacuolised, and may exhibit an enlarged nucleus (Herranz and Gil, 2018, Humphreys, El Ghazaly and Frisan, 2020). Senescence can be induced by a number of stressors including oxidative stress, ionising radiation, mitochondrial dysfunction and chemotherapy drugs and is often preceded by a period of sustained DDR (Coppe et al, 2008, Herranz et al., 2018, Basisty et al., 2019, Kale et al., 2020).

In 2008, Coppe et al. used antibody assays to assess the myriads of factors secreted by senescent cells in response to genotoxic stress. These secretions were similar across different cell types and found to be associated with inflammation. This was termed the senescence-associated secretory phenotype or SASP and comprises a complex range of cytokines and proteases (Basisty et al., 2019). A number of components have been found to be core features of the SASP. These comprise the proinflammatory cytokines interleukin-6 (IL-6), and CXC ligand 8 (CXCL8/IL-8) and monocyte chemoattractant protein 1 (MCP1) and are common across many types of senescence (Di Micco et al., 2020). Around the same time Xue et al (2007) discovered that reactivating p53 in a hepatocarcinoma mouse model led to an upregulation in inflammatory cytokines and the recruitment of selective immune cells. This in turn led to the removal of senescent cells by the immune system and tumour regression, linking the SASP to an immune response for the first time.

Cell cycle arrest in senescence is maintained by two main pathways. The first is controlled by tumour suppressor p53 in conjunction with p21, a cell-cycle inhibitory protein known as a cyclin-dependent kinase inhibitor (CDK). The other is governed

by another CDK, $p16^{INK4}$ (p16) and phosphorylated retinoblastoma protein (p-pRb) another tumour suppressor (Kale et al., 2020). When p16 is impaired in mice it leads to a predisposition to spontaneous tumour formation (Serrano et al., 1996). A cell is also maintained in a senescent state through the SASP via positive feedback loop known as autocrine signalling (Gonzalez-Meljem et al., 2018), however it has also been found that senescence is transmissible to neighbouring cells known as a 'bystander effect'. This is sustained via paracrine signalling and occurs through gap junction-mediated cell to cell contact and the release of soluble factors such as IL1, IL6, IL8 and CC2 (Gonzalez-Meljem et al., 2018, Nelson et al., 2012).

Senescence was found to have other beneficial effects in cellular processes besides tumour suppression and immune clearance. It has also been linked to important roles within embryonic development as part of a natural programming mechanism and was linked to wound healing process with a rapid upregulation of p16 found after wounding in mouse models (Jun and Lau, 2010, Demaria et al., 2014) with removal of senescent cells causing a delay in cutaneous wound healing (Demaria et al., 2014). However, many of the beneficial effects of senescence effects of senescence are dependent on timely removal by the immune system (He and Sharpless et al., 2017). Over time the immune system begins to deteriorate resulting in an accumulation of senescent cells. Clearing cells positive for p16 resulted in delayed tumorigenesis and reduced age-related deterioration in several organs along with an increased median life span in mice (Baker et al., 2016). This suggests that while senescence may initially be instrumental in preventing tumorigenesis, an increase in proinflammatory molecules resulting from the decline in immune system function associated with advancing age and accumulation of senescent cells becomes detrimental, leading to pathogenesis of age-related diseases, including cancers.

3.3.3 Apoptosis

When a cell becomes damaged beyond repair, the most extreme fate is programmed cell death such as apoptosis. This is form of cell death displays significant changes in cell morphology. Early apoptosis induces cell shrinkage which progresses to

plasma membrane blebbing, karyorrhexis and finally cell fragmentation into apoptotic bodies during late-stage apoptosis (Elmore, 2007, Wong, 2011, Nossing and Ryan, 2022).

Apoptosis occurs via one of two core pathways; the intrinsic and the extrinsic pathway. Although both lead to the same terminal outcome (Reed, 2000, Elmore, 2007, Jan and Chaudhry, 2019).

The Extrinsic Pathway: this pathway is otherwise known as the death receptor pathway and is activated by extracellular pro-death signals from immune cells such as natural killer (NK) lymphocytes. The apoptosis process begins when death ligands bind to their corresponding death receptor. The best described death receptors are TNFR1 (type 1 TNF receptor) and Fas (CD95) and their respective ligands, TNF (tumour necrotising factor) and FasL (Fas ligand) (Jan and Chaudhry, 2019, Nossing and Ryan, 2023). Adapter proteins such as FADD (Fas-associated death domain) and TRADD (TNF receptor-associated death domain), along with caspase 8, are recruited to intracellular death domains on the death receptors. Binding by the adapter protein is permitted once the ligand has bound to the receptor and the whole complex becomes known as the DISC (death-inducing signalling complex) (Jan and Chaudhry, 2019). This new complex activates caspase 8 which is the initiator of a caspase cascade which drives apoptosis (Wong et al., 2011).

The Intrinsic Pathway: this is the mitochondrial pathway, so called because pro-apoptotic molecules are released into the cytoplasm via increased mitochondrial permeability. This pathway is triggered by cellular stressors such as oxidative stress, irradiation or severe DNA damage, and is mediated by BCL-2 (B-cell lymphoma-2) (Wong, 2011, Jan and Chaudhry, 2019). Upon sensing DNA damage, the DDR is activated and depending on the type of damage sustained, either triggers ATM-Chk2 (Ataxia telangiectasia mutated-Checkpoint kinase 2) in the case of DSBs and ATR-Chk1 (Ataxia telangiectasia and Rad3-related gene-Checkpoint kinase 2) if SSBs. Both cause activation of p53 which is the transcription factor for pro-apoptotic genes

such as BAX (Bcl-2 Associated X-protein), PUMA (BBC3/BCL2 Binding Component 3) and NOXA (PMAIP1/Phorbol-12-Myristate-13-Acetate-Induced Protein 1) (Nossing and Ryan, 2023). MDM2 (Mouse double minute 2) inhibits the activity of p53 until DNA damage is detected. ATM then phosphorylates MDM2, breaking the negative feedback loop and releasing p53, leading to its stabilisation (Cheng and Chen., 2010).

PUMA and NOXA are members of the BCL-2 protein family along with others such as BIM (Bcl-2-like 11), BID (BH3 Interacting Domain Death Agonist) and HRK (Harakiri, BCL2 Interacting Protein). These inhibit the action of anti-apoptotic members of the BCL-2 family and activate BAX and BAK (BCL2 Antagonist/Killer 1), signalling the point of no return. This is the catalyst for mitochondrial permeability, triggering release of cytochrome c, subsequently permitting formation of the apoptosome and a cascade of caspases that begin fragmenting the cell (Jan and Chaudhry, 2019, Nossing and Ryan, 2023).

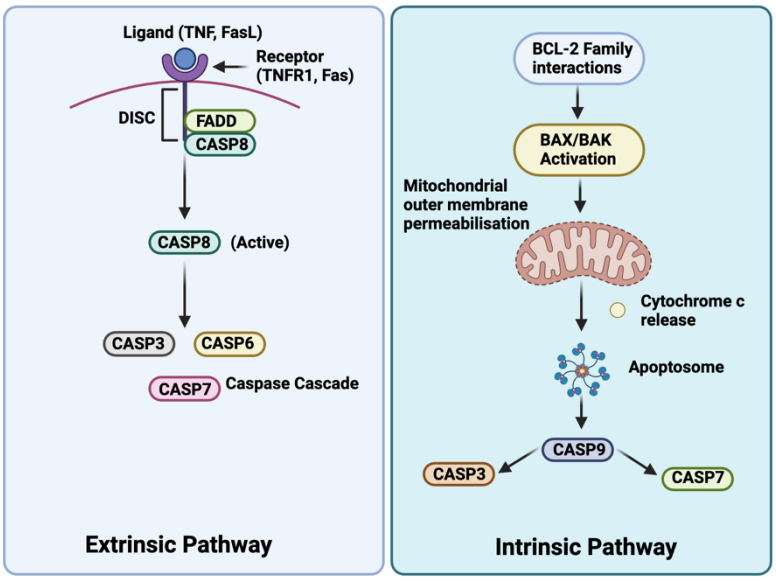

Fig 1.3 **The Extrinsic and Intrinsic Apoptosis Pathways.** The extrinsic pathway is activated by binding of ligands to death receptors and consequent recruitment of FADD and caspsade 8. This causes activation of caspase 8 leading to a caspase cascade and apoptosis. Conversely the intrinsic pathway is triggered by inhibition of anti-apototic members of the BCL-2 family leading to activation of BAK/BAX and increased permeabilisation of the mitochondrial outer membrane. This results in relwase of cytochrome c and formation of the apoptosome. This then leads to a caspase cascade in a similar manner to the extrinsic pathway.

3.4 The Typhoid Toxin and DNA Damage

The Humphreys lab has studied the effects of the typhoid toxin *in vitro* and found that the toxin caused wide spread DNA damage in host cells. DSBs were induced in HT1080 cells and were detected by γH2AX and 53BP1 labelling in phase G0/1 of the cell cycle. The toxin also induced SSBs through detection of γH2AX and hyperphosphorylation of RPA (Replication protein A), a protein which binds to single stranded DNA, in cells in S/G2. This caused activation of ATR and phosphorylation of p53 and CHK1, which are also components of the ATR pathway (Ibler et al., 2019).

The replication stress induced by the typhoid toxin was also found to activate cell fate decisions. Cells displayed cell distension and permanent cell cycle arrest suggesting the cells underwent senescence. This senescence phenotype was induced in naïve cells by treating them with the secretome harvested from intoxicated cells and demonstrating that the toxin triggered release of the SASP and drove secondary senescence in bystander cells. These cells also showed greater susceptibility to infection by *S.* Javiana supporting the theory that the typhoid toxin promotes infection (Ibler et al., 2019). Following this, the toxin-induced host secretome was identified by proteomics, which revealed host proteins Wnt5a, INHBA and GDF15 as mediators of SASP (El Ghazaly et al 2023). For example, secreted Wnt5a protected HCT116 intestinal cells from toxin-induced damage and in the absence of Wnt5a, HCT116 cells underwent apoptosis rather than senescence.

The underlying mechanism for toxin induced replication stress and senescence was found to be excessive numbers of SSBs which caused saturation of RPA and prevented repair by SSBR. Once repair was not achievable the cells turned to senescence to try and maintain genomic stability, but in turn may have inadvertently facilitated infection.

Our results fit with other published studies such as those by Del Bel Belluz et al. (2016), Miller et al. (2018) and Gibani et al. (2019). The typhoid toxin causes DNA

damage forcing cell to make cell fate decisions. DNA damage has been implicated in a number of human diseases and persistent damage by *S.* Typhi has been linked to carcinogenesis. Therefore, I will begin this project by investigating the host responses to purified toxin in both primary and epithelial cells.

Chapter 4: The Interferon Response

The innate response is the body's first line of defence against pathogen invasion. This is a fast-acting response and is a non-specific, antigen-independent response. This differs from the adaptive immune response which relies on specific antigen recognition (Tosi, 2005). Pathogen's release PAMPs which are microbial products that upon entry into the host trigger activation of signalling pathways designed to detect invasion, which are defined as pattern recognition receptors (PRRs). Several of these receptors exist such as Toll-like receptors, AIM2-like receptors and RIG-I-like receptors (Tang et al., 2012). Once detected, the innate immune system can release its other defence mechanisms which can be categorised as: immune cells (macrophages, neutrophils, dendritic cells), acute phase proteins (complement, C-reactive protein), anti-microbial peptides (defensins) and enzymes (lysozyme), and inflammatory mediators such as cytokines (TNF, interferons, interleukins) (Marshall et al., 2018). This extensive host defence strategy aims to quickly eliminate pathogens and limit infection (Aristizábal et al., 2013).

4.1 Interferons

Interferons (IFNs) were discovered by Isaacs and Lindemann (1957) after they discovered a secretion factor that appeared to "interfere" with viral infection (Walker, Sridhar and Baldridge, 2021). There are now three families of interferons categorised as type I, type II and type III. The receptors for these IFNs are IFNα (IFNAR), IFNγ (IFNGR) and IFNλ (IFNLR) respectively (Kopitar-Jerala, 2017, Alphonse et al., 2021). Type I interferons are expressed by almost all cells with the most widely studied being IFNα and IFNβ, whereas the type II family contains a sole member -

IFNγ. It is also unique compared to other interferons as its inducement come from immune cells as part of a response to other cytokines. The type III family consists of IFNλ 1,2,3 and 4, but expression of its receptor is limited to epithelial cells and a few immune cells (Alphonse et al., 2021).

IFNs are important for the expression of interferon stimulated genes (ISGs), a group of 300-600 genes that are involved in the innate immune response and are inducible by all types of interferon (Alphonse et al., 2021). IFN signalling occurs via their receptor which activates the Janus kinase/Signal transducer and activator of transcription (JAK-STAT) pathway (Platanias et al., 2005, Alphonse et al., 2021).

When it comes to bacterial infection ISGs have been shown to have an inhibitory effect on the life cycle of intracellular bacteria. The expression of the ISG viperin inhibited cellular number of both *Shigella* flexneri (*S*. flexneri) and *Listeria* monocytogenes (*L*. monocytogenes) by as much as 80% 5hrs post infection (Helbig et al., 2019). Type I IFN was also shown to have a similar inhibitory ability by preventing the transmigration of bacteria across endothelial and epithelial membranes. Mice either possessing deficiency in the type I IFN receptor, IFNAR, displayed elevated levels of bacteraemia after pneumococcal infection, despite showing similar bacteria numbers in the lung. Mice treated with IFNβ showed a reduction in bacteraemia (Le Messurier et al., 2013).

However, IFNs have also been found to exacerbate infection and enhance bacterial pathogenesis. A positive correlation was found in the blood transcriptome of patients between disease pathogenesis of Mycobacterium tuberculosis (*M. tuberculosis*) and the profusion of type I IFN-inducible transcripts (Berry et al., 2010) and influenza infected mice deficient in type I IFN displayed better survival and were better able to clear a *Streptococcus pneumoniae* (*S. pnuemoniae*) compared to the similarly infected control group (Shahangian et al., 2009).

There has been considerable research conducted into the role of IFNs/ISGs in viral infection but distinctly fewer studies have investigated their role in bacterial infection.

The studies that have been done indicated that the effects of IFNs/ISGs can either promote or inhibit infection depending on the pathogen and experimental context (Alphonse et al., 2014). This offers an exciting and novel research opportunity which this project aims to undertake.

4.2 The Interferon Response

Type I IFN signalling occurs through its receptor IFNAR in both an autocrine and paracrine manner. Production of IFNα and IFNβ triggers classic JAK-STAT signalling **(Fig 4.1)** by binding to IFNAR which induces conformational changes in the receptor site allowing phosphorylation by JAK1 (Janus kinase 1) and TYK2 (tyrosine-protein kinase 2). The phosphorylation action attracts STAT 1 and 2 (Signal transducer and activator of transcription proteins 1 and 2) to the cell membrane where they also become phosphorylated by TYK2. Phosphorylated STAT1 and STAT2 are bound by methylated IRF9 (Interferon regulatory protein 9) to form a tertiary complex known as the SSI complex. IRF9 is subsequently demethylated triggering translocation of the SSI complex to the nucleus. Once in the nucleus, binding of the SSI complex to the (ISRE) interferon-stimulated response element activates upregulation of hundreds of ISGs (Mathieu et al., 2021).

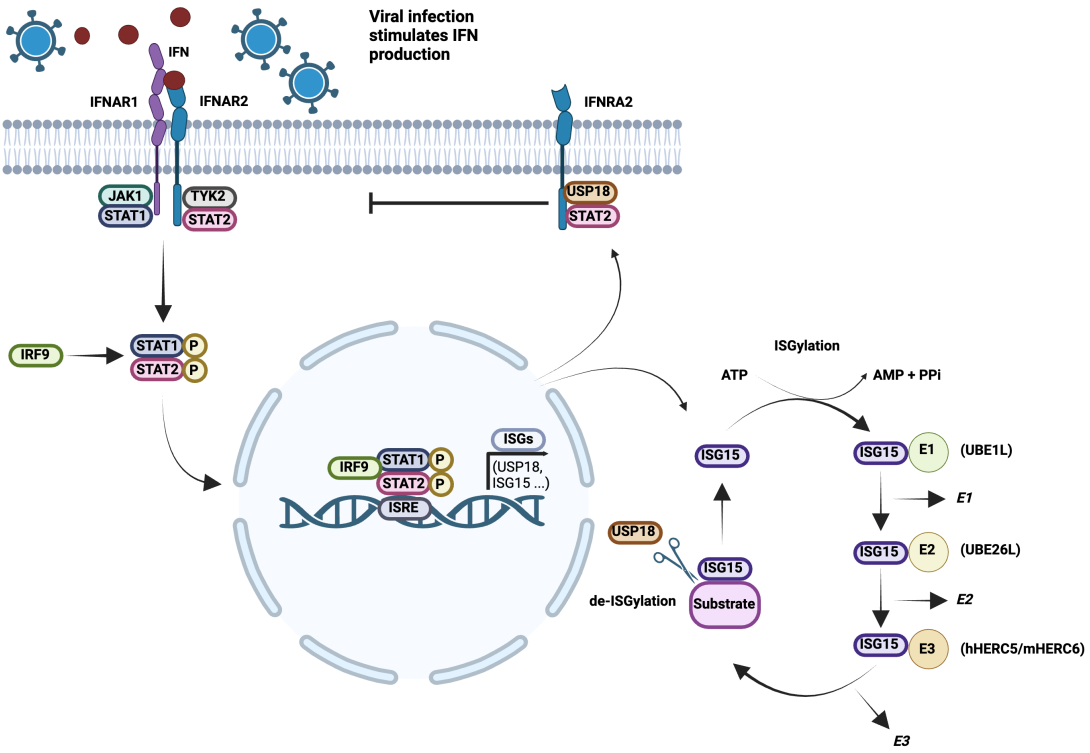

Fig 4.1 **The Interferon Response via JAK/STAT Signalling.** IFNα and IFNβ bind to the receptor IFNAR causing phosphorylation of STAT1 and STAT2 and formation of the SSI complex with IRF9. This migrates to the nucleus activating upregulation of hundreds of ISGs. ISG15 activity is regulated by ISGylation with deISGylation mediated by USP18. Downregulation of the IFN response is also mediated by USP18 through a negative feedback loop in conjunction with STAT2.

4.2 ISG15 and ISGylation

One of the most prominent ISGs to be upregulated as part of the interferon response is ISG15 (interferon stimulated gene 15) (Sadler and Williams, 2008). This is a ubiquitin-like protein plays a number of roles within the cell outside of the antiviral response, for example it has been identified as a key modulator of both p53 and autophagy (Sandy, De Costa and Schmidt, 2020). ISG15 can be in a free or conjugated state.

Free ISG15 is found both extracellular and intracellular. The presence of extracellular ISG15 has been detected near various immune cell types after type I IFN activation, enhancing their cytotoxicity by acting as a cytokine (Yuan et al.,

2023). ISG15 in this environment has been shown to suppress tumour growth in breast cancer (Burks, Reed and Desai et al., 2015). However, the reverse was true PDAC (pancreatic ductal carcinoma) (Sun et al., 2020). Intracellular ISG15 has been found to regulate other intracellular proteins modulating the antiviral response from within. ISG15 disrupts the function of VP40 and inhibited budding of the Ebola virus by interacting with NEDD4 (Neural precursor cell expressed developmentally down-regulated 4), preventing its ligation and consequently downregulating ubiquitination of VP40 (Okumura, Pitha and Harty, 2008). ISG15 can also cause persistent antiviral signalling by prolonging activation of proteins like IRF3 and STAT1, leading to an elevated interferon response (Shi et al., 2010, Ganesan et al., 2016).

The role of intracellular ISG15 centres around its conjugation via its lysine (K) residues in a process called ISGylation. This is a cyclical pathway involving a three-enzyme cascade. The three enzymes are E1 (UBE1L) the activating enzyme, E2 (UBE26L) the conjugating enzyme and the ligase E3 (HERC5/mHERC6) (Sandy et al., 2015). First UBE1L activates ISG15 in an ATP-dependent manner, forming a thioester bind between UBE1L and ISG15. Once actvated ISG15 is transferred to the active cysteine active site of UBE26L, forming another thioester bond. Finally, HERC5 (or another E3 ligase such as TRIM25 or ARIH1) catalyzes the covalent binding of ISG15 to its target protein. In mice, HERC6 is the main E3 ligase for ISGylation, while in humans HERC6 is devoid of a ISGylation function (Dastur et al., 2006, Jacquet, Pontier and Etienne, 2020). ISGylated proteins are then detected by RNF213 (Ring Finger Protein 213), an E3 ligase and cellular sensor which has been shown to play a role in antimicrobial defence by targeting RTA, a key viral protein (Thery et al., 2021). It has also been shown to restrict the proliferation of cytostolic *Salmonella* by ubiquitination of LPS, inducing anti-bacterial autophagy (Otten et al., 2021).

Post ISGylation ISG15 is released from its substrate in a process called deISGylation mediated by USP18 (ubiquitin-specific protease 18). USP18 also plays a further role outside of deISGylation by downregulating IFN signalling by binding STAT2. This prevents IFNAR modification by JAK1 and phosphorylation of STAT1

which consequently prevents the activation of ISGs (Dzimianski et al., 2019, Freitas et al., 2020).

4.3 ISGylation and Ubiquitination

The process of ISGylation and ubiquitination are very similar. Both are post-translation modifications and involve covalent conjugation of ubiquitin-like proteins (ISG15 and ubiquitin, respectively) in order to target proteins through a enzymatic cascade using E1, E2 and E3 enzymes (Chen, Li and McGilvray, 2011, Kang, Kim and Jeon, 2022). Some enzymes such as TRIM25 and UBE2L6 are shared across both reactions (Telcaco-Cruz and Zepeda-Cervantes, 2023). Both processes are also reversible with specific deconjugating proteins (USP18 and proteasome) removing ISG15 and ubiquitin from their target protein (Chen, Li and McGilvray, 2011, Jeon and Chung, 2022).

However the relationship between ISGylation and ubiquitination is complex. While both are involved in various cellular processes, ISGylation is induced by interferon and is involved in antiviral defence and innate immunity, whereas ubiquitination is involved in a broader range of activities such as DNA repair, cell cycle regulation and protein degradation (Villarroya-Beltri, Guerra and Sanchez-Madrid, 2017). The two also appear to have an antagonistic relationship with ISGylation competing with or altering ubiquitination, and vice versa. Viral induced ISG15 and HERC5 expression enhanced NLPR3 (NOD-, LRR-, and pyrin domain–containing protein 3) ISGylation leading to a NLPR3 inflammasome response and subsequently inhbiting K48-linked ubiquitination and proteasomal degradation (Qin et al., 2023). ISG15 and ISGylation has also been found to promote apoptosis in response to toxic stimuli by increasing degradation-independent polyubiquitination of tAIF (truncated AIF) (Jeon and Chung, 2022). Conversely, SUMO1, a small ubiquitin-like modifier, increases poly-SUMOylation in response to IFN activation, stabilsing ISG proteins and enhancing antiviral defences (Chelbi-Alix and Thibault, 2021).

4.4 ISG15 and Antiviral Activity

ISG15 plays a vital role in antiviral defences through its function as a cytokine and by conjugating to target proteins involved in the immune response. One of the key ways it accomplishes this is by interefering with viral replication, disrupting the function, localisation and interaction of viral proteins (Dzimianski et al., 2019, Zhang et al., 2021). ISG15 has been found to inhibit influenza A infection by targeting NS1A, a protein essential for counteracting the cells antiviral activities, by modifying the K41, a critical lysine residue and ISG15 acceptor site. This inhibits the function of NS1A and thereby restricts influenza A infection (Zhao et al., 2010). During ebola infection the virus relies on ubiquitination of its VP40 matrix protein by the E3 ligase NEDD4 to assist its entry into the host cell. ISG15 targets VP40, preventing its ubiquitination and inhibiting budding, a crucial step in the ebola virus life cycle (Freitas et al, 2021). ISG15 also helps inhibits HIV-1 infection in a similar manner by specifically inhibiting Gag (Group-specific antigen) and Tsg101 (Tumour susceptibility gene 101) ubiquitination, preventing HIV-1 budding and virion release (Okumura et al., 2006). These strategies demonstrate that ISG15 is an important component in the antiviral response and specifically targets viral proteins to inhibit infection.

4.5 Viral Evasion Strategies to ISG15

The battle between ISG15 and viral infection is not a one sided battle however. Viruses have adapted strategies to combat the interefering effects of ISG15. The NS1B protein released by influenza B inhibits ISGylation of host proteins by blocking ISG15 conjugation through preventing the interaction of ISG15 and UBE1L (Jeon, Yoo and Chung, 2010). Similarly, the E3 protein produced by the vaccinia virus blocks ISG15 conjugation by binding to the C-terminal of ISG15 (Guerra et al., 2008). Contrary to the findings in Jeon, Yoo and Chung (2010), the work of Zhao et al. (2016) suggests that instead of preventing ISGylation, NS1B sequesters ISGylated proteins, inhibiting their action. Whatever the exact mechanism it is clear that NS1B is an important component in the viral invasion strategy.

In addition to interfering with ISG15 conjugation, viruses may also counteract the antiviral activities of ISG15 through other methods. HIV-1 targets the STAT1 and STAT3 (both ISGylated proteins) for proteasomal degradation and thereby negatively affecting JAK/STAT signalling (Gargan et al., 2018). Some viruses such as Middle East respiratory syndrome coronavirus (MERS-CoV) have the ability to reverse ISGylation through the action of a papain-like protease (PLpro) which both deubiquitinates and ISGylates conjugated proteins (Daczkowski et al., 2017). These strategies demonstrate how, despite rapid ISG15 release and a strong immune response, viruses are able to overcome the host antiviral mechanisms and establish infection.

4.6 ISG15 Deficiency and Human Disease

ISG15 deficiency is a rare, inheritable condition with currently less than 100 cases reported globally (Burleigh et al., 2023). Clinical presentation of ISG15 deficiency manifests as an increased susceptibility to mycobacterial infection, intracranial calcifications and development of necrotising skin lesions (Hermann and Bogunovich, 2017, Martin-Fernandez et al., 2020). Surprisingly, patients did not show increased susceptibility to viral infections due to sustained enhanced type I IFN signalling (Hermann and Bogunovich, 2017). Increased susceptibility to mycobacterial infection was found to be uncoupled from ISGylation and instead was attributed to loss of mycobacterium induced ISG15 secretion by leukocytes (Bogunovich et al., 2012). Interestingly, attenuated *Mycobacterium bovis* Bacille Calette-Guerin (BCG), a vaccine strain, triggered a life-threatening infection in ISG15-deficient individuals while BCG typically only elicits a mild inflammatory response in healthy people. ISG15 has also been associated with protecting humans against infection by the intracellular pathogen *Listeria monocytogenes* due ISG15-dependent restriction (Radoshevich 2015). Following *Listeria* infection, bacterial DNA triggered an IFN-independent ISG15 response that relied upon cytosolic DNA surveillance proteins STING (Stimulator of interferon genes), TBK1 (Tank binding kinase 1), IRF3 (Interferon regulatory factor 3) and IRF7 (Interferon regulatory factor 7) . *Listeria* infections triggered ISGylation and increased secretion of cytokines,

which were speculated to mediate antimicrobial responses. Indeed, siRNA-mediated depletion of ISG15 in cultured cells or ISG15 gene knockouts in mice, led to an increased *Listeria* infection. In a a later study, ISGylation was linked *Listeria*-induced autophagy through the modification of mTOR, WIPI2, AMBRA1, and RAB7 (Zhang et al 2019) and autophagy is a major host defence pathway against intracellular pathogens (Hu et al 2020, Kimmy & Stallings 2016). ISG15 has also been implicated in epithelial cell infections by the intracellular pathogen *Chlamydia trachomatis* (Wu et al 2024), which causes urinary tract infections. *Chlamydia* infection triggered IFN-independent ISG15 expression depending on STING-TBK1-IRF3. ISG15-depletion increased cytokine and chemokine production and mediated its effects against *Chlamydia* independently of ISGylation (Wu et al 2024), which contrasted with *Listeria* (Radoshevich 2015). Delayed clearance of *Chlamydia* was observed in ISG15-deficient mice further indicating that ISG15 protects mammalian hosts from infection (Wu et al 2024).

Compared to viral infection, there is a lack of knowledge regarding how ISG15 deficiency impacts bacterial infection, which mainly focuses on *Listeria* and *Chlamydia*. Infection by *L. monocytogenes* highly induced expression ISG15 independently of type I IFN signalling in Hela cells. Detection of bacterial cytostolic DNA rapidly induced ISG15 and ISGylation leading to restriction of infection (Radoshevich and Cossart., 2018). Similarly, infection with *C. trachomatis* in epithelial cells also triggered ISG15 activation. Absence of ISG15 resulted in an increase in cytokines IL-6 and IL-8 suggesting that ISG15 acts as a brake on the immune response, preventing excessive inflammation. Bacterial load also increased without ISG15 demostrating that ISG15 limits bacterial numbers (Wu et al., 2024).

A review of the current literature reveals even less on the interaction with *Salmonella enterica*, one of the most common sources of bacterial infection. No studies could be found investigating ISG15 deficiency and infection by toxigenic bacteria. Therefore, this project aims to fill this knowledge gap.

4.7 Aims and Hypothesis

From the published literature it has been shown that ISG15 expression can be triggered by type 1 IFN, but can also be induced by pathways IFN independent pathways. Does the typhoid toxin activate one of these pathways?

The aims of this project are as follows:

1. Investigate the host responses to the typhoid toxin in different cell types.
2. Explore the role of ISG15 and determine if this modulates differing host responses to the typhoid toxin.
3. Determine if deficiency of ISG15 promotes or inhibits infection of toxigenic *Salmonella*.

Given that deficiency of ISG15 increases the susceptibility to mycobacterial infection, I would hypothesise the same is true of *Salmonella* infection. As the typhoid toxin has been shown to elicit DNA damage, I would expect that the combined effect of the toxin and lack of ISG15 would further promote infection.

Part 2: Materials & Methods

Chapter 5: Mammalian Cell Culturing

The following cell lines were used in this project:

Cell Line	Source	Culture Media
$A549^{WT}$	Laboratory of Dr. Radoshevich, University of Iowa	DMEM Glutamax (Gibco # 31966-021)
$A549^{ISG15-/-}$	Laboratory of Dr. Radoshevich, University of Iowa	DMEM Glutamax
BMDMs	C57BL/6 mice, Laboratory of Prof. Walter Marcotti, University of Sheffield	RPMI (Sigma Aldrich #R8758)
$HCT116^{WT}$	Laboratory of Dr. Patrick Herr, University of Sheffield	DMEM Glutamax
$HCT116^{p53-/-}$	Laboratory of Dr. Patrick Herr, University of Sheffield	DMEM Glutamax
MEF^{WT}	Laboratory of Dr. Radoshevich, University of Iowa	DMEM high glucose (Sigma Aldrich # D65796)
$MEF^{ISG15-/-}$	Laboratory of Dr. Radoshevich, University of Iowa	DMEM high glucose
$U2OS^{WT}$	Laboratory of Dr. Radoshevich, University of Iowa	DMEM Glutamax
$U2OS^{ISG15-/-}$	Laboratory of Dr. Radoshevich, University of Iowa	DMEM Glutamax

Table 5.1 **Cell Lines and Media Used.** Complete list of all cell lines and the corresponding growth media used in this project.

All cell lines were cultured in complete growth media containing 10% FBS (Sigma Aldrich #F7524), 0.1% Kanamycin (BioBasic #KB0286), 0.1% Penicillin/streptomycin (P.S.) (Gibco #11548876).

A549, MEF and U20S cell lines were kindly provided by Dr Lilliana Radoshevich, Microbiology and Immunology Department, University of Iowa.

5.1 Generation of A549 Knockout Cell Lines

ISG15 knockout cell lines were generated by the Radoshevich lab, University of Iowa using a CRISPR/Cas9 approach. The target sequences were designed using www.benchling.com and oligonucleotides synthesised via Integrated DNA Technologies (www.IDT.com). These were cloned into the following plasmids:

pX330-U6-Chimeric_BB-CBh-hSpCas9 (#42230, Addgene)
pSpCas9(BB)-2A-GFP (#48138, Addgene)

Both plasmids were gifted by Feng Zhang (Department of Biological Engineering, MIT). The cells were co-transfected with ISG15-targeting plasmids along with FU gene® HD transfection reagent (BD Science) then GFP positive cells were isolated and plated in 96-well plates for single-clone selection using Becton Dickinson FACS Aria Fusion (BD Science). Transfected cells were challenged with IFNα and subsequent lack of ISG15 expression confirmed through Western blotting. Additionally, knock out of ISG15 was further confirmed by genomic PCR and next-generation sequencing of the ISG15 amplicon.
Primers - ISG15 NCBI FWD 5' gtgtgcctcaggcttataatagg 3'
ISG15 NCBI REV5' cggccatttctctttacaacagcc 3'

Both primers were synthesised by Integrated DNA Technologies.

5.2 General Maintenance of Cell Lines

Cell stocks were stored at -80°C in 10% sterile DMSO and 90% complete media. For experimental use, cells were thawed at 37°C and transferred into a cell culture flask at a 1:10 dilution with complete media. Flasks were placed into a humidified incubator (Panasonic, MCO-170AICUV-PE) at 37°C, 5% CO_2. Cell passage was carried out every 3 days, or when cells reached approximately 80% confluence.

To seed for experiments, the media was aspirated from the flask and washed with sterile PBS. Trypsin (Thermo Fisher Scientific #R001100) was then added (5mls), and the flask incubated at 37°C for 5 mins, or until the cells were fully detached. The trypsin was neutralised 1:1 volume with growth media containing 10% FBS and cells counted using a glass haemocytometer.

5.3 Harvesting and Differentiation of BMDMs

Mice were obtained from the animal facility at the University of Sheffield and humanely culled according to Schedule 1 of the Animals (Scientific Procedures) Act 1986. The mice were then sprayed with 70% ethanol and dissection carried out in a fume hood according to the protocol described in Madaan et al., 2014.
To differentiate the harvested monocytes into macrophages, 2ml of cell culture was added to 6.5ml of DMEM high glucose growth medium containing 10% FBS and 0.1% P.S., along with 1.5ml of L929 supernatant (kindly supplied by the Dept of Infection, Immunity and Cardiovascular Disease, University of Sheffield), 80ul of L-glutamine (Cytiva #SH30034.02). Differentiation was judged to be fully completed after 7 days by the change from monocytes in suspension to the presence of adherent macrophage cells.

5.4 Standard Intoxication Assay

Cells were seeded at $1x10^5$ per well of 24-well plate and incubated overnight at 37°C, 5% CO_2 in complete growth media as Table 2.1 with appropriate supplements (10% FBS, 0.1% Kanamycin, 0.1% PS). The next day the media was removed and replaced with fresh media containing purified typhoid toxin (TxWT) or a mutant control toxin (TxHQ) (0.1/1/10 ng/µl), 0.1 µg/ml IFN2α (NKMAX #IFN0502) or 3µM ETP (Cayman Chemicals #12092). The cells were then harvested using a trypsin at the appropriate time point (24hrs, 48hrs, 4 days, 7days).

5.5 *Salmonella* Javiana Infection (1)

Cells were seeded at the following densities in a 24 well plate

Cell Line	Seeding Density
$A549^{WT}$ - IFNα	$2x10^4$
$A549^{WT}$ + IFNα	$3x10^4$
$A549^{ISG15-/-}$ - IFNα	$2x10^4$
$A549^{ISG15-/-}$ + IFNα	$8x10^4$

Table 5.2 **Seeding densities for cell lines used for infection.** Given the cell killing effects of IFNα, an attempt was made to normalise cell numbers prior to infection.

After overnight incubation of A549 cells, IFNα was added (0.1µg/ml) to each well and the plate placed back into the incubator for a further 3 days at 37°C, 5% CO_2. The evening before infection, a 50ml falcon containing 10ml of LB broth was inoculated with isolate S5-0395 of wild-type *Salmonella* Javiana (SJ^{WT}) or with isolate M8-0540 of *Salmonella* $Javiana^{\Delta cdtB}$ ($SJ^{\Delta cdtB}$), provided by from Prof. Martin Weidmann (Cornell University, New York). As alternatives, *S.* Typhimurium SL1344 (provided by Prof. Vassilis Kornakis, University of Cambridge) and *S.* Typhimurium ST313 (provided by Prof. Gordon Dougan, University of Cambridge) were used for overnight cultures and infection. The next morning 100µl of the overnight culture was added to

a new 50ml falcon containing 10ml fresh LB broth. Upon reaching OD 1, the cells were infected at multiplicity of infection (MOI) 20 for 1 hour. Cells were washed x2 with sterile PBS and then 500μl of DMEM Glutamax added to each well. In order to eliminate extracellular bacteria, gentamicin (Thermo Fisher Scientific #15750060) was also added at 50μg/ml. After 1hr of treatment with DMEM Glutamax/gentamicin, 2hr samples were harvested and DMEM Glutamax containing 10μg/ml gentamicin was added to the other wells. Cells were then harvested at 8hrs and 24hrs post-infection.

5.6 *Salmonella* Javiana Infection (2)

Cells were seeded at $5x10^4$ in a 24 well plate. In parallel, 10ml of LB broth was inoculated with bacterial colonies of isolate S5-0395 of wild-type *Salmonella* Javiana (SJ^{WT}) or with isolate M8-0540 of *Salmonella* Javiana$^{\Delta cdtB}$ ($SJ^{\Delta cdtB}$), provided by from Prof. Martin Weidmann (Cornell University, New York). The next morning 100μl of the overnight culture was added to a new 50ml falcon containing 10ml fresh LB broth to generate a logarithmic culture. Upon reaching OD 1, the cells were infected at MOI 100 for 1hr. Cells were washed x2 with sterile PBS and then 500ul of DMEM Glutamax containing 50ug/ml gentamicin (+/- IFNα 0.1μg/ml) was added to kill extracellular *Salmonella*. At this point 2hr samples were harvested for CFU assays and DMEM Glutamax containing 10μg/ml gentamicin (+/- IFNα 0.1μg/ml) was added to the other wells until the appropriate time point was reached.

5.7 CFU Assay

At the appropriate timepoint the growth media was removed and the cells washed x2 with sterile PBS. The cells were then lysed to release intracellular *Salmonella* by adding 500μl 1% Triton in PBS and incubating at 37°C for 3 mins. 200ul of this mixture was transferred to a 96 well plate and a serial dilution was created by adding 20ul of the previous culture to 180μl PBS. 5ul of each dilution was spot pipetted onto an agar plate containing ampicillin (Melford Lab #A0104) which was then placed into

an incubator at 37°C overnight. The next day the number of CFUs at each dilution were counted and infection rate quantified.

5.8 siRNA Knockdown of A549 Cells

$A549^{WT}$ cells were seeded at $1x10^4$ overnight in a 24 well plate in antibiotic-free complete growth media. The next day siRNAs were transfected into the cells to knockdown USP18 (human siRNA, Horizon smartpool #L-004236-00-0005), ISG15 (human siRNA, Horizon smartpool #L-004235-03-0005 and UBE1L (human siRNA, Horizon smartpool #L-019759-00-0005). A non-targeting human siRNA pool was used as a control (Horizon smartpool #D-001810-10-05). Lipofectamine RNAiMax (Invitrogen, # 13778–150) was used to perform siRNA transfection using the following protocol:
https://www.thermofisher.com/uk/en/home/references/protocols/cell-culture/transfection-protocol/a549-cells-protocol.html

In summary for a 24-well plate, tube 1 containing 200µL Opti-MEM I medium (Gibco, #31985062) and 4µL Lipofectamine was combined with tube 2 containing 200µL Opti-MEM I medium and 10nM siRNA. Incubate for 15 minutes at room temperature. Add 50µL of mixture to A549 cells before incubation of transfected cells at 37°C, 5% CO_2. At 24 hours post-transfection, the cells were washed with PBS and the transfection mixture replaced with DMEM Glutamax complete (with 0.1% kanamycin, 0.1% PS) and IFNα (0.1 µg/ml) was added to the +IFNα wells. The plate was then incubated in an incubator at 37°C, 5% CO_2 for 7 days. Knock downs were then validated via MTT assay or Western blotting.

5.9 Transfection of USP18 Plasmid into A549 Cells

A549 wild type cells were seeded at $2x10^5$ seeded in a 6-well plate in antibiotic-free media overnight. Transfection was carried out as above, however instead of siRNA a Flag-HA-USP18 plasmid (Addgene #22572) was used. Again, an empty vector

plasmid (pHCMV) was used as a control. Following transfection, a 7-day incubation was carried as previously described. Transfection was validated via MTT assay.

Chapter 6: Biological Cell Assays

6.1 MTT Assay

Cells were seeded at the following densities overnight in a 24 well plate:

Cell Line	24hr	7 Day
MEFs	0.5×10^4	0.15×10^4
All other cell lines	1×10^4	2.5×10^4

Table 6.1 **Seeding density for MTT Assay.** Given the accelerated growth rate of the MEF cells, these were seeded at a lower density than other cell lines used.

The next day the cells were intoxicated as per the standard intoxication protocol. Upon reaching the appropriate time point the growth media was removed and the cells washed once with sterile PBS and 300ul of 3-(4,5-dimethylthiazol-2-yl)-2,5-diphenyltetrazolium bromide (MTT) reagent (Thermo Fisher Scientific #158990050)(5mg/ml) added to the wells. The plate was then placed into a humidified incubator at 37^{o}C, 5% CO_2 for 45 mins. The MTT solution was removed taking care not to disturb the purple-coloured formazan in the bottom of the well. 240ul of isopropanol was added with 160μl transferred to a 96 well plate once the formazan had fully dissolved. The plate was then run on a FLUOstar Omega plate reader at 550nm and 690nm. To determine the true absorbance value, the background control (690nm) was subtracted from the 550nm measurements.

6.2 Beta-Galactosidase (β-Gal) Assay

Cells were seeded in a 24 well plate as per the MTT protocol then intoxicated using the standard intoxication protocol. Upon reaching the appropriate time point the senescence β-Gal staining kit (Cell Signalling Technology, #9860) was performed according to manufacturer's instructions –

https://www.cellsignal.com/products/cellular-assay-kits/senescence-b-galactosidase-staining-kit/9860

The stained cells were imaged using a microscope (Nikon Eclipse TS2). Plates were then stored at 4°C by removing the staining solution and replacing with 70% glycerol.

6.3 Live/Dead Assay

Following 7 days of differentiation, BMDMs were harvested and the growth media was replaced with fresh DMEM complete containing 20ng/ml of purified typhoid toxin. The cells were then incubated for a further 6 days at 37°C, 5% CO_2.
A positive control for cell death was created by added 70% ethanol to live cells and incubating at room temperature for 5 mins. 5ul of both the Calcein, AM (component A) and the SYTOX™ Deep Red Nucleic Acid Stain (component B) from the LIVE/DEAD™ Viability/Cytotoxicity Kit, for mammalian cells (Invitrogen, #L3224) was added to 10ml of growth media with 500ul added to each well. The plates were shielded from light and immediately imaged on a Nikon Widefield Live Cell System microscope.

6.4 Immunofluorescence (IF)

To fix cells, coverslips covered in adherent cells were washed in the plate x2 with sterile PBS then 4% PFA was added to each well for 10 mins. Cells were again washed x2 with sterile PBS then stored with ~500µl PBS in each well.

If required, EdU staining was carried out using the Click-iT™ EdU Cell Proliferation Kit for Imaging, Alexa Fluor™ 647 dye (Invitrogen #10340). Staining was carried out according to the manufacturer's protocol –

https://www.thermofisher.com/uk/en/home/references/protocols/cell-and-tissue-analysis/protocols/click-it-edu-imaging-protocol.html

To stain for proteins of interest, coverslips were removed from the plate and placed face down on 50µl of blocking solution (3% BSA, 0.2% triton Tx100 in PBS) at room temperature for 1 hour. Coverslips were briefly washed in PBS before being placed face down on 50µl of primary antibody in PBS (antibodies and dilutions **table 2.4**) and left for 1 hour. Coverslips were this time washed in PBS + 0.2% triton Tx100 and placed face down on 50µl of secondary antibody (antibodies and dilutions **table 2.4**) and incubated in the dark for 30 mins. After washing in PBS 0.2% triton Tx100, coverslips were placed face up and allowed to dry whilst in the dark. Once dry the coverslips were placed face down on a microscope slide with 5µl Vectashield antifade mounting medium with DAPI (Vector Labs #H-1200-10). Coverslips were then sealed with nail varnish and then imaged on a Nikon Widefield Live-cell System microscope.

Primary antibody	Species	Manufacturer	Product code	Dilution
AIM2	Mouse monoclonal	Abcam	ab204995	1:500
ISG15	Rabbit polyclonal	Protein tech	15981-1-AP	1:50
p53	Mouse monoclonal	Santa Cruz Biotechnology	sc-126	1:50
pRb	Mouse monoclonal	Cell Signalling Technology	9309	1:2000
PUMA	Rabbit monoclonal	Cell Signalling Technology	24633	1:800
STAT1	Rabbit monoclonal	Cell Signalling Technology	7649	1:50
SUMO-1	Rabbit polyclonal	Cell Signalling Technology	4930	1:400
γH_2AX	Mouse monoclonal	Merck Millipore	05-636	1:1000
LAMP1	Mouse monoclonal	Santa Cruz Biotechnology	sc-17768	1:500
Secondary antibody				
488 Goat anti-rabbit		Thermo Fisher Scientific	A11008	1:10 000
594 Donkey anti-mouse		Thermo Fisher Scientific	A21203	1:10 000

Table 6.2 **List of Primary and Secondary Antibodies used in Immunofluorescence.**

6.5 Protein Gels

6.5.1 Preparation of Whole Cell Lysates

Cells were seeded in a 6-well plate at density that would reach 70-80% confluency after 48hrs and treated with IFNα, TxWT or TxHQ as appropriate. The cells were then harvested by trypsinisation and transferred into 2ml tubes. The cells were centrifuged at 5000 rpm for 1 min and resuspended in 1ml of sterile PBS. To calculate the volume of SDS-Urea (50mM Tris pH 6.8, 8M urea, 2% SDS, 0.3% bromophenol blue)/ 1% β-mercaptoethanol (Merck #805740) the following equation was used:

Vol of SDS Urea (µl) = OD_{600} x 250 x vol of cells in suspension

The cells were centrifuged as before, the PBS removed and the calculated volume of sample buffered added. The samples were briefly vortexed and placed onto a heat block at 95°C for 5 mins. Samples were stored at room temperature until running on an SDS-page gel.

6.5.2 SDS-PAGE

Gels were cast using the Biorad Mini PROTEAN Tetra Cell Casting Stand Clamps (Biorad #1658050). The gel's comprised of a resolving gel that allows separation of the proteins and a stacking gel on top containing the samples in loaded wells. To polymerise the stacking gel, TEMED (N, N, NN- Tetramethylethylenedi) (Sigma Aldrich #T9281) and APS (ammonium persulphate) (Melford #A1512) was added.

37:5:1 Acrylamide/Bis Solution (40%) (Biorad #16101148)	7.5ml
2.5M Bis-Tris pH6.5	3.6ml
20% SDS	150µl
MQ H_2O	13.8ml

Table 6.3 **12% Resolving gel for Immunoblotting (25ml).** Once pipetted into the gel chamber, isopropanol was added to remove air bubbles and ensure an even level to add the stacking gel on top.

29:1 Acrylamide/Bis Solution (30%) (Biorad #1610156)	996µl
2.5M Bis-Tris pH6.5	86µl
20% SDS	3µl
MQ H_2O	4.11ml
TEMED	6µl
APS	30µl

Table 6.4 **5% Stacking gel for Immunoblotting (6ml).** Approximately 1.5ml was used per gel. The stacking gel mixture after the resolving gel has fully polymerised and the isopropanol has been removed.

Approximately 9ml of resolving gel was pipetted in between glass plates in the casting chamber and isopropanol was added to remove bubbles and ensure the top of the gel was level, then allowed to set. Once the gel had fully set the isopropanol was removed and the stacking gel pipetted on top. A 10-well or 15-well comb was added before polymerisation. Gels were stored in a humidified container until use. To run the gel the samples were briefly heated on a heat block and then loaded into the well in the gel using Fisherbrand™ Gel-loading Tips (Fisher Scientific #11937734). The gel was then run in MOPS buffer at 40mA/gel, 200V for approximately 90 mins.

6.5.3 Immunoblotting

Prior to transfer, Immun-Blot PVDF membranes (Biorad #1620174) were activated by briefly placing into methanol. The membrane was then placed on top of the protein gel and sandwiched between stacks of filter paper before being run on a Trans-blot® Turbo™ Transfer System (Biorad #1704150EDU). Protein transfer was conducted as per the manufacturer's instructions and using the recommended settings.

The membranes were then blocked using 5% non-fat milk in TBS for 1hr with agitation before washing x3 with TBS/0.1% tween (TBS-TW) for 5 mins. The primary antibody **(Table 2.7)** was added at the manufacturer's recommended dilution and left overnight on a rolling mixer at room temperature. The next day the membrane was

washed x3 with TBS-TW before addition of the secondary antibody at 1:10000 in TBS-TW for 30mins on a rolling mixer. The membrane was then washed at least x3 with TBS-TW for 5mins each before imaging on an Odyssey SA Li-Cor scanner. Image processing was conducted using ImageLiteStudio v5.2.5.

Primary antibody	Species	Manufacturer	Product code	Dilution
AIM2	Mouse monoclonal	Abcam	ab204995	1:500
AKT	Mouse monoclonal	Cell Signalling Technology	2920	1:2000
p-AKT	Rabbit polyclonal	Cell Signalling Technology	9275	1:1000
BAX	Rabbit monoclonal	Cell Signalling Technology	5023	1:1000
GAPDH	Rabbit monoclonal	Cell Signalling Technology	2118	1:1000
IFIT1	Rabbit polyclonal	Invitrogen	PA3-848	1:2000
ISG15	Rabbit polyclonal	Cell Signalling Technology	2743	1:1000
MAVS	Rabbit polyclonal	Cell Signalling Technology	3993	1:1000
p-pRb	Mouse monoclonal	Cell Signalling Technology	9309	1:2000

USP18	Rabbit monoclonal	Cell Signalling Technology	4813	1:1000
Tubulin	Mouse monoclonal	Abcam	Ab7291	1:5000
γH2AX	Rabbit polyclonal	Novusbio	NB100-384	1:10000
Secondary antibody				
680RD Donkey anti-rabbit	Rabbit polyclonal	Thermo Fisher Scientific	12-4739-81	1:20000
800CW Donkey anti-mouse	Donkey polyclonal	LICOR Bio	926-32212	1:20000

Table 6.5 **Primary and Secondary Antibodies used for Immunoblotting.**

6.6 Flow Cytometry of Apotracker-labelled cells

Cells were seeded at $2x10^4$ overnight in a 24-well plate in DMEM Glutamax complete. The next day the cells were intoxicated using the standard intoxication protocol and incubated at 37°C, 5% CO_2. 4 days post-intoxication cells were harvested by trypsinisation, transferred into a 1.5ml tube and then washed 2x by centrifuging at 1500 rcf for 1 min, removing the supernatant and reconstituting with sterile PBS. On the final wash, 1 ml of PBS was added to the cells and then 2.5µl of Apotracker™ (#427403, Biolegend). The tubes were mixed by briefly vortexing and then allowed to incubate at room temperature for 10 mins. Flow cytometry analysis

was carried out using an Attune™ NxT Acoustic Focusing Cytometer. Data were analysed and figures generated using the Attune™ NxT software (V2.5).

6.7 RNA Extraction

RNA was extracted prior to RNA Seq using the RNAspin Mini Kit (Cytiva #25050071) according to the manufacturer's protocol - https://www.scientificlabs.co.uk/handlers/libraryFiles.ashx?filename=Manuals_2_25050072_A.pdf

30µl of sample was removed and the rest of the sample stored at -20°C prior to delivery to Novogene. The presence of high-quality RNA was confirmed using an Invitrogen Qubit™. Samples were prepared using the Invitrogen Qubit™ RNA IQ Assay Kit according to the manufacturer's instructions - https://assets.fishersci.com/TFS-Assets/BID/manuals/MAN0017405_Qubit_RNA_IQ_Assay_Kit_UG.pdf

A minimum quality threshold was set at an RNA IQ (or quality score) of 6. All samples sent for RNA Sequencing attained a score of 6 or above.

6.8 RNA Sequencing

After isolation, the RNA was fragmented into strands measuring 150 bp (base pairs) and converted to cDNA by Novogene. Next-generation sequencing (NGS) is carried out after the cDNA is ligated to synthetic adapters immobilised on a flow cell and amplified by PCR. A reaction mix is then added which contains primers, DNA polymerase and modified nucleotides containing a fluorophore which not only acts as a reversible terminator of DNA synthesis, but also functions as a nucleotide identifier. Cycles of incorporation are repeated until the sequence of the cDNA is determined (Bentley et al., 2003, Deshpande et al., 2023).

High quality base detection is imperative for accurate mapping to a reference genome. The likelihood that a base has been called incorrectly is called the Sequencing quality score, or Q score and is determined by the following equation:

$$Q = -10\log_{10}(e)$$

Where Q is the quality score and (e) is the error rate. A high Q score denotes a small probability of error where a low score may indicate a large portion of unusable reads or false positives (Illumina, 2024). The correlation between Q score and base call accuracy is outlined in the table below.

Quality Score	Probability of Incorrect Base Call	Inferred Base Call Accuracy
10 (Q10)	1 in 10	90%
20 (Q20)	1 in 100	99%
30 (Q30)	1 in 1000	99.9%

Table 6.6 **The Relationship between Sequencing quality score (Q Score) and accuracy of base calling.** A high-quality score indicates a higher degree of base calling accuracy. Table produced courtesy of Illumina, 2024.

Quality control (QC) was performed by Novogene using HISAT2, an in-house program developed to map NGS reads to the reference sequence. All samples scored well over 90% of bases identified attaining a Q30 score, or a base call accuracy of 99.9% (**Table 8.1**). There was relatively low variability between samples with the lowest percentage achieved being 93.33%. This meant that subsequent analysis could be carried out with confidence that the underlying base sequence was highly accurate.

Sample ID	Raw Reads	Clean Reads	Total No of bases in clean reads	Total % of bases with Q30
WT_Cont1	52182310	51735418	7.76G	94.13
WT_Cont2	44671944	44287456	6.64G	94.19
WT_Cont3	79750180	79029784	11.85G	94.59
WT_IFN1	47816940	47441586	7.12G	94.34
WT_IFN2	69217422	68699936	10.3G	94.26
WT_IFN3	45406684	45053356	6.76G	93.84
WT_TX1	45281570	44915782	6.74G	93.45
WT_TX2	49077068	48645034	7.3G	93.37
WT_Tx3	44734094	44368994	6.66G	93.87
ISG15_Cont1	45975726	45610892	6.84G	94.14
ISG15_Cont2	46089518	45703314	6.86G	93.53
ISG15_Cont3	45765454	45372588	6.81G	93.43
ISG15_IFN1	45129962	44748604	6.71G	93.68
ISG15_IFN2	48883694	48414900	7.26G	93.33
ISG15_IFN3	72005988	71252840	10.69G	93.82
ISG15_TX1	43363348	43013950	6.45G	94.24
ISG15_TX2	79880888	79286188	11.89G	94.36
ISG15_Tx3	41140574	40789738	6.12G	93.66

Table 6.7 **Summary of filtered reads and the quality score for each sample.** The table summarises the number of clean reads for each sample and the total number of bases within these reads. The percentage of bases scoring within Q30 – the highest degree of base call accuracy is also shown. Sample ID refers to A549^{WT} or A549I$^{SG15-/-}$ treated with TxWT (TX), IFNα (IFN) or untreated (CONT). 1,2 or 3 refers to the replicate number.

6.9 Statistical and Data Analysis

Unless stated, all data analyses were performed using GraphPad Prism (version 10.2.3). Significance was defined as $P \leq 0.05$ when compared to an untreated control. Where it was possible, analyses are representative of 3 independent experiments each containing 3 technical replicates. Experiments containing fewer experiments or replicates have been denoted accordingly. The absorbance readings from the three technical replicates were averaged and the relative absorbance calculated as a percentage of the untreated control. This value was used to determine statistical significance by two-way ANOVA.

Part 3: Results

Chapter 7: Host Responses to Purified Typhoid Toxin and IFNα

7.1 Introduction

The typhoid toxin produced by *Salmonella* Typhi is an important virulence factor associated with *Salmonella* pathogenesis and the establishment of typhoid infection (Thakur et al. 2022). Although *in vivo* the toxin is only produced once the bacteria are intracellular within SCVs, mice injected with purified typhoid toxin have been shown to develop typhoid-like symptoms and fatality (Song et al. 2014). The typhoid toxin has demonstrated DNase activity through its catalytic H160 residue in the CdtB subunit, resulting in activation of the DDR and cell death via apoptosis when DNA damage is severe (Frisan, 2015). The initial aim of this project was to investigate the effects of the typhoid toxin on primary immune cells and cultured fibroblast cell populations.

7.2 Purification and Testing of the Typhoid Toxin

Two models are currently employed in our laboratory to investigate the activity of the typhoid toxin in cultured cells: (i) incubate cells with purified HIS-tagged recombinant typhoid toxin, or (ii) infect cells with toxigenic *Salmonella enterica* serovars Javiana or Typhi. To directly test the activity of the typhoid toxin and uncouple from additional virulence factors encoded by *Salmonella,* I first opted to investigate host responses using purified typhoid toxin.

The T7 vector encoding pETDuet1-pltB-HIS/pltA-MYC/cdtB-FLAG was transformed into chemically competent *E.coli* BL21 to purify wild-type typhoid toxin (Tx-WT).

Transformed colonies were used to express HIS-tagged typhoid toxin following addition of Isopropyl β-D-1- thiogalactopyranoside (IPTG). HIS-tagged PltB in the typhoid toxin was used to harvest covalently bound subunits PltA-MYC and CdtB-FLAG from lysed *E.coli* by NiNTA affinity chromatography as previously reported (Ibler et al 2019, ElGhazaly et al 2023) **(Fig 3.1).**

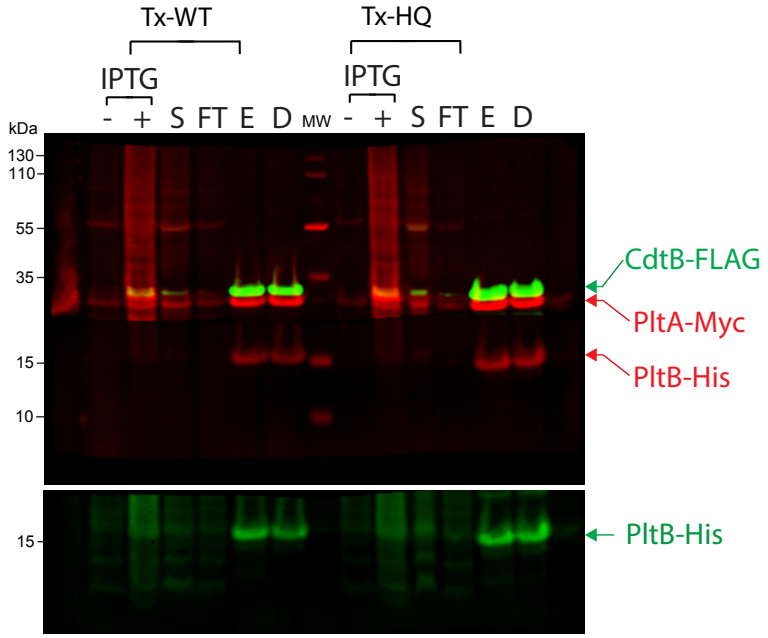

Fig 7.1 **Immunoblot of Purified Typhoid Toxin.** 3L of BL21 *E.coli* encoding TxWT (pET-Duet1-pltB-His-pltA-Myc/cdtB-FLAG) or the DNase mutant TxHQ (pET-Duet1-pltB-His-pltA-Myc/cdtB-H160Q-FLAG) were expressed to an OD of 1.0 before addition of IPTG (-/+) before incubation overnight at 30C. The bacteria were lysed using a cell disruptor and the soluble (S) fraction harvested by centrifugation (60,000 RCF, 1h). The soluble fraction was incubation with 1.5ml of NiNTA agarose before immobilising the beads on an affinity chromatography column and collecting the flow through (FT). The toxin was eluted (E) using buffer containing 200mM imidazole before dialysation in TBS (D) and storage at -80C. The collected fractions were immunoblotted with antibodies to HIS (PltB-HIS), Myc (PltB-Myc) and FLAG (CdtB-FLAG). Green colour signifies primary antibodies raised in mice while red indicates rabbit. MW indicates molecular weight as indicated in kDa left. Immunoblot and purification performed by Dr. Daniel Humphreys.

Before further experimentation it was important to investigate whether the purified typhoid toxin performed in line with previous results produced by the lab in a dependable manner (Ibler et al 2019). To achieve this wild type HT1080 fibroblast cells were intoxicated by continuous incubation with 10ng/ml purified typhoid toxin (Tx-WT) and a control toxin containing a H160Q mutation in CdtB (Tx-HQ) – henceforth referred to as the standard intoxication protocol **(Methods 5.4)**. The H160Q mutation in CdtB prevents DNAse activity (Ibler et al 2019) while also providing a control for the presence of PAMPs (e.g. LPS) present from the purification process of TxWT and TxHQ from *E.coli* **(Fig 7.1)**. HT1080 intoxication

experiments were performed alongside controls: (i) topoisomerase inhibitor etoposide (ETP), which induces double strand breaks preventing cell cycle progression and causes cell death (Karpinich et al, 2002), and (ii) purified interferon 2 alpha (IFNα) to mimic PAMP-mediated activation of the interferon pathway. The doubling time of HT1080s is 26-30hrs therefore cell cycle arrest was assayed at 48h to observe effects of typhoid toxin. Also, if cell cycle arrest is prolonged beyond 7 days, then this can be indicative of senescence (Ibler et al 2019), and thus, the effects of the typhoid toxin were also assayed at 7 days to identify pronounced senescence-like effects.

To determine the activity of the typhoid toxin, the MTT assay was employed to measure cellular metabolism of MTT per well. The MTT reagent is a mono-tetrazolium salt (3-(4,5-dimethylthiazol-2-yl)-2,5-diphenyl-2H-tetrazolium bromide) and due to its positive charge and lipophilic nature, is able to pass through the cellular membrane as well as the mitochondrial inner membrane of viable cells. Metabolically active cells are able to break this compound down to a violet-blue and water-insoluble product called formazan (Ghasemi et al., 2021). Higher levels of MTT metabolism, typically indicative of increased number of cells, directly correlate to increased formation of formazan and therefore greater intensity of colour. This became a standard assay used in this project.

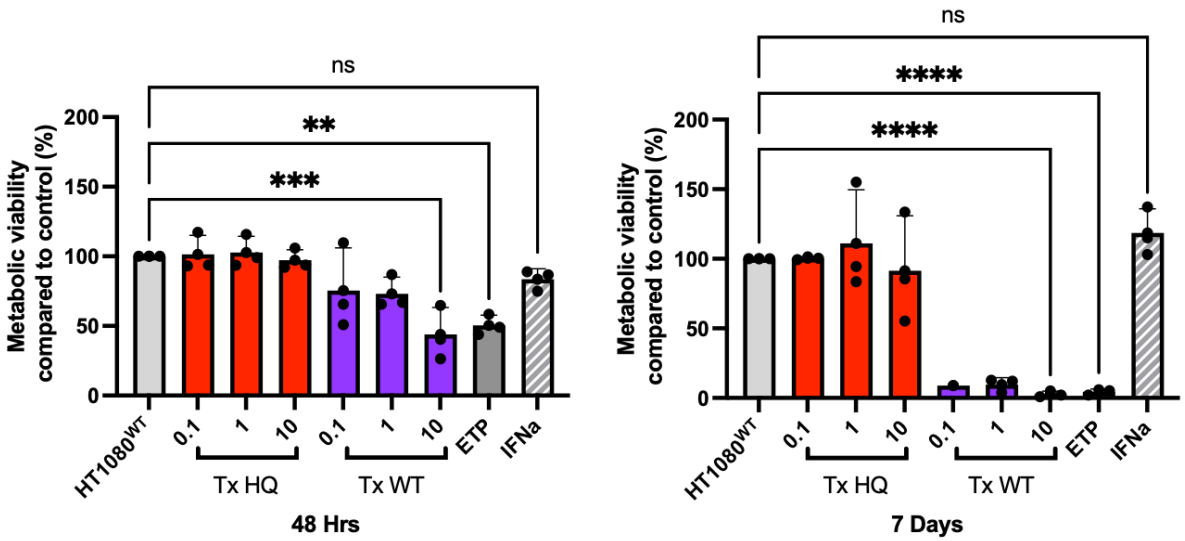

Fig 7.2 **MTT Assay of Intoxicated HT1080 Cells.** Cells were treated with either the wild type (TxWT) or the control toxin (TxHQ) at 0.1, 1 or 10ng/ml with an absorbance reading taken at 48hrs or 7 days. Etoposide (3µm) was used as a positive control for cell death and IFNα (0.1µg/ml) was used to trigger an immune response. Each circle represents one biological replicate consisting of three technical replicates. An average of the absorbances within each biological replicate was taken. The relative absorbance compared to the untreated control was calculated with the control representing 100%. The bars indicate the mean and the error bars indicate standard deviation (SD). Statistical significance was calculated using a two-way ANOVA with asterisks denoting significance. (n=4)

At 48h, HT1080 cells treated with TxHQ exhibited equivalent MTT metabolism to the untreated controls **(Fig 7.2**). However, MTT metabolism was reduced to ~75% by relatively low concentrations of TxWT (0.1ng/ml, 1ng/ml) and was further reduced to ~50% by higher concentrations of TxWT (10ng/ml). By 7 days, MTT metabolism had been reduced to ~5% with all concentrations of TxWT while TxHQ was equivalent to control. TxWT matched the HT1080 cell responses to ETP indicating DDRs while activating innate immune responses with IFNα had no effect. Thus, the typhoid toxin reduces MTT metabolism in HT1080 cells in a manner dependent on nuclease activity. This was likely due to senescence caused by toxin nuclease activity rather than apoptosis as typhoid toxin did not activate caspase 3-mediated apoptosis in HT1080 cells (Ibler et al 2019).

7.3 The Typhoid Toxin Impairs Early-Stage Differentiation of Monocytes

Purified typhoid toxin has been shown to reduce the number of monocytes in a mouse model (Song et al 2013). Upon infection, monocytes are rapidly differentiated into IFN-producing dendritic cells and macrophages. During the initial stages of differentiation, the monocytes undergo a cascade of biochemical and morphological changes requiring high levels of transcription (Yang et al. 2014). This may leave the cells vulnerable to the damaging effects of the typhoid toxin. Macrophages become activated by inflammatory signals in 4 stages (Mak et al., 2005). Once inflammation occurs a signal is sent to a resting macrophage causing it to become responsive. Low levels of cytokines (particularly IFN-y) trigger the second stage causing the macrophage to change from responsive to activated. Most of the functions associated with macrophages are activated at this stage, accompanied by morphological and biochemical changes. Thus, I investigated the effects of TxWT in mouse bone marrow-derived macrophages.

Bone marrow was harvested from murine femur and tibia bones with the monocyte population then separated. Differentiation into macrophages was induced using conditioned L929 fibroblast media and incubated in DMEM complete for 7 days **(Methods 5.4**). Post-differentiation, macrophage cells were treated with 20ng/ml purified typhoid toxin (TxWT) and the Live/Dead™ Viability/Cytotoxicity assay used to determine if the addition of the purified toxin led to cell death on day 6 of intoxication **(Fig 7.3)**. The Live/Dead assay utilises two stains: calcein-AM (yellow) is metabolised by live cells while the ethidium homodimer-1 (magenta) can only penetrate and stain DNA in dead cells. If cells encounters high levels of IFN-y along with a bacterial toxin, such as the typhoid toxin, the macrophage becomes hyperactivated leading to enhanced antimicrobial fighting abilities. Once activated, macrophages release over 100 secretory products (Mak & Saunders, 2006) however the same mechanisms that allow the release of these secretions also allow the Live/Dead stains to enter the cell. The result is calcein-AM staining in the cytoplasm

and ethidium homodimer-1 staining of the nucleus. A positive control for cell death was created by treating cells with 70% ethanol for 5 mins just prior to conducting the assay.

As expected, the untreated control showed no cell death as fields of view were dominated by living cells (**Fig 7.3:** live control). In contrast, ethanol treatment successfully killed all cells (**Fig 7.3:** dead control). Interestingly, treatment with TxWT showed predominantly live cells in yellow with cells also containing a mixture of both the live and the dead stains in the same cell (**Fig 7.3:** TxWT). This was determined not to be cell death as there was no noticeable reduction in cell number, even after 6 days of intoxication. Thus, the data indicates the typhoid toxin does not kill macrophages but does promote cell permeability to ethidium homodimer-1.

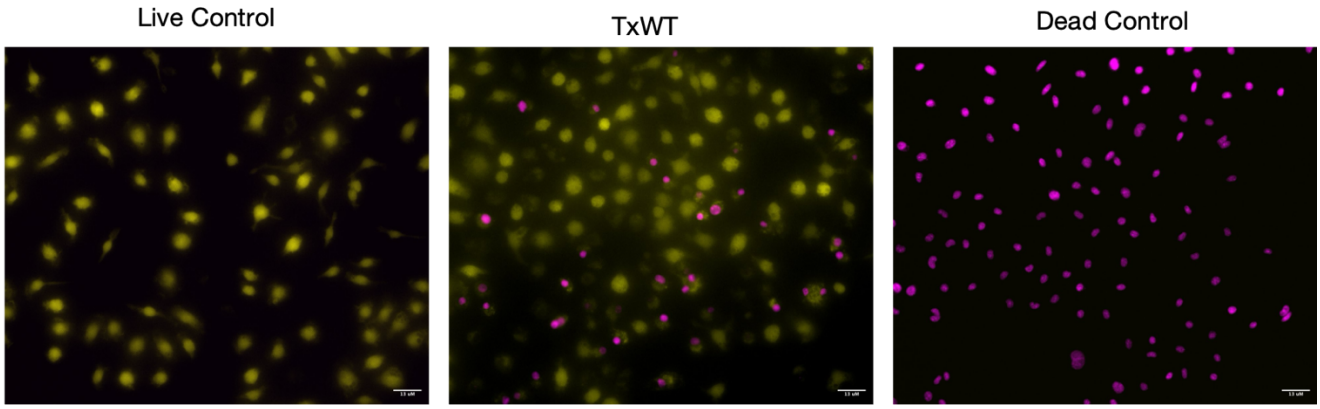

Fig 7.3 **Hyperactivation of Bone-Marrow Derived Macrophages.** Fluorescence images of the Live/Dead™ assay. Differentiated BMDMs were either untreated (live control) or treated with purified toxin (20ng/ml) for 6 days. BMDMs treated with 70% ethanol for 5mins at room temp was used as a positive control for cell death. The Live/Dead stains were added to the cells and immediately imaged on a Nikon Widefield Live Cell System microscope at x20 magnification, scale bar = 13uM. Live cells are shown above in yellow, dead cells are shown in magenta and hyperactivated macrophages show both yellow and magenta staining. (n=3)

Typhoid toxin was shown to cause replication stress on host cells with only modest damage observed in non-replicating cells (Ibler et al 2019), which could explain the lack of cell death in **Fig 7.3**. Using BMDMs also offered a chance to investigate the effects of the typhoid toxin on monocyte differentiation. Differentiation was initiated by treating freshly harvested monocytes with L929 media for 7 days. At the same time the cells were treated with either 0.1ng/ml typhoid toxin or the control TxHQ. After optimisation it was found that the effects of the toxin could be observed even at

low concentrations. By intoxicating the monocytes at 0.1ng/ml it ensured that the harmful effects of the typhoid could be realised whilst not risking complete destruction of the cells. The intoxicated cells were left to incubate at 37^{o}C, 5% CO_2 for 72 hrs then imaged. Mature macrophages (7 days post differentiation) were treated in the same way.

It was found that neither the typhoid toxin nor the control toxin caused any significant morphological changes in macrophages or loss of cell number 7 days post differentiation **(Fig 7.4A)**. However, the typhoid toxin inhibited monocyte differentiation into macrophages, most likely via apoptosis as marked by an increase in cell debris visible at the end of the intoxication period. The control toxin TxHQ had little effect on either cell type. Thus, typhoid toxin prevents monocytes from differentiating into macrophages, seemingly through cell death.

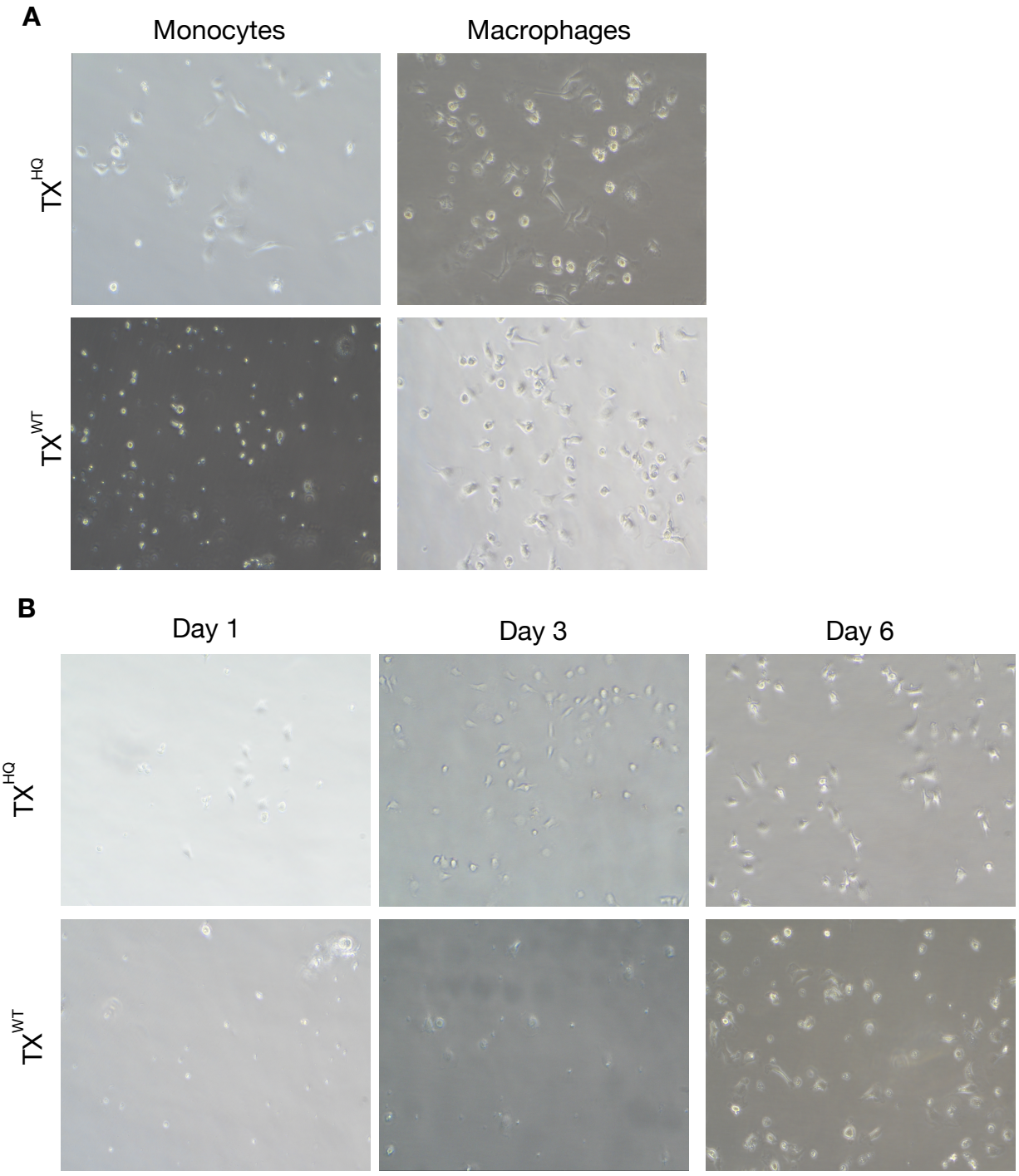

Fig 7.4 **intoxication of Differentiating Monocytes and Mature Macrophages. (A)** Freshly harvested monocytes or mature macrophages were intoxicated with either the purified toxin (TxWT) or the control toxin (TxHQ) (both 0.1ng/ml). Images were taken after 72hrs intoxication on a Nikon Eclipse TS microscope. **(B)** Monocytes were intoxicated with either purified typhoid toxin or the control toxin (both 10ng/ml) at days 1, 3 or 6 of differentiation. Images were taken after 72hrs on a Nikon Eclipse TS microscope. (n=3)

Next, to determine at which point in the differentiation process does the typhoid toxin act on monocytes the same protocol was used as before, however this time monocytes were intoxicated on days 1, 3 or 6 of the 7-day differentiation protocol

and imaged after 72 hrs. The concentrations of both toxins were increased from 0.1ng/ml to 10ng/ml to maximise any damaging effects. It was determined that differentiation of monocytes intoxicated on day 1 was greatly impacted in comparison to the control TxHQ **(Fig 7.4B)**. For monocytes intoxicated on day 3 there is still a significant effect, however there a small number of fully formed adherent macrophages are visible; although this number is far fewer than with the control toxin. Finally, as could reasonably be predicted, there was little observable change in the monocytes intoxicated on day 6 of differentiation. By this point the process is near completion and therefore gives a similar result to intoxication of mature macrophages in **Fig 7.4A**.

From these experiments it can be concluded that the effects of the typhoid toxin are greatest during early differentiation (days 1-3). This suggests that the high plasticity of monocytes that allows a rapid innate immune response to environmental stimuli may also provide an opportunity for typhoid toxin to cause DNA damage and inhibit this response. In summary, the findings are consistent with observations showing that monocyte numbers are reduced in a mouse model (Song et al 2013), and that this is likely due to toxin-mediated cell death in monocytes rather than macrophages.

7.4 The Typhoid Toxin Stimulates ISG15 Expression and Triggers the Interferon Response

It was decided to build from experiments in **Fig 3.2**, which show HT1080 fibroblast cells are susceptible to typhoid toxin. To examine HT1080 responses to the typhoid toxin in more detail, Dr. Angela Ibler in the Humphreys laboratory performed whole genome GenChip microarray analysis on HT1080 cells intoxicated for 48h with TxWT or TxHQ (ElGhazaly et al 2023). The data is publicly available at ArrayExpress (E-MTAB-12333), which enabled me to investigate transcriptional changes by the typhoid toxin in more detail. Pathway analysis using GSEA showed that one of the top upregulated pathways was the ‘response to type 1 interferon’ **(Fig 7.5A).**

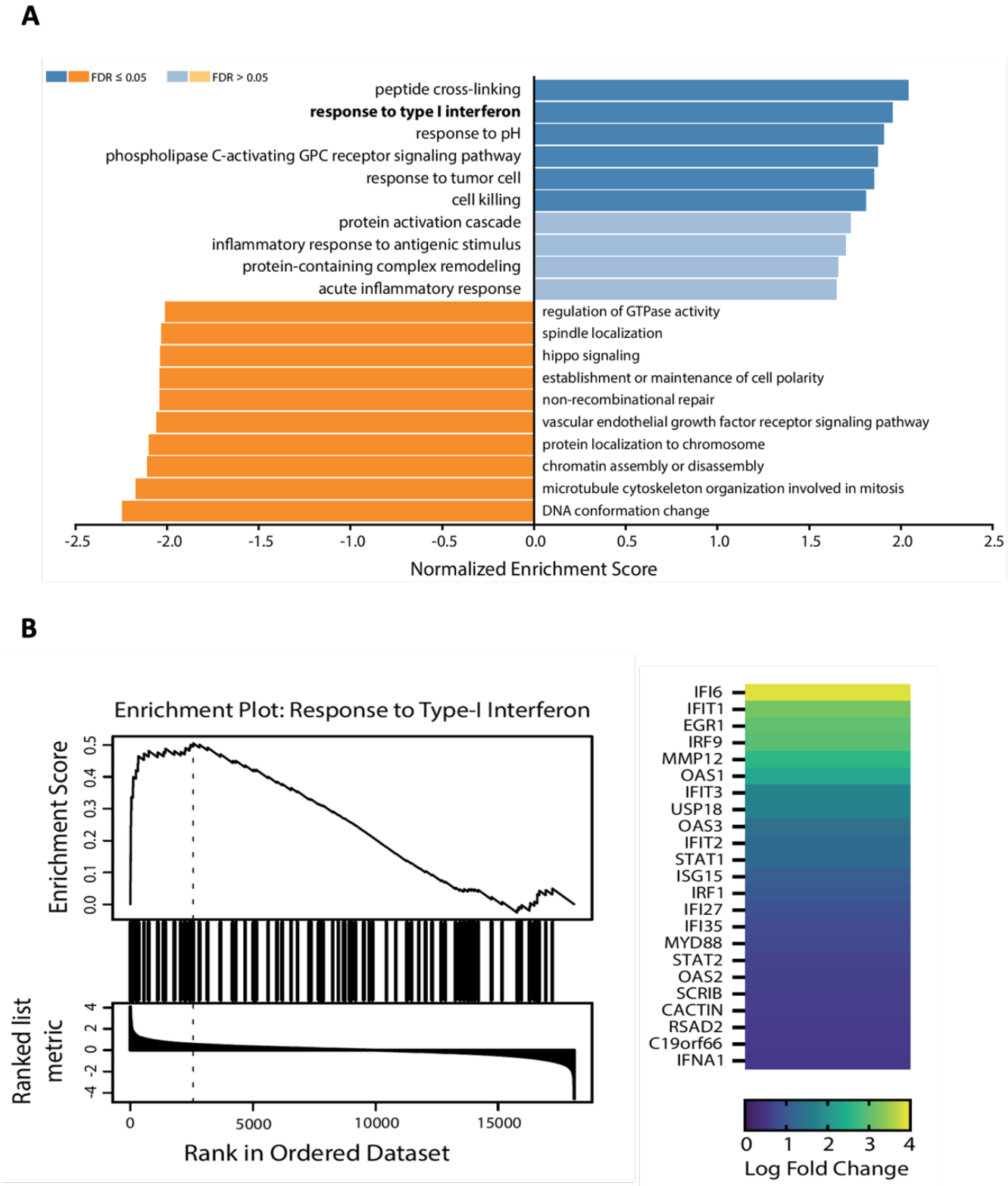

Fig 7.5 **Microarray Data from Intoxicated HT1080 Cells.** (A) Pathways that are upregulated (blue) or downregulated (orange) when comparing enrichment scores between cells intoxicate with the typhoid toxin compared to the control toxin. (B) The enrichment plot reflects the extent to which a gene is overrepresented within the top or bottom of a ranked list of genes. The heatmap shows all the genes within this plot and represents the fold change between the two toxin treatments.

The IFN response included genes such as IFN1α, as well as interferon-stimulated genes (ISGs) such as IFIT1-3 and OAS1-3 **(Fig 7.5B)**. Upon further investigation into the genes within this pathway that are activated in response to the typhoid toxin, it was found that ISG15 and its partner protein USP18 were both upregulated **(Fig 7.5B)**. In addition to being an important regulator of the interferon response, deficiency of ISG15 has also been implicated in promoting infection: ISG15 has been shown to play a role in infections by intracellular pathogens *Listeria* (Radoshevich et al., 2015) and *Mycobacterium* (Bogunovich et al., 2012). For these reasons it was decided to further investigate the role ISG15 plays in *Salmonella enterica* infection.

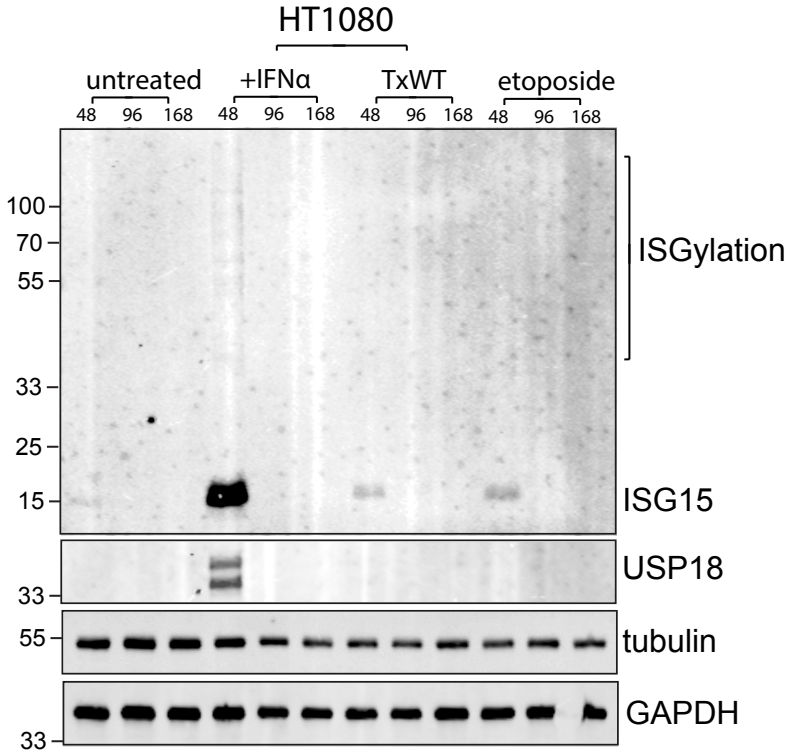

Fig 7.6 **Influences of TxWT on the ISG15 Pathway in HT1080 Cells.** Immunoblot showing expression of ISG15 and USP18 in response to TxWT (10ng/ml), IFNα (0.1μg/ml) and etoposide (3μM).

ISG15 is a ubiquitin-like protein that can be conjugated to other proteins and modify their function (Villarroya-Beltri et al., 2017, Perng et al., 2018., Mirzalieva et al., 2022) in a manner dependent upon the conjugators Ube1L (E1 protein), UbcH8 (E2)

and HERC5 (also TRIM25, ARIH1) (E3). The conjugation process is referred to as ISGylation (Zhang et al., 2021). USP18 plays a role in de-ISGylation. It was thus first examined whether increased expression of ISG15 was observed in response to typhoid toxin **(Fig 7.6)**. In untreated HT1080 cells, a faint band of ISG15 was observed at 48h but was not observed at the 96h or 168h timepoints. USP18 was not detected at any point. In contrast, treatment with either TxWT or the control ETP induced ISG15 expression at 48h with possible expression of USP18 also observed. No ISGylation was observed. As a positive control, cells were treated with IFNα, which induced robust ISG15 expression at 48h with evidence of ISGylation. USP18 was also expressed with two bands evident, which is consistent with its known ubiquitination (Basters et al., 2017). In summary, DDRs induced by TxWT trigger ISG15 expression, which confirms the microarray findings.

7.5 ISG15 Regulates the Response to the Typhoid Toxin in MEF Cells

It was clear from the immunoblot in **Fig 7.6**, that TxWT and ETP elicit similar levels of ISG15 expression indicating a role for DDRs. In addition to the interferon response, ISG15 also plays a role in stabilising p53 enabling downstream functions, which include cell-cycle arrest and apoptosis (Huang et al., 2014). To investigate the effects of ISG15 deficiency in response to intoxication, the focus switched from HT1080 cells to mouse embryonic fibroblast (MEF) cells as an $ISG15^{-/-}$ derivative was available from the laboratory of Dr. Lilliana Radoshevich. Both wild-type and $ISG15^{-/-}$ MEF cells were intoxicated using the standard intoxication protocol for 72hrs before imaging of DAPI-stained nuclei to observe DNA. Neither MEF^{WT} nor $MEF^{ISG15-/-}$ showed any noticeable effects in response to TxHQ however, MEF^{WT} cells showed clear indication that TxWT induced cell-cycle arrest, apparent by the decrease in cell number and the increase in nuclear size **(Fig 7.7)**. The same was true in $ISG15^{-/-}$ MEFs ($MEF^{ISG15-/-}$), which also underwent cell-cycle arrest in response to TxWT. However, closer inspection made the effects of ISG15 deficiency immediately clear **(Fig 7.7)**. Morphological changes could be observed such as cell distension, nuclear fragmentation and membrane “blebbing” (a key characteristic of apoptosis). Blebbing

was more pronounced in the ISG15$^{-/-}$ cells compared to the wild type MEFs (inset) and not observed in the cells treated with the control TxHQ.

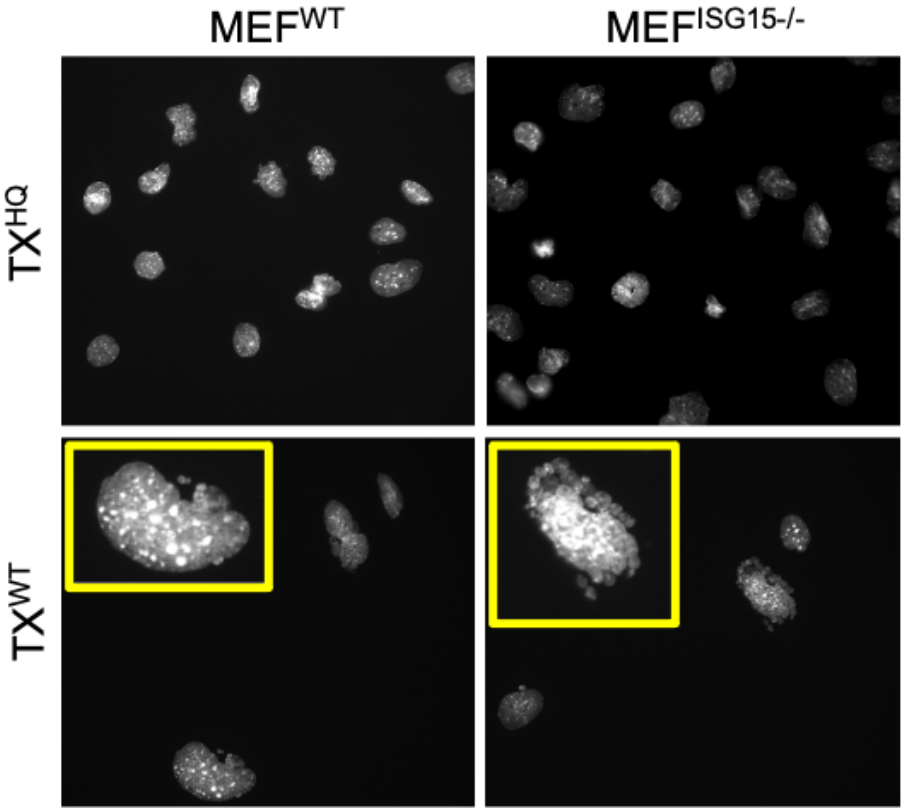

Fig 7.7 **Intoxication of Wild Type and ISG$^{-/-}$ MEF Cells.** Both cell lines were intoxicated using either purified typhoid toxin (TxWT) or the control toxin (TxHQ) (both 10ng/ml) for 72hrs. Cells were stained with DAPI and imaged at x40 magnification on a Nikon Widefield Live-Cell System microscope. During editing the images were turned to greyscale to more clearly show morphological changes in response to the typhoid toxin. The yellow inserts are zoomed in images of a single cell showing nuclear distension and fragmentation.

The morphological changes to the nuclei indicate DDRs. A master regulator of DDRs is p53, which is rapidly and continuously degraded in non-damaged cells but is stabilised by post-translational modifications during DDRs (Williams and Schumacher, 2016). Stabilised p53 translocates to the nucleus to effect downstream transcriptional responses. Thus, p53 was imaged inside intoxicated cells treated with either TxWT or TxHQ in parallel while imaging the fluorescently-labelled nucleotide analogue EdU to mark DNA synthesis and cell cycle progression (**Fig 7.8**). During optimisation, it was noted that MEF cells were sensitive to the typhoid toxin and were

killed at concentrations above 0.1ng/ml making imaging difficult. Thus, the following imaging was performed at 0.1ng/ml typhoid toxin concentrations. During this imaging it was surprising to observe that, all cellular conditions showed upregulation of p53, although arguably the most intense fluorescence could be observed in the wild type MEFs in response to the typhoid toxin. It is possible that the control TxHQ toxin is also triggering a DNA damage response due to the harmful effects of bacterial PAMPs remaining after purification. The fields of view of both wild type and ISG15 knockout cells intoxicated with the typhoid toxin show a distinct reduction in cell number when compared to TxHQ suggesting that the control toxin may elicit a DDR, but it is not able to drive cell cycle arrest or cell death to the same extent as the typhoid toxin. All the cells imaged after intoxication with the typhoid toxin were positive for EdU, which demonstrates that a small number of cells are able to survive a low concentration (0.1ng/ml) of the typhoid toxin and continue to proliferate.

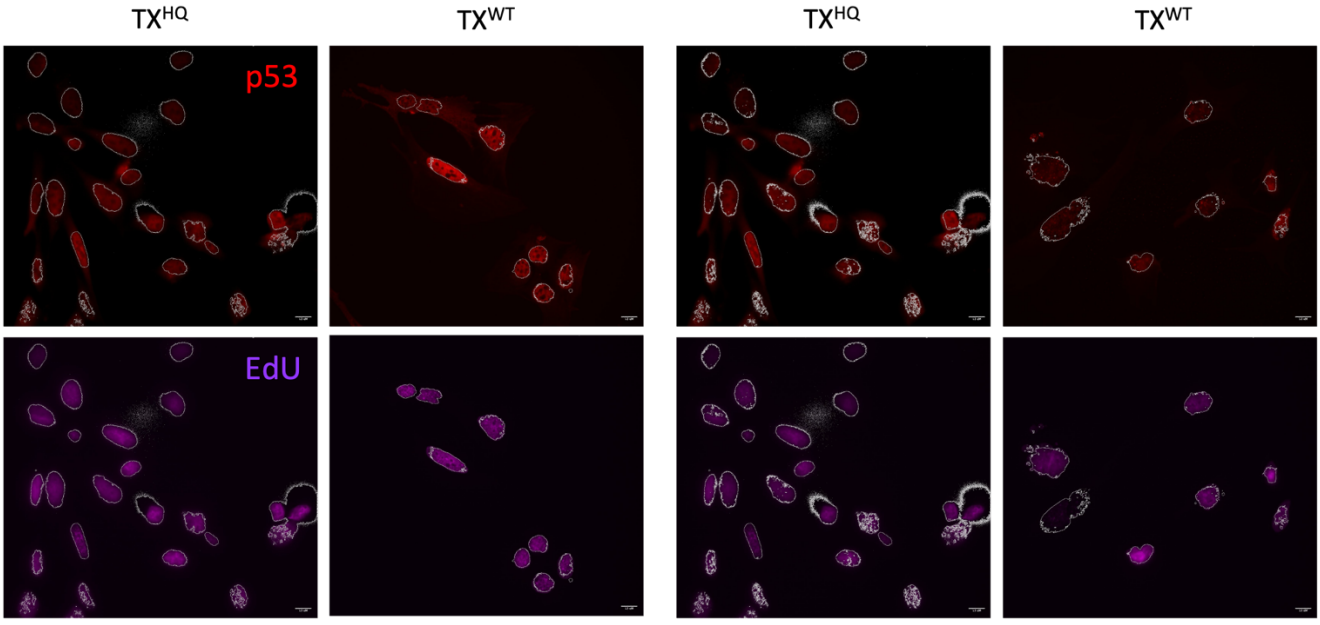

Fig 7.8 **Activation of the p53 Pathway.** Wild type and ISG15$^{-/-}$ cells were intoxicated with purified typhoid toxin (TxWT) and the control toxin (TxHQ) (both 0.1ng/ml) for 72hrs. The cells were stained for EdU and p52 before imaging on a Nikon Widefield Live Cell System microscope at x40 magnification. Nuclei is (4′,6-diamidino-2-phenylindole) DAPI stained and outlined in greyscale. Scale bar = 13uM.

Overall, the typhoid toxin appears to induce a slightly stronger p53 response in wild type MEFs compared to the ISG15 knockouts. Although the typhoid toxin is still able to drive either cell cycle arrest or cell death in ISG15 deficient cells, this result does not fully support the theory that p53 is stabilised by ISG15 in published literature.

The effects of the typhoid toxin on the p53 pathway could also be investigated by imaging PUMA (p53 upregulated modulator of apoptosis). MEF^{WT} and $MEF^{ISG15-/-}$ cell lines were intoxicated with either TxWT or TxHQ (0.1ng/ml) and labelled with anti-PUMA antibodies before imaging by fluorescence microscopy at 72h (**Fig 7.9**). In MEF^{WT}, PUMA was expressed in a small number of cells treated with TxHQ. This increased in response to TxWT. It was found that expression of PUMA is lost when cells are deficient in ISG15 regardless of whether the cells are treated with TxWT or TxHQ. This means that while loss of ISG15 results in a decrease in p53 upregulation, it almost completely knocks out expression of its downstream effector PUMA.

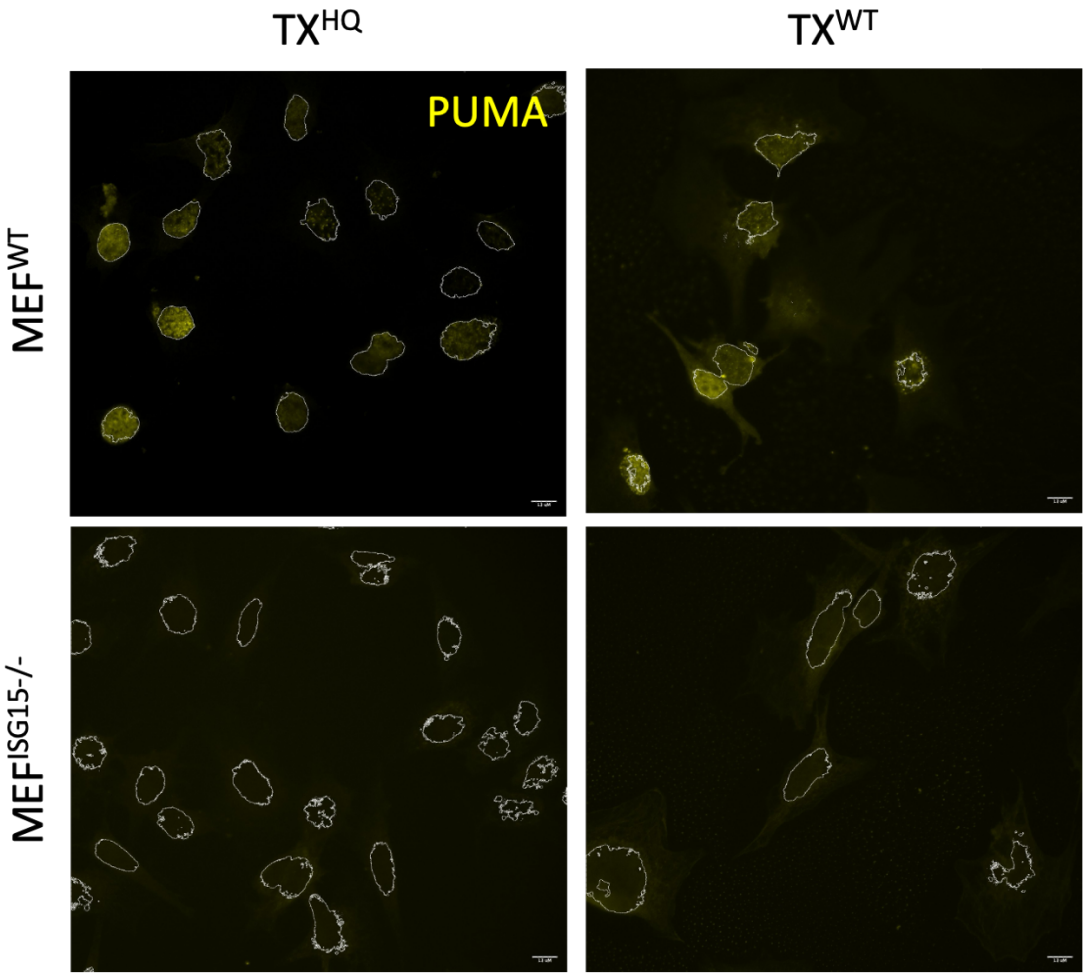

Fig 7.9 **Inducement of PUMA in Response to Intoxication in MEF Cells..** Both wild type and ISG15$^{-/-}$ cells were intoxicated with purified typhoid toxin (TxWT) and the control toxin (TxHQ) (both 0.1ng/ml) for 72hrs before staining for PUMA. Images were taken on a Nikon Widefield Live Cell System at x40 magnification. Nuclei is DAPI stained and outlined in greyscale. Scale bar = 13uM.

Finally, the DNA damage response to the typhoid toxin was assayed by looking at phosphorylation of the histone H2AX (γH2AX), which mediates DNA repair and maintains genome stability (Prabhu et al., 2024). Consequently, γH2AX is a commonly used marker for assaying DNA damage.

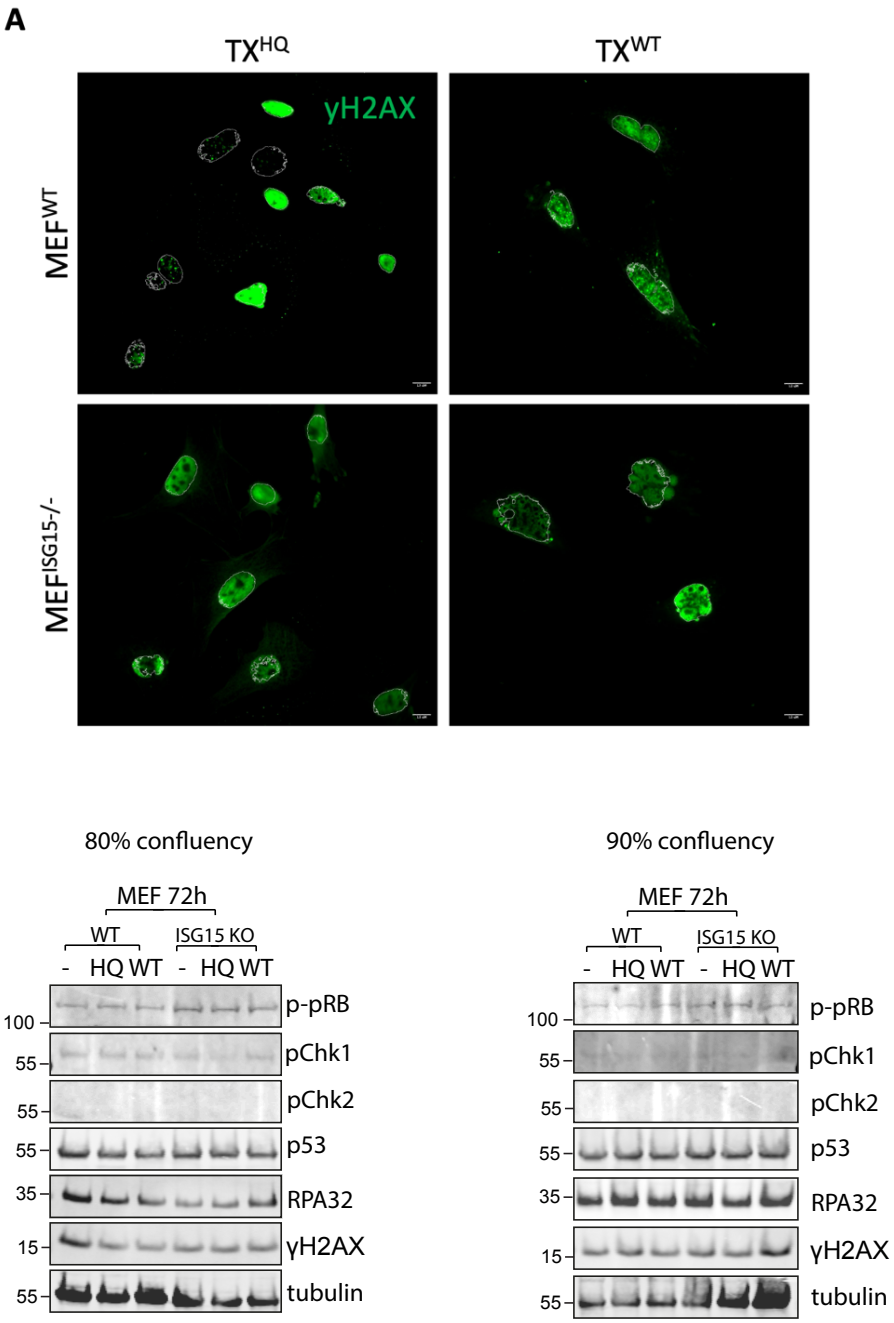

Fig 7.10 **Expression of γH2AX in Response to Intoxication.** (A**)** Both wild type and ISG15$^{-/-}$ cells were intoxicated with purified typhoid toxin (TxWT) and the control toxin (TxHQ) (both 0.1ng/ml) for 72hrs before staining for γH2AX. Images were taken on a Nikon Widefield Live Cell System at x40 magnification. Nuclei is DAPI stained and outlined in greyscale. (B) DDRs observed in untreated control and intoxicated MEFs. Both MEF^{WT} and MEFISG15-/- showed upregulation of DDR markers across all conditions. Scale bar = 13uM.

It was unexpectedly found that γH2AX production was evident across all conditions regardless of toxin or cell genotype **(Fig 7.10A)**. Although the ISG15 knockouts did show unusual staining when intoxicated with the typhoid toxin compared to the other conditions, e.g. increased blebbing indicative of cell death. To examine this further, wild-type and ISG15 -/- null MEF cells were immunoblotted following either no treatment (-), or treatment for 72h with TxHQ or TxWT (**Fig 7.10B**). In all cases, γH2AX was present at equivalent levels, as was p53, and markers of cell cycle progression (i.e. p-pRb, pChk1, and RPA32). Together, the results from **Fig 7.9** and **Fig 7.10** results may indicate either elevated γH2AX DDRs, even in control cells or no response to typhoid toxin. Equivalent responses were observed in replicating cells (80% confluency) as well as cells nearing quiescence (90% confluency). Upon further investigation, it was realised that the MEF cells had been immortalised using Simian Virus 40 (SV40), a process which has been shown to lead to stabilisation of p53 and elevated γH2AX (Cheng et al., 2009). This complicates interpretation of toxin-induced DDRs, their effects on p53-driven responses, and most importantly p53 regulation by factors such as ISG15.

7.6 Typhoid Toxin and IFNα Reduce Viability of ISG15 Deficient Cells

Given the difficulties of using the MEF cells, a decision was made to obtain an alternative ISG15 knockout cell line. Further experimentation for this project was conducted in wild type and ISG15$^{-/-}$ null A549 cells, which were provided by the laboratory of Dr. Lilliana Radoshevich. A549 is a lung epithelial cell line with a doubling time of approximately 22hrs. The ISG15$^{-/-}$ null (A549$^{ISG15-/-}$) cell line was generated through a CRISPR/Cas9 approach that deletes ISG15 expression by introducing an INDEL in exon 2 creating a missense out-of-frame ISG15 mRNA **(Methods 5.1)** thus circumventing the complications encountered with SV40-immortalised MEF cells.

In order to confirm the effects of the typhoid toxin were consistent with this new cell line, both wild type and ISG15$^{-/-}$ null cells were intoxicated with 0.1ng/ml, 1ng/ml or

10ng/ml TxWT or TxHQ before assaying MTT metabolism at 48hrs and 7 days **(Fig 7.11)**. With the typhoid toxin both the wild type and ISG15-/- null cells replicated the results previously reported in HT1080 cells (**Fig 7.2**)**.** Here, using A549 cells, TxHQ had no effect as MTT was metabolised equivalent to control at 48h in both wild-type A549 ($A549^{WT}$) and $A549^{ISG15-/-}$ cells **(Fig 7.11).** In contrast, MTT metabolism in the presence of TxWT was reduced with the most significant effect being observed with 10ng/ml TxWT that reduced MTT metabolism to ~50% of untreated. There was no difference between wild-type and ISG15-deficient A549 cells. The trend with TxWT and TxHQ was also observed at the 7-day timepoint though the effects were more significant. All concentrations of TxWT reduced MTT metabolism to ~5% of untreated while 10ng/ml of TxHQ reduced MTT metabolism relative to the untreated control. In agreement with the observations in HT1080 cells, ETP also reduced MTT metabolism in A549 cells at 48h with even greater effects observed at 7 days.

Interestingly, unlike the HT1080 cells in **Fig 7.2**, IFNα generated significant reductions in MTT metabolism in A549 cells **(Fig 7.11)**: IFNα had no effect at 48h in $A549^{WT}$ cells but by 7 days metabolism was reduced by approximately 70%. Loss of MTT metabolism was even more significant in the $A549^{ISG15-/-}$ cells with a loss of 45% metabolism at 48hrs and a complete loss by 7 days. This result suggests that prolonged exposure to IFNα has a harmful effect on cell viability, which is amplified by the loss of ISG15.

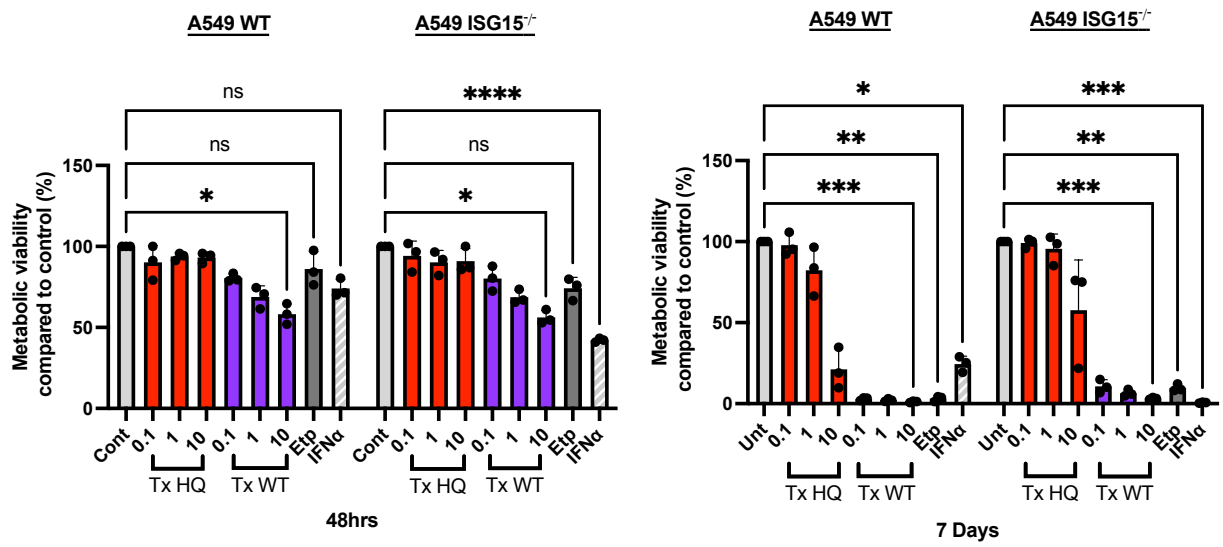

Fig 7.11 **MTT Assay of Intoxicated A549 Cells.** Wild type and ISG15$^{-/-}$ cells were intoxicated with purified typhoid toxin (TxWT) and the control toxin (TxHQ) at 0.1, 1 and 10ng/ml with an absorbance reading taken at 48hrs or 7 days. Etoposide (3µm) was used as a positive control for cell death and IFNα (0.1µg/ml) was used to trigger an immune response. Each circle represents one biological replicate consisting of three technical replicates. An average of the absorbances within each biological replicate was taken. The relative absorbance compared to the untreated control was calculated with the control representing 100%. The bars indicate the mean and the error bars indicate standard deviation (SD). Statistical significance was calculated using a two-way ANOVA with asterisks denoting significance. (n=3)

To validate this result and confirm the effects of IFNα on cell viability is not a phenotype unique to A549 cells, the assay was replicated exactly in U2OS cells, a human epithelial bone cell, using wild type (U2OS^{WT}) and ISG15-/- null (U2OS$^{ISG15-/-}$) cell lines **(Fig 7.12)**. When examining U2OS^{WT} cells at 48h, neither TxHQ, TxWT, ETP or IFNα had a marked effect. The same was true in U2OS$^{ISG15-/-}$ cells, the only difference being a reduction in MTT metabolism in response to IFNα **(Fig 7.12)**, as observed in ISG15-/- null A549 cells **(Fig 7.11).** At 7 days, there was a significant loss of MTT metabolism with the TxWT and ETP in U2OS^{WT} and U2OS$^{ISG15-/-}$ with very little difference between cell types **(Fig 7.12).** However, both cell lines appeared more resistant to any harmful effects of TxHQ, even at the highest concentration. In U2OS^{WT} IFNα had no effect of MTT metabolism even at 7 days. The U2OS$^{ISG15-/-}$ cells mirrored the phenotype shown by the A549$^{ISG15-/-}$ cells with IFNα driving loss of metabolism at 48hrs and a complete loss by 7 days. This suggests that while the

effects of IFNα on wild type cell populations may be determined by cell type, ISG15 is vital for maintaining cell viability in the presence of IFNα.

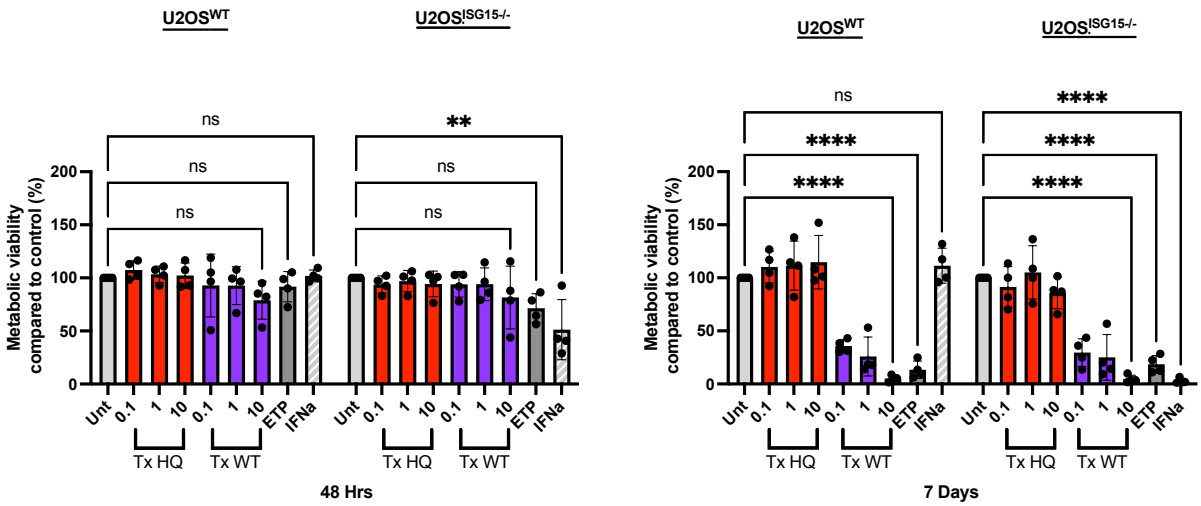

Fig 7.12 **MTT of Intoxicated U2OS cells.** Wild type and ISG15$^{-/-}$ cells were intoxicated with purified typhoid toxin (TxWT) and the control toxin (TxHQ) at 0.1, 1 and 10ng/ml with an absorbance reading taken at 48hrs or 7 days. Etoposide (3μm) was used as a positive control for cell death and IFNα (0.1μg/ml) was used to trigger an immune response. Each circle represents one biological replicate consisting of three technical replicates. An average of the absorbances within each biological replicate was taken. The relative absorbance compared to the untreated control was calculated with the control representing 100%. The bars indicate the mean and the error bars indicate standard deviation (SD). Statistical significance was calculated using a two-way ANOVA with asterisks denoting significance. (n=3)

Chapter 8: The Effects of ISG15 Deficiency on Cell Survival

8.1 Introduction

Typhoid toxin induces IFN-like responses in HT1080 fibroblast cells, which includes increased expression of interferon-α1, ISG15 and USP18. Investigation in ISG15-deficient A549 cells underwent cell cycle arrest in response to the toxin equivalently to wild-type A549 cells. However, the ISG15-deficient A549 cells had increased sensitivity to IFNα, which caused cell death in both ISG15-deficient A549 and U2SO cells. ISG15-deficiency has been implicated in increased susceptibility during infection by intracellular pathogens such as *Listeria* and *Mycobacteria* (Bogunovich et al., 2012, Radoshevich et al., 2015). Thus, in this next chapter, IFNα responses in ISG15-deficient cells are investigated in more detail.

8.2 Preparing ISG15 knockout A549 for Transcriptomics

It was decided that the loss of MTT metabolism displayed by the A549$^{ISG15-/-}$ cells in response to IFNα warranted further exploration.

First, the expression of ISG15 was examined in untreated and IFNα-treated A549 cells by immunofluorescence (**Fig 8.1**). In parental A549^{WT} cells, ISG15 was observed in untreated cells but ISG15 was dramatically increased following 96h treatment with IFNα. ISG15 was also examined in A549 cells where endogenous USP18 has been replaced with an isopeptidase dead mutant USP18$^{C61A/C61A}$, which leads to enhanced ISGylation and resistance to viral infection (Ketscher et al., 2015). ISG15 expression was observed equivalently in A549^{USP18} cells to A549^{WT} cells. In contrast, ISG15 was not observed in untreated or IFNα-treated A549$^{ISG15-/-}$ cells, which confirms the loss of ISG15.

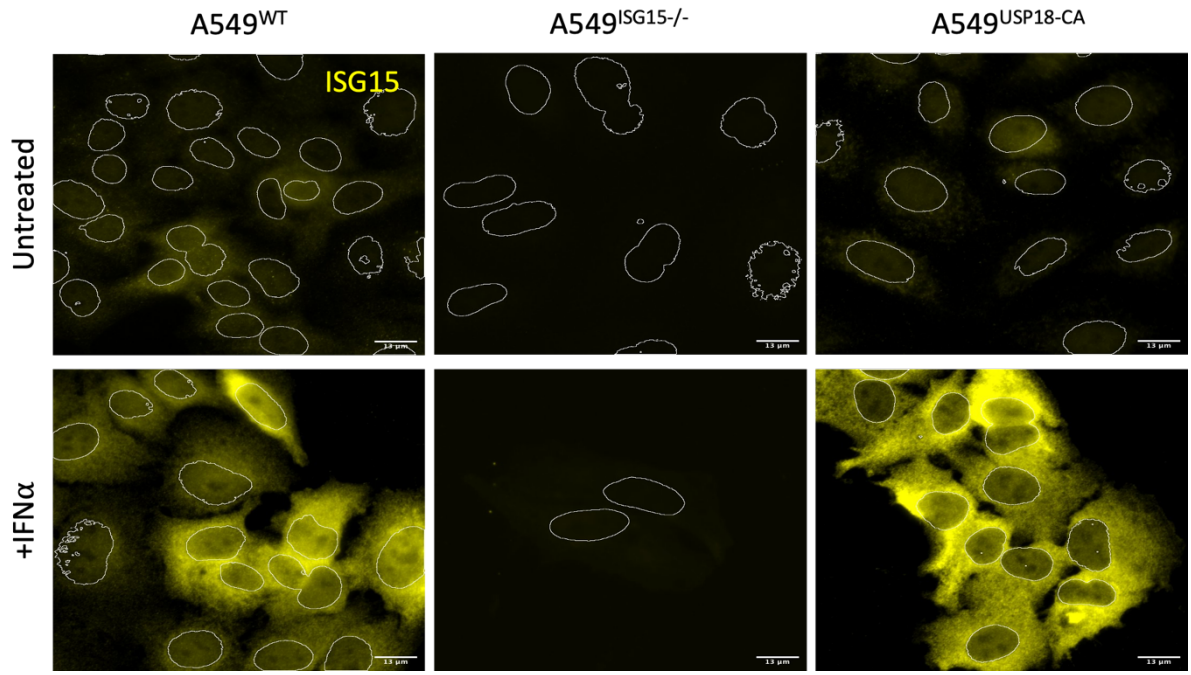

Fig 8.1 **Expression of ISG15 in A549 Cells.** A549^{WT}, A549$^{ISG15-/-}$ and A549^{USP18} cells were treated with IFNα (0.1μg/ml) for 96hrs. Cells were labelled for ISG15 (yellow) and imaged using a Nikon Widefield Live Cell System. DAPI-stained nuclei were outlined in greyscale during processing, scale bar = 13uM.

It was also noted that treatment with IFNα resulted in fewer cells being observed indicative of cell cycle arrest and/or apoptosis (**Fig 8.1**). RNA sequencing would provide a deeper understanding not only of the transcriptional changes and differential gene expression driving this phenotype, but also the pathways impacted by the effects of the typhoid toxin. To this end, $A549^{WT}$ and $A549^{ISG15-/-}$ cells were intoxicated using the standard intoxication protocol for 96hrs and then harvested. RNA was extracted and the presence of high-quality RNA was confirmed using a Qubit 4 fluorometer (Invitrogen) **(Methods 6.8).** To validate the effects of the TxWT and IFNα, an MTT assay was performed in parallel prior to RNA sequencing by Novogene (**Fig 8.2**). This showed that both the TxWT and IFNα performed as expected and duplicated the results shown in **Fig 7.11**.

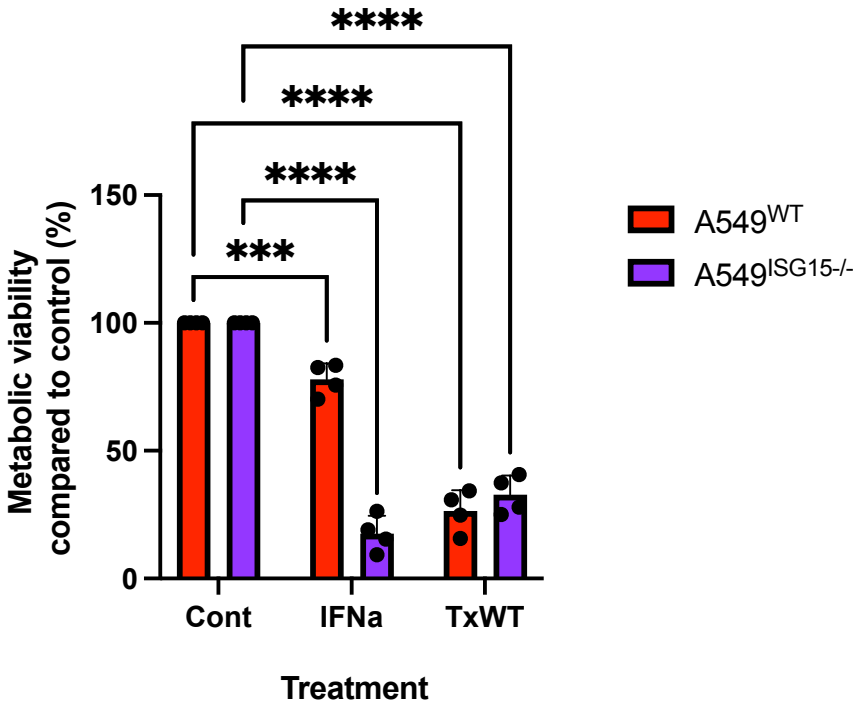

Fig 8.2 **MTT Validation for RNA Sequencing.** $A549^{WT}$ and $A549^{ISG15-/-}$ were treated for 96hrs with TxWT and IFNα to confirm effects prior to RNA sequencing. Each circle represents a biological repeat consisting of three technical replicates. (n=3)

8.3 RNA Sequencing Analysis of ISG15-deficient cells

To fully investigate the underlying effects of the typhoid toxin and IFN on ISG15 deficiency, RNA sequencing was carried out on untreated, toxin treated and IFN treated A549^{WT} and A549$^{ISG15-/-}$ cells. QC analysis was carried out by normalising the RNA-saq data to account for read depth or the total reads of each sample. The number of reads that align to a single location is summarised using a program called 'Feature counts' and then the reads are assigned to a gene. From here Principal Component Analysis (PCA) can be carried out. This is a machine learning, dimensionality reduction method that reduces a large set of variables into a smaller one (or principal components) whilst retaining as much information as possible, enabling the identification of inter- and intra- sample group variation. In order to perform a PCA the axis of greatest variation (a line of best fit) is identified. This then becomes known as PC1. The next highest variation (that is uncorrelated to PC1) is calculated and not surprisingly becomes PC2. This continues until all the principal components have been calculated and should be equal to the number of variables. As PC1 and PC2 contain the highest amount of variance these are normally the only principal components to be visualised on a PCA graph. Biological replicates should contain a low level of variation and should be expected to cluster together due to having similar transcript profiles, however samples having undergo different treatments or conditions should show less similarity and therefore not cluster (Novogene, 2023).

RNA Sequencing was performed by Novogene (UK). Biological replicates of both A549^{WT} and A549$^{ISG15-/-}$ cells were sent in triplicate for each 96hr treatment condition (untreated control, TxWT and IFNα) with a total of 18 samples sequenced. PCA data indicate little difference between untreated control A549^{WT} and A549$^{ISG15-/-}$ cells, which grouped together (**Fig 8.3**). Toxin-treated A549^{WT} and A549$^{ISG15-/-}$ cells also grouped together, though in a distinct cluster from untreated control cells. This indicates that there is little difference in the response in A549^{WT} and A549$^{ISG15-/-}$ cells. However, there is some difference in the clustering between the two populations suggesting that there are subtle differences in transcriptomic changes which could

be investigated. In contrast, IFNα-treated A549$^{ISG15-/-}$ cells form a distinct group from A549^{WT} cells. Indeed, IFNα-treated A549$^{ISG15-/-}$ cells formed the most distinct group as apparent from their isolation on the right-hand side of the PCA plot. In summary, the PCA data agree with findings so far that IFN responses in the absence of ISG15 are divergent from those found in parental cells.

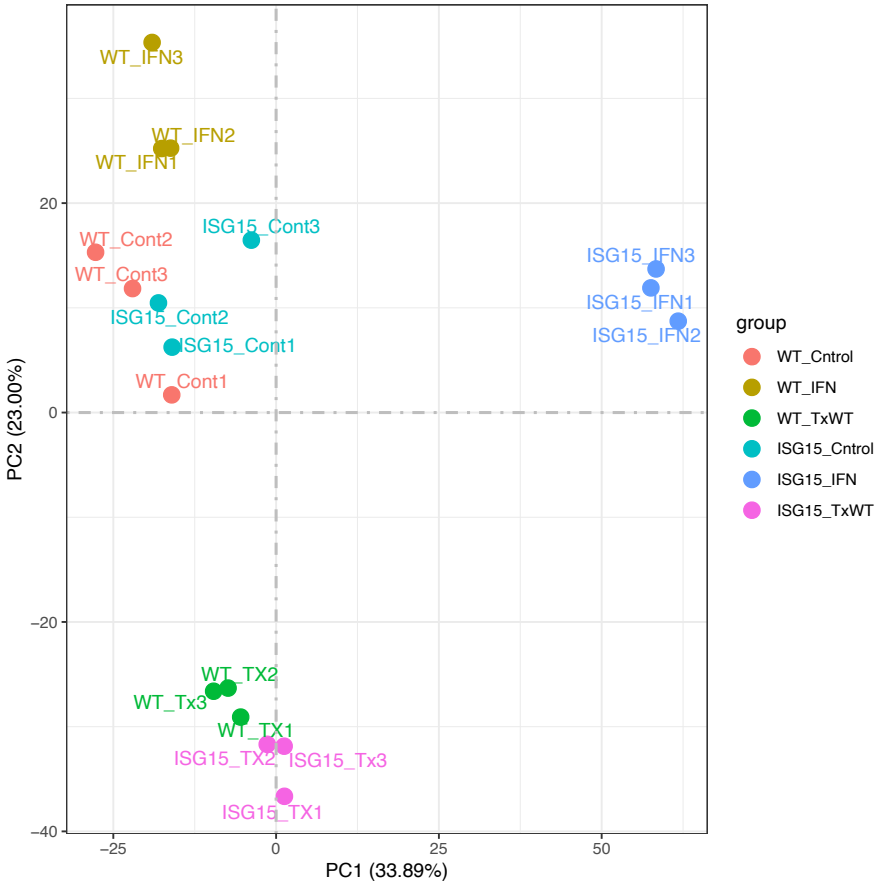

Fig 8.3 **Principal Component Analysis of parental and ISG15-deficient A549 cells in the presence of typhoid toxin or IFNα**. A549^{WT} (WT) or A549$^{ISG15-/-}$ (ISG15) were either untreated (cont), or treated with either typhoid toxin (TX) or IFNα (IFN) for 96h prior to harvest of total RNA. X and Y axes denote the distance of projected values of each data point from the origin (or centre of the dataset) and highlight variation or correlation between samples in terms of their transcriptomes. PC1 accounts for 33.89% of transcriptomic variation around the PC axes, while PC2 accounts for 23% of that variation. Colours represent individual biological replicates, and numbers after sample name, e.g., TX1, TX 2 and TX 3 represent sample replicates. Illumina RNA sequencing and PCA plot were provided by Novogene.

In agreement with this observation, Reactome analysis (http://www.reactome.org) of differentially expressed gene sets identified divergent responses to IFNα by A549^{WT} and A549$^{ISG15-/-}$ cells (**Fig 8.4**). In A549^{WT} cells treated with IFNα, the top ranked genes were associated with interferon signalling (38 genes), interferon alpha/beta

signalling (25 genes) and ISG15-dependent anti-viral mechanisms (9 genes) (**Fig 8.4A**). In contrast, type 1 interferon signalling genes were not identified in IFNα-treated A549$^{ISG15-/-}$ cells (**Fig 8.4B**). Instead, the top ranked pathways included chromosome maintenance (54 genes) and DNA strand elongation (24 genes) suggesting an impact on genome stability and loss of control in IFN responses.

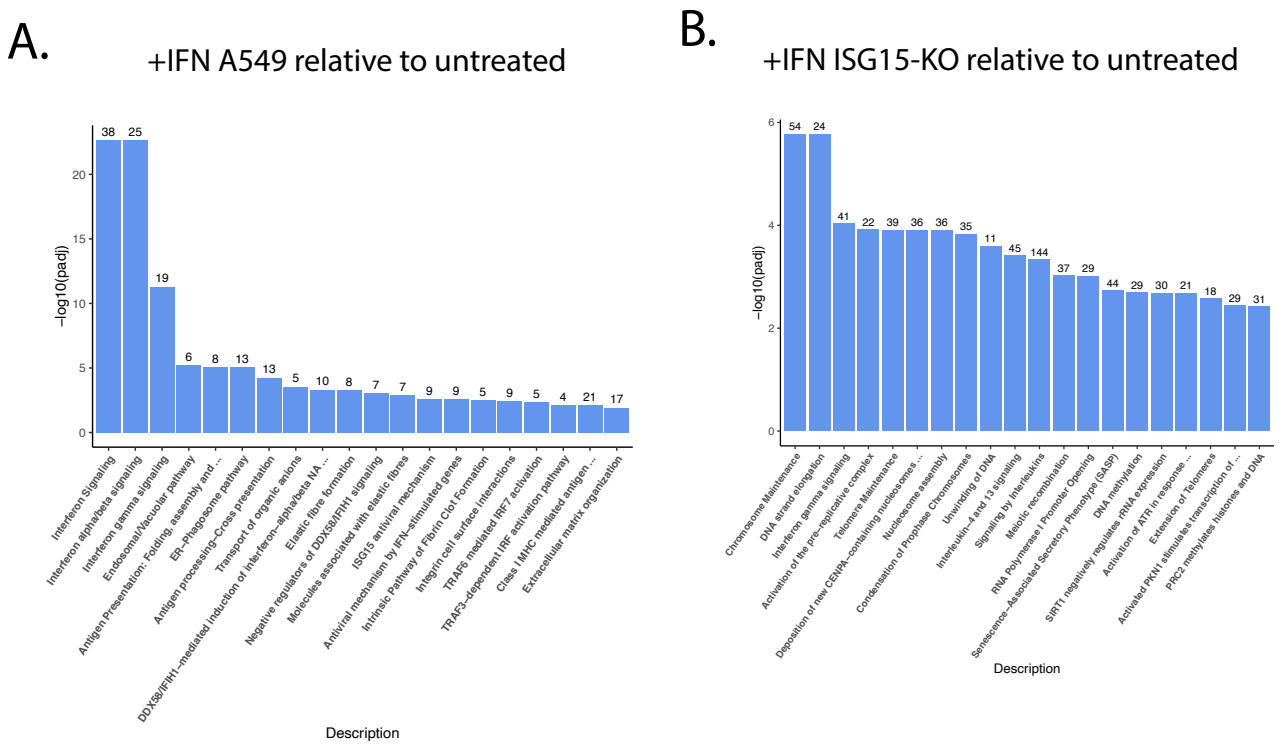

Fig 8.4 **Reactome Analysis of ISG15-deficient A549 cells in the presence of IFNα**. (**A**) A549^{WT} or (**B**) A549$^{ISG15-/-}$ cells were either untreated or treated with IFNα for 96h prior to harvest of total RNA. Differentially expressed gene sets from RNA sequencing was used by Novogene to identify pathways of Reactome (http://www.reactome.org) that were significantly enriched in IFNα relative to untreated cells for each cell line (analysis performed by Novogene).

Unfortunately the RNA Seq data was received very late in the project during the writing of this thesis so it was not possible to conduct an indepth analysis of the data. Therefore most of the conclusions are drawn by investigating changes at the pathway level.

8.5 IFNα and typhoid toxin trigger cell cycle arrest in ISG15 Deficient Cells

Other than heatmaps of curated groups of genes, the RNA seq data from this project is the result of Kyoto Encyclopedia of Genes and Genomes (KEGG) analysis performed by Novogene. Rather than focusing on the activity of individual genes, this analysis links a set of genes to a network of interacting molecules in a higher biological function, such as a pathway. KEGG currently consists of 16 databases split into 4 categories – systems, genomic, chemical and health information. The KEGG/PATHWAY database contains species specific graphical diagrams (or pathway maps) of 90 metabolic pathways. Differentially expressed gene sets are mapped to relevant pathways with downregulated genes indicated in green and upregulated genes indicated in red (Kanehisa and Goto, 2000, Novogene, 2023).
It has so far been shown that loss of ISG15 in A549 cells consistently causes loss of MTT metabolism in response to exposure to IFNα. However, although the MTT assay effectively demonstrates a curtailment of cell viability, it does not definitively identify the underlying cause of this loss. Therefore, further investigation was needed to try and answer this question. First it could be theorised that IFNα stimulation may result in cell cycle arrest rather than apoptosis.

To determine whether RNA seq analysis provided evidence of IFNα-induced cell cycle arrest in A549$^{ISG15-/-}$ cells, KEGG analysis files were used, which is a resource that annotate differentially expressed genes in cellular pathways **(Fig 8.5)**. In untreated A549^{WT} or A549$^{ISG15-/-}$ cells, there was very little difference in cell cycle gene expression showing that A549$^{ISG15-/-}$ cells replicate equivalently to parental cells in untreated conditions **(Fig 8.5A)**. In contrast, relative to A549^{WT} cells, IFNα treatment in A549$^{ISG15-/-}$ cells reduced the expression of cyclins (e.g. CycE, CycA, CycB) and cyclin-dependent kinases (e.g. CDK2, CDK1), which drive cell cycle progression **(Fig 8.5B)**. Interestingly, expression of the E3 ubiquitin-protein ligase Mdm2, that mediates ubiquitination and degradation of p53, increased. This

suggests downregulation of p53, however, expression of the p53 effector p21 (Cip1) increased, which suggests increased p53 activity. Moreover, post-translational modifications of p53 suppresses its targeting by Mdm2 (Clark et al., 2022). The findings are consistent with IFNα-induced cell cycle arrest only in A549$^{ISG15-/-}$ cells, which would explain the loss of cells in MTT assays.

A.

untreated A549$^{ISG15-/-}$ relative to untreated A549^{WT} cells

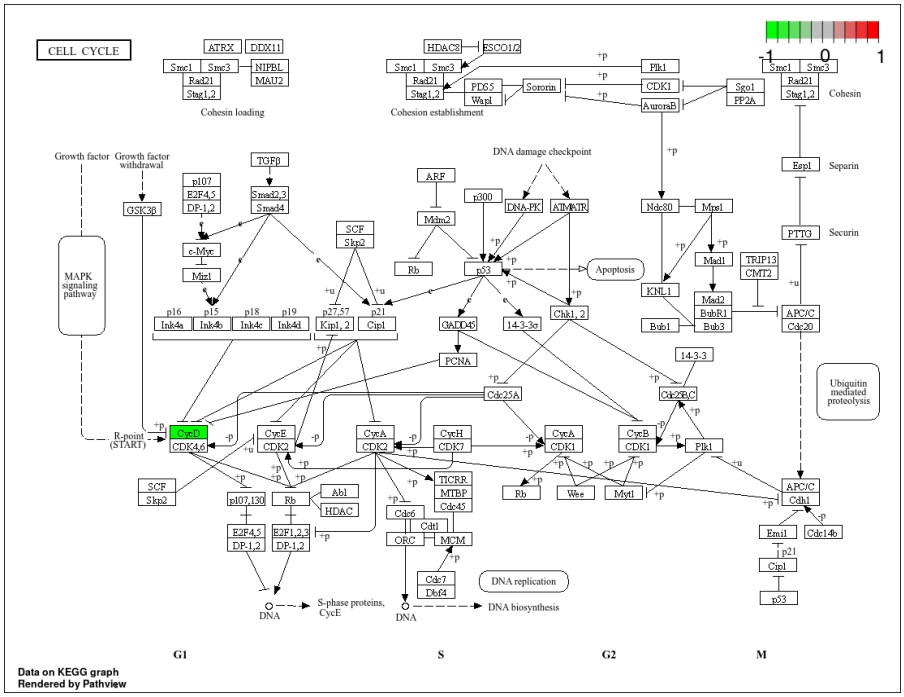

B.

+IFN-treated A549$^{ISG15-/-}$ relative to +IFN-treated A549^{WT} cells

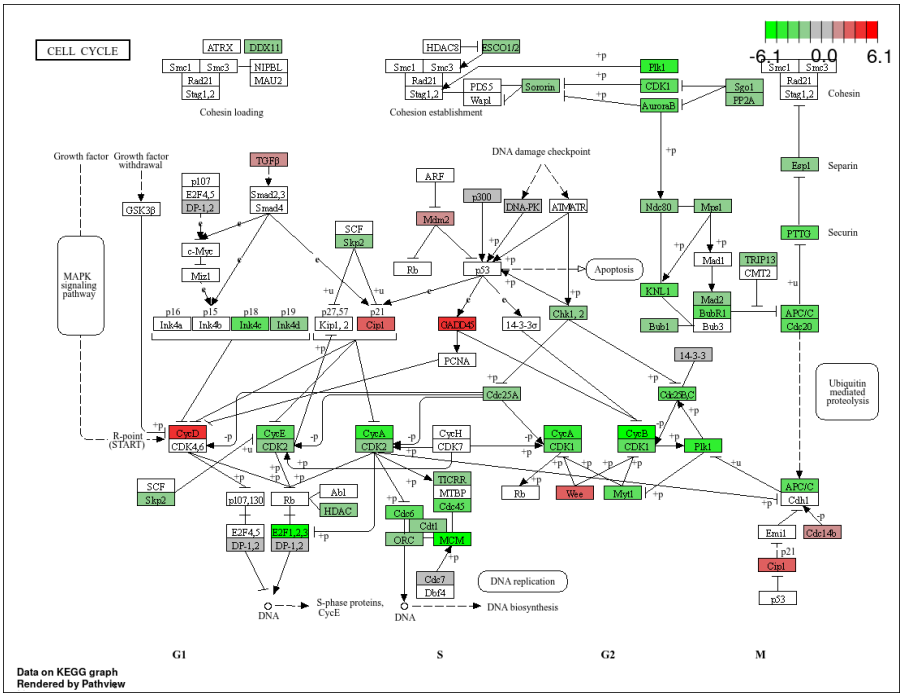

Fig 8.5 **KEGG Analysis of ISG15-deficient A549 cells in the presence of IFNα**. A549^{WT} or A549$^{ISG15-/-}$ were either (**A**) untreated, or (**B**) treated with IFNα, for 96h prior to harvest of total RNA. Differentially expressed gene sets from RNA sequencing was used by Novogene to identify pathways of KEGG that were significantly enriched, which in this case included the Cell cycle (analysis performed by Novogene). Genes with no change (grey), decreased (green) or increased (red) gene expression are indicated in the pathway.

Next, it was decided to investigate cell cycle arrest experimentally. Cell cycle arrest was also accordingly assayed after typhoid toxin or IFNα treatment in A549^{WT} and A549$^{ISG15-/-}$ cells, which were labelled with EdU and imaged using fluorescence microscopy at 72hrs **(Fig 3.14)**. The number of EdU positive cells per field of view for each condition was then quantified to determine DNA synthesis due to DNA replication**.**

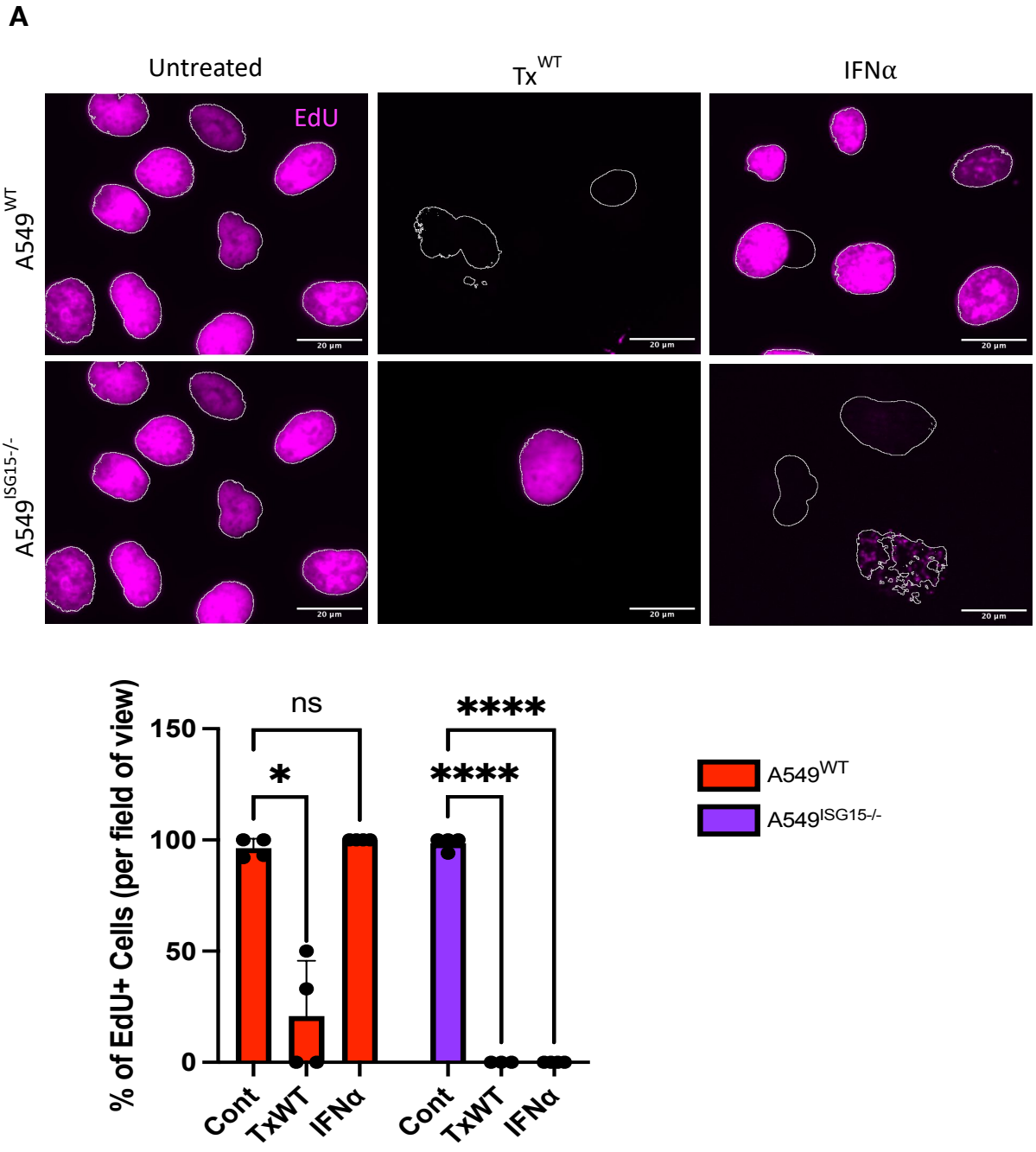

Fig 8.6 **EdU Expression of Toxin and IFNα Treated A549 Cells** (A) Immunofluoresence images of A549^{WT} and A549$^{ISG15-/-}$ cells treated with TxWT (0.1ng/ml) and IFNα (0.1ug/ml) and labelled with EdU (magenta) after 96hrs. Images were taken on a Nikon Widefield Live Cell System at x40 magnification. Scale bar = 20uM. (B) Quantification of EdU positive cells in (A). The percentage of EdU positive cells per field of view was calculated and statistical significance determined using a two-way ANOVA in GraphPad Prism. Each circle represents one biological repeat. (n=3)

The untreated controls for both A549^{WT} and A549$^{ISG15-/-}$ showed no noticeable difference demonstrating that knocking out ISG15 does not impact cell proliferation and allowing comparison between the two cell lines following treatment. The TxWT produced similar effects in both cell lines with a noticeable reduction in cell number in **Fig 8.6A** which was confirmed by quantification of EdU positive cells per field of view in **Fig 8.6B.** In TxWT-treated cells, A549^{WT} showed some variability ranging from a 50% loss of EdU to a complete loss of EdU positive cells. For A549$^{ISG15-/-}$, very few EdU positive cells could be found in the presence of TxWT and a single EdU-positve cell is shown in **Fig 8.6A**. Surprisingly, whereas A549$^{ISG15-/-}$ treated with IFNα showed a loss of EdU therefore implying a disruption to cell proliferation, the A549^{WT} showed little difference to the untreated cells which was confirmed by the quantification. Cell cycle arrest provides an explanation for the loss of MTT metabolism in A549$^{ISG15-/-}$ in response to IFNα in **Fig 7.11**.

To investigate the response to IFNα further, cell proliferation was also assayed by labelling cells with the phosphorylated form of p-pRb (retinoblastoma protein), a regulator of cell growth and division. A549^{WT} and A549$^{ISG15-/-}$ were treated with or without IFNα for 96hrs before imaging by fluorescence microscopy **(Fig 8.5A).** Again, there was little difference between the untreated controls showing there are no underlying growth defects with either cell line. However, while there was partial loss of pRb with A549^{WT} in the presence of IFNα, there was complete loss of pRb with A549$^{ISG15-/-}$ under the same conditions. This result was further corroborated by immunoblotting **(Fig 8.5B).** There was no difference between untreated and + IFNα in A549^{WT} cells as the immunoblot showed a decrease in p-pRb from 48hr to 96hr with a complete loss at 168h likely due to quiescence. There was p-pRb at 48h in A549$^{ISG15-/-}$ but this was reduced relative to the same timepoint in A549^{WT} cells. In contrast, IFNα abolished p-pRb production at 48h in A549$^{ISG15-/-}$ cells. At 96h, no p-pRB was detectable in untreated or IFNα-treated A549$^{ISG15-/-}$ cells, which contrasted with the presence of p-pRb in A549^{WT} cells. At 168h, p-pRB was not detected in any cell type.

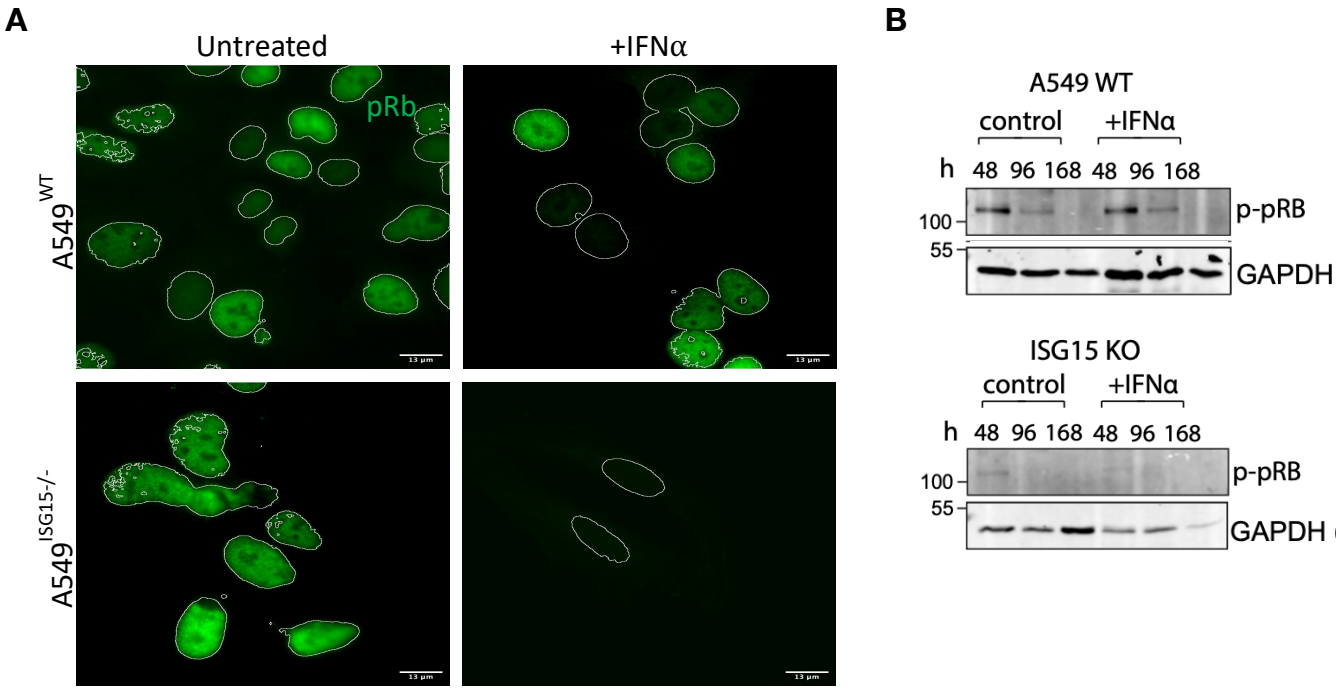

Fig 8.7 **Expression of p-pRb in Response to IFNα.** (A) Immunofluorescence images of pRb expression (green) in A549^{WT} and A549$^{ISG15-/-}$ cells after 96hrs of IFNα (0.1ug/ml) exposure. Magnification – x40, scale bar = 13uM. (B) Immunoblot showing pRb expression at 48, 96 and 168hrs. A549^{WT} and A549$^{ISG15-/-}$ (ISG15 KO) cells were untreated or treated with or 0.1µg/ml IFNα before generating whole cell lysates (WCL) at 48, 96 and 168hrs. WCLs were immunoblotted with antibodies to phosphorylated RB (pRB-pS807/811) or the loading control GAPDH. MW markers shown on the left in kDa.

It is so far clear that IFNα causes a striking effect on replication in ISG15 deficient cells. The substantial defect in DNA synthesis (**Fig 8.6**) and p-pRB (**Fig 8.7**) indicate senescence in A549$^{ISG15-/-}$ cells. A senescence-associated Beta-galactosidase (β-Gal) assay was carried out to see if A549$^{ISG15-/-}$ cells entered into a state of senescence in response to IFNα. This is a simple colorimetric assay where cells are incubated with a chromogen called X-Gal (5-bromo-4-chloro-3-indoyl β-d-galactopyranoside). This is a direct substrate for Beta-galactosidase, a lysosomal enzyme that increases in concentration during senescence, which cleaves the substrate into two products - galactose and 5-bromo-4-chloro-3-hydroxyindole. The latter of the two is oxidised resulting in a blue colour, giving a visual confirmation of β-Gal activity (Valieva et al., 2022).

A549^{WT} and A549$^{ISG15-/-}$ cells were treated with TxWT or IFNα for 7 days before the β-Gal assay was carried out. Images were taken at x10 magnification to allow a greater overview of the number of surviving cells and β-Gal expression **(Fig 8.8)**.

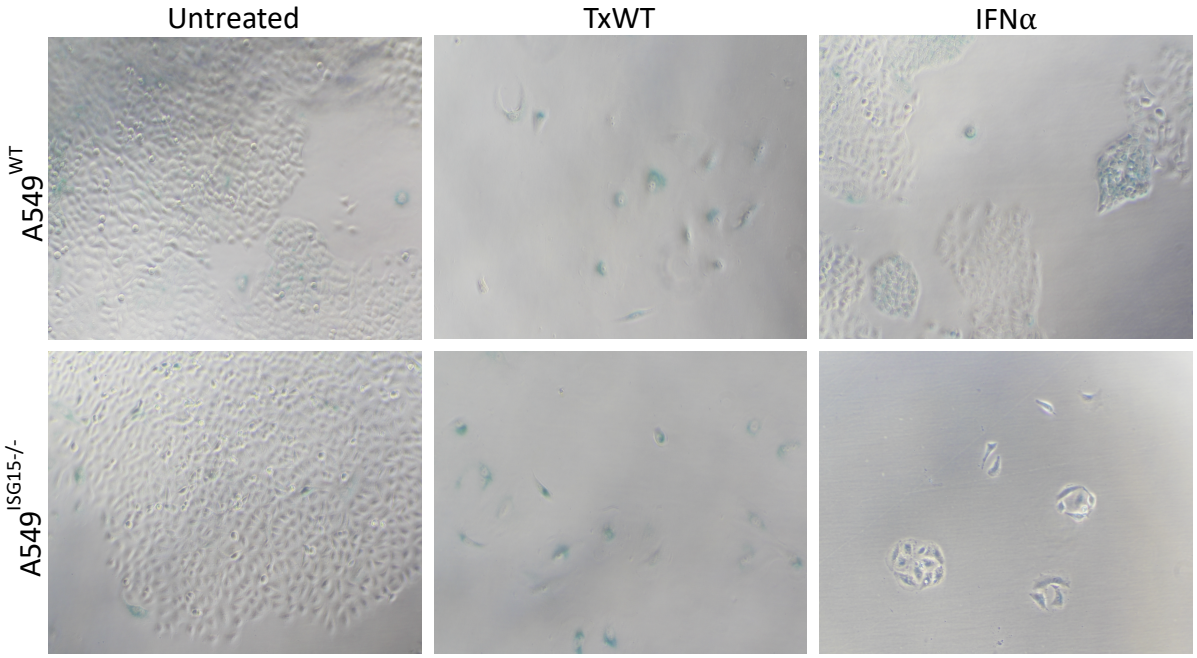

Fig 8.8 **β-Gal Assay of Intoxicated A549 Cells.** Both A549^{WT} and A549$^{ISG15-/-}$ cells were treated with TxWT (0.1ng/ml) and IFNα (0.1μg/ml) for 7 days after which a β-Gal assay was performed. Cells were imaged after 48hrs at x10 magnification on a Nikon TS Eclipse microscope. (n=3)

The untreated controls for both cell lines showed normal cell growth and large areas covered by proliferating cells with little evidence of senescence. With the TxWT treatment both A549^{WT} and A549$^{ISG15-/-}$ showed a similar outcome – a significant reduction in cell number and greater dispersion of visible cells rather than the large patches of growth seen in the untreated controls. The surviving cells showed increase in β-Gal expression and identified cells that were able to withstand TxWT and enter into a senescent state. However, the most interesting result came from the cells treated with IFNα. A549^{WT} cells demonstrated that despite a comparable loss of MTT metabolism to A549$^{ISG15-/-}$ after 7 days of IFNα treatment **(Fig 7.11)**, the cellular outcomes were in fact very different: A549^{WT} were able to withstand the harmful effects of IFNα to a certain extent, although there are fewer cells visualised compared to the untreated controls. There are also patches of blue visible showing increased senescence-associated β-Gal activity. This implies that prolonged

exposure to IFNα possibly pushes cells towards a quiescent state as there was no evidence of cell cycle arrest. For example, there were many more cells visible relative to treatment with the senescence inducer TxWT. Also, IFN-treated A549^{WT} were comparable to untreated in DNA synthesis (**Fig 8.6**) and p-pRB (**Fig 8.7**). This greatly contrasts to A549$^{ISG15-/-}$ in the presence of IFNα, which shows much fewer cells surviving and no senescence-associated β-Gal activity. The results indicate that A549$^{ISG15-/-}$ cells have a replication defect in the presence of IFNα but this does not lead to senescence and the loss of cells is likely due slow growth and possibly apoptosis, though this has not beed resolved. The loss of A549$^{ISG15-/-}$ cells is due to cell cycle aresst and not senescence, which further explains the phenotype in MTT assays where loss of MTT metabolism was observed for A549$^{ISG15-/-}$ cells.

The reduction in A549$^{ISG15-/-}$ cells, the loss of EdU-labelled DNA synthesis and p-pRB, in the presence of IFNα suggested senescence but this was not observed in the senescence-associated β-Gal assay. This was despite evidence that the typhoid toxin induced senescence in A549$^{ISG15-/-}$ cells. To examine this further, A549^{WT} and A549$^{ISG15-/-}$ cells were immunoblotted in the presence of typhoid toxin, etoposide and IFNα before examining markers of senescence (p21), cell cycle progression (p-pRb), and DDRs (p-p53, γH2AX) at 48h or 168h (**Fig 8.9)**.

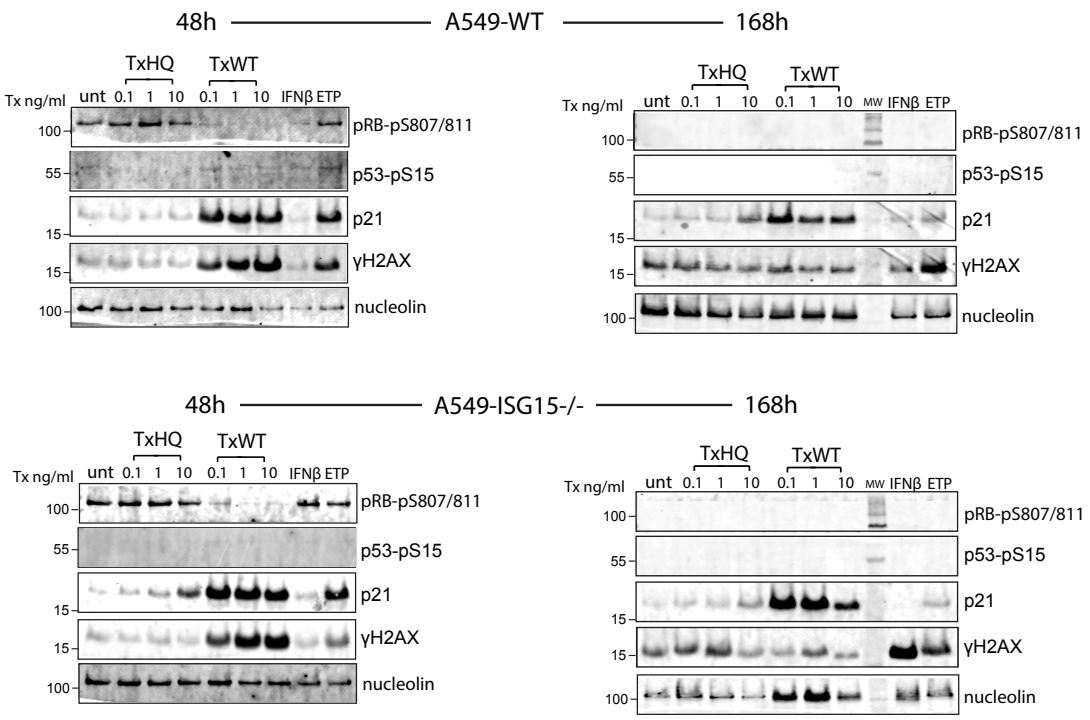

Fig 8.9 Senescence and DDR responses in A549 cells. Cells were untreated or treated with 01. 1, or 10ng/ml DNase-deficient typhoid toxin (TxHQ) or wild-type toxin (TxWT), 3μM etoposide (ETP) or 0.1μg/ml IFNα before generating whole cell lysates (WCL) at 48h or 168h. WCLs were immunoblotted with antibodies to phosphorylated RB (pRB-pS807/811), phosphorylated p53 (p53-pS15), p21, γH2AX or the loading control nucleolin. MW markers shown on the left in kDa.

The immunoblot showed that typhoid toxin and etoposide induced senescence responses characterised by elevated p21, γH2AX and reduced p-pRb at 48h in A549^{WT} cells. Phosphorylated p53 was also observed at 48h. At 168h, elevated p21 was still observed relative to controls cells (untreated, TxHQ). The same trend was found in A549$^{ISG15-/-}$ cells. These observations are consistent with senescence. In agreement with the senescence-associated β-Gal assay, IFNα exposure in A549^{WT} cells did not induce senescence as indicated by p21, γH2AX and p-pRb levels that were equivalent to untreated A549^{WT} cells. Interestingly, a marked increase in γH2AX was apparent in IFNα-treated A549$^{ISG15-/-}$ cells at 168h (**Fig 8.9)**, which coincides with the reduction in MTT metabolism (**Fig 7.11**). Elevated p21 was absent in IFNα-treated A549$^{ISG15-/-}$ cells at 168h with increased γH2AX (**Fig 8.9)**, which contrasted with KEGG analysis of differentially expressed genes showing increased p21 gene expression (**Fig 8.5B**). Indeed, there is still the possibility that IFNα-treated

A549$^{ISG15-/-}$ cells undergo apoptosis, which has not been discounted and was investigated next.

8.6 IFNα triggers apoptosis in ISG15 Deficient Cells

It is clear from the results so far that ISG15 is key is maintaining viable cells in response to IFNα. During my PhD studies, ISG15 was implicated in apoptosis of macrophages during IFNα treatment (Fakhar-ul-Hassnain Wagas et al., 2022). To determine whether RNA seq analysis provided evidence of IFNα-induced cell death in A549$^{ISG15-/-}$ cells, KEGG analysis was performed by Novogene to annotate differentially expressed genes in cellular pathways **(Fig 8.10)**. KEGG pathway analysis indicated that IFNα-treated A549^{WT} cells were predominantly associated with pathways implicated in IFN responses to viral infection (e.g. Epstein-Barr virus, 20 genes; influenza A, 18 genes) **(Fig 8.10A)**. In contrast, the second most enriched pathway in IFNα-treated A549$^{ISG15-/-}$ cells was tumour necrosis factor (TNF) signalling (59 genes), which is associated with apoptotic pathways **(Fig 8.10B).**

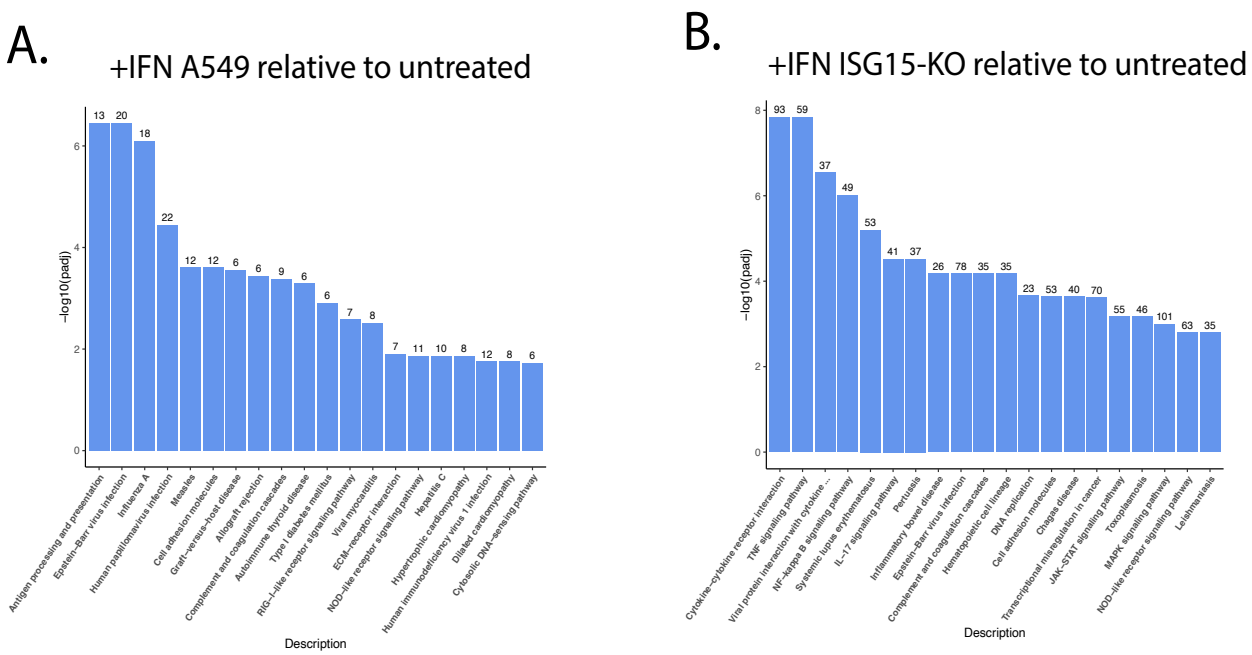

Fig 8.10 Cellular pathways upregulated in ISG15-deficient A549 cells in the presence of IFNα. (**A**) A549^{WT} or (**B**) A549$^{ISG15-/-}$ cells were either untreated or treated with IFNα for 96h prior to harvest of total RNA. Differentially expressed gene sets from RNA sequencing were used by Novogene to identify gene sets enriched in cellular pathways of KEGG in IFNα relative to untreated cells for each cell line (analysis performed by Novogene).

The TNFα was examined in closer detail by KEGG pathway analysis **(Fig 8.11).** Relative to untreated, IFNα had no effect of the TNFα pathway in A549^{WT} cells **(Fig 8.11A)**. In IFNα-treated A549$^{ISG15-/-}$ cells however, expression of TNFα pathway genes exhibited increased expression **(Fig 8.11B).** This included increased expression of TNF itself, the receptor TNFR2, Fas, caspase 8/10, which are implicated in cell death by apoptosis. The findings are consistent with IFNα-induced apoptosis in A549$^{ISG15-/-}$ cells, which would explain the loss of cells in MTT assays.

A.

+IFN A549 relative to untreated

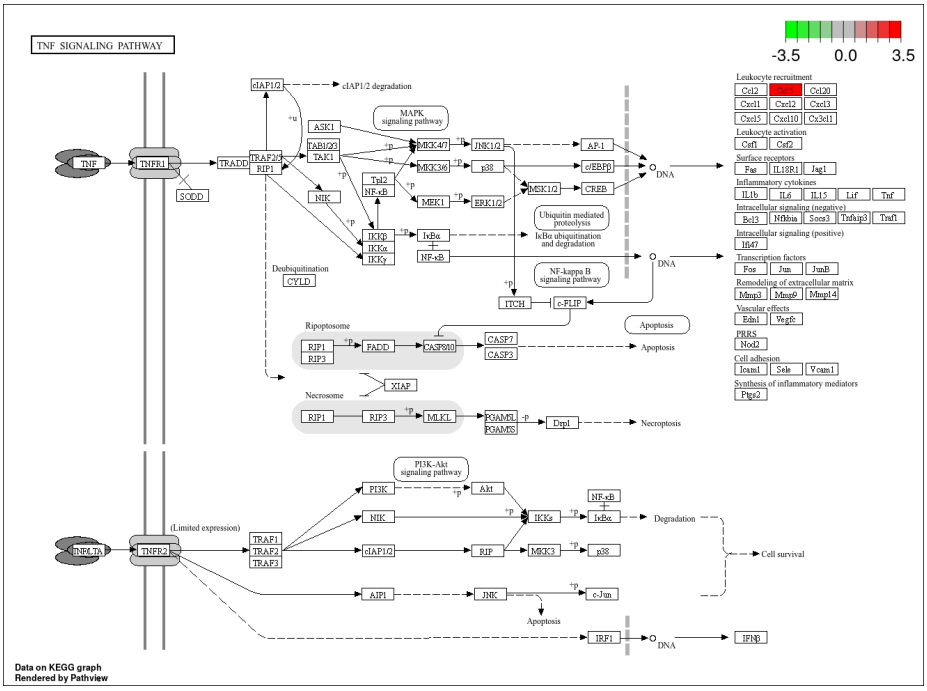

B.

+IFN ISG15-KO relative to untreated

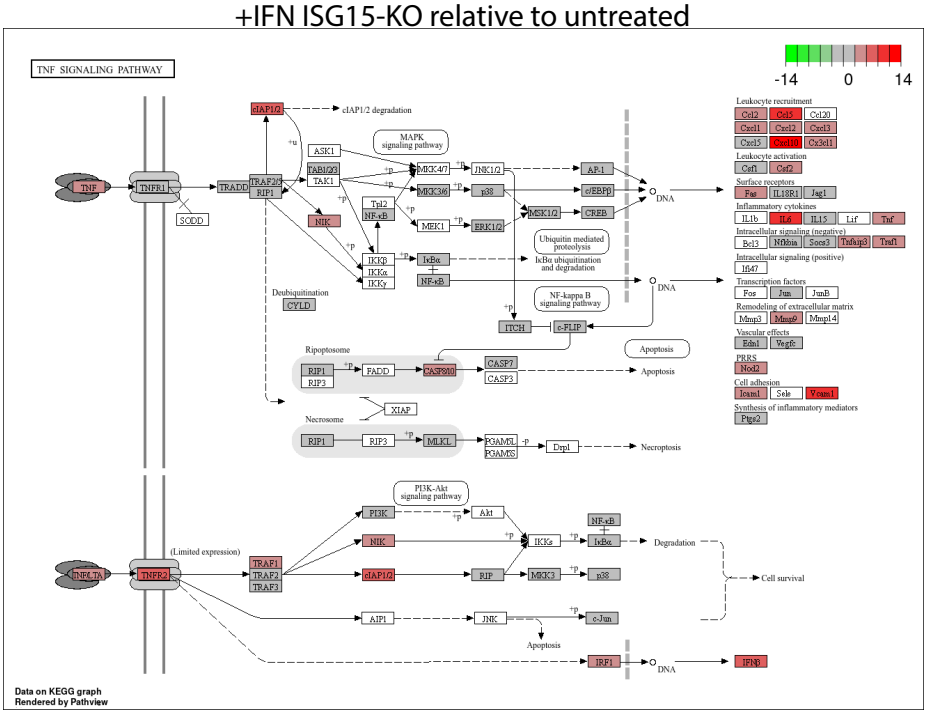

Fig 8.11 KEGG Analysis of ISG15-deficient A549 cells in the presence of IFNα. A549^{WT} or A549$^{ISG15-/-}$ were either (**A**) untreated, or (**B**) treated with IFNα, for 96h prior to harvest of total RNA. Differentially expressed gene sets from RNA sequencing was used by Novogene to identify pathways of KEGG that were significantly enriched, which in this case included the TNFα signalling pathway (analysis performed by Novogene). Genes with no change (grey), decreased (green) or increased (red) gene expression are indicated in the pathway.

To delve deeper into the transcriptional changes associated with ISG15 deficiency, the upregulation of specific apoptotic markers was explored by generating a heat map **(Fig 8.12)**. A549$^{ISG15-/-}$ showed at least a two-fold upregulation in 13 genes associated with apoptosis when compared to A549^{WT} after IFNα treatment. Of these the most highly upregulated was TRAF1 (TNF receptor associated factor 1) with a 5.42-fold-change compared to A549^{WT} under the same conditions. As its name suggests it interacts with receptors of the TNF family. Although it is usually regarded as having an anti-apototic effect, Jang et al., 2001 demonstrated that if cleaved it can enhance the effects of TNF-mediated apoptosis (Lu et al., 2013). Significant upregulation was also seen in genes associated with the Nuclear factor kappa-light-chain-enhancer of activated B cells (NF-κB) pathway (MAP3K14, NFKBIA) which attempts to combat the apoptotic actions of the TNF pathway (Baichwal and Baeuerle, 1997) suggesting that the cells also try to activate pro-survival strategies. However, upregulation of FAS (Fas cell surface death receptor), another TNF receptor, and genes associated with DNA damage (DDIT3, GADD45A) suggests this strategy is not successful

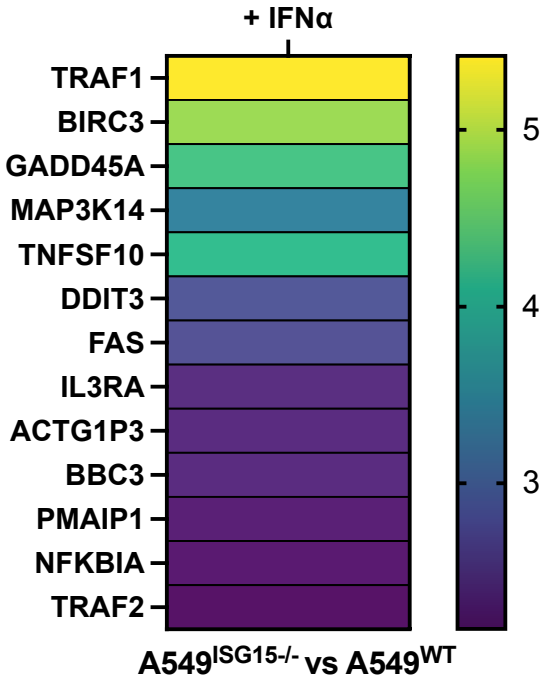

Fig 8.12 **Upregulation of apoptosis related genes in ISG15-deficient A549 cells in response to IFNα.** The list of apoptosis related genes upregulated in A549ISG15-/- in response to IFNα compared to A549WT was filtered to only include those with at least a two-fold upregulation. The results were then visualised by creating a heat map in GraphPad Prism.

To address IFNα-induced cell death experimentally, immunofluorescence was first used to assay apoptosis in IFNα treated A549^{WT} and A549$^{ISG15-/-}$ cells for 96hrs **(Fig 8.13)**. Apotracker^{TM} (Apo-15 peptide) was then added to label apoptotic cells and imaged. This is a calcium-independent probe which detects translocation of the phospholipid phosphatidylserine to the extracellular leaflet of the plasma cell membrane during apoptosis (https://www.biolegend.com/en-gb/products/apotracker-green-18527?GroupID=GROUP22).

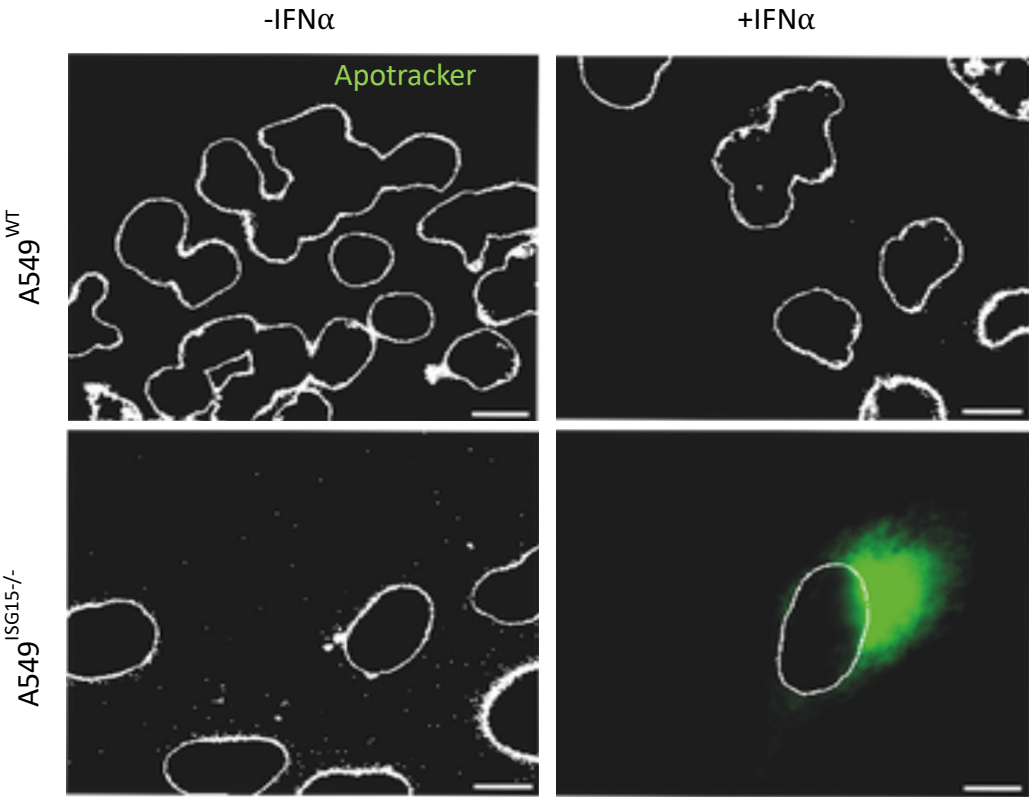

Fig 8.13 **Immunofluorescence of Apotracker expression in A549 Cells.** A549^{WT} and A549$^{ISG15-/-}$ were treated with IFNα (0.1ug/ml) for 96hrs and then labelled with Apotracker (green). Images were taken on a Nikon Widefield Live Cell System ay x40 magnification. DAPI-stained nuclei were outlined in greyscale during processing in Fiji. Scale bar = 13uM.

No expression of Apotracker was detected in A549^{WT} or A549$^{ISG15-/-}$ without IFNα indicating no apoptotic activity **(Fig 8.13;** -IFNα). However, A549$^{ISG15-/-}$ cells in the presence of IFNα showed labelling with Apotracker and a reduction in cell number

compared to A549^{WT} further reinforcing the idea that IFNα drives apoptosis in ISG15 deficient cells **(Fig 8.13;** +IFNα).

Apotracker can be used in multiple applications so it was possible to further investigate this phenotype by quantifying apoptosis using flow cytometry. A549^{WT} and A549$^{ISG15-/-}$ were treated with TxWT, IFNα and ETP using the standard intoxication protocol for 96hrs before harvesting. Live cells were analysed on a Attune NxT Flow Cytometer immediately after labelling with the Apotracker^{TM} probe and the consequent fluorescent output measured.

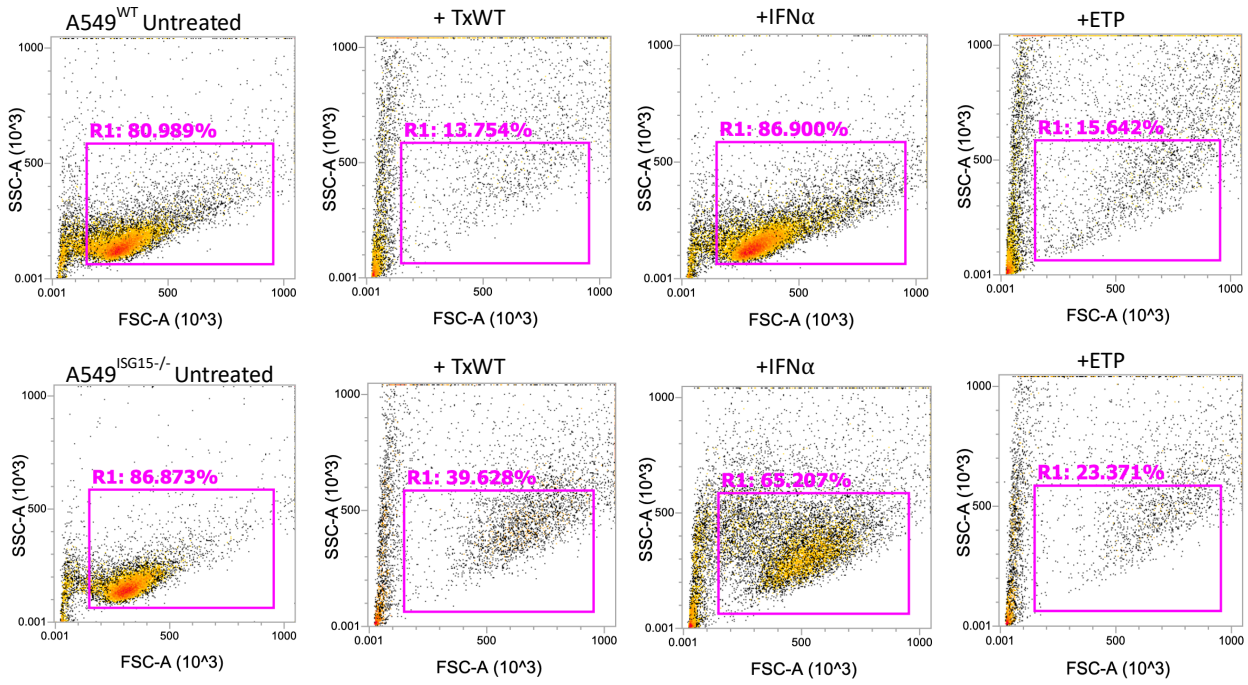

Fig 8.14 **Flow Cytometry Analysis of Intoxicated A549 Cells.** Dot plots of forward scatter (FSC-A) vs side-angle light scatter (SSC-A) of intoxicated A549^{WT} and A549$^{ISG15-/-}$ cells. Collection was stopped at either 10,000 cells or when 500ul of sample was analysed.

The forward scatter (FSC) vs side angle scatter plot **(Fig 8.14)** shows ~80% of untreated A549^{WT} cells in the gated population and ~86% of untreated A549$^{ISG15-/-}$ cells. Relative to untreated, TxWT reduced the number of A549^{WT} and A549$^{ISG15-/-}$ cells to ~13% and ~39%, respectively, which was due to cell cycle arrest. The same trend was also observed with ETP (A549^{WT} cells, ~15%; A549$^{ISG15-/-}$ cells, ~23%). After IFNα treatment, ~86.9% of A549^{WT} were gated, however only 65.207% of

A549$^{ISG15-/-}$ were gated suggesting a loss of cells population even before fluorescence quantification of apotracker.

In flow cytometry the excitation maximum is the wavelength at which the fluorochrome absorbs the most photons, resulting in the most intense emission of fluorescence. By plotting the percentage of maximum fluorescence due to apotracker **(Fig 8.15)** it is possible to determine how much fluorescence is emitted at a specific excitation percentage. The untreated control peaks were almost identical for A549^{WT} and A549$^{ISG15-/-}$ and both showed a similar shift to the right for cells treated with TxWT and ETP therefore demonstrating an increase in apotracker labelling and therefore an increase in apoptotic cells. However, where A549^{WT} showed a slight shift to the right after IFNα indicating some apoptosis occurring, there was a significant shift with A549$^{ISG15-/-}$ overlapping with the TxWT and ETP peaks. This shows that IFNα causes apoptosis in ISG15 deficient cells to a similar level as TxWT as well as ETP, the positive control for cell death.

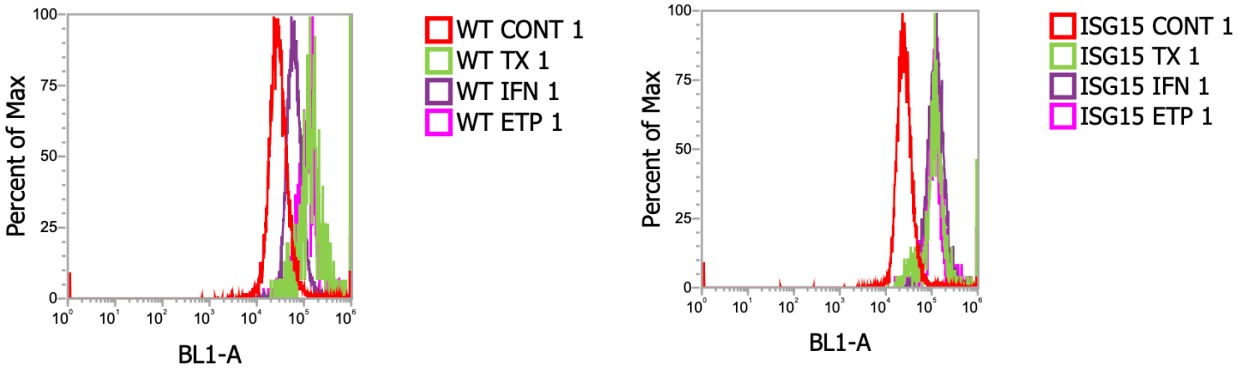

Fig 8.15 **Percentage of Maximum Fluorescence Plot.** This shows the fluorescence emission of the labelled A549 cells under excitation by the BL1 laser (488nm). Peaks are shown for A549WT and A549ISg15-/- treated with TxWT (10ng/ml), IFNα (0.1ug/ml) or ETP (3uM) alongside an untreated control. Cells were labelled after 96hrs with ApoTracker™ and assayed for apoptosis using a Attune NXT flow cytometer.

This result was confirmed by plotting the average mean fluorescence under each condition **(Fig 8.16)**. Both cell lines showed a significant increase in fluorescence in response to TxWT and ETP compared to the untreated controls, showing that the typhoid toxin drives apoptosis. However, there was no significance in average mean

fluorescence between A549^{WT} untreated and IFNα treated. This contrasts the result for A549$^{ISG15-/-}$ under IFNα conditions which showed an increase of apotracker fluorescence intensity comparable to TxWT and ETP. This confirms that whereas the typhoid toxin causes cell death regardless of ISG15 status in A549 cells, IFNα drives apoptosis in ISG15 deficient cells, but not in wild type.

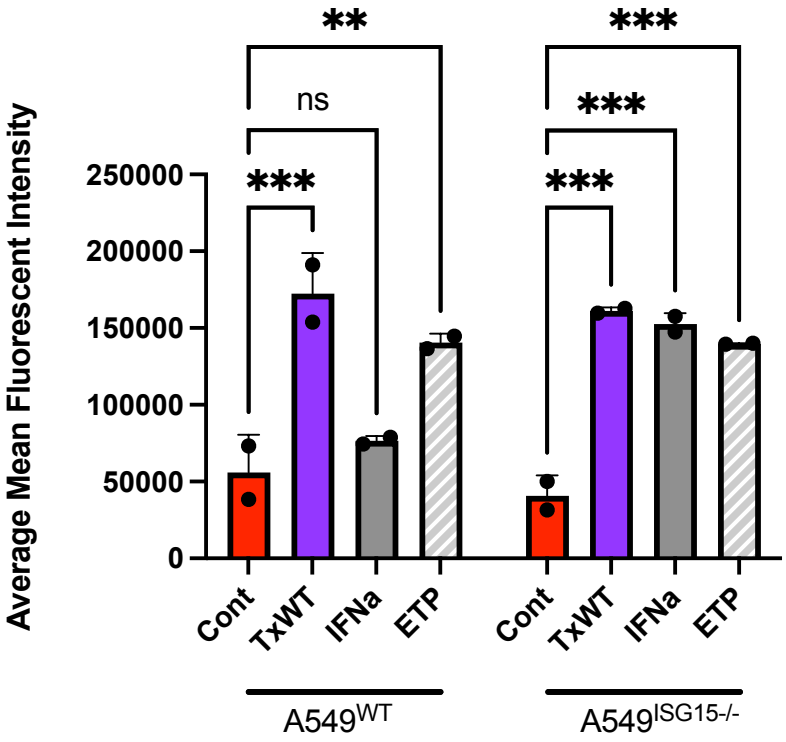

Fig 8.16 **Mean Fluorescent Intensity of Apotracker-labelled A549 cells in response to intoxication.** Fluorescence emission of ApoTracker™-labelled A549WT and A549ISg15-/- treated with TxWT (10ng/ml), IFNα (0.1ug/ml) or ETP (3uM) alongside an untreated control under excitation by the BL1 laser (488nm) were assayed for apoptosis using a Attune NXT flow cytometer. The average mean intensity for each condition was calculated and plotted in the bar chart. Each circle represents one biological replicate consisting of three technical replicates. Statistical significance was determined by two-way ANOVA. (n=3)

8.7 Apoptosis Occurs Independently of p53

P53 is a regulator of DNA repair and cell division and will drive apoptosis to prevent damaged or mutated cells from dividing (Park et al. 2016). As ISG15 has been shown to stabilise p53 and plays a role in regulating its functions (Huang et al. 2014) it was decided to investigate the impact ISG15 deficiency causes on p53 and its

ability to cause apoptosis in response to IFNα. After intoxication using the standard intoxication protocol, p53 expression was visualised after 96hrs in A549^{WT} and A549$^{ISG15-/-}$ cells by immunofluorescence **(Fig 8.17)**. It was found that p53 is expressed even in the untreated A549^{WT} however this has been previously observed in wild-type A549 cells (Douarre at el., 2013). After TxWT treatment or IFNα, p53 was expressed. However, with A549$^{ISG15-/-}$ cells there was complete loss of p53 expression regardless of treatment. This suggests that apoptosis occurs by pathways independently of p53. The observation also indicates an importance of ISG15 in p53 expression. This agrees with the immunoblotting experiment in **Fig 8.9** where phosphorylated p53 was faintly detected in A549^{WT} but not A549$^{ISG15-/-}$ cells.

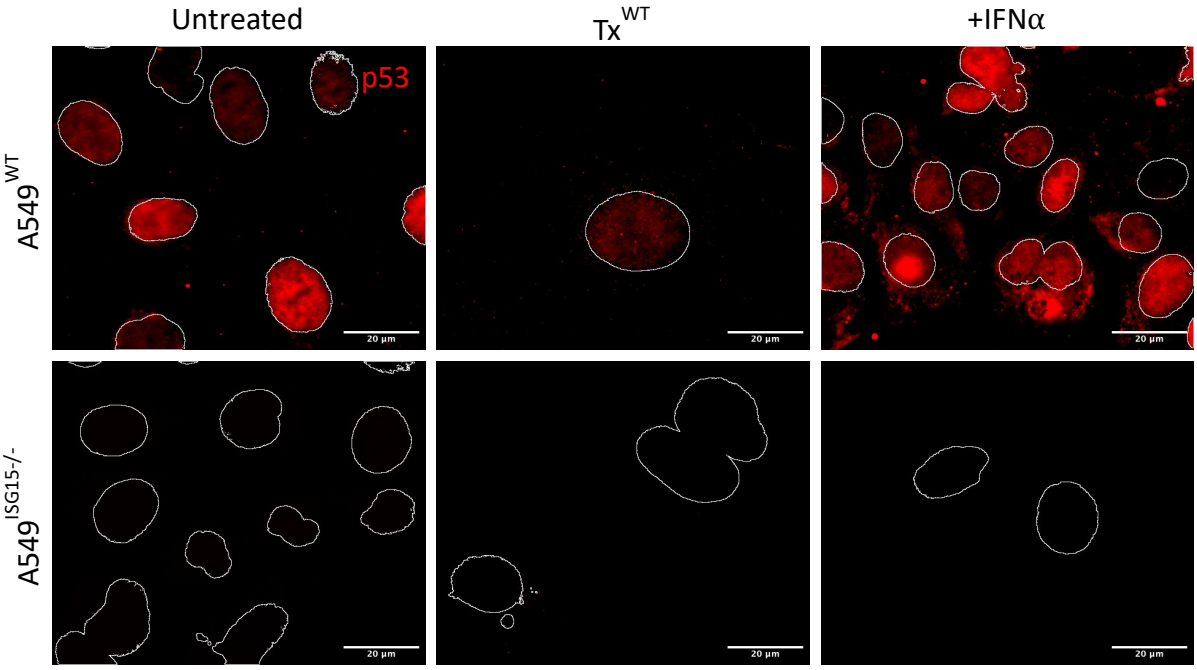

Fig 8.17 **p53 Expression in A549 Cells.** A549^{WT} and A549$^{ISG15-/-}$ were intoxicated for 96hrs with TxWT (0.1ng/ml) and IFNα (0.1ug/ml). Expression of p53 (red) was visualised on a Nikon Widefield Live Cell System and DAPI-stained nuclei were outlined in grey scale during processing in Fuji. Scale bar = 20um.

To further unpick this relationship and examine whether loss of p53 contributes to cell death in the presence of IFNα, cell survival was assayed in wild type and p53 null -/- HCT116 intestinal epithelial cells, which divide every 16-18hrs. After intoxication using the standard intoxication protocol an MTT assay was conducted at 48hr and 7 days **(Fig 8.18).** Treatment with TxHQ showed no loss of metabolism after 48hrs and only slight reduction after 7 days when compared to the untreated

control. However, after intoxication with TxWT there was a loss MTT metabolism with both HCT116^{WT} and HCT116$^{p53-/-}$ from 48hrs with a reduction of approximately 50% and 60% respectively and an almost complete loss by 7 days which was mirrored by ETP. This phenotype has been consistent across all cell types tested so far under identical conditions. For TxWT, this means that loss of MTT metabolism due to cell cycle arrest and apoptosis occurs in HCT116 cells in response to TxWT independently of p53.

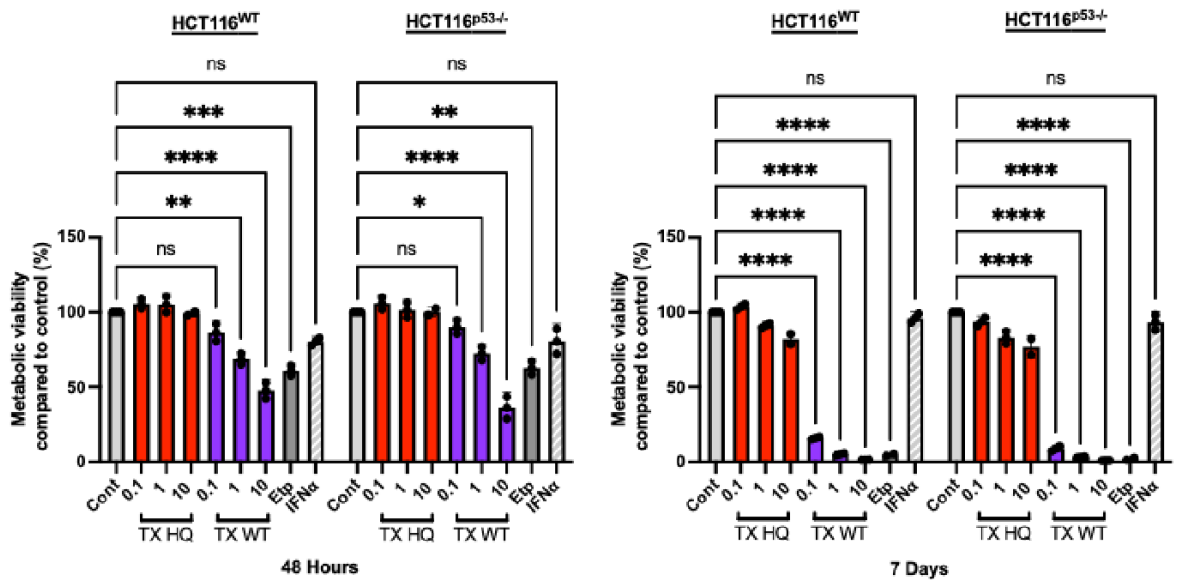

Fig 8.18 **MTT Assay of Intoxicated HCT116 Cells.** Cells were treated with either the typhoid toxin (TxWT) or the control toxin (TxHQ) at concentration of 0.1, 1 or 10ng/ml and an absorbance reading taken at either 48hrs or 7 days. Etoposide (3uM) was used as a positive control for cell death and IFNα (0.1ug/ml) was used to trigger an immune response. Each circle represents one biological replicate consisting of three technical replicates. An average of the absorbances within each biological replicate was taken. The relative absorbance was calculated compared to the untreated control with the control representing 100%. The bars indicate the mean and error bars shown indicate standard deviation (SD). Statistical significance was calculated using a two-way ANOVA with asterisks indicating significance. (n=3)

After treatment with IFNα neither HCT116^{WT} nor HCT116$^{p53-/-}$ showed significant loss of MTT metabolism. A slight reduction was observed after 48hrs, however this recovered and was identical to the untreated control by 7 days.

To confirm there were no underlying differences in responses to IFNα between HCT116^{WT} and HCT116$^{p53-/-}$ being obscured by the MTT assay, a senescence-associated β-Gal assay was also performed as per **Fig 8.8**

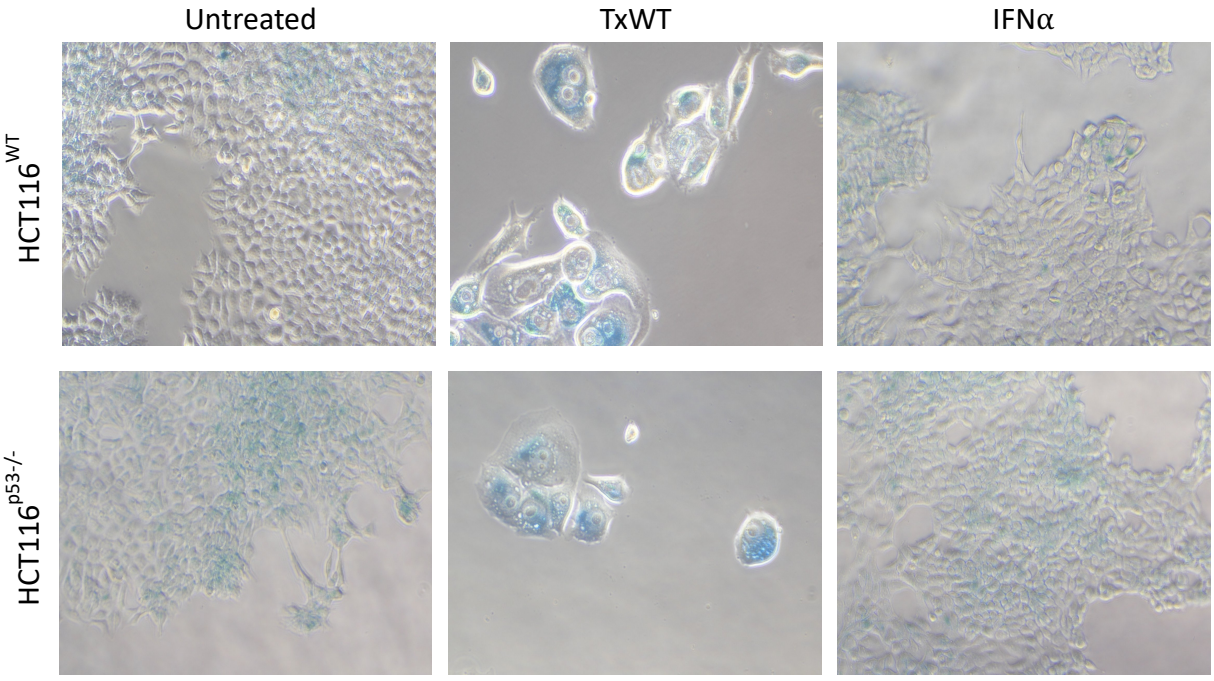

Fig 8.19 **β-Gal Assay of Intoxicated HCT116 Cells.** HCT116WT and HCT116p53-/- cells were treated with TxWT (0.1ng/ml) or IFNα (0.1ug/ml) for 7 days after which a β-Gal assay was performed. Cells were imaged after 48hrs at x10 maginification using a Nikon TS Eclipse microscope. (n=3)

No difference was found between $HCT116^{WT}$ and $HCT116^{p53-/-}$ in response to either TxWT or IFNα **(Fig 8.18)**.. Treatment with TxWT resulted in cell distension, fewer numbers of cells and expression of β-Gal, giving a similar result to A549 cells and suggesting the effects of the typhoid toxin are universal across cell types, Treatment with IFNα produced a result identical to the untreated controls with large patches of normal cells growth. The accompanying expression of β-Gal indicating areas of high confluence.

Thus, no changes in sensitivity to IFNα were observed $HCT116^{p53-/-}$ cells. Parental HT1080, U2SO and MEF cells were also unaffected by IFNα.

8.8 ISG15 is responsible for USP18 stabilisation in response to IFNα

Given that ISG15 and USP18 were upregulated together in HT1080 cells (**Fig 7.5**), it was possible that ISGylation played a role in A549 cell survival. For example, it was possible that loss of ISGylation in ISG15 cells increased impairments in DNA replication and increased apoptosis in the presence of IFNα. To test this possibility, the A549^{USP18} cell line where USP18 had been replaced with USP18$^{C61A/C61A}$ (Ketscher et al., 2015) was exploited as it was speculated that this cell line would exhibit enhanced ISGylation and therefore cell survival in MTT assays **(Fig 8.20)**. However, both A549^{WT} and A549^{USP18} cells were equivalently sensitive typhoid toxin, etoposide and IFNα. Importantly, any increase in ISGylation found in A549^{USP18} cells did not promote cell survival relative to A549^{WT} cells.

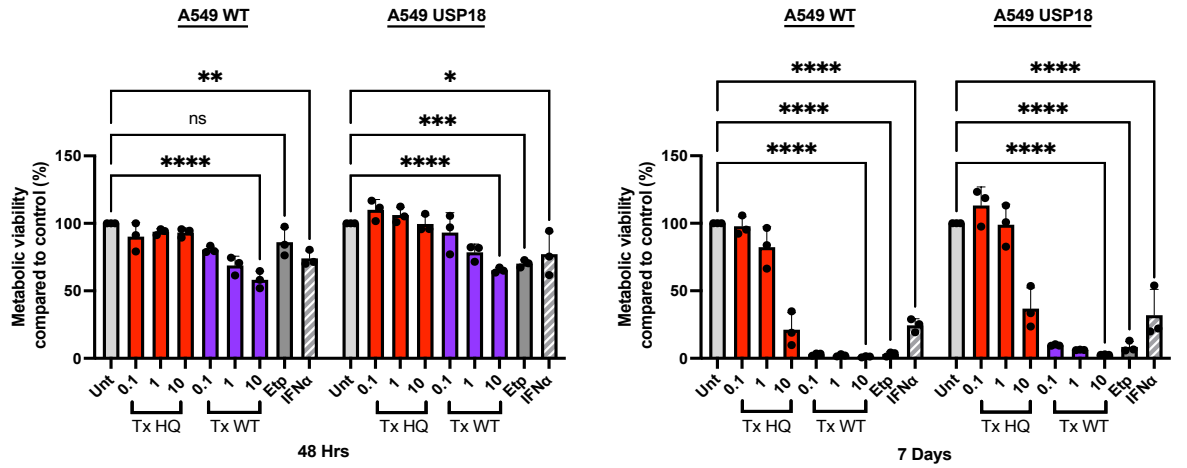

Fig 8.20 MTT Assay of intoxicated A549 USP18-CA cells. Cells were treated with either the typhoid toxin (TxWT) or the control toxin (TxHQ) at concentration of 0.1, 1 or 10ng/ml and an absorbance reading taken at either 48hrs or 7 days. Etoposide (3uM) was used as a positive control for cell death and IFNα (0.1ug/ml) was used to trigger an immune response. Each circle represents one biological replicate each consisting of three technical replicates. An average of the absorbances within each biological replicate was taken. The relative absorbance was calculated compared to the untreated control with the control representing 100%. The bars indicate the mean and error bars shown indicate standard deviation (SD). Statistical significance was calculated using a two-way ANOVA with asterisks indicating significance. (n=3)

It remained possible that increased ISGylation was not observed in A549^{USP18} cells. To examine this possibility, A549 cells were immunoblotted for ISG15 and USP18 following no treatment (control) or treatment with IFNα (+IFNα) at 48h, 96h, and 168h (**Fig 8.21**). ISG15 and USP18 were expressed in A549^{WT} and in A549^{USP18}

(USP18-CA) cells. USP18 was present but difficult to detect by immunoblotting. ISGylation was found in A549^{WT} cells but this was substantially increased in A549^{USP18} cells, which was consistent with the faint USP18 bands in A549^{WT} and A549^{USP18} cells. Moreover, ISGylation was maximal at 96h in A549^{WT} and A549^{USP18} cells but was still evident at 168h in A549^{USP18} cells. As expected, ISG15 was not expressed in the A549$^{ISG15-/-}$ cells. This result confirmed that increased ISGylation in response IFNα plays no role in promoting cell survival as observed in the MTT assay above in **Fig 8.19**. Interestingly however, USP18 was not expressed in the A549$^{ISG15-/-}$ cells in the presence of IFNα.

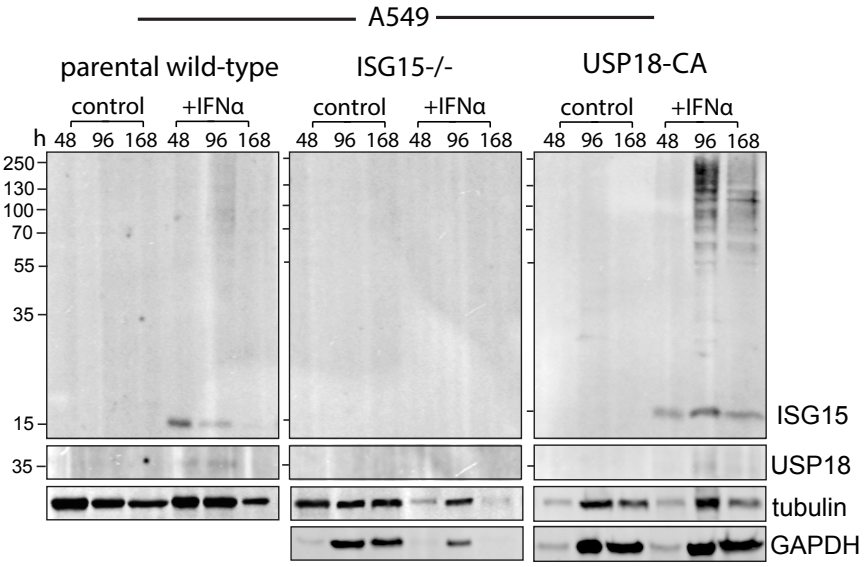

Fig 8.21 IFN-dependent ISG15 expression in A549 wild-type, ISG15-KO and USP18-CA cells. All cells were untreated or treated with IFNα (0.1ug/ml) before generating whole cell lysates at 48h, 96h, or 168h. To observe free ISG15 (15kDa) as well as ISGylation (high MW ISG15-positive conjugate proteins), entire PVDF membranes were immunoblotted with antibodies to ISG15 (indicated right). Antibodies to USP18, and loading controls tubulin and GAPDH were also using in the immunoblotting experiment. MW markers shown on the left in kDa.

The results suggest ISG15 was required for expression of USP18. However, USP18 expression was difficult to detect. Thus, the experiment was repeated in the hope of obtaining more convincing data (**Fig 8.22**). The repeat experiment showed that ISG15 was only expressed in A549^{WT} cells. This time however, USP18 was readily detected as was a higher molecular weight species, which was presumed to be

ubiquitinated USP18 as reported (Honke et al., 2016). In the A549$^{ISG15-/-}$ cells, ISG15 was lost as was USP18, which showed ISG15 drives USP18 expression. A faint USP18 band was observed in A549$^{ISG15-/-}$ cells indicating that alternative mechanisms also promote ISG15 expression though this was predominantly regulated by ISG15.

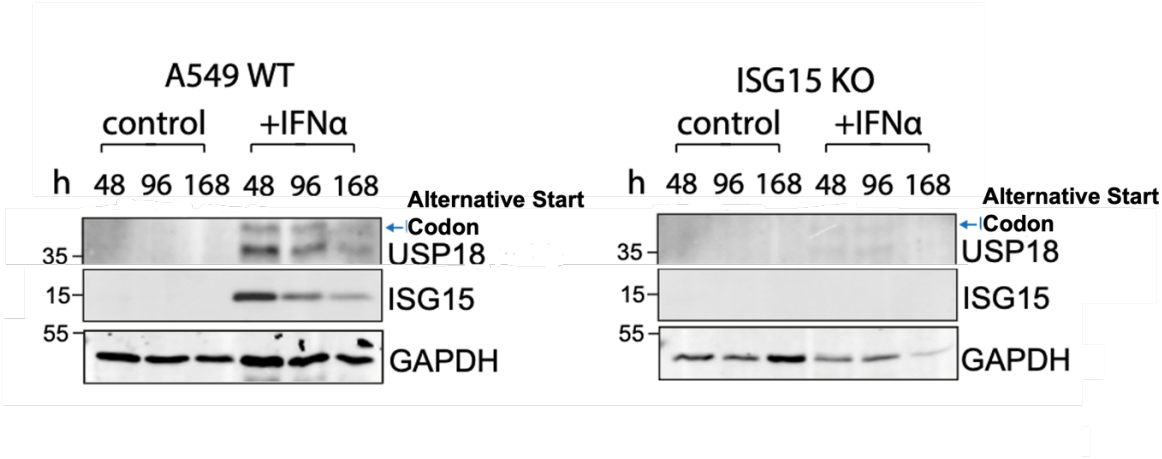

Fig 8.22 **IFNα-driven ISG15-dependent USP18 expression in A549 cells.** Cells were untreated or treated with IFNα (0.1ug/ml) before generating whole cell lysates at 48h, 96h, or 168h. Antibodies to ISG15, USP18, and loading controls GAPDH were used in the immunoblotting experiment (indicated right). Ubiquitinated USP18 indicated with blue text. MW markers shown on the left in kDa.

8.9 IFNα-induced cell death is specific to ISG15-deficient human- and not mouse-derived cells.

ISG15 has been shown to have species-specific roles that rely on interplay with USP18. For example, ISG15 is known to sustain USP18 levels in humans but not mice (Speer et al., 2016). It was shown that ISG15-mediated stabilisation of USP18 was needed for negative regulation of the IFN response while in mice ISG15 was dispensable for USP18 expression and can regulate the IFN response in the absence of ISG15 (Speer et al., 2016). Thus, it was proposed that human A549$^{ISG15-/-}$ cells would be susceptible to IFNα-induced cell death while mouse MEF$^{ISG15-/-}$ cells treated with IFNα would survive due to ISG15-independent control of USP18 expression.

IFNα-induced cell cycle deficiency and cell death A549$^{ISG15-/-}$ cells was apparent during loss of MTT metabolism in **Fig 7.11**. Thus, the MTT assay was initially performed to examine MTT metabolism in IFNα-treated MEF^{WT} and MEF$^{ISG15-/-}$ cells at 48hrs and 7 days **(Fig 8.23)**. MEF^{WT} and MEF$^{ISG15-/-}$ cells lost the ability to metabolise MTT only at relatively high concentrations of typhoid toxin (10ng/ml TxWT), which was best observed at 7 days where ISG15-deficient cells appeared more susceptible to typhoid toxin (right). MEF cells were susceptible to etoposide at both 48h and 7 days. In contrast, MEF^{WT} and MEF$^{ISG15-/-}$ cells were not affected by IFNα at 48hrs or 7 days. This is consistent with the proposed hypothesis that human ISG15-deficient cells undergo cell death due to loss of USP18 expression, which is not observed in mice-derived cells.

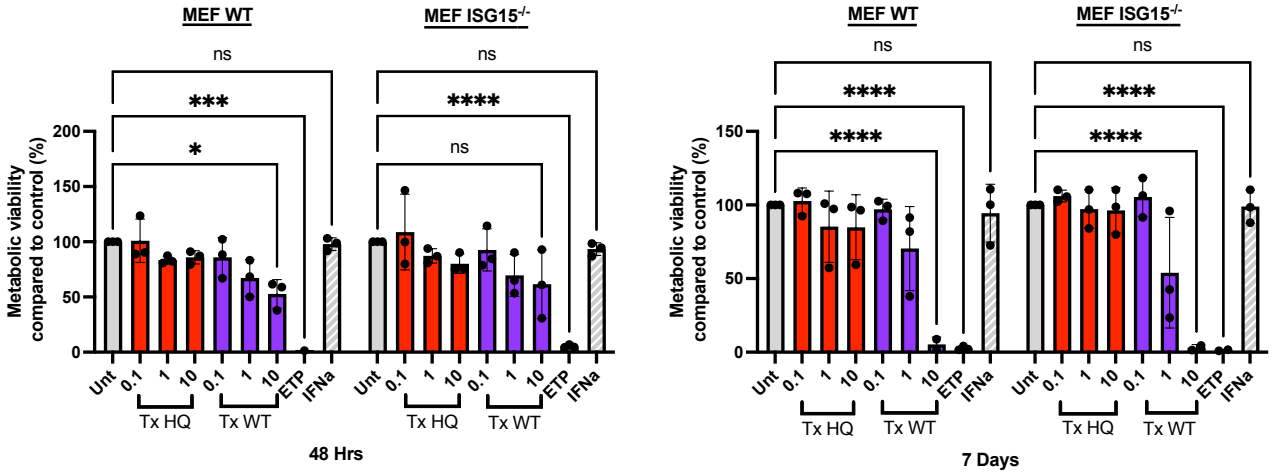

Fig 8.23 **MTT Assay of Intoxicated MEF Cells.** MEF^{WT} and MEF$^{ISG15-/-}$ were treated with either the typhoid toxin (TxWT) or the control toxin (TxHQ) at concentration of 0.1, 1 or 10ng/ml and an absorbance reading taken at either 48hrs or 7 days. Etoposide (3uM) was used as a positive control for cell death and IFNα (0.1ug/ml) was used to trigger an immune response. Each circle represents one biological replicate consisting of three technical replicates. An average of the absorbances within each biological replicate was taken. The relative absorbance was calculated compared to the untreated control with the control representing 100%. The bars indicate the mean and error bars shown indicate standard deviation (SD). Statistical significance was calculated using a two-way ANOVA with asterisks indicating significance. (n=3)

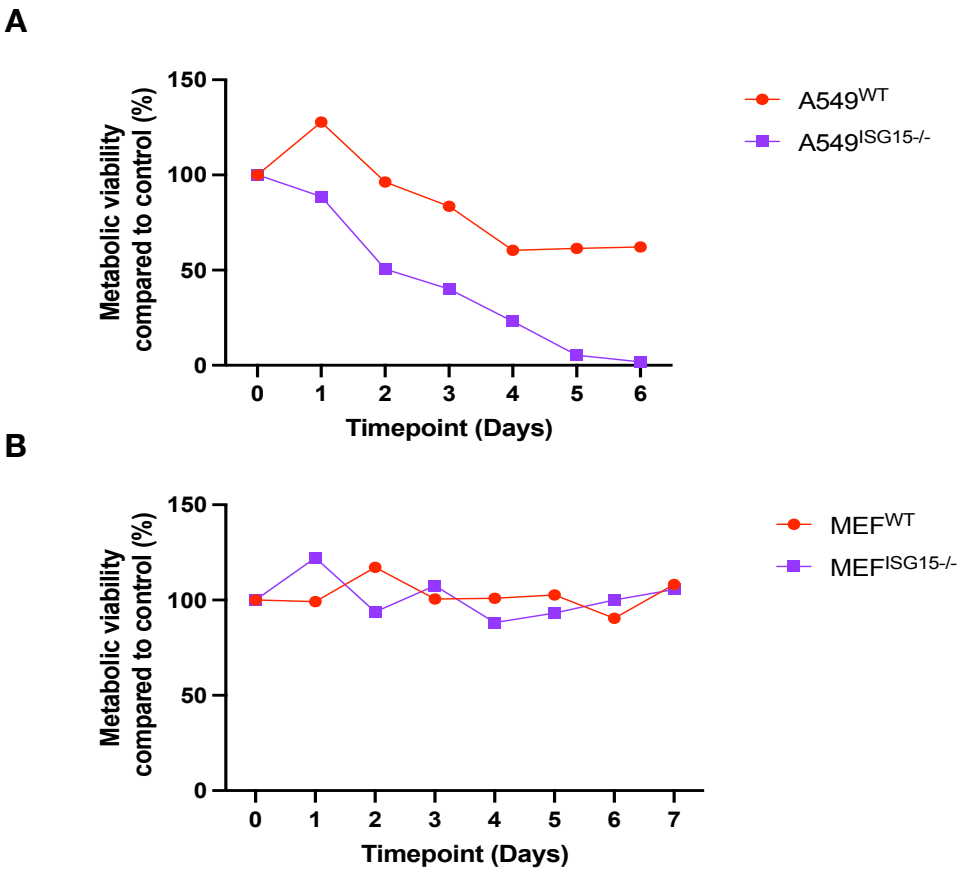

Fig 8.24 **MTT Assay of IFNα treated A549 and MEF Cells.** A549 (A) and MEF (B) cells were treated with 0.1μg/ml IFNα with absorbance readings taken daily from days 1-6 (A549) and days 1-7 (MEFs). Relative compared to an untreated control was calculated. (n=1)

Next, ISG15-deficient human A549 and mouse MEF cells were compared directly following treatment with IFNα each day up to 7 days using the MTT assay **(Fig 8.24)**. Building from **Fig 7.11**, the results with A549$^{ISG15-/-}$ cells showed that IFNα induced loss of MTT metabolism after 48h (day 2), which continued to complete loss of MTT metabolism by day 5 **(Fig 8.24A)**. A549^{WT} cells were also susceptible to IFNα-induced loss of MTT metabolism, which was apparent from 4 days with a 50% reduction. In contrast, IFNα had no effect on MTT metabolism in MEF$^{ISG15-/-}$ cells, which remained equivalent to MEF^{WT}, cells across all 7 days **(Fig 8.24B)**. Unfortunately, attempts to verify the results in MEF cells by immunoblotting by assaying ISG15 and USP18 expression were unsuccessful. Nevertheless, the findings agree with published literature that ISG15 controls USP18 in human, but not mouse, cells.

The slight reduction in MTT metabolism in $MEF^{ISG15-/-}$ cells treated with 1ng/ml typhoid toxin relative to MEF^{WT} cells in **Fig 8.23** prompted further investigation. This result suggests that MEF cells are more resistant to the typhoid toxin compared to A549 cells, but in contrast to A549 cells, MEF cells lose resistance without ISG15 at 7 days.

$A549^{WT}$ and $A549^{ISG15-/-}$ showed similar responses to TxWT with a gradual loss of MTT metabolism over the timepoints with a complete loss by day 6 **(Fig 8.25A)**. This phenotype was replicated across all 3 concentrations of TxWT (0.1ng/ml, 1ng/ml, 10ng/ml). However, the MEF cells showed a different response **(Fig 8.25B)**. Interestingly, both $A549^{WT}$ and $MEF^{ISG15-/-}$ showed increased MTT metabolism at day 1 relative to day 0. At the lowest concentration (0.1ng/ml) MEF^{WT} appeared relatively unaffected by TxWT however, $MEF^{ISG15-/-}$ showed an initial loss of metabolism until day 5 at which the cell population shows signs of recovery. At 1ng/ml, MEF^{WT} showed little difference in MTT metabolism to 0.1ng/ml but $MEF^{ISG15-/-}$ demonstrated loss of metabolism from day 2 and complete loss by day 4 with no sign of recovery, which was indicative of cell death. At 10ng/ml, the highest concentration, $MEF^{ISG15-/-}$ showed a similar response with irrecoverable loss of MTT metabolism at day 3. The MEF^{WT} cells displayed a similar, although more gradual loss of MTT metabolism until day 5 until metabolism increased, suggesting an increase in the number of viable cells. The potential for cell populations to overcome the effects of TxWT and recover is the reason that the experiment length was increased from 6 to 7 days for MEF cells. In summary, ISG15 maintains host survival in response to toxin-induced DDRs in MEF cells but not A549 cells further displaying species-specific roles for ISG15. Unfortunately due to time constraints it was only possible to complete one replicate of this experiment. Given the published literature it is highly likely that further replicates would confirm these results. It would have been interesting to see if the spike in cell metabolic activity observed in both wild-type A549 and MEF cells after 1 day of treatment was replicated.

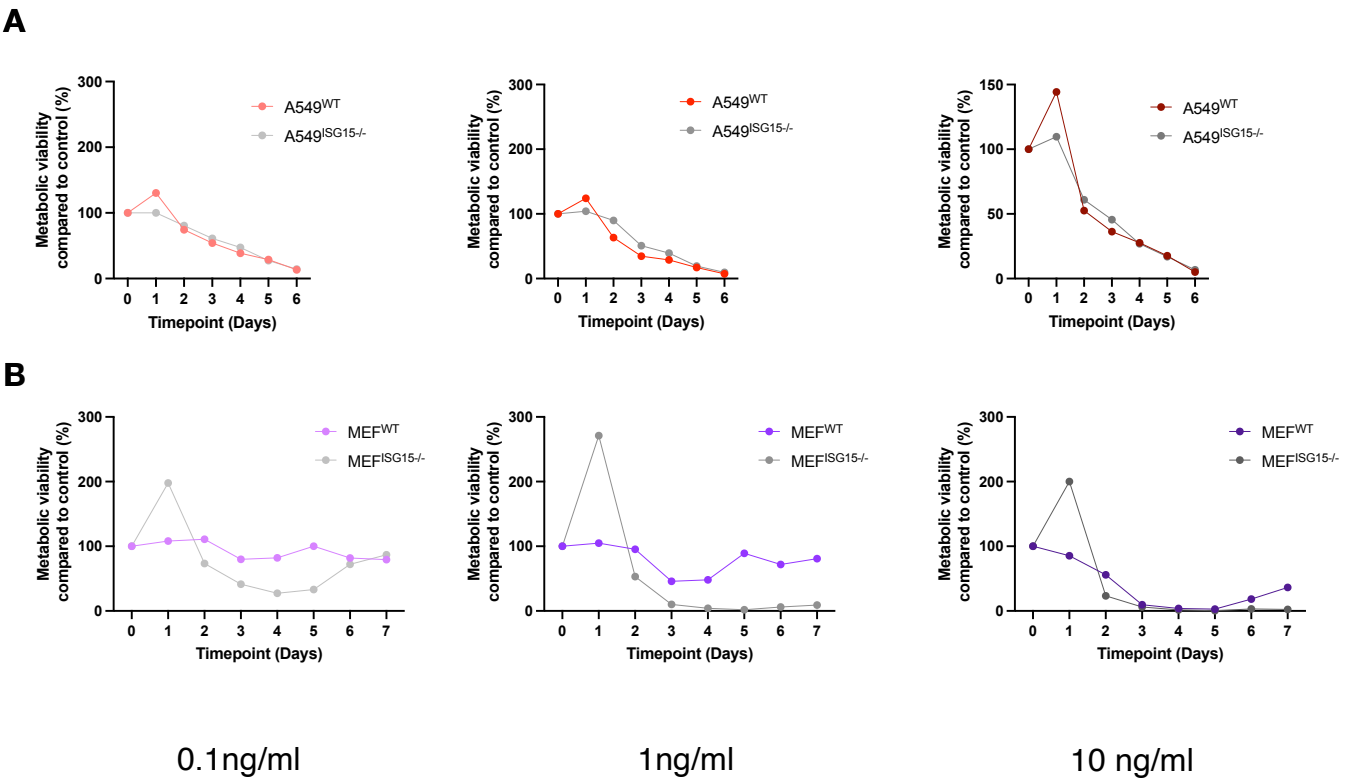

Fig 8.25 **MTT Assay of TxWT Induced Cell Death.** A549 (A) and MEF (B) cells were intoxicated with TxWT with an MTT assay conducted every 24hrs from day 1 to day 6/7 to determine cell death. The absorbance relative to the untreated control was calculated and plotted. (n=1)

8.10 USP18 is the Driving Force behind Apoptosis in Response to IFNα.

There is a clear relationship between ISG15 and USP18 however it is not yet clear if ISGylation is crucial in preventing apoptosis when activated by IFNα, or whether apoptosis is driven by USP18 independently of ISGylation. To try and answer this question, it was decided to target different parts of the pathway and determine the effects on cell survival (depicted in the illustration **Fig 4.1**). To block ISGylation, but not ISG15-independent roles of USP18, MTT metabolism was quantified in A549^{WT} cells treated with IFNα for 7 days following transfection with siRNA to the E1 enzyme UBE1L (i.e. ISGylation-disabled conditions). In parallel, the same experiment was performed in cells transfected with siRNA to USP18, which would block ISGylation but not interfere with free ISG15 (i.e. ISG15-competent/USP18-deficient conditions).

Cells were also treated with ISG15 siRNA as a control to phenocopy the effects observed in ISG15-deficient A549 cells (i.e. ISG15-/USP18-deficient conditions).

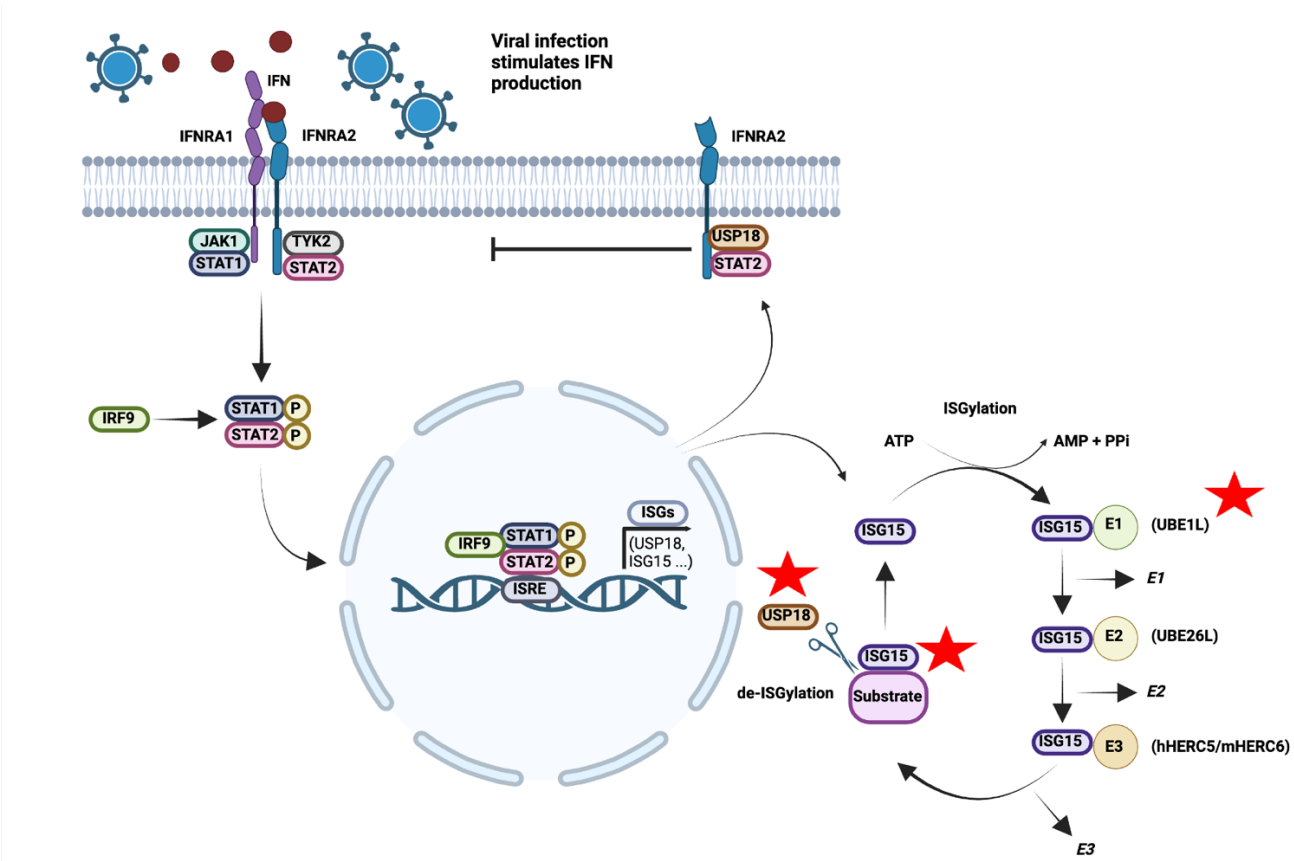

Fig 8.26 **siRNA Knockdown of ISGlyation and USP18.** SiRNAs were used to knockdown expression of USP18, ISG15 and UBE1L. This would help determine if apoptosis occurred after IFNα treatment due to loss of ISGlyation or some other part of the JAK/STAT pathway.

As expected, IFNα-treated A549 cells transfected with a non-targeting siRNA ($WT^{NT\ siRNA}$) showed no significance difference to untreated as MTT metabolism remained at ~100% at the 7-day point **(Fig 8.27A)**. The $ISG15^{siRNA}$ showed some loss of MTT metabolism (~40%) but did not show the complete loss in metabolism displayed by $A549^{ISG15-/-}$ (ISG15-/-). This is perhaps explained by the presence of USP18 in immunoblotting experiments (**Fig 8.27B**) indicating further optimisation of ISG15 is required or that the transfection process has activated ISG15-independent expression of USP18. $USP18^{siRNA}$ however, closely mirrored $A549^{ISG15-/-}$ with a significant loss of ~80% MTT metabolism. No significance was found in the $UBE1L^{siRNA}$ after IFNα treatment. ISG15, USP18 and UBE1L knock-down were investigated in parallel by immunoblotting **(Fig 8.27B).** Immunoblotting showed that there was no ISG15 or USP18 expression after their respective siRNA transfections. Loss of the de-ISGylation enzyme USP18 resulted in increased ISGylation. In support of this observation, increased ISGylation was also observed by immunoblotting in IFNα-treated $A549^{WT}$ cells (**Fig 8.26B**). UBE1L was not detected and though no firm conclusion can be drawn as to its contribution, the lack of ISGylation may indicate loss of UBE1L. Taken together, the result shows that cell survival was likely dependent on USP18 activities independent of ISG15.

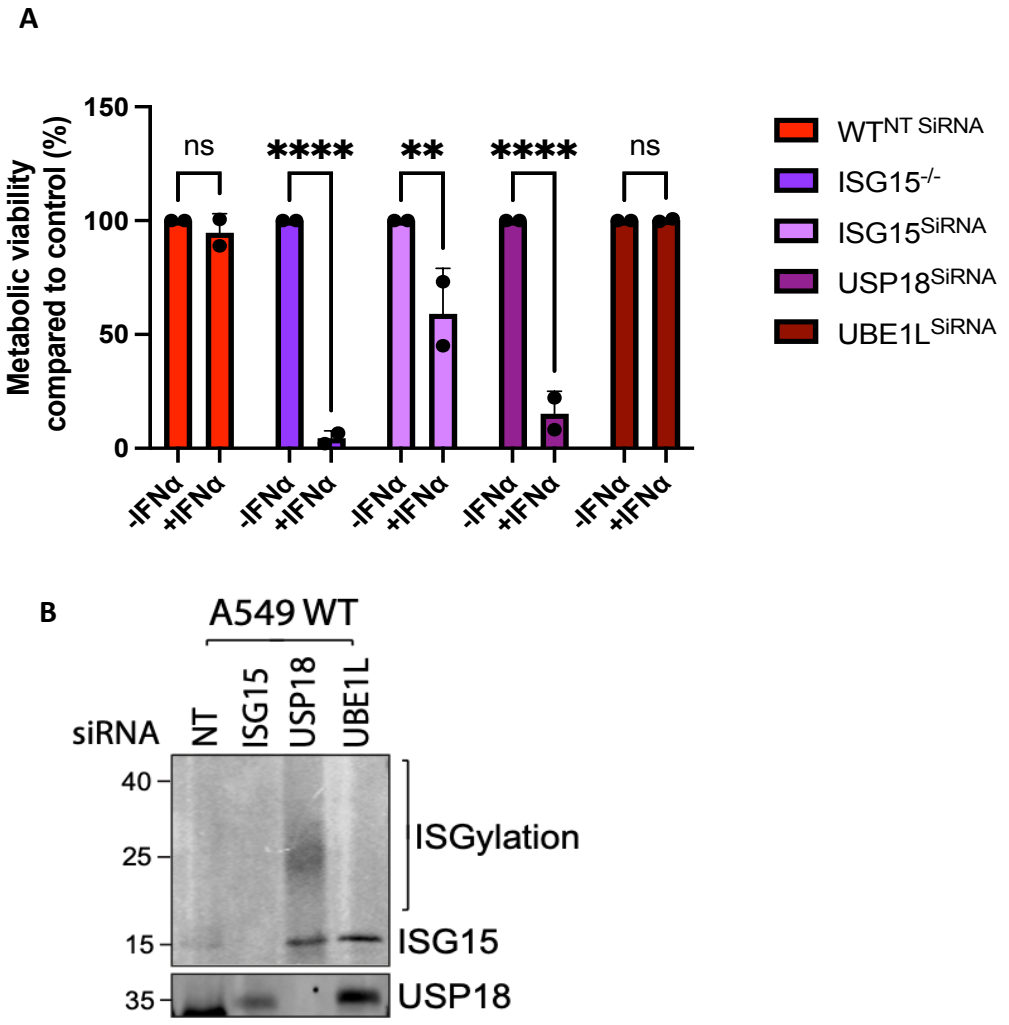

Fig 8.27 **MTT Assay of siRNA Knockdowns.** (A) MTT assay of SiRNAs in A549^{WT} cells. IFNα (0.1ug/ml) was added 24hrs post transfection and the MTT assay conducted after 7 days of treatment. Each circle represents one biological replicate comprising of three technical replicates. Relative absorbance was calculated compared to the -IFNα control and statistical significance determined by two-way ANOVA. (B) Immunoblot of ISG15 and USP18 expression to validate effectiveness of the knockdowns. Cells were either non-targeting (NT) siRNA or transfected with siRNA to ISG15, USP18 or UBE1L for 48h prior to preparation of whole cell lysates. Antibodies to ISG15 and USP18 were used in the immunoblotting experiment (indicated right). Immunoblotting with antibodies to UBE1L and the loading control GAPDH were unsuccessful (not shown). ISGylation indicative of ISG15 and USP18 activity is indicated right. MW markers shown on the left in kDa. (n=2)

To try and prove that cells rely on USP18 for cell survival after activation of the interferon pathway, an USP18-rescue was attempted in ISG15-deficient cells. This was attempted by transfecting cells with a mammalian plasmid expressing USP18 (Flag-HA-USP18 plasmid - #22572, Addgene). As a first step, transfection was performed in A549^{WT} cells along with transfection with an empty vector (pHCMV) as

a control. The plasmids were transfected following a similar protocol to the siRNA transfection and with the cells also treated with IFNα for 7 days. Any restoration of cell viability was assessed by MTT assay **(Fig 8.28)**.

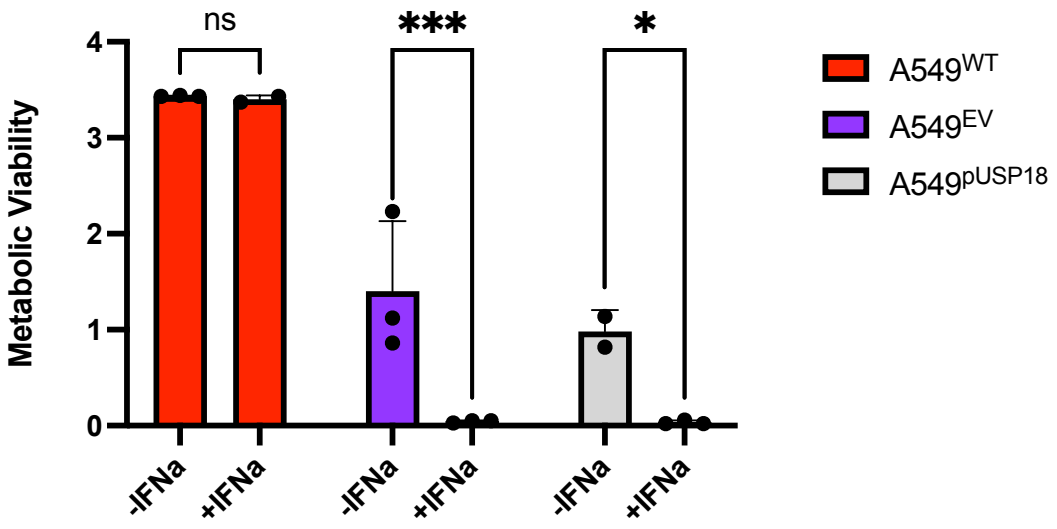

Fig 8.28 **MTT Assay of USP18 Plasmid Insertion into A549 wild type Cells.** A Flag-HA-USP18 plasmid was transfected into A549^{WT} cells. As a negative control, an empty vector (pHCMV) was also transfected. Cells were then subjected to IFNα (0.1μg/ml) for 7days. An MTT assay was then conducted. Each circle represents one technical replicate. Absorbance was plotted compared to the -IFNα control. Statistical significance was determined by two-way ANOVA. (n=3)

Unfortunately, despite several attempts at optimisation the plasmid transfection was found to be too harsh for cells to survive and even transfected cells without the added stress of IFNα suffered a loss of ~70% loss of MTT metabolism compared to A549^{WT}. Neither A549^{EV} or A549^{pUSP18} showed any signs of recovery and thus this investigative angle was not continued with at the late stage of the PhD studies.

8.10 ISG15-mediated suppression of USP18 deregulates ISG expression

ISG15 has been shown to regulate ISG expression via control of USP18 and the absence of ISG15 leads to an enhanced IFN response due to low levels of USP18 (Zhang et al 2014). Thus, ISGs MAVS, IFIT1, and AIM2 were examined alongside ISG15 and USP18 in A549^{WT} and A549$^{ISG15-/-}$ cells following treatment with IFNα (**Fig**

8.29). These proteins were of interest as ISG15 is a downstream effector of MAVS (Mitochondrial anti-viral signalling) and activation of the RIG-I/MAVS pathway during viral infection leads to an upregulation of ISG15 (Zhang et al., 2024). IFIT1 (Interferon induced protein with tetratricopeptide repeats 1) was shown to be highly upregulated in response to TxWT in the microarray data **(Fig 7.5)**, but also plays a role in the antiviral response and its expression is increased by ISGlyation (Kespohl et al., 2020).

Immunoblotting confirmed that ISG15 was expressed in A549^{WT} cells in the presence of IFNα only, which coincided with USP18 expression (**Fig 8.29A**). Neither ISG15 nor USP18 were observed in A549$^{ISG15-/-}$ cells. In contrast, ISGs MAVS, IFIT1 and AIM2 were expressed in untreated (-) A549^{WT} cells, and their expression was increased with IFNα. The same trend was observed in A549$^{ISG15-/-}$ cells albeit slightly lower expression of MAVS, IFIT1 and AIM2 was observed in untreated (-) and IFNα-treated cells. Due to the subtle changes in ISG expression, immunoblotting of A549^{WT} and A549$^{ISG15-/-}$ cells was repeated in the presence of IFNα or its absence (control) at 48h, 96h, or 168h to increase the likelihood of observing a difference (**Fig 8.29B, 8.29C**). However, the same trend was observed for MAVS with very little difference between A549^{WT} and A549$^{ISG15-/-}$ cells. In contrast, it was clear that IFIT1 expression was reduced during IFNα responses in A549$^{ISG15-/-}$ cells (**Fig 8.29B, 8.29C**).

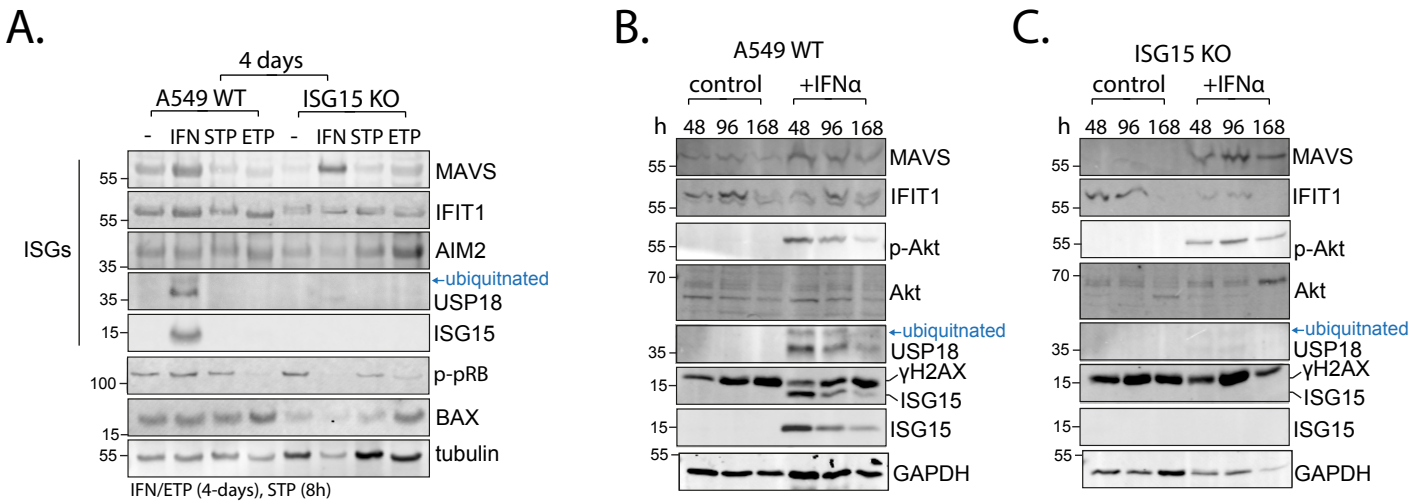

Fig 8.29 **Immunoblots of ISGs and Markers of Replication Stress.** (A) Expression of proteins in A549^{WT} and A549I$^{SG15-/-}$ after 96hrs of treatment with IFNα (0.1ug/ml). STP and ETP were used as controls for DNA damage and apoptosis with tubulin used as a loading control for the immunoblot. (B A549^{WT} were treated as for (A) but with protein expression detected at 48, 96 and 168hrs. (C) The same experiment as (B) but with A549$^{ISG15-/-}$ cells.

In parallel, the ISGs were examined in response to etoposide and the inducer of apoptosis staurosporine (**Fig 8.29A**). This provided an opportunity to examine cell cycle progression with phosphorylated RB (i.e. IFNα vs etoposide) and apoptosis by examining BAX (i.e. IFNα vs staurosporine). BAX is increased during p53-mediated apoptosis and was upregulated during macrophage apoptosis of IFNα-treated macrophages (Waqas et al 2022).

Phosphorylated RB (p-Rb) was observed in untreated (-) A549^{WT} and A549$^{ISG15-/-}$ cells showing cell cycle progression, which was unchanged during IFNα responses in A549^{WT} cells. In contrast, p-Rb was reduced in A549$^{ISG15-/-}$ cells indicating cell cycle arrest, which was equivalent to that observed with known DDR-inducer ETP (**Fig 8.29A**). When BAX was examined, there was no change in A549^{WT} cells regardless of treatment (**Fig 8.29A**). However, BAX was suppressed in untreated (-), IFNα- or STP-treated A549$^{ISG15-/-}$ cells, and only increased with ETP. BAX is a known mediator of apoptosis upregulated by p53 (Reyna and Gavathiotis, 2016). Thus, suppression of BAX agrees with defective p53 signalling observed by microscopy in **Fig 7.8**.

The data indicates that IFNα-treated A549$^{ISG15-/-}$ cells undergo apoptosis in a manner independent of p53. Recently, ISG15-deficient macrophages were found to elicit apoptosis via reduced phosphorylation of the survival kinase AKT (Waqas et al 2022,). Thus, phosphorylation of AKT (p-AKT) was examined during IFNα treatment of A549$^{ISG15-/-}$ cells (**Fig 8.29B, 8.29C**). Relative to A549^{WT} cells, IFNα treatment in A549$^{ISG15-/-}$ cells induced elevated γH2AX, particularly at 96h, indicating cell stress in the absence of ISG15. Nevertheless, no differences in p-AKT were observed between A549^{WT} and A549$^{ISG15-/-}$ cells.

From the immunoblot MAVS was expressed at a low level in both the control and +IFNα conditions across all time points with a slight increase in expression with +IFNα (**Fig 8.29B, 8.29C**). A similar result was produced for IFIT1. With A549$^{ISG15-/-}$ there was no expression of MAVS in the untreated control, but strong expression

with +IFNα when compared to A549^{WT}. With IFIT1 there was expression at 48 and 96hrs, but this was lost by 168hrs.

AKT is a survival kinase whose phosphorylation of AKT was was lost in apoptotic ISG15-deficient macrophages (Waqas et al 2022). Expression of phosphorylated Akt (p-Akt) was only induced by IFNα and was not present in the untreated control (**Fig 8.29B, 8.29C**). The levels of p-Akt were similar between A549^{WT} and A549$^{ISG15-/-}$. Both cell lines showed low levels of p-Akt across all timepoints in the untreated and +IFNα, however there did appear to be stronger phosphorylation with A549$^{ISG15-/-}$ in response to IFNα at 168hrs.

Taken together, these results indicate that MAVS expression can occur independently of ISG15 after activation by IFNα whereas IFIT1 expression is lost in ISG15 deficient cells under the same conditions. Phosphorylation of Akt is triggered by IFNα but is unaffected by ISG15 status, however p-Akt is sustained in ISG15 deficient cells.

8.11 ISG15 deregulates other IFN Associated Proteins.

Finally, given that ISG15 has multiple functions in the cell and that deficiency has been shown to have serious and wide-ranging consequences to health, it was decided to explore if loss of ISG15 impacts other parts of the JAK/STAT pathway and the expression of other related proteins.

The expression of STAT1 (Signal transducer and activator of transcription 1) and AIM2 (Interferon-inducible protein AIM2) was explored, this time by immunofluorescence. STAT1 is one of the earliest mediators of the interferon response and triggers the transcription of hundreds of ISGs. Deficiency of STAT1 leaves cells unable to defend against infection and is vital in the antiviral response (Tolomeo et al., 2022). AIM2 is a cytostolic DNA sensor which detects microbial DNA and sheared DNA resulting from DNA damage. Upon activation it assembles the

AIM2 inflammasome, resulting in inflammation and innate immune responses (Kumari et al., 2020, Lammert at al., 2020).

STAT1 was not detected in the untreated controls and upregulation was not triggered by TxWT in either A549^{WT} or A549$^{ISG15-/-}$ **(Fig 8.30)**. Not surprisingly STAT1 was detected after activation by IFNα in A549^{WT} via the interferon response. However, STAT1 expression was lost in all treatments with A549^{ISG15} suggesting ISG15 may have a stabilising role outside of ISGlyation.

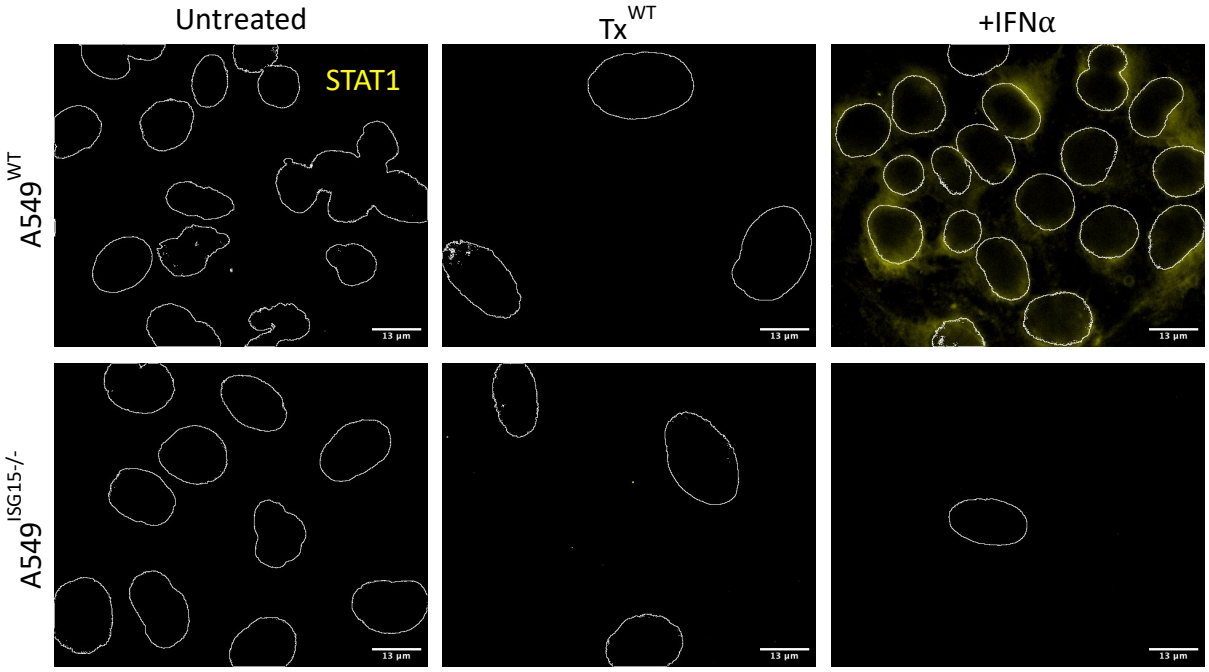

Fig 8.30 **Expression of STAT1 in Intoxicated A549 Cells.** A549WT and A549ISG15-/- cells were intoxicated with TxWT (0.1ng/ml) and IFNα (0.1ug/ml) for 96hrs. STAT1 expression (yellow) was detected using immunofluorescence. Images were taken on a Nikon Widefield Live Cell System at x40 magnification. Nuclei were outlined in greyscale during processing. Scale bar = 13uM.

AIM2 gave a similar result although some cells showed AIM2 expression in the untreated A549^{WT} **(Fig 8.31)** This is not entirely unexpected as within a normal proliferating cell population some cells may incur DNA damage leading to AIM2 activation. Surprisingly, TxWT did not induce AIM2 expression for either A549^{WT} or A549$^{ISG15-/-}$. It could be that as has been previously shown that toxin-induced senescent cells have suppressed AIM2 expression. AIM2 was strongly induced in response to IFNα in A549^{WT} demonstrating a link between the AIM2 inflammasome and activation of the interferon pathway but this was absent in A549$^{ISG15-/-}$ cells.

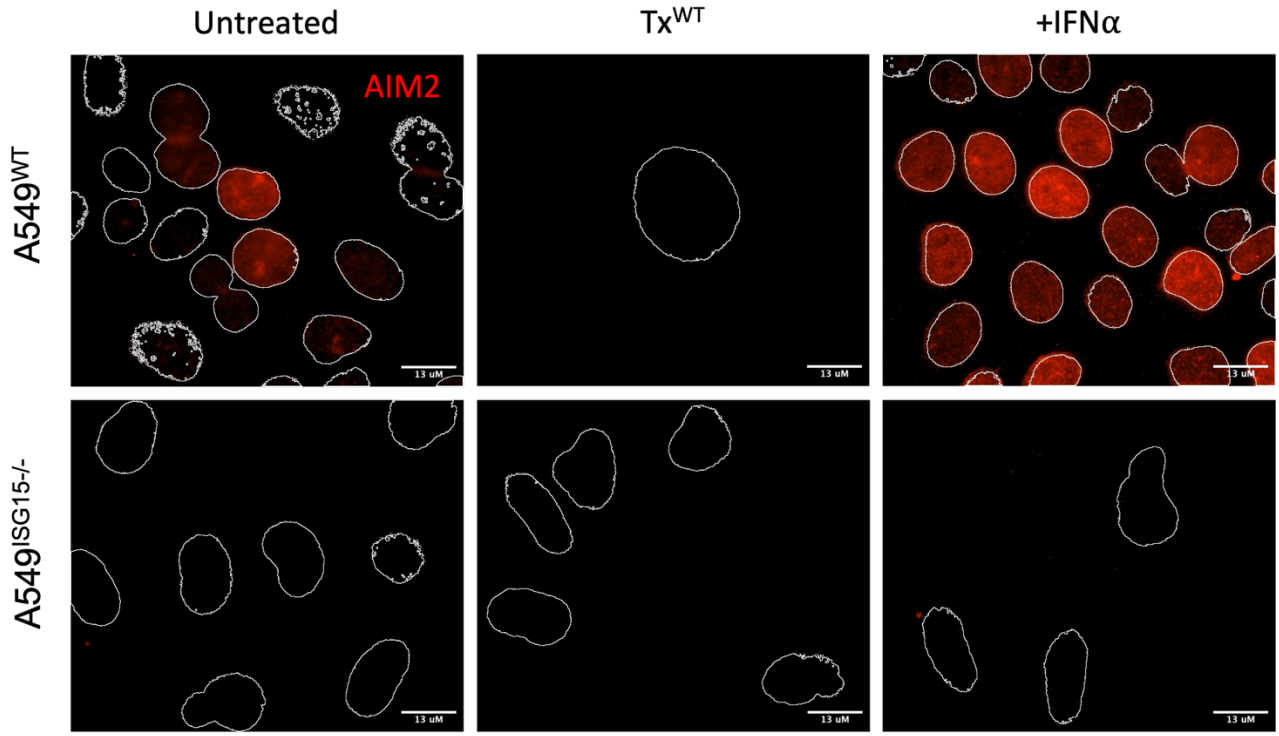

Fig 8.31 **Expression of AIM2 in Intoxicated A549 Cells.** A549WT and A549ISG15-/- cells were intoxicated with TxWT (0.1ng/ml) and IFNα (0.1ug/ml) for 96hrs. AIM2 expression (red) was detected using immunofluorescence. Images were taken on a Nikon Widefield Live Cell System at x40 magnification. Nuclei were outlined in greyscale during processing. Scale.bar = 13uM.

Finally, it was decided to determine if ISG15 affects the effectiveness of the SUMO (Small ubiquitin-related Modifier) pathway. This pathway is able to alter ISG restriction factors and JAK/STAT signalling (El-Asmi et al., 2020). IFNα results in an increase in both ISGlyation and SUMOylation although the exact relationship between the two is not entirely clear (Chelbi-Alix & Thibault, 2021).

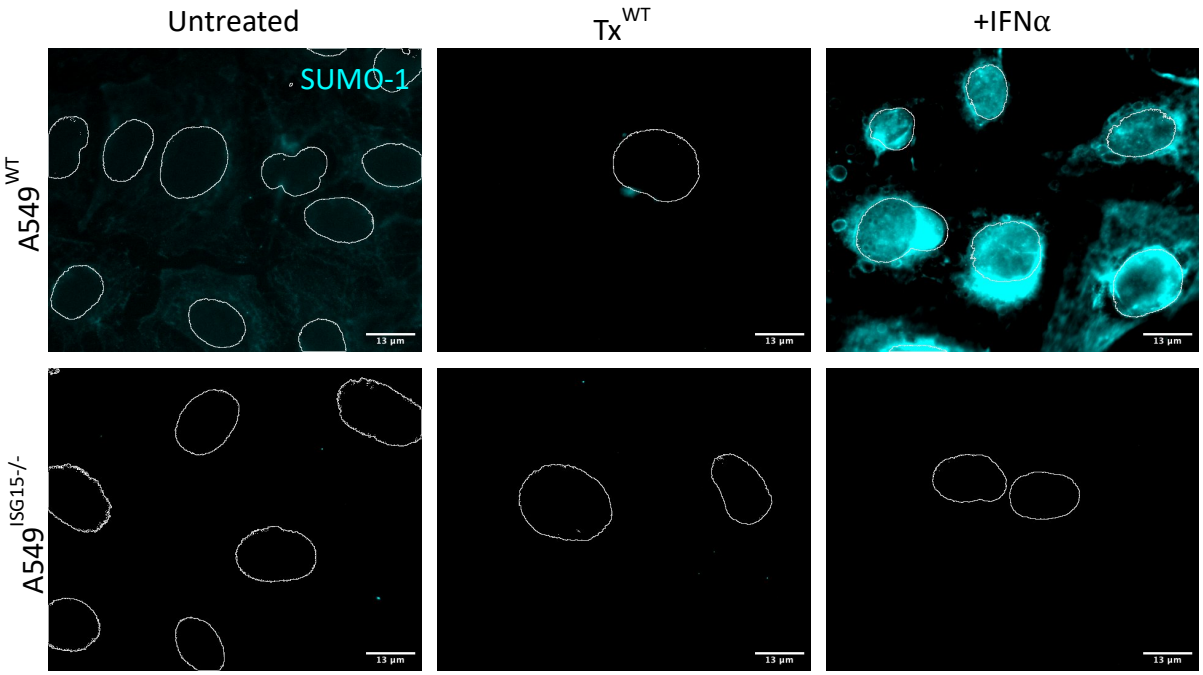

Fig 8.32 **Expression of SUMO-1 in Intoxicated A549 Cells.** A549WT and A549ISG15-/- cells were intoxicated with TxWT (0.1ng/ml) and IFNα (0.1ug/ml) for 96hrs. SUMO-1 expression (cyan) was detected using immunofluorescence. Images were taken on a Nikon Widefield Live Cell System at x40 magnification. Nuclei were outlined in greyscale during processing. Scale bar = 13uM.

SUMO-1 (a component of the SUMO pathway) was expressed at low levels in A549^{WT} untreated cells however, as SUMOylation is involved in an extensive number of cellular processes (Friedlander & Melchior, 2007) this is not unexpected **(Fig 8.32)**. Again, TxWT did not induce expression of SUMO-1 in either A549WT or A549$^{ISG15-/-}$. SUMO-1 was strongly expressed in response to IFNα in A549^{WT} but not in A549$^{ISG15/-}$ suggesting that ISG15 deficiency curtails crosstalk between ISGlyation and SUMOylation.

These results were compared to the results of the RNA seq analysis. The expression of genes associated with the JAK/STAT pathway was compared between A549^{WT} untreated and those stimulated with IFNα **(Fig 8.33)**. Upregulation was found in STAT1 and STAT2, the key mediators in the interferon response (Yeung, Mandhana and Horvath, 2013). IRF7 was also highly expressed. This is triggers further production of IFNα and is crucial for its regulation in infection (Ning, Pagano and Barber, 2011). Upregulation of USP18 and HERC5 demonstrated active ISGlylation occurring. In contrast, when comparing differential expression in A549$^{ISG15-/-}$ to

A549^{WT} after IFNα treatment, it was found that AIM2 was highly upregulated with an 8.31-fold-change when compared to A549^{WT} indicating extensive DNA damage. This contrasts with the immunofluorescence data which would have predicted no AIM2 expression. No significant difference was found in the expression of STAT1 or SUMO, suggesting these effects may only occur at the protein level, ISGlylation was also shown to occur through USP18/HERC5 activation. Finally, upregulation was shown in member of the SOCS family which negatively regulate the JAK STAT pathway and SMAD1/7 which can also inhibit the JAK STAT pathway to modulate the TGF-β (transforming growth factor beta) pathway. The TGF-β pathway is involved in a number of biological processes such as cell proliferation and apoptosis. This result suggests that in the absence of ISG15 and upon detection of DNA damage, attempts are made to down regulate the JAK STAT pathway to promote cell survival.

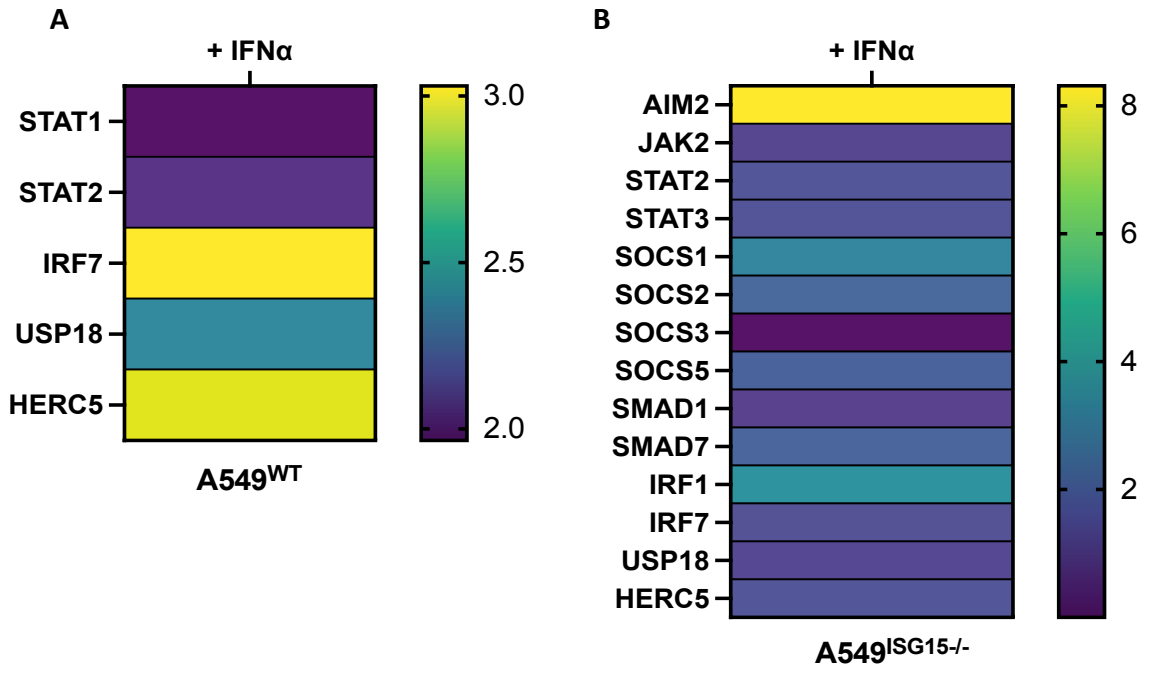

Fig 8.33 **Differential expression in A549 cell in response to IFNα.** (A) Upregulation of genes associated with the JAK/STAT pathway in A549^{WT} (+) IFNα compared to the untreated control. (B) Upregiulation of genes in the JAK/STAT pathway in A549$^{ISG15-/-}$ to A549^{WT} after both were treated with IFNα. In both (A) and (B) the fold change was visualised in a heat map using GraphPad Prism.

Chapter 9: ISG15 Deficiency and *Salmonella* Enterica Infection

9.1 Introduction

ISG15 deficiency has been implicated in the manifestation of human disease such as necrotizing skin lesions (Martin-Fernandez et al., 2020, Waqas et al., 2022, Malik et al., 2022) and intracranial calcification (Zhang et al., 2015). Dysregulation of ISG15 expression and ISGlyation has also been linked to a number of cancers, in particular those of the digestive system (Zu et al., 2016). Indeed, some evidence of this was found through the RNA Seq analysis. Novogene provides a file of differentially expressed genes associated with human disease. The most highly upregulated gene in A549$^{ISG15-/-}$ cells in response to intoxication with the Typhoid toxin was CSMD2 (CUB and Sushi multiple domains 2) which controls the complement cascade of the immune system and acts as a tumour suppressor in colorectal cancer. The data was then processed by selecting genes showing at least a two-fold change in expression and then further filtered by listing those annotated with terms like “colorectal carcinoma” and “colorectal neoplasms”. A comparison in expression was then made between genes that were appeared in the gene list for both Typhoid toxin intoxication and cells treated with IFNα.

A549$^{ISG15-/-}$ cells showed at least a two-fold upregulation of a number of genes associated with colorectal cancer when compared to A549^{WT} **(Fig 9.1)**. This was true in both the untreated and TxWT conditions, but treatment with IFNα showed a marked increase in expression of PRRX1 (paired related homeobox 1), which is important for tumour progression, (Du et al., 2021) and WISP1 (WNT1-inducible-signaling pathway protein 1), which promotes cell proliferation and invasion, as well as acting as an indicator of clinical prognosis in colon cancer (Tao et al., 2020)

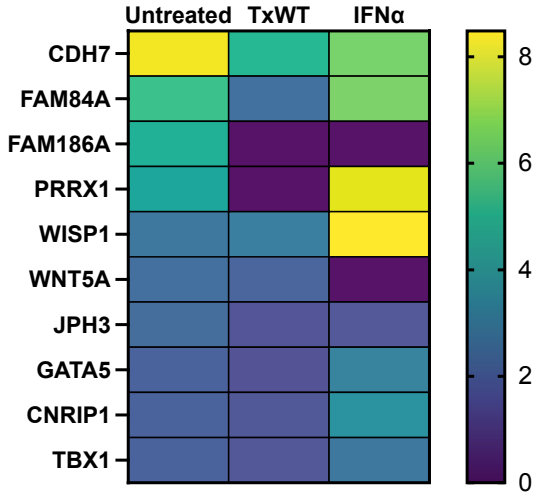

Fig 9.1 **Upregulation of Colorectal Associated Genes in ISG15-deficient A549 Cells.** After treatment with TxWT (0.1ng/ml) or IFNα (0.1ug/ml) RNA seq analysis was conducted. The heat map shows at least two-fold upregulation of colorectal associated genes in untreated A549$^{ISG15-/-}$ vs untreated A549^{WT} along with subsequent expression after treatment with TxWT or IFNα.

The links between ISG15 deficiency and viral infection have been extensively researched (Lenschow et al., 2007, Zhao et al., 2010, Liu et al., 2022, Sarkar et al., 2023). Although ISG15 deficiency is an extremely rare autoinflammatory condition, patients deficient in ISG15 have shown an increased susceptibility to mycobacterial infection (Bogunovich et al., 2012). However, significantly less research has been conducted into how ISG15 deficiency affects infection by *Salmonella enterica*, and even less into infection by toxigenic bacteria such as *Salmonella enterica* serovar Javiana (henceforth *S.* Javiana).

9.2 Host Responses to Toxigenic and Non-Toxigenic *Salmonella*

To begin with it was decided to determine how host cells would respond to different serovars of *Salmonella enterica*. This was achieved by infecting wild type HT1080 cells (HT1080^{WT}) for 96h with *S.* Javiana, a non-typhoidal serovar of *Salmonella enterica* that produces the typhoid toxin. A non-toxigenic mutant (*S.* Javiana$^{\Delta cdtB}$) was used as a control to identify toxin specific phenotypes. In addition, purified TxWT and TxHQ (20ng/ml) was used as positive controls for *Salmonella*-induced

toxicity. Non-toxigenic serovars were used as additional controls: non-typhoidal *Salmonella* (NTS) strain *S*. Typhimurium ST19 (sequence type 19) and invasive NTS (iNTS) strain *S*. Typhimurium ST313 were used to infect HT1080 cells in parallel.

In the untreated control, there was low level production of γH2AX in the untreated HT1080^{WT}, which corresponded with a lack of the p53 effector p21 **(Fig 9.2)**. In the absence of p21, HT1080 cells replicated their genome marking progression of the cell cycle as indicated by EdU incorporation **(Fig 9.2)**. In contrast, there was an increase in γH2AX during infection with ST19 and to a lesser extent with ST313, which indicate increased DNA damage **(Fig 9.2)**. However, despite higher levels of γH2AX with ST19 infection, this did not correlate to cell cycle arrest as only a few cells showed strong upregulation of p21 and there was only a slight reduction in EdU incorporation compared to the untreated control. Conversely, HT1080^{WT} infected with ST313 showed only slight upregulation of γH2AX and p21, however incorporation of EdU was not detected at all suggesting cell cycle arrest. In summary, ST19 and ST313 inhibit cell cycle progression, which was independent of p21 and therefore p53 activity.

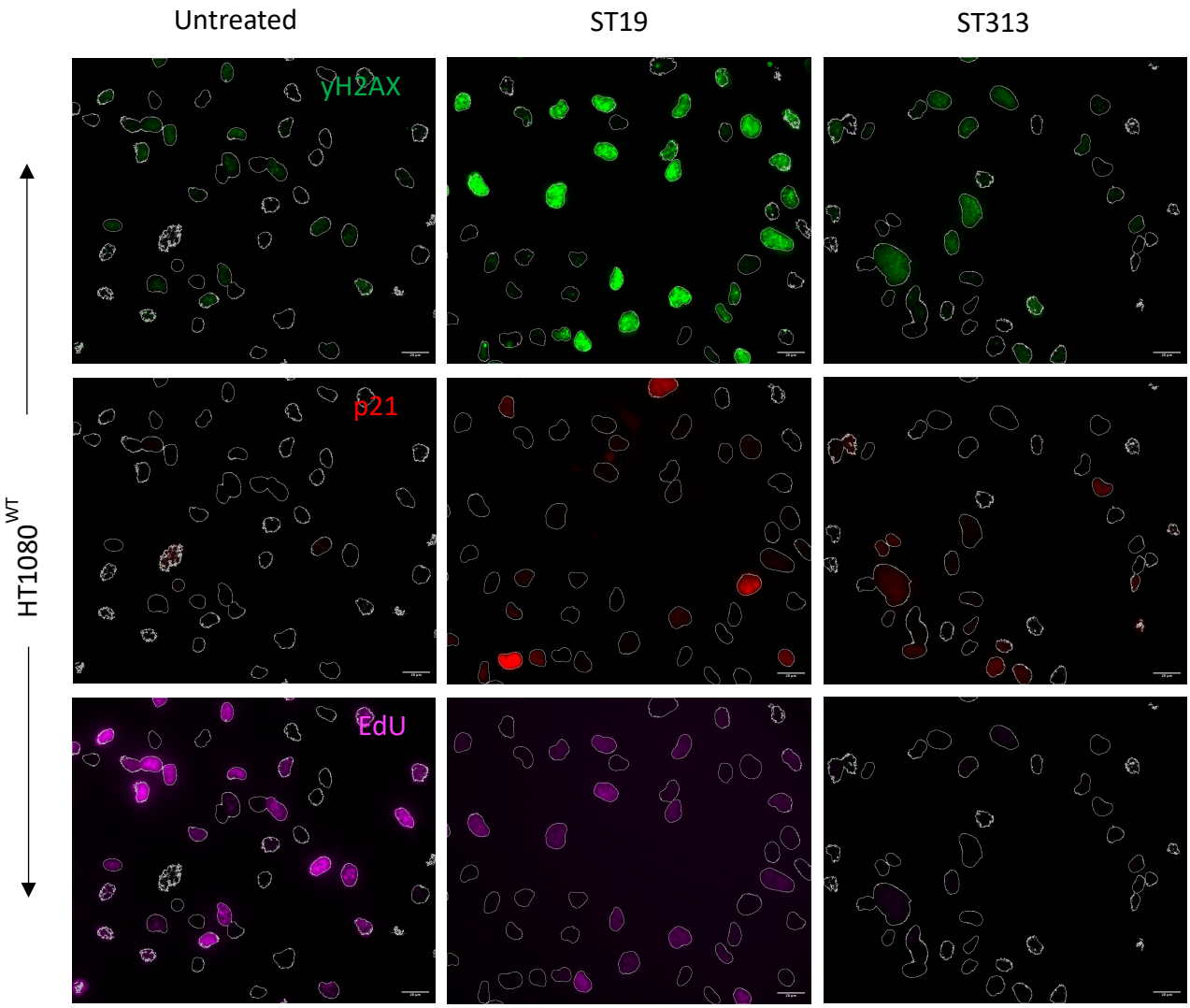

Fig 9.2 **Immunofluorescence of Non-toxigenic *Salmonella* Infection.** HT1080 cells were either untreated, or infected for 30 minutes with non-toxigenic *Salmonella* serovars ST19 and ST313 (MOI 20) followed by incubation for a further 96h in gentamicin-containing media, an antibiotic that cannot penetrate cells allowing assessment of intracellular infections. EdU (magenta) was added to living cells for the last 2h of infection prior to fixation with PBS 4% paraformaldehyde. At 96h, fixed cells were stained with antibodies to γH2AX (green) and p21 (red). Cells were imaged on a Nikon Widefield Live Cell System at x20 magnification. DAPI-stained nuclei outlined in greyscale during processing in Fiji.

Next HT1080^{WT} was treated with purified TxWT or TxHQ to determine the effects of the typhoid toxin **(Fig 9.3)**. Relative to untreated and TxHQ controls, the difference in TxWT-treated cells was immediately clear as there were noticeably fewer cells imaged and the surviving cells were distended. Not only was there an increase in γH2AX compared to the controls, but phosphorylation of γH2AX led to the formation of nuclei foci (i.e. micronuclei) **(Fig 9.3)**, indicating lethal levels of replication stress

(Moeglin et al., 2019, Noubissi at el., 2021). This was accompanied by strong expression of p21 and a complete loss of EdU showing cell cycle arrest has occurred. Toxin-induced p21 expression contrasted to TxHQ, which was equivalent to control. Thus, the toxin causes p21-mediated cell cycle arrest via toxin nuclease activity.

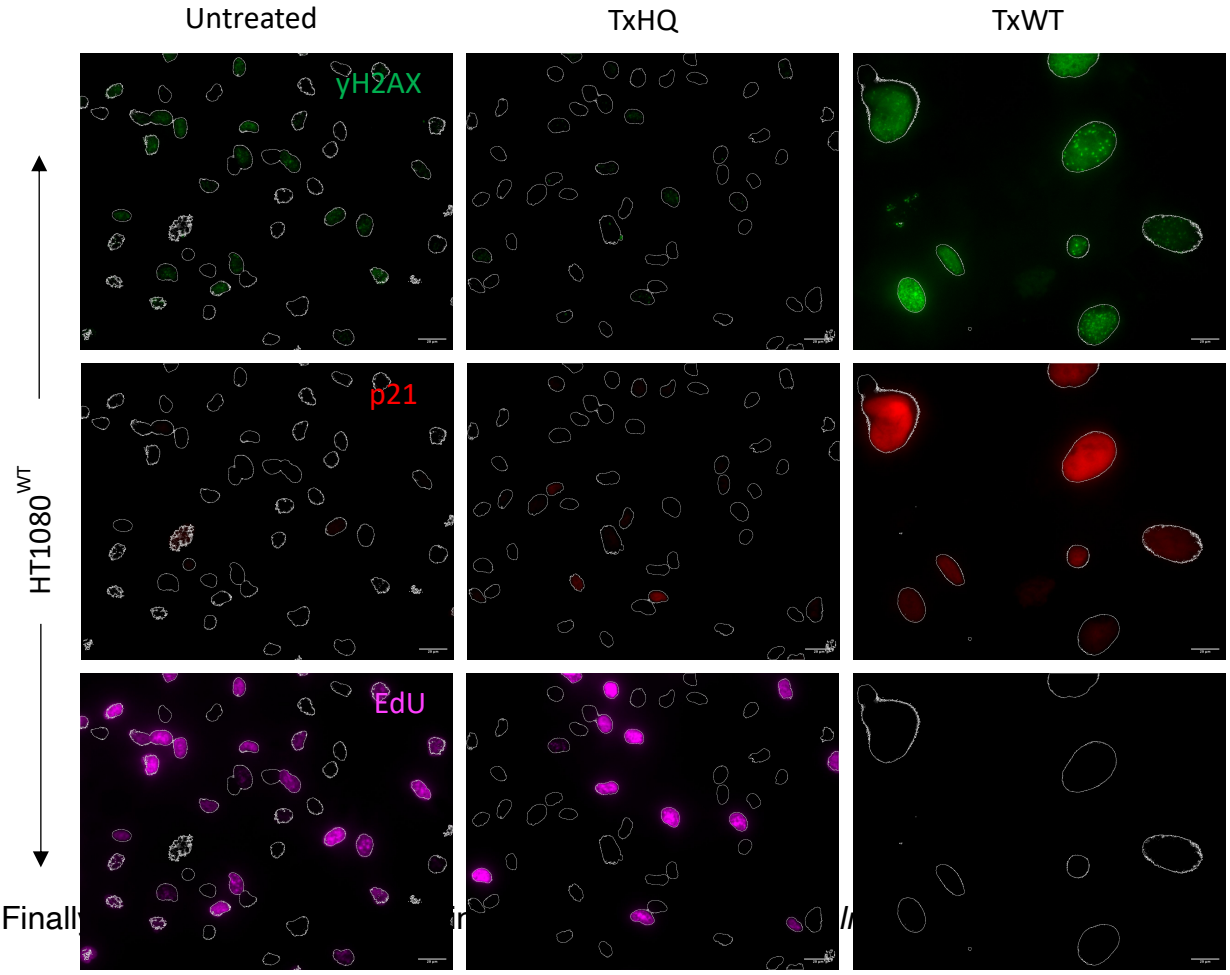

Finall[illegible]

Fig 9.3 **Immunofluorescence of Intoxicated HT1080 Cells.** HT1080 cells were either untreated, or treated with purified TxWT or TxHQ (20ng/ml) and incubated for 96h. EdU (magenta) was added to living cells for the last 2h of experimentation prior to fixation with PBS 4% paraformaldehyde. At 96h, fixed cells were stained with antibodies to γH2AX (green) and p21 (red). Cells were imaged on a Nikon Widefield Live Cell System at x20 magnification. DAPI-stained nuclei outlined in greyscale during processing in Fiji.

Javiana^{WT} showed similar results to TxWT with HT1080s showing cell distention, upregulation of both γH2AX and p21, and loss of EdU **(Fig 9.4)**. Relative to untreated, *S.* Javiana$^{\Delta cdtB}$ showed cell distension and upregulation of γH2AX and p21 but this was to a lesser extent than *S.* Javiana^{WT}. Consistent with this, some *S.* Javiana$^{\Delta cdtB}$-infected cells imaged remained positive for EdU. However, the effects of

S. Javiana$^{\Delta cdtB}$ were noticeably greater than untreated and TxHQ controls indicating that even in the absence of the typhoid toxin, the presence of bacterial PAMPs illicits low level DNA damage and cell cycle arrest.

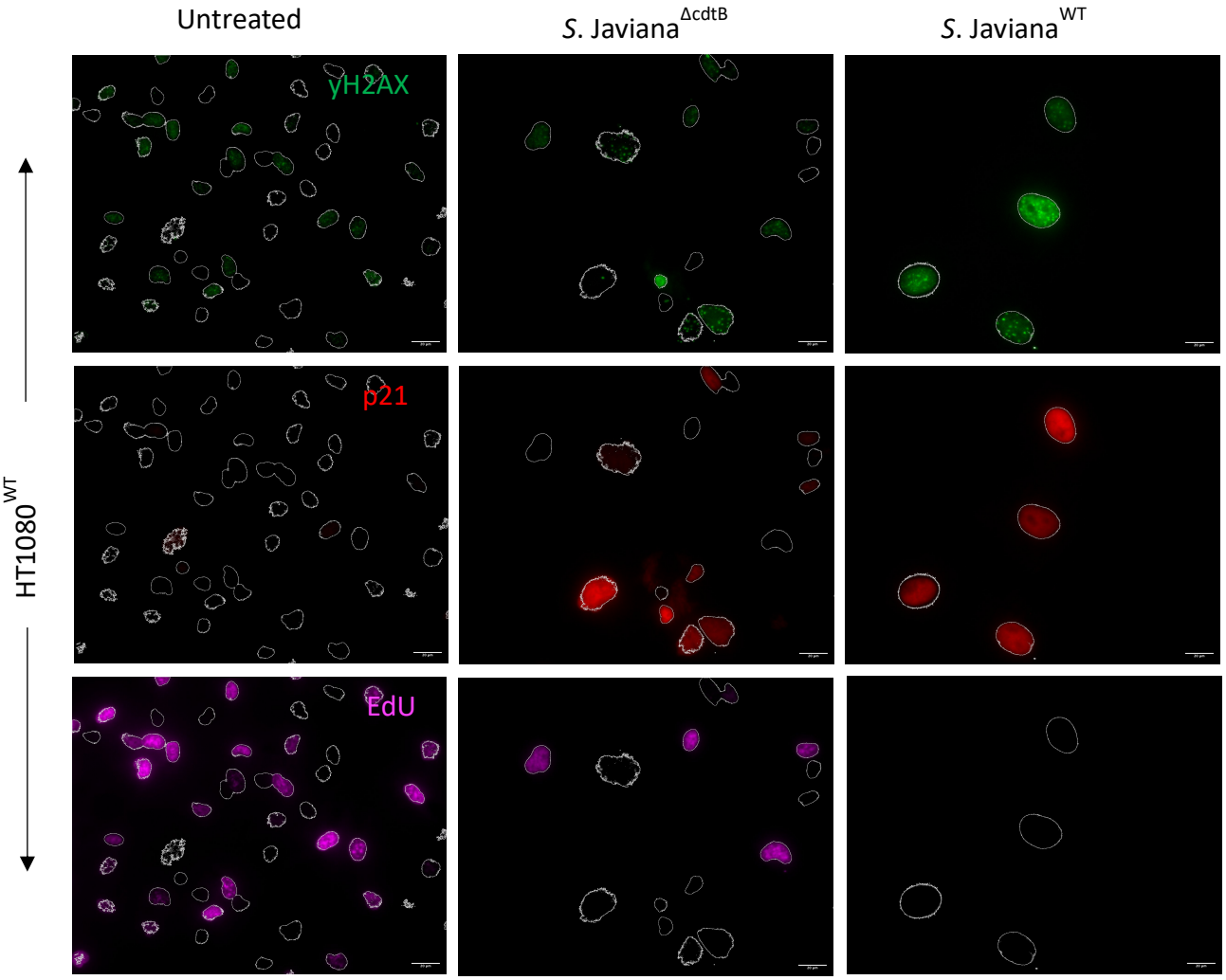

Fig 9.4 **Immunofluorescence of Toxigenic Salmonella Infection.** HT1080 cells were either untreated, or infected for 30 minutes with toxigenic *Salmonella* serovar S. Javiana^{WT} or the control mutant S. Javiana$^{\Delta cdtB}$ (MOI 20) followed by incubation for a further 96h in gentamicin-containing media, an antibiotic that cannot penetrate cells allowing assessment of intracellular infections. EdU (magenta) was added to living cells for the last 2h of infection prior to fixation with PBS 4% paraformaldehyde. At 96h, fixed cells were stained with antibodies to γH2AX (green) and p21 (red). Cells were imaged on a Nikon Widefield Live Cell System at x20 magnification. DAPI-stained nuclei outlined in greyscale during processing in Fiji.

9.3 Optimisation and Validation of *Salmonella* Enterica Infection

Although it is clear that ISG15 deficiency has wide ranging and often devastating effects on host cells, it is impossible to determine if this promotes or inhibits infection

using purified typhoid toxin alone. Therefore, A549^{WT} and A549$^{ISG15-/-}$ cells were infected with *S.* Javiana^{WT} and *S.* Javiana$^{\Delta cdtB}$ as illustrated in **Fig 9.5**

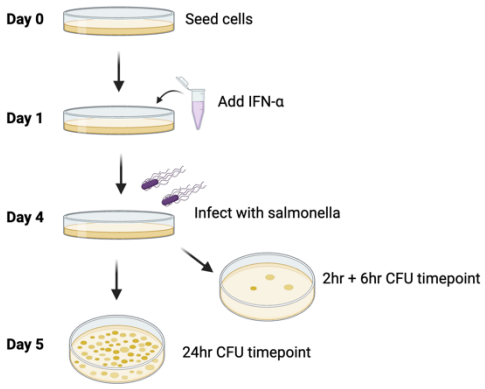

Fig 9.5 ***Salmonella* Javiana Infection Experiment Design.** A549^{WT} and A549$^{ISG15-/-}$ cells were seeded overnight before IFNα (0.1ug/ml) was added for 72hrs. *S.* Javiana^{WT} and *S.* Javiana$^{\Delta cdtB}$ infection was carried out for 30 mins at MOI 20 prior to replacing media containing *Salmonella* with media containing gentamicin that kills extracellular bacteria. *Salmonella* colony forming units (CFUs) were plated at 2, 6 and 24hrs onto LB agar plates and grown overnight at 37C. *Salmonella* colonies were counted after 24hrs to quantify infection. Image created with Biorender.

Initially, infections were performed in cells already expressing ISG15 to maximise effects: after seeding, the A549 cells were treated with IFNα and infection carried out after 72hrs in cells undergoing IFN responses. A549 cell lysates containing *Salmonella* colony forming units (CFUs) were plated onto agar plates at 2, 6 and 24hrs before being placed in an incubator at 37^{o}C overnight. Infection success for each timepoint was determined by the number of colonies formed after 24hrs.

Prior to performing infections, control experiments were performed with *S.* Javiana. Typhoid toxin is only expressed intracellularly within SCVs from 3h (Spano et al 2008). Nevertheless, to confirm that any differences in infection was down to the effects of ISG15 deficiency, *S.* Javiana^{WT} and *S.* Javiana$^{\Delta cdtB}$ were analysed beforehand by examining the secretion of virulence effectors **(Fig 9.6)**.
First to test differences in secretome and bacterial effector expression a Coomassie SDS-PAGE gel was run to test for variations in protein expression between

S. Javiana^{WT} and *S*. Javiana$^{\Delta cdtB}$ with a mutated strain of *Salmonella* Typhimurium (ΔT4) lacking secreted effectors *sopE, sopE2, sipA* and *sopB* used as a control **(Fig 9.6A)**. This showed no difference in bacterial protein expression in whole cell lysates (bacteria) across the three strains. Analysis of the secretome showed differences in *S.* Typhimurium ΔT4 relative to both strains of *S.* Javiana, which limited its usefulness as a control in Coomassie Blue staining experiments. No difference in secretion between the two *S*. Javiana strains were observed. The expression of SipA (Salmonella invasion protein A), a virulence factor used to promote bacterial entry into host cells (Galkin et al., 2002), was detected and showed similar levels of upregulation in the *S*. Javiana strains when compared to ΔT4. This shows that there are no significant differences in the expression of bacterial proteins and effectors that may impact infection. However, a band for SipA in the *S.* Typhimurium ΔT4 lane indicated possible cross-reactivity with an unknown protein.

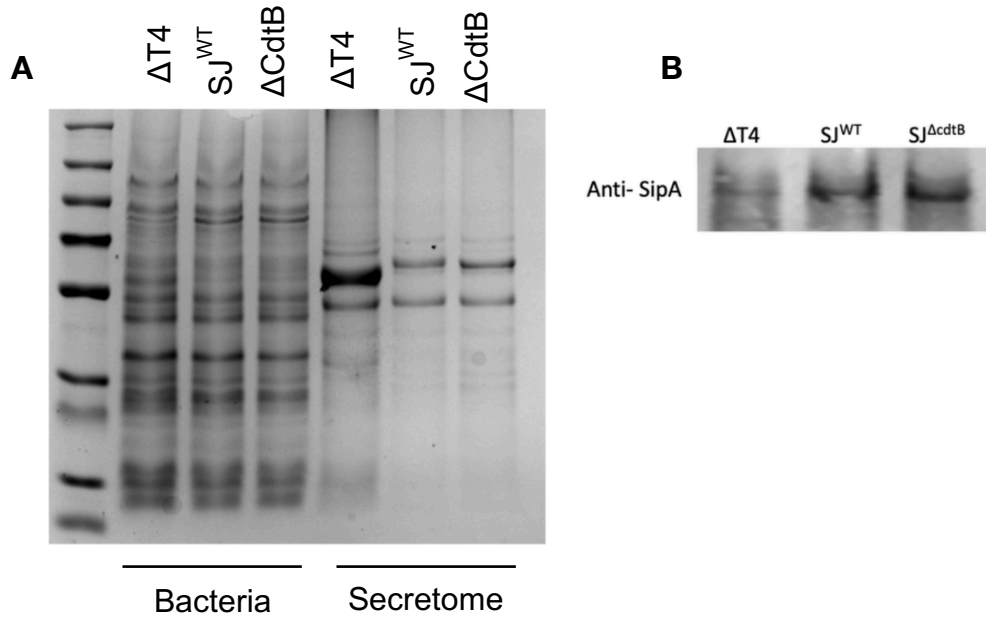

Fig 9.6 **The activity of the T3SS in Salmonella Javiana. (A)** *S.* Javiana^{WT} and *S.* Javiana$^{\Delta cdtB}$ or the *S.* Typhimurium ΔT4 strain lacking *sipA, sopB, sopE,* and *sopE2* were grown in LB broth at 37C in a shaking incubator to mimic human host. At OD 1.0, *Salmonella* were resuspended in SDS-UREA to generate a whole cell lysate (bacteria). In parallel, the supernatant was harvested by centrifugation and precipitated using 10% trichloroacetic acid before secreted proteins were resuspended in SDS-UREA (secretome). Samples were analysed by SDS-PAGE by loading on a 12% Bis-Tris Gel, run at 200V, prior to Coomassie Blue staining. (**B**) Immunoblotting of SipA was performed by blotting the secretome shown in (A) with anti-SipA antibodies as indicated.

The growth rate of *S.* Javiana^{WT} and *S.* Javiana$^{\Delta cdtB}$ was tested to ensure that differences in colony numbers could not be attributed to variation in doubling rates due to mutation of *cdtB* under the same extracellular conditions. This was achieved by inoculating growth media with the same volume of bacterial culture and incubating for 8hrs. At this point a serial dilution was performed and CFUs plated onto agar plates overnight **(Fig 9.7)**. No differences in growth rate were found from the CFU serial dilution which was further confirmed by quantification and statistical analysis **(Fig 9.7A+B)**.

Following a 30 min infection, gentamicin is added to infected cells to prevent further rounds of infection from extracellular *Salmonella* as gentamicin cannot penetrate cells and therefore only affects extracellular bacteria. To ensure that gentamicin kills *S.* Javiana, gentamicin was tested by adding gentamicin at both a low concentration (LG – 10ug/ml) and a high concentration (HG- 50ug/ml) to LB broth containing *S.* Javiana **(Fig 9.7C)**. CFUs were plated at 2hrs and 24hrs. It was found that more

extracellular survived at 2hrs with the low gentamicin treatment with *S.* Javiana$^{\Delta cdtB}$ compared to *S.* Javiana^{WT} however, the killing effect was complete by 24hrs for both strains **(Fig 9.7C)**. The high gentamicin treatment was successful for both timepoints in *S.* Javiana^{WT} and *S.* Javiana$^{\Delta CdtB}$. Therefore, the infection could be performed with some confidence that differences between *S.* Javiana^{WT} and *S.* Javiana$^{\Delta cdtB}$ (other than expression of the typhoid toxin) would not influence the outcome of the experiment.

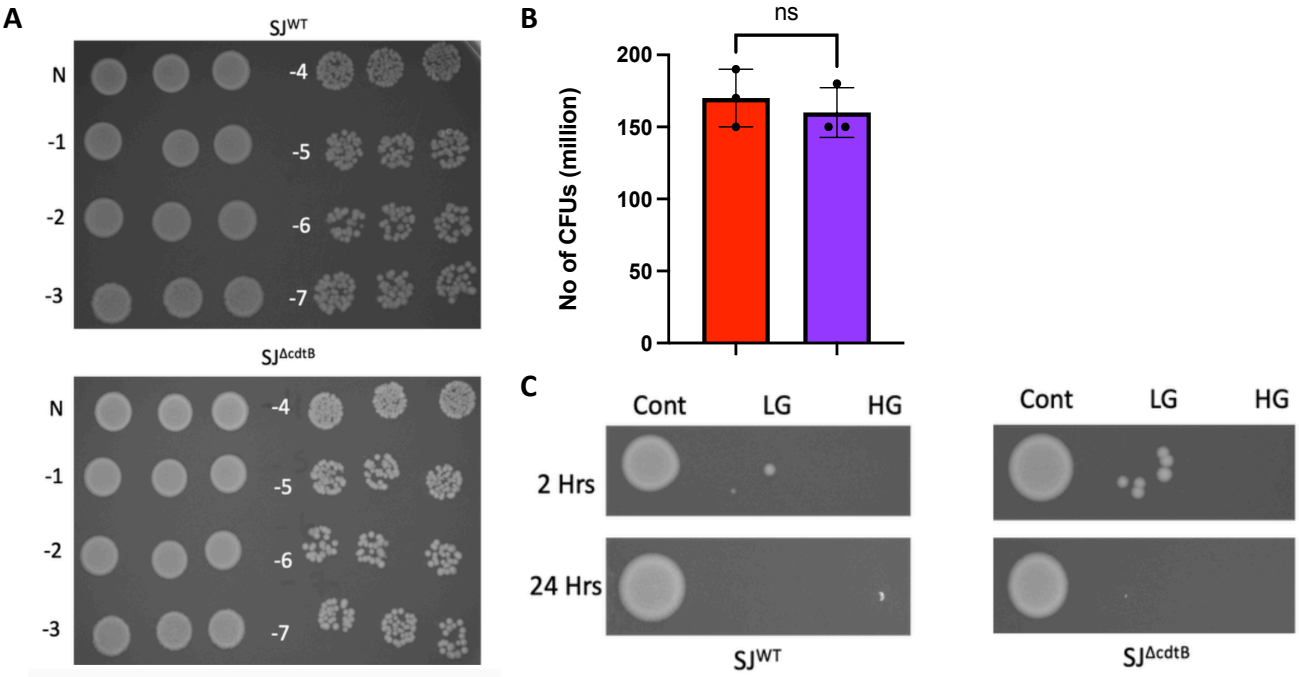

Fig 9.7 **Validation of Bacterial Growth Rates and Killing Effects of Gentamicin.** (A) LB broth was inoculated with 5ul of *S.* Javiana^{WT} and *S.* Javiana$^{\Delta cdtB}$ for 8hrs. A serial dilution was then performed with 5ul of culture spotted onto an agar plate containing ampicillin. Colonies were counted after 24hrs. (B) Quantification of CFUs in (A). Statistical significance was determined by paired T-test. Each circle represents one technical replicate. (C) CFUs formed after treatment with a low concentration (LG – 10ug/ml) or a high concentration (HG – 50ug/ml) of gentamicin. LB broth was inoculated with either *S.* Javiana^{WT} or *S.* Javiana$^{\Delta cdtB}$ and allowed to grow for 1hr before gentamicin was added. Bacterial culture was spotted onto agar plates at 2hrs and 24hrs.

Following these validation steps an infection of HT1080 cells was performed as per **Fig 9.5.** A549 cells were treated with IFNα for 72hrs prior to a 30 min infection followed by replacing infection media with media containing gentamicin. *Salmonella* begins to replicate from 3-4h (Hautefort et al., 2008), thus, *Salmonella* invasion by cytoskeleton remodelling can be quantified at 2h by counting CFUs. It was found that after 2hrs of infection there was a striking increase in the number of CFUs in both A549^{WT} and A549$^{ISG15-/-}$ infected with *S.* Javiana$^{\Delta cdtB}$ (SJ$^{\Delta cdtB}$) compared to *S.* Javiana^{WT} (SJ^{WT}), a surprising observation consistent throughout infection assays. No significant difference was found in infection rates for either A549^{WT} or A549$^{ISG15-/-}$ infected with SJ$^{\Delta cdtB}$ regardless of 72hr IFNα treatment prior to infection **(Fig 9.8)**. This was also true for A549$^{ISG15-/-}$ infected with SJ^{WT} however some significance was found in A549^{WT} treated with IFNα, which showed an increase in the number of CFUs compared to the untreated control. This would suggest that initial infection of A549^{WT} by toxigenic *Salmonella* is promoted by IFNα.

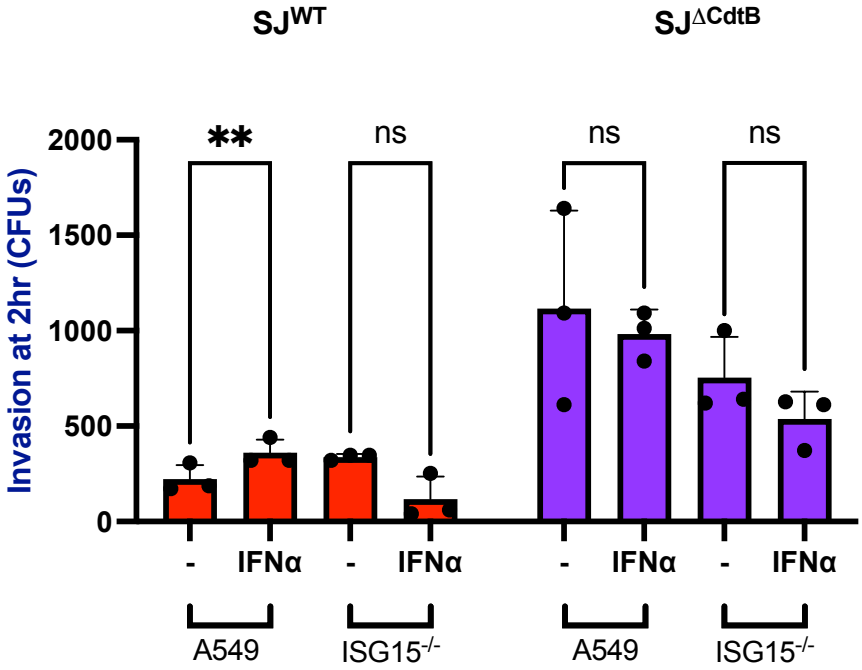

Fig 9.8 ***S.* Javiana invasion into ISG15-deficient cells.** A549^{WT} and A549$^{ISG15-/-}$ were treated +/- IFNα (0.1ug/ml) for 72hrs then infected with *S.* Javiana^{WT} or *S.* Javiana$^{\Delta cdtB}$ for 30 minutes at MOI 20. CFUs were plated at 2hrs infection and the colonies counted after 24hrs. The average number of CFUs was calculated and significance calculated using a two-way ANOVA. Each circle represents one biological replicate consisting of three technical replicates. (n=3)

To investigate the continuing impact of infection and measure intracellular *Salmonella* replication, the fold change in CFU number compared to 2hrs invasion with *S.* Javiana^{WT} (SJ^{WT}) or *S.* Javiana$^{\Delta cdtB}$ (SJ$^{\Delta cdtB}$) was calculated at 6hrs and 24hrs **(Fig 9.9)**.

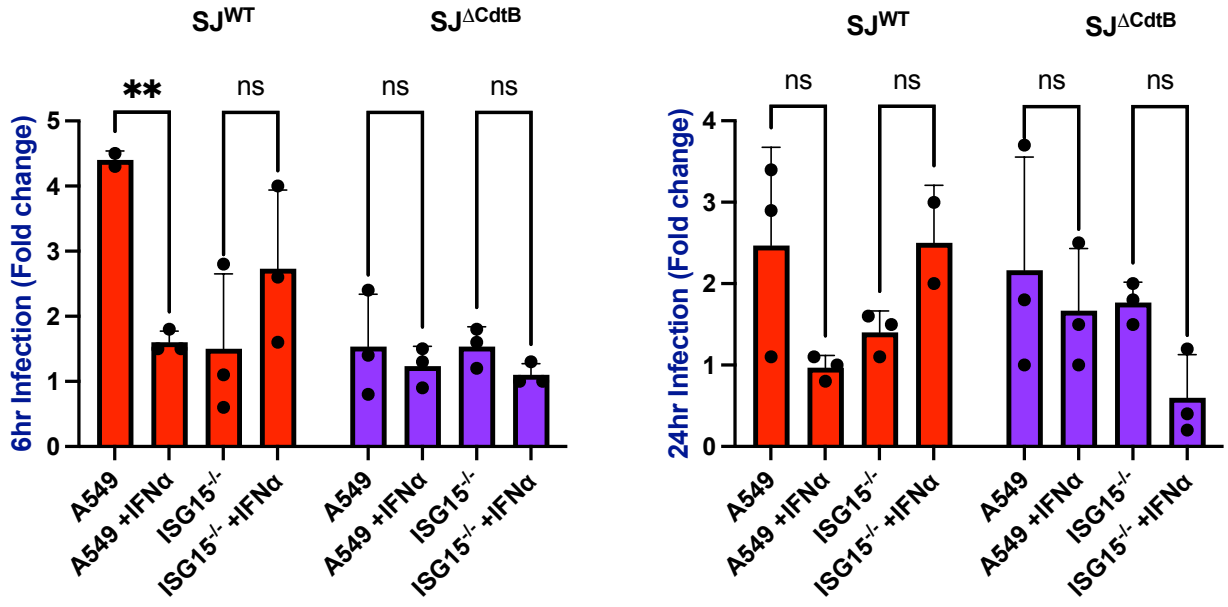

Fig 9.9 **Intracellular replication of *S.* Javiana in ISG15-deficient cells.** A549^{WT} or A549$^{ISG15-/-}$ cells were either untreated or treated with IFNα for 72h prior to infection. At 72h, the cells were infected for 30 minutes with toxigenic *Salmonella* serovar S. Javiana^{WT} (SJ^{WT}) or the control mutant S. Javiana$^{\Delta cdtB}$ (SJ$^{\Delta cdtB}$) at an MOI 20 followed by incubation for a further 6h (left) or 24h (right) in gentamicin-containing media, an antibiotic that cannot penetrate cells allowing assessment of intracellular infections. The fold change in the number of CFUs was calculated at 6hrs and 24hrs infection represents bacterial replication relative to 2hrs invasion, which was performed in parallel. The average number of CFUs in each condition was calculated and significance determined using a two-way ANOVA. Each circle represents one biological replicate consisting of three technical replicates. (n=3)

Again, significance was only found at 6hrs infection in A549^{WT} +/- IFNα infected with SJ^{WT} where IFNα suppressed intracellular replication of toxigenic *Salmonella* **(Fig 9.9)**. Statistical analysis and interpretation were complicated by a large degree in variation between replicates bringing doubt into the validity of the results and making it difficult to draw any definite conclusions. This can be attributed to the effects of

IFNα added 72h prior to infection and its harmful effects on A549 cells that likely affected the MOI at the start of infections.

9.4 ISG15 Deficient A549 Cells are Unable to Support Infection

In light of the complications described above, changes were made to the infection protocol. Instead of adding IFNα prior to infection, it was instead added alongside the *Salmonella*, which would ensure the same number of cells at the start of the infection (**Fig 9.10)**. The MOI was also increased from MOI 20 to MOI 100 and the infection time was increased from 30 minutes to 1 hour. The decision was made to change the experimental timepoints to 2hrs, 24hrs and 48hrs. This would allow the effects of IFNα to be fully realised. As some of the previous experiments had shown signs of potential recovery after extended treatment with IFNα, an additional timepoint of 72hrs was added for the final replicate.

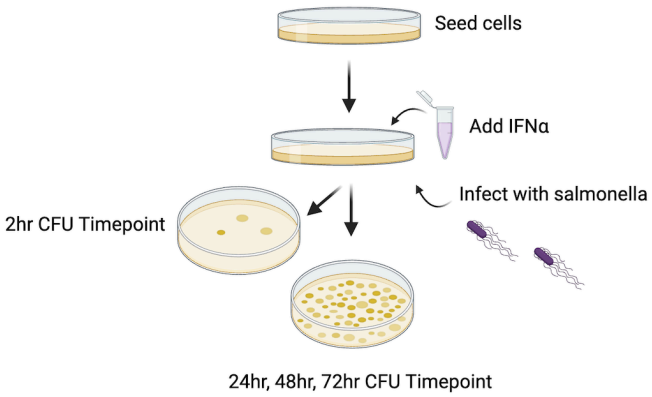

Fig 9.10 **Updated Infection Protocol.** Instead of adding IFNα prior to infection, it was added alongside the *Salmonella*. Timepoints were amended to 2hrs, 24hrs, 48hrs and 72hrs, infection time was increased to 1 hour and MOI was increased to MOI 100.

A549^{WT} and A549$^{ISG15-/-}$ cells were infected with *S.* Javiana^{WT} using the updated infection protocol. Initial infection success was once again determined by quantification of CFUs after 2hrs **(Fig 9.11)**.

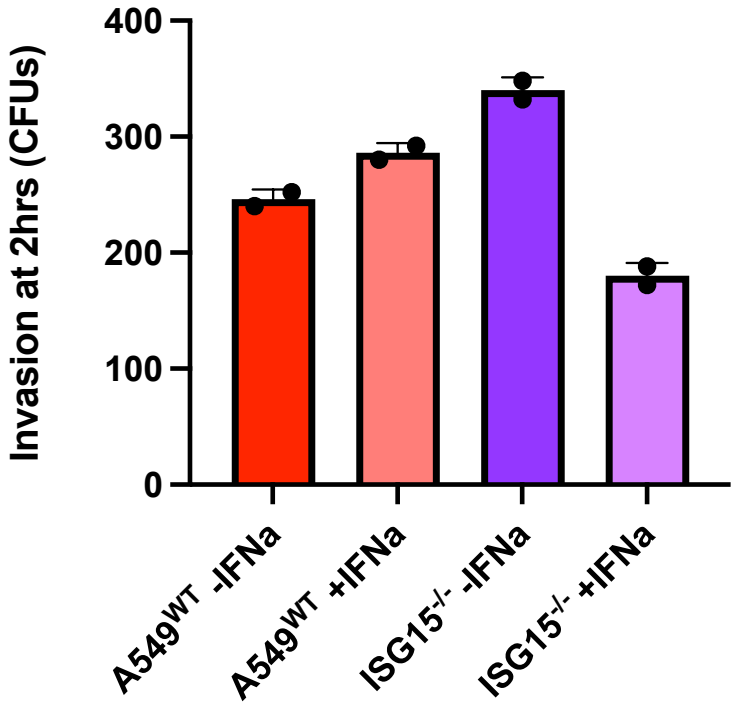

Fig 9.11 **Number of CFUs after 2hrs Infection.** A549^{WT} and A549$^{ISG15-/-}$ cells were infected with SJ^{WT} for 2hrs along with +/- IFNα (0.1ug/ml). 5ul of bacterial culture was plated onto agar plates and CFUs counted after 24hrs. The average number of CFUs was calculated with each circle representing one biological replicate consisting of three technical replicates. (n=2)

A549$^{ISG15-/-}$ treated with IFNα showed noticeably fewer CFUs forming after 2hrs suggesting that even though IFNα was added at the time of infection, the effects on the ISG15 deficient cells occurs quickly.

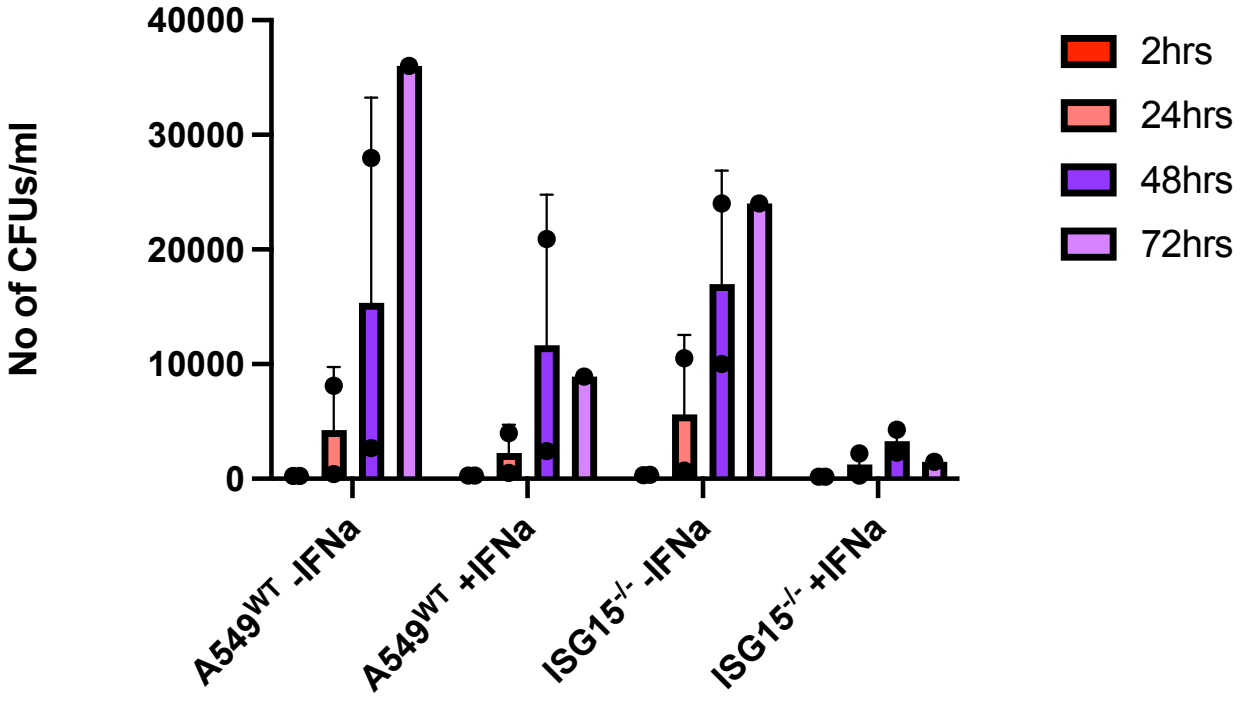

Fig 9.12 **Infection of A549 Cells with wild type *Salmonella* Javiana..** A549^{WT} and A549$^{ISG15-/-}$ cells were infected with SJ^{WT} along with +/- IFNα (0.1ug/ml). After 30 minutes infection, infected cells were incubated in gentamicin-containing media for 24h, 48h or 72h prior to culturing of 5ul from 200µl of *Salmonella* infected cell lysate. The average number of CFUs was calculated with each circle representing one biological replicate consisting of three technical replicates. (n=2)

Both A549^{WT} and A549$^{ISG15-/-}$ showed no barrier to infection when in a null IFNα state with the number of *Salmonella* CFUs increasing with each timepoint **(Fig 9.12)**. Relative to 2h invasion, *Salmonella* inside A549^{WT} cells in the presence of IFNα showed an increase in CFUs up to 48hrs but this plateaued or slightly decreased even at 72hrs indicating suppression of infection via the IFN response. However, the most striking result occurred with A549$^{ISG15-/-}$ + IFNα which showed overall fewer CFUs forming across all timepoints. This could be attributed to the apoptotic effects of IFNα on ISG15 deficient cells which releases the bacteria from the cells into the host environment.

To investigate the extent to which the typhoid toxin contributed to this phenotype, the experiment was also conducted using SJ$^{\Delta CdtB}$ under the same conditions **(Fig 9.13)**. This time the result was less clear but A549^{WT} +/- showed similar results with an increase in CFUs up to 48hrs and then a decrease at 72hrs. Again, variation

between the replicates makes interpretation difficult but A549$^{ISG15-/-}$ showed approximately the same result in both +/- IFNα however there was an observable increase in CFUs for A549$^{ISG15-/-}$ +/- IFNα from 24hrs onwards when compared to A549^{WT}. In summary, this indicates that more ISG15-deficient host cells are able to withstand infection in the absence of typhoid toxin. This implies that the combined effects of IFNα and the typhoid toxin overloads ISG15 deficient cells and accelerates apoptosis.

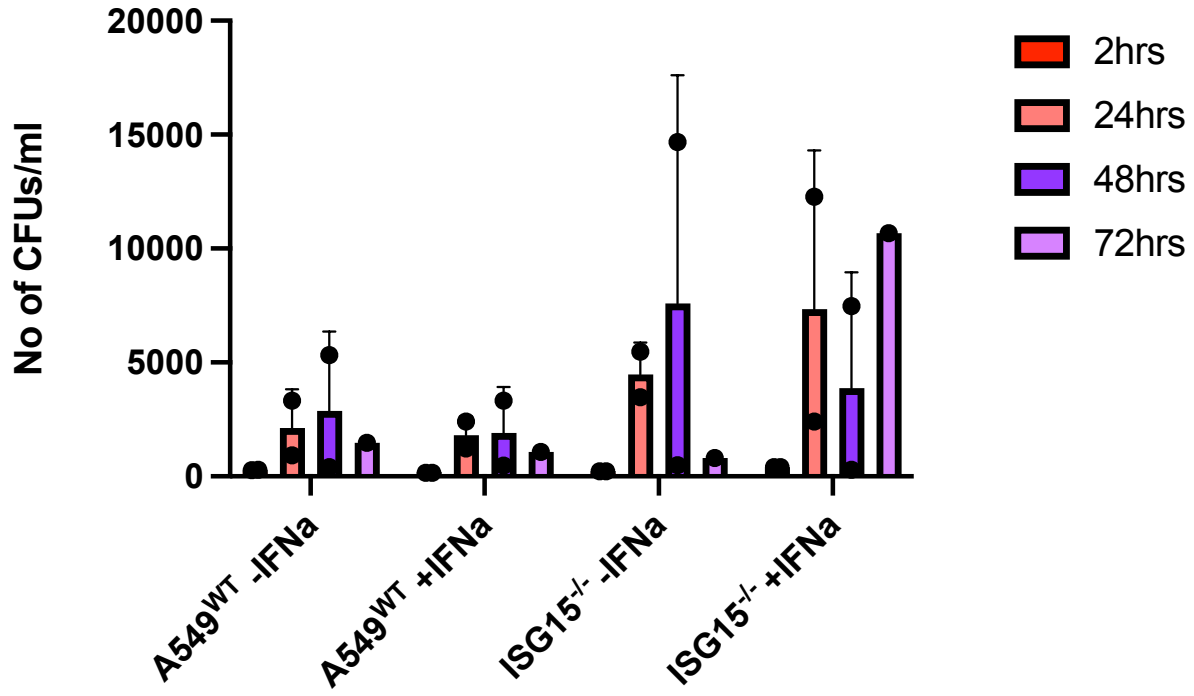

Fig 9.13 **Infection of A549 Cells with non-toxigenic Salmonella Javiana.** A549^{WT} and A549$^{ISG15-/-}$ cells were infected with SJ$^{\Delta cdtB}$ along with +/- IFNα (0.1ug/ml). After 30 minutes infection, infected cells were incubated in gentamicin-containing media for 24h, 48h or 72h prior to culturing of 5ul from 200µl of *Salmonella* infected cell lysate. The average number of CFUs was calculated with each circle representing one biological replicate consisting of three technical replicates. (n=2)

Finally, to try and confirm the observation that fewer CFUs in ISG15 deficient cells is due to cell killing effects of the typhoid toxin and IFNα, immunofluorescence of infected cells was conducted **(Fig 9.14)**. A549^{WT} and A549$^{ISG15-/-}$ cells were infected and IFNα treated in parallel with infection as before however, instead of CFUs, this time the localisation of LAMP1 (lysosomal-associated membrane protein 1) was

visualised. This is a host lysosomal protein that is recruited by *Salmonella* and marks the *Salmonella*-containing vacuole (Madan et al., 2011). The SJ^{WT} strain contained pM975, a plasmid that expresses GFP from a SPI-2 promoter ssaV (Misselwitz et al., 2011), which is activated when the bacteria are within the vacuole, allowing visualisation of infection.

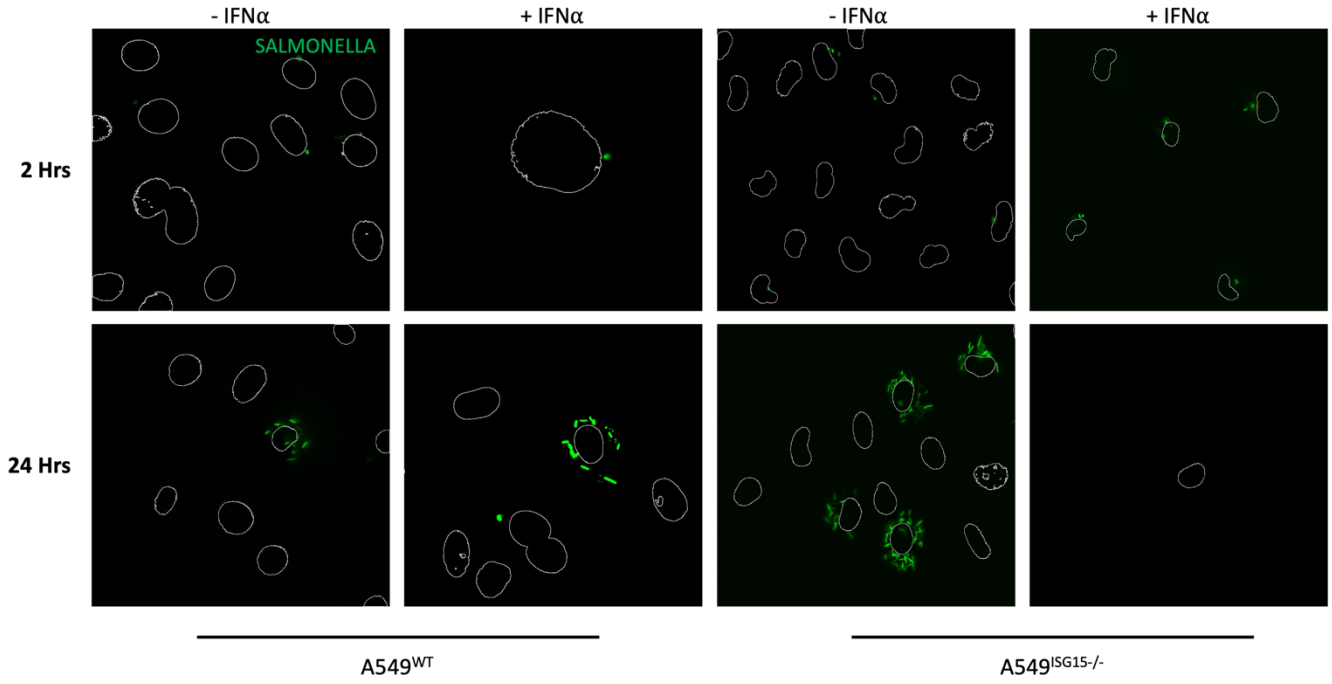

Fig 9.14 **Immunofluorescence of Infected A549 Cells.** $A549^{WT}$ and $A549^{ISG15-/-}$ cells in the presence or absence of IFNα were infected with GFP-emitting SJ^{WT} encoding pM975 for indicating timepoints. IFNα treatment and infection occurred simultaneously. GFP expression marked *Salmonella* (green) was visualised at 2hrs and 24hrs. DAPI-stained nuclei outlined in greyscale during processing in Fiji. Images were taken on a Nikon Widefield Live Cell System at x40 magnification.

With A549^{WT} -IFNα there was an increase in the number of bacteria from 2hrs to 24hrs (**Fig 9.14**). Treatment of A549^{WT} with IFNα appears to have no effect on *Salmonella* number though IFNα-mediated suppression of infection was observed by CFU counts in **Fig 9.12**. A549^{WT} also inexplicably shows some signs of cell distension at 2hrs in the presence of IFNα which was absent in conditions lacking IFNα (**Fig 9.14**). In the absence of IFNα, A549$^{ISG15-/-}$ cells showed a significant increase in the number of *Salmonella* from 2hrs to 24hrs, lending credence to the theory that ISG15 deficiency promotes infection (Bogunovich et al, 2012). Conversely, although there was a small number of intracellular *Salmonella* visualised with A549$^{ISG15-/-}$ +IFNα at 2hrs, none could be seen by 24hrs. However, as predicted there were significantly fewer cells visualised at 2hrs compared to the other conditions and almost no cells visible by 24hrs. IFNα was added simultaneously with the *Salmonella,* which indicates that the effects of IFNα occur quickly and the cell killing effects of the typhoid toxin and IFNα are devastating to ISG15 deficient cells, preventing them from supporting infection. However, this is turn may promote disease by releasing intracellular *Salmonella* allowing disseminated infections and increased invasive infections *in vivo*.

.

Part 4: Discussion

Chapter 10: Discussion of Results

My project aimed to explore the host responses to the typhoid toxin. It was found that type I IFN signalling was upregulated as part of the innate immune response which activates the transcription of pathogen fighting ISGs. One of the most important of these is ISG15. Persistent IFN signalling by IFNα was found to cause apoptosis in ISG15 deficient cells and rendered them unable to support infection by toxigenic *S.* Javiana, thus, ISG15 deficieny increases host susceptibility to cell death and pathogen release in the presence of interferon

10.1 The Effects of the Typhoid Toxin on Host Cells

The typhoid toxin has been shown to induce DNA damage in host cells (Ibler et al., 2019, Chen et al., 2024, Chiloeches et al., 2024). In this study, the typhoid toxin causes upregulation of markers of DNA damage and cycle arrest. This was true of both purified typhoid toxin and infection with *S.* Javiana which also expresses the typhoid toxin. These effects were not seen in cells treated with TxHQ, which possesses a mutation in H160. This single mutation has been shown to prevent toxicity (Nešić, Hsu and Stebbins, 2004) and shows that DNA damage resulted from the catalytic action of the cdtB active subunit of the typhoid toxin.

As explained previously the typhoid toxin is part of a family of bacterial genotoxins that specifically translocate to the nucleus and act upon DNA (Jindasa et al., 2011, Grasso and Frisan, 2015). Intoxicating primary immune cells during differentiation caused widespread damage to the differentiating monocytes characterised by increased levels of cell debris and lack of fully matured macrophages after 7 days. Differentiation offers the perfect target for the typhoid toxin as cell differentiation requires global transcriptive hyperactivity which decreases as the process progresses. Transcription requires separation of the DNA strand allowing access for the typhoid toxin (Elfroni et al. 2009). Additionally, monocytes are non-proliferating which are more likely to undergo cell death than arrest in response to DNA damaging agents (Granada et al., 2022). Intoxication during the early stages of differentiation (day 1-3) had the greatest impact of differentiation supporting this idea. Consistent with my results, Song et al. (2013) showed that the Typhoid toxin reduced the number of mononuclear cells in mice, which had been administered with the Typhoid toxin.

The typhoid toxin also caused significant morphological changes normally associated with apoptosis, such as membrane blebbing, after 72hrs intoxication suggesting that prolonged exposure to the typhoid toxin drives apoptosis. In chapter 7 $HCT116^{WT}$ and $HCT^{p53-/-}$ cells were treated with TxWT, TxHQ, ETP and IFNα and MTT metabolism assayed. Both cell lines showed complete loss of MTT metabolism

after 7 days of intoxication with the typhoid toxin. Cell death was confirmed by a β-Gal assay which showed fewer cell numbers and cell distension. P53 is a key mediator of apoptosis and it could be theorised that cells deficient in p53 would be resistant to p53. However, this result suggested that cell death was able to occur independently of p53 via death receptor mediated extrinsic apoptosis. Ray et al. (2016) used crocetin, a natural compound found in saffron, to induce cell death in HCT116 cells containing a range of p53 mutations. They found that cell death was able to occur independently of p53 by activating p73, a paralogue of p53. This upregulates FAS and triggering apoptosis via the extrinsic pathway. The results in this thesis suggest that the typhoid toxin may also cause cells to utilise this pathway in the absence of p53.

The typhoid toxin was shown to elicit an immune response in HT1080 cells by upregulation of the type I IFN pathway. IFNα production is stimulated by the typhoid toxin which activates transcription of hundreds of ISGs, one of them being ISG15 (Platanias et al., 2005, Alphonse et al., 2021). IFNα was used as a control for type 1 IFN activation, however when used in the MTT assay with A549WT and A549$^{ISG15-/-}$ unexpectedly showed loss of MTT metabolism in response to IFNα. A decision was then made to probe this result further

10.2 IFNα Drives Cell Death in ISG15 Deficient Cells via the Extrinsic Apoptosis Pathway

The MTT assay is a quick and easy method of assaying cell viability, however it only gives a snapshot and does not point to the underlying cause of the loss of metabolism. IFNα treatment of ISG15 deficient cells caused cell cycle arrest, DNA damage and loss of cells. The next step of this project was to determine the fate of ISG15 deficient cells.

Evidence of apoptosis was found using flow cytometry and immunofluorescence. The typhoid toxin was found to drive apoptosis in both A549^{WT} and A549$^{ISG15-/-}$ cells but IFNa drove much higher levels of apoptosis in A549$^{ISG15-/-}$. Analysis of apoptosis

markers from the RNA seq data showed TRAF1 was highly upregulated. This interacts with receptors of the TNF family and forms part of the extrinsic apoptosis pathway (Leo et al., 2001). Other members of this pathway (FAS and DDIT3) were also found to be upregulated. One of the functions of ISG15 is the stabilisation of p53 (Huang et al. 2014) and such high levels of TRAF1 expression suggests that ISG15 deficiency prevents intrinsic apoptosis and instead forces the cell towards the same alternate pathway described above by p53 deficient cells. However, members of the NF-κB pathway (MAP3K14, NFKBIA) which inhibit the TNF pathway were also up regulated suggesting the cell deploys both pro- and anti-apoptotic strategies. IFNa induced cell death in ISG15 deficient macrophages has also been observed (Waqas et al., 2022) and also found upregulation of members of the TNF family and down regulation of the NF-κB pathway.

10.3 USP18 is Critical for Cell Survival

ISG15 deficiency was shown to be fatal with prolonged exposure to IFNα. However, ISG15 exists in both a free and conjugated form (Perng et al., 2018, Kang et al., 2022). SiRNA was used to try and determine if cell death resulted from loss of ISGylation. Knock downs were generated of ISG15, USP18 and UBE1L and MTT metabolism assayed after 7 days of IFNα treatment. No loss of metabolism was found in the UBE1L knock down (the E1 enzyme in the ISGylation cycle) suggesting that ISGylation was not responsible for the cell death phenotype. UBE1L has been found to not be essential for IFNα signalling (Kim et al., 2006) and does not appear to influence the outcome of ISG15 deficiency. Unfortunately, UBE1L expression was not detected by immunoblotting in any of the knock downs or control sample so it was not possible to confirm this theory. Conversely, knock down of USP18 showed massive loss of MTT metabolism to almost the same levels as A549$^{ISG15-/-}$.

As inhibition of ISGylation was not found to be the reason for driving cell death then this pointed towards the secondary function of USP18, downregulation of the IFN response through a negative feedback loop in conjunction with JAK2 (Dzimianski et

al., 2019, Freitas et al., 2020). It has also been suggested that ISG15 plays a role in stabilising USP18 as part of IFNα regulation (Zhang et al., 2015). Attempts to restore cell survival by restoring USP18 function via plasmid insertion were unsuccessful and required further experimental optimisation. Confirmation that apoptosis resulted as a failure to downregulate the IFN response could be achieved by knocking down expression of JAK2. I would hypothesise that cells who were deficient in JAK2 but displayed normal ISG15 and USP18 function would undergo apoptosis in response to IFNα treatment.

10.4 ISG15 Causes Dysregulation of Proteins Associated with IFN Signalling

Loss of ISG15 has been found to cause sustained elevated expression of ISGs leadling to chronic inflammation (Malik et al., 2022). Similarly, Wu et al. (2024) found ISG15 deficieny lead to increased cytokine action. In this thesis the effects of ISG15 deficency were found to impact the expression of other proteins associated with iFN signalling. Immunoblotting in Fig 8.28 showed ISG15 deficient cells expressed MAVs, AIM2 and IFIT1 in response to IFNα, although at lower levels than wild type. Immunofluorescence showed that ISG15 deficiency knocked out expression of STAT1, AIM2 and SUMO-1. In mice ISG15 was not found to be required for STAT1 activation (Osiak et al., 2005). However, a later study found that ISG15 and ISGylation was increased stability for numerous proteins including STAT1 in microglia cells (Przanowski et al., 2018). SUMO-1 is part of the SUMO family and can downregulate the IFN response by inhibiting phosphorylation of STAT1. If the IF accurate then this could mean that ISG15 deficiency breaks cross talk between ISGylation and SUMOylation and suggests that ISG15 may play a role in modulating other inhibitiors of the IFN response. AIM2 was the most surprising result. The IF suggested that absence of ISG15 knocks out AIM2, however the RNA seq analysis showed massive upregulation in ISG15 deficient cells after IFNα treatment. It may be that while the mRNA transcript for AIM2 is present, the protein itself is degraded in the absence of ISG15. Thus, AIM2 is lost at the post-translational level.

The RNA seq analysis also showed up regulation of both JAK2 and members of the SOCs family of proteins which play a role in down regulating the IFN response (Blumer et al., 2017) and so may be effective at dampening the expression of some IFN associated proteins. The study conducted by Waqas et al. (2022) showed a similar upregulation of proteins associated with the extrinsic apoptosis pathway in ISG15 deficient macrophages, but they did not show differential expression for SOCS proteins. This difference may be due to cell type and it would be interesting to compare the transcriptomic profile of other cell types under the same conditions.

10.5 ISG15 Deficient Cells are Unable to Support *Salmonella* Infection

Finally, it was impossible to explore the role of ISG15 deficiency in *Salmonella enterica* infection using purified toxin alone. Infection using wild type *S*. Typhi was not possible due to covid restrictions in place at the time and the attenuated strain used in the lab showed low infection efficacy. Therefore, infection was carried out using *S*. Javiana. This is a NTS serovar of *S*. Javiana that also produces the typhoid toxin, which has a narrower tissue tropism than typhoid toxin of *S.*Typhi (Lee et al., 2020). A549^{WT} and A549$^{ISG15-/-}$ cells were infected with both toxigenic and non-toxigenic S. Javiana for up to 72hrs.

Infection by *L. monocytogenes* was found to induce ISGylation whereas infection by *C. trichomatis* did not. In **Fig 7.6** it was found that the typhoid toxin did not induce ISGylation and suggests that ISG15 activation occurs by an alternative pathway. (Radoshevich and Cossart., 2018, Wu et al., 2024). In both studies ISG15 was found to inhibit infection regardless of the activation pathway used. In the *L. monocytogenes* study infection was restricted by ISGylation of cytokines such as MAG1 whereas *C. trichomatis* infection triggered ISG15 and cytokine expression through the STING/TBK1/IRF3 pathway, rather than through ISGylation. It can be theorised that similar mechanisms could be used during *Salmonella enterica* infection.

While ISG15 has been shown to play a role in modulating the immune response, but does it also combat infection by ISGylation of effectors, taking the fight to the bacteria? SopB is not known to be modified by ISG15 with translocation and ubiquitination of SopB continuing for hours after infection (Knodler et al., 2009). However, ISGylation of other bacterial effectors remains relatively unknown. This offers an opportunity for further research.

10.5 Choice of Cell Lines and Bacterial Strains, and Possible Alternatives

This project primarily used A549 cells, an epithelial cell line isolated from a lung carcinoma patient. This cell line has been used extensively to investigate the interactions between ISG15 and viral infection (Gonzalez-Sanz et al., 2016, Rabbani et al., 2016, Holthaus et al., 2020) They have also been used to investigate the effects of ISG15 on bacterial infection (Radoshevich et al., 2015, Zhang et al., 2019). As this had been shown to be an established cell line for use in similar types of research, it was deemed suitable for this project and a $A549^{WT}$ and $A549^{ISG15-/-}$ cell line was kindly provided by the Radoshevich lab. It was shown that ISG15 deficieny in A549 cells caused loss of metabolic activity and apoptosis in response to IFNα, and increased rates of infection by *S.* Javiana. These effects were exacerbated by the Typhoid toxin. However, later in the project the MTT assay was repeated, initially to show that greater loss of metabolic activity in ISG15 deficient cells in response to IFNα when compared to WT was replicable across different cell lines. In U2OS cells – a human osteosarcoma cells, this was found to produce an even more pronounced phenotype that A549 cells **(Fig 7.12)**, and subsequent experiments in the lab have found them to produce more robust and reproducible CFUs after infection. With hindsight this may have been a preferable cell line to use for this project.

Another consideration is the origin of the cell lines used. Although A549 and U2OS cells gave strong phenotypes in response to IFNα, they were harvested from a human lung and tibia respectively. As *S.* Typhi infects through the small intestine in order to more accurate replicate the infection environment a gut epithelial cell line could have been used. Candidates for this could be HIEC, a continuously growing

human intestinal epithelial cell line, or Caco-2 cells, a colorectal adenocarcinoma cell line commonly used to model the small intestine.

The attenuated *S*. Typhi strain currently available within the Humphreys lab has been found to not be effective when used in infection assays so a decision was made to use *S*. Javiana instead. Although this is a non-typhoidal *Salmonella* strain it produces the Typhoid toxin therefore, it can be used to investigate the effects of intoxication on cells. This is also a class 2 pathogen and so infection assays using this bacteria could be conducted within the department. Infecting cells with wild-type *S*. Typhi would have been preferable as it would not only have shown the effects of the Typhoid toxin, but would have also highlighted phenotypes deriving from the bacteria themselves. However, due to covid access to the class 3 lab this work would have to be carried out in was severely limited and thus it was not possible to conduct these experiments within the scope of this project.

Although alternatives were identified that may have produced more optimal experimental conditions, the cell lines and bacterial strains chosen in this project were effective in demonstrating the effects of ISG15 on *Salmonella* enterica infection.

10.6 ISG15 and the Host-Pathogen Interaction

This project has shown that deficiency of ISG15 promotes infection, but its place within the host-pathogen interaction is still not entirely clear. Much of the published literature describes the role of ISG15 in combating viral infection, but comparatively little has been wriiten in regards to bacterial infection. This leaves the questions - do bacterial effectors target ISG15 and conversely how does ISG15 prevent infection by *Salmonella* enterica?

It has been shown that both overexpression of ISG15 and interferon treatment induced expression of a number of proteins associated with the endoplasmic reticulum and the Golgi apparatus. This results in increased cytokine secretion which

are known to fight infection. Three of these (MAGT1, RTN4 and Atlastin-3) were also induced following *Listeria* infection and are known targets of ISGylation (Radoshevich et al., 2015). In **Fig 8.10** it was shown that IFNα treatement stimulated many of the same pathways associated with combatting viral infection. This was lost in the absence of ISG15 which instead saw upregulation of pathways associated with apoptosis. More indepth analysis of the RNA Seq data would have allowed highlighted individual genes associated with this response and if there was a similar upregulation of ER and Golgi related proteins.

Salmonella possess a number of bacterial effectors that helps increase survival and replication during infection. In *S*. Typhimurium the effector SarA has been shown to activate STAT3 (which is induced by IFNα signalling and modulated by ISG15) (Jaslow et al., 2019). This results in inhibition of IL-10, an anti-inflammatory cytokine, and increased intracellular replication suggesting that *Salmonella* enterica serovars may be able to promote infection by disrupting ISG15 interactions (Jaslow et al., 2019). *S*. Typhi does not possess SarA, but it is possible that interactions may occur between ISG15 and some of its other effectors. Over time *S*. Typhi has evolved a degraded genome in order to evade detection by the immune system and adapt to a human host (Machado and Galan, 2024), it is possible that as part of its box of tricks it utilises its array of bacterial effectors to target ISG15 and its associated proteins to enhance its survival in the intracellular environment. The next step of this project would have explored these potential interactions further.

10.7 Suggestions for Further Work and Improvements

This project began with investigating the effects of ISG15 deficiency on A549 cells in response to IFNα and toxin treatment, which showed loss of cell metabolism and apoptosis, and finished with determining the results of infecting these same cells with *S*. Javiana. This again showed that the absence of ISG15 resulted in increased apoptosis and enhanced infection. U2OS cells, as described previously, gave an even stronger phenotype in the MTT assay **(Fig 7.12)** so it naturally follows to repeat

some of the later experiments and infection assay with this cell line. This may give more robust results and produce stronger phenotypes than A549 cells.

The infection assays could also be improved by determining numbers of intracellular *S*. Javiana by methods other than CFU counting, which sometimes proved to be unreliable. A suggestion for this would be to lyse the infected cells and harvest the bacteria. As the *S*. Javiana strain used contains pM975 (a plasmid that produces the green fluorescent protein (GFP)) this could be detected using flow cytometry with bacteria harvested from cells containing a higher infection burden producing increased levels of GFP.

In this project the focus fell on the role of ISG15 in preventing infection, but with more time the next step of the project would have been to look at how ISG15 interacts with bacterial effectors. It has been shown that ISG15 does not interact with SopB (Knodler et al., 2009) however, there are other bacterial effectors such as SipA, SipC and Sse1 that may be isgylated. By either knocking out or over expressing these proteins it would be possible to explore the host-pathogen relationship between *Salmonella* and the ISG15 pathway.

Finally, as the RNA Seq data was only received whilst writing this thesis it was not possible to fully explore the transcriptional changes resulting from IFNα and Typhoid toxin treatment. Most of the results focus on changes at the pathway level and did not fully explore the genes within these pathways that were differentially expressed in wild type and ISG15 deficient cells. The PCA analysis also showed slightly differential clustering between A549^{WT} and A549$^{ISG15-/-}$ treated with the Typhoid toxin and it would have been interesting to further investigate the underlying changes in gene expression despite giving similar phenotypes with the MTT assay.

10.8 Conclusion

My project aimed to explore the host responses to the typhoid toxin. It was found that type I IFN signalling was upregulated as part of the innate immune response which

activates the transcription of pathogen fighting ISGs. One of the most important of these is ISG15. Persistent IFN signalling by IFNα was found to cause apoptosis in ISG15 deficient cells and rendered them unable to support infection by toxigenic *S*. Javiana. However, some evidence was found that ISG15 deficiency promoted *Salmonella Javiana* infection. Although the role of ISG15 has been well documented in viral infection, there has been little research conducted into its impact on typhoidal *Salmonella*. This offers an opportunity for further work to fully explore the effect ISG15 has on *Salmonella enterica* infection.

Part 5: Bibliography

Abbotts R, Wilson DM 3rd. Coordination of DNA single strand break repair. Free Radic Biol Med. 2017 Jun;107:228-244. doi: 10.1016/j.freeradbiomed.2016.11.039. Epub 2016 Nov 24. PMID: 27890643; PMCID: PMC5443707.

Acheson, D, Hohmann EL. Nontyphoidal salmonellosis. Clin Infect Dis. 2001 Jan 15;32(2):263-9. doi: 10.1086/318457. Epub 2001 Jan 15. PMID: 11170916.

Ajibola O, Mshelia MB, Gulumbe BH, Eze AA. Typhoid Fever Diagnosis in Endemic Countries: A Clog in the Wheel of Progress? Medicina (Kaunas). 2018 Apr 25;54(2):23. doi: 10.3390/medicina54020023. PMID: 30344254; PMCID: PMC6037256.

Alphonse N, Dickenson RE, Odendall C. Interferons: Tug of War Between Bacteria and Their Host. Front Cell Infect Microbiol. 2021 Mar 10;11:624094. doi: 10.3389/fcimb.2021.624094. PMID: 33777837; PMCID: PMC7988231.

Als D, Radhakrishnan A, Arora P, Gaffey MF, Campisi S, Velummailum R, Zareef F, Bhutta ZA. Global Trends in Typhoidal Salmonellosis: A Systematic Review. Am J Trop Med Hyg. 2018 Sep;99(3_Suppl):10-19. doi: 10.4269/ajtmh.18-0034. Epub 2018 Jul 24. PMID: 30047364; PMCID: PMC6128363.
Andrews JR, Ryan ET. Diagnostics for invasive Salmonella infections: Current challenges and future directions. Vaccine. 2015 Jun 19;33 Suppl 3(0 3):C8-15. doi: 10.1016/j.vaccine.2015.02.030. Epub 2015 Apr 30. PMID: 25937611; PMCID: PMC4469564.

Aristizábal B, González Á. Innate immune system. In: Anaya JM, Shoenfeld Y, Rojas-Villarraga A, et al., editors. Autoimmunity: From Bench to Bedside [Internet]. Bogota (Colombia): El Rosario University Press; 2013 Jul 18. Chapter 2.

Arya SC. Field effectiveness of Vi polysaccharide typhoid vaccine in the People's Republic of China. J Infect Dis. 2002 Mar 15;185(6):845; author reply 845-6. doi: 10.1086/339191. PMID: 11920305.

Au-Yeung N, Mandhana R, Horvath CM. Transcriptional regulation by STAT1 and STAT2 in the interferon JAK-STAT pathway. JAKSTAT. 2013 Jul 1;2(3):e23931. doi: 10.4161/jkst.23931. Epub 2013 Jun 18. PMID: 24069549; PMCID: PMC3772101.

Baker S, Favorov M, Dougan G. Searching for the elusive typhoid diagnostic. BMC Infect Dis. 2010 Mar 5;10:45. doi: 10.1186/1471-2334-10-45. PMID: 20205702; PMCID: PMC2846943.

Baker DJ, Childs BG, Durik M, Wijers ME, Sieben CJ, Zhong J, Saltness RA, Jeganathan KB, Verzosa GC, Pezeshki A, Khazaie K, Miller JD, van Deursen JM. Naturally occurring p16(Ink4a)-positive cells shorten healthy lifespan. Nature. 2016 Feb 11;530(7589):184-9. doi: 10.1038/nature16932. Epub 2016 Feb 3. PMID: 26840489; PMCID: PMC4845101.

Balasubramanian R, Im J, Lee JS, Jeon HJ, Mogeni OD, Kim JH, Rakotozandrindrainy R, Baker S, Marks F. The global burden and epidemiology of invasive non-typhoidal *Salmonella* infections. Hum Vaccin Immunother. 2019;15(6):1421-1426. doi: 10.1080/21645515.2018.1504717. Epub 2018 Sep 5. PMID: 30081708; PMCID: PMC6663144.

Basisty N, Kale A, Jeon OH, Kuehnemann C, Payne T, Rao C, Holtz A, Shah S, Sharma V, Ferrucci L, Campisi J, Schilling B. A proteomic atlas of senescence-associated secretomes for aging biomarker development. PLoS Biol. 2020 Jan 16;18(1):e3000599. doi: 10.1371/journal.pbio.3000599. PMID: 31945054; PMCID: PMC6964821.

Basters A, Geurink PP, Röcker A, Witting KF, Tadayon R, Hess S, Semrau MS, Storici P, Ovaa H, Knobeloch KP, Fritz G. Structural basis of the specificity of USP18 toward ISG15. Nat Struct Mol Biol. 2017 Mar;24(3):270-278. doi: 10.1038/nsmb.3371. Epub 2017 Feb 6. PMID: 28165509; PMCID: PMC5405867.

Bentley DR, Balasubramanian S, Swerdlow HP, Smith GP, Milton J, Brown CG, Hall KP, Evers DJ, Barnes CL, Bignell HR, Boutell JM, Bryant J, Carter RJ, Keira Cheetham R, Cox AJ, Ellis DJ, Flatbush MR, Gormley NA, Humphray SJ, Irving LJ, Karbelashvili MS, Kirk SM, Li H, Liu X, Maisinger KS, Murray LJ, Obradovic B, Ost T, Parkinson ML, Pratt MR, Rasolonjatovo IM, Reed MT, Rigatti R, Rodighiero C, Ross MT, Sabot A, Sankar SV, Scally A, Schroth GP, Smith ME, Smith VP, Spiridou A, Torrance PE, Tzonev SS, Vermaas EH, Walter K, Wu X, Zhang L, Alam MD, Anastasi C, Aniebo IC, Bailey DM, Bancarz IR, Banerjee S, Barbour SG, Baybayan PA, Benoit VA, Benson KF, Bevis C, Black PJ, Boodhun A, Brennan JS, Bridgham JA, Brown RC, Brown AA, Buermann DH, Bundu AA, Burrows JC, Carter NP, Castillo N, Chiara E Catenazzi M, Chang S, Neil Cooley R, Crake NR, Dada OO, Diakoumakos KD, Dominguez-Fernandez B, Earnshaw DJ, Egbujor UC, Elmore DW, Etchin SS, Ewan MR, Fedurco M, Fraser LJ, Fuentes Fajardo KV, Scott Furey W,

George D, Gietzen KJ, Goddard CP, Golda GS, Granieri PA, Green DE, Gustafson DL, Hansen NF, Harnish K, Haudenschild CD, Heyer NI, Hims MM, Ho JT, Horgan AM, Hoschler K, Hurwitz S, Ivanov DV, Johnson MQ, James T, Huw Jones TA, Kang GD, Kerelska TH, Kersey AD, Khrebtukova I, Kindwall AP, Kingsbury Z, Kokko-Gonzales PI, Kumar A, Laurent MA, Lawley CT, Lee SE, Lee X, Liao AK, Loch JA, Lok M, Luo S, Mammen RM, Martin JW, McCauley PG, McNitt P, Mehta P, Moon KW, Mullens JW, Newington T, Ning Z, Ling Ng B, Novo SM, O'Neill MJ, Osborne MA, Osnowski A, Ostadan O, Paraschos LL, Pickering L, Pike AC, Pike AC, Chris Pinkard D, Pliskin DP, Podhasky J, Quijano VJ, Raczy C, Rae VH, Rawlings SR, Chiva Rodriguez A, Roe PM, Rogers J, Rogert Bacigalupo MC, Romanov N, Romieu A, Roth RK, Rourke NJ, Ruediger ST, Rusman E, Sanches-Kuiper RM, Schenker MR, Seoane JM, Shaw RJ, Shiver MK, Short SW, Sizto NL, Sluis JP, Smith MA, Ernest Sohna Sohna J, Spence EJ, Stevens K, Sutton N, Szajkowski L, Tregidgo CL, Turcatti G, Vandevondele S, Verhovsky Y, Virk SM, Wakelin S, Walcott GC, Wang J, Worsley GJ, Yan J, Yau L, Zuerlein M, Rogers J, Mullikin JC, Hurles ME, McCooke NJ, West JS, Oaks FL, Lundberg PL, Klenerman D, Durbin R, Smith AJ. Accurate whole human genome sequencing using reversible terminator chemistry. Nature. 2008 Nov 6;456(7218):53-9. doi: 10.1038/nature07517. PMID: 18987734; PMCID: PMC2581791.

Berry MP, Graham CM, McNab FW, Xu Z, Bloch SA, Oni T, Wilkinson KA, Banchereau R, Skinner J, Wilkinson RJ, Quinn C, Blankenship D, Dhawan R, Cush JJ, Mejias A, Ramilo O, Kon OM, Pascual V, Banchereau J, Chaussabel D, O'Garra A. An interferon-inducible neutrophil-driven blood transcriptional signature in human tuberculosis. Nature. 2010 Aug 19;466(7309):973-7. doi: 10.1038/nature09247. PMID: 20725040; PMCID: PMC3492754.

Blumer T, Coto-Llerena M, Duong FHT, Heim MH. SOCS1 is an inducible negative regulator of interferon λ (IFN-λ)-induced gene expression *in vivo*. J Biol Chem. 2017 Oct 27;292(43):17928-17938. doi: 10.1074/jbc.M117.788877. Epub 2017 Sep 12. PMID: 28900038; PMCID: PMC5663890.

Bogunovic D, Byun M, Durfee LA, Abhyankar A, Sanal O, Mansouri D, Salem S, Radovanovic I, Grant AV, Adimi P, Mansouri N, Okada S, Bryant VL, Kong XF, Kreins A, Velez MM, Boisson B, Khalilzadeh S, Ozcelik U, Darazam IA, Schoggins JW, Rice CM, Al-Muhsen S, Behr M, Vogt G, Puel A, Bustamante J, Gros P, Huibregtse JM, Abel L, Boisson-Dupuis S, Casanova JL. Mycobacterial disease and impaired IFN-γ immunity in humans with inherited ISG15 deficiency. Science. 2012 Sep 28;337(6102):1684-8. doi: 10.1126/science.1224026. Epub 2012 Aug 2. PMID: 22859821; PMCID: PMC3507439.

Bolado-Carrancio A, Lee M, Ewing A, Muir M, Macleod KG, Gallagher WM, Nguyen LK, Carragher NO, Semple CA, Brunton VG, Caswell PT, von Kriegsheim A. ISGylation drives basal breast tumour progression by promoting EGFR recycling and Akt signalling. Oncogene. 2021 Nov;40(44):6235-6247. doi: 10.1038/s41388-021-02017-8. Epub 2021 Sep 23. PMID: 34556814; PMCID: PMC8566238.

Brem R, Hall J. XRCC1 is required for DNA single-strand break repair in human cells. Nucleic Acids Res. 2005 May 2;33(8):2512-20. doi: 10.1093/nar/gki543. PMID: 15867196; PMCID: PMC1088068.

Buchlis G, Odorizzi P, Soto PC, Pearce OM, Hui DJ, Jordan MS, Varki A, Wherry EJ, High KA. Enhanced T cell function in a mouse model of human glycosylation. J Immunol. 2013 Jul 1;191(1):228-37. doi: 10.4049/jimmunol.1202905. Epub 2013 May 24. PMID: 23709682; PMCID: PMC3691298.

Burleigh A, Moraitis E, Al Masroori E, Al-Abadi E, Hong Y, Omoyinmi E, Titheradge H, Stals K, Jones WD, Gait A, Jayarajan V, Di WL, Sebire N, Solman L, Ogboli M, Welch SB, Sudarsanam A, Wacogne I, Price-Kuehne F, Jensen B, Brogan PA, Eleftheriou D. Case Report: ISG15 deficiency caused by novel variants in two families and effective treatment with Janus kinase inhibition. Front Immunol. 2023 Dec 5;14:1287258. doi: 10.3389/fimmu.2023.1287258. PMID: 38115997; PMCID: PMC10728638.

Burkinshaw BJ, Strynadka NC. Assembly and structure of the T3SS. Biochim Biophys Acta. 2014 Aug;1843(8):1649-63. doi: 10.1016/j.bbamcr.2014.01.035. Epub 2014 Feb 7. PMID: 24512838.

Burks J, Reed RE, Desai SD. Free ISG15 triggers an antitumor immune response against breast cancer: a new perspective. Oncotarget. 2015 Mar 30;6(9):7221-31. doi: 10.18632/oncotarget.3372. PMID: 25749047; PMCID: PMC4466680.

Cannan WJ, Pederson DS. Mechanisms and Consequences of Double-Strand DNA Break Formation in Chromatin. J Cell Physiol. 2016 Jan;231(1):3-14. doi: 10.1002/jcp.25048. PMID: 26040249; PMCID: PMC4994891.

Caldecott KW. Single-strand break repair and genetic disease. Nat Rev Genet. 2008 Aug;9(8):619-31. doi: 10.1038/nrg2380. PMID: 18626472.

Caldecott KW. Causes and consequences of DNA single-strand breaks. Trends Biochem Sci. 2024 Jan;49(1):68-78. doi: 10.1016/j.tibs.2023.11.001. Epub 2023 Nov 30. PMID: 38040599.

Carver A, Zhang X. Rad51 filament dynamics and its antagonistic modulators. Semin Cell Dev Biol. 2021 May;113:3-13. doi: 10.1016/j.semcdb.2020.06.012. Epub 2020 Jul 3. PMID: 32631783.
Ceccaldi R, Rondinelli B, D'Andrea AD. Repair Pathway Choices and Consequences at the Double-Strand Break. Trends Cell Biol. 2016 Jan;26(1):52-64. doi: 10.1016/j.tcb.2015.07.009. Epub 2015 Oct 1. PMID: 26437586; PMCID: PMC4862604.

Melton-Celsa AR. Shiga Toxin (Stx) Classification, Structure, and Function. Microbiol Spectr. 2014 Aug;2(4):EHEC-0024-2013. doi: 10.1128/microbiolspec.EHEC-0024-2013. PMID: 25530917; PMCID: PMC4270005.

Chatterjee N, Walker GC. Mechanisms of DNA damage, repair, and mutagenesis. Environ Mol Mutagen. 2017 Jun;58(5):235-263. doi: 10.1002/em.22087. Epub 2017 May 9. PMID: 28485537; PMCID: PMC5474181.

Chaudhuri RA, Nussenzweig A. The multifaceted roles of PARP1 in DNA repair and chromatin remodelling. Nat Rev Mol Cell Biol. 2017 Oct;18(10):610-621. doi: 10.1038/nrm.2017.53. Epub 2017 Jul 5. PMID: 28676700; PMCID: PMC6591728.

Chelbi-Alix MK, Thibault P. Crosstalk Between SUMO and Ubiquitin-Like Proteins: Implication for Antiviral Defense. Front Cell Dev Biol. 2021 Apr 21;9:671067. doi: 10.3389/fcell.2021.671067. PMID: 33968942; PMCID: PMC8097047.

Chemello AJ, Fowler CC. Alternate typhoid toxin assembly evolved independently in the two *Salmonella* species. mBio. 2024 Apr 10;15(4):e0340323. doi: 10.1128/mbio.03403-23. Epub 2024 Mar 19. PMID: 38501873; PMCID: PMC11005416.

Chen H, Ang CJ, Crowder MK, Brieher WM, Blanke SR. Revisiting bacterial cytolethal distending toxin structure and function. Front Cell Infect Microbiol. 2023 Nov 14;13:1289359. doi: 10.3389/fcimb.2023.1289359. Erratum in: Front Cell Infect Microbiol. 2024 Jan 16;14:1366193. doi: 10.3389/fcimb.2024.1366193. PMID: 38035327; PMCID: PMC10682658.

Chen L, Li S, McGilvray I. The ISG15/USP18 ubiquitin-like pathway (ISGylation system) in hepatitis C virus infection and resistance to interferon therapy. Int J Biochem Cell Biol. 2011 Oct;43(10):1427-31. doi: 10.1016/j.biocel.2011.06.006. Epub 2011 Jun 16. PMID: 21704181.

Cheng Q, Chen J. Mechanism of p53 stabilization by ATM after DNA damage. Cell Cycle. 2010 Feb 1;9(3):472-8. doi: 10.4161/cc.9.3.10556. PMID: 20081365; PMCID: PMC2977994.

Cheng J, DeCaprio JA, Fluck MM, Schaffhausen BS. Cellular transformation by Simian Virus 40 and Murine Polyoma Virus T antigens. Semin Cancer Biol. 2009 Aug;19(4):218-28. doi: 10.1016/j.semcancer.2009.03.002. Epub 2009 Mar 31. PMID: 19505649; PMCID: PMC2694755.

Chiloeches M, Bergonzini A, Frisan T. Bacterial Toxins Are a Never-Ending Source of Surprises: From Natural Born Killers to Negotiators. Toxins (Basel). 2021 Jun 17;13(6):426. doi: 10.3390/toxins13060426. PMID: 34204481; PMCID: PMC8235270.

Chiloeches M, Bergonzini A, Martin OCB, Bergstein N, Erttmann SF, Aung KM, Gekara NO, Avila Cariño JF, Pateras IS, Frisan T. Genotoxin-producing *Salmonella enterica* induces tissue-specific types of DNA damage and DNA damage response outcomes. Front Immunol. 2024 Jan 11;14:1270449. doi: 10.3389/fimmu.2023.1270449. PMID: 38274797; PMCID: PMC10808668.

Clark JS, Kayed R, Abate G, Uberti D, Kinnon P, Piccirella S. Post-translational Modifications of the p53 Protein and the Impact in Alzheimer's Disease: A Review of the Literature. Front Aging Neurosci. 2022 Apr 28;14:835288. doi: 10.3389/fnagi.2022.835288. PMID: 35572126; PMCID: PMC9096077.

Chong A, Lee S, Yang YA, Song J. The Role of Typhoid Toxin in *Salmonella* Typhi Virulence. Yale J Biol Med. 2017 Jun 23;90(2):283-290. PMID: 28656014; PMCID: PMC5482304.

Coppé JP, Patil CK, Rodier F, Sun Y, Muñoz DP, Goldstein J, Nelson PS, Desprez PY, Campisi J. Senescence-associated secretory phenotypes reveal cell-nonautonomous functions of oncogenic RAS and the p53 tumor suppressor. PLoS Biol. 2008 Dec 2;6(12):2853-68. doi: 10.1371/journal.pbio.0060301. PMID: 19053174; PMCID: PMC2592359.

Cooper, G. M. The Cell: A Molecular Approach. 2nd Edition. Sinauer Associates, 2000

Daczkowski CM, Goodwin OY, Dzimianski JV, Farhat JJ, Pegan SD. Structurally Guided Removal of DeISGylase Biochemical Activity from Papain-Like Protease Originating from Middle East Respiratory Syndrome Coronavirus. J Virol. 2017 Nov 14;91(23):e01067-17. doi: 10.1128/JVI.01067-17. PMID: 28931677; PMCID: PMC5686735.

Del Bel Belluz L, Guidi R, Pateras IS, Levi L, Mihaljevic B, Rouf SF, Wrande M, Candela M, Turroni S, Nastasi C, Consolandi C, Peano C, Tebaldi T, Viero G, Gorgoulis VG, Krejsgaard T, Rhen M, Frisan T. The Typhoid Toxin Promotes Host Survival and the Establishment of a Persistent Asymptomatic Infection. PLoS Pathog. 2016 Apr 7;12(4):e1005528. doi: 10.1371/journal.ppat.1005528. PMID: 27055274; PMCID: PMC4824513.

Dastur A, Beaudenon S, Kelley M, Krug RM, Huibregtse JM. Herc5, an interferon-induced HECT E3 enzyme, is required for conjugation of ISG15 in human cells. J Biol Chem. 2006 Feb 17;281(7):4334-8. doi: 10.1074/jbc.M512830200. Epub 2005 Dec 28. PMID: 16407192.

Demaria M, Ohtani N, Youssef SA, Rodier F, Toussaint W, Mitchell JR, Laberge RM, Vijg J, Van Steeg H, Dollé ME, Hoeijmakers JH, de Bruin A, Hara E, Campisi J. An essential role for senescent cells in optimal wound healing through secretion of PDGF-AA. Dev Cell. 2014 Dec 22;31(6):722-33. doi: 10.1016/j.devcel.2014.11.012. Epub 2014 Dec 11. PMID: 25499914; PMCID: PMC4349629.

Deng W, Marshall NC, Rowland JL, McCoy JM, Worrall LJ, Santos AS, Strynadka NCJ, Finlay BB. Assembly, structure, function and regulation of type III secretion systems. Nat Rev Microbiol. 2017 Jun;15(6):323-337. doi: 10.1038/nrmicro.2017.20. Epub 2017 Apr 10. Erratum in: Nat Rev Microbiol. 2017 May 12;15(6):379. doi: 10.1038/nrmicro.2017.54. PMID: 28392566.

Deshpande D, Chhugani K, Chang Y, Karlsberg A, Loeffler C, Zhang J, Muszyńska A, Munteanu V, Yang H, Rotman J, Tao L, Balliu B, Tseng E, Eskin E, Zhao F, Mohammadi P, P Łabaj P, Mangul S. RNA-seq data science: From raw data to effective interpretation. Front Genet. 2023 Mar 13;14:997383. doi: 10.3389/fgene.2023.997383. PMID: 36999049; PMCID: PMC10043755.

Di Domenico EG, Cavallo I, Pontone M, Toma L, Ensoli F. Biofilm Producing Salmonella Typhi: Chronic Colonization and Development of Gallbladder Cancer. Int J Mol Sci. 2017 Aug 31;18(9):1887. doi: 10.3390/ijms18091887. PMID: 28858232; PMCID: PMC5618536.

Di Micco R, Krizhanovsky V, Baker D, d'Adda di Fagagna F. Cellular senescence in ageing: from mechanisms to therapeutic opportunities. Nat Rev Mol Cell Biol. 2021 Feb;22(2):75-95. doi: 10.1038/s41580-020-00314-w. Epub 2020 Dec 16. PMID: 33328614; PMCID: PMC8344376.

Douarre C, Mergui X, Sidibe A, Gomez D, Alberti P, Mailliet P, Trentesaux C, Riou JF. DNA damage signaling induced by the G-quadruplex ligand 12459 is modulated by PPM1D/WIP1 phosphatase. Nucleic Acids Res. 2013 Apr 1;41(6):3588-99. doi: 10.1093/nar/gkt073. Epub 2013 Feb 8. PMID: 23396447; PMCID: PMC3616712.

Du W, Liu X, Yang M, Wang W, Sun J. The Regulatory Role of PRRX1 in Cancer Epithelial-Mesenchymal Transition. Onco Targets Ther. 2021 Jul 16;14:4223-4229. doi: 10.2147/OTT.S316102. PMID: 34295164; PMCID: PMC8291965.

Dueva R, Iliakis G. Replication protein A: a multifunctional protein with roles in DNA replication, repair and beyond. NAR Cancer. 2020 Sep 25;2(3):zcaa022. doi: 10.1093/narcan/zcaa022. PMID: 34316690; PMCID: PMC8210275.

Dutta U, Garg PK, Kumar R, Tandon RK. Typhoid carriers among patients with gallstones are at increased risk for carcinoma of the gallbladder. Am J Gastroenterol. 2000 Mar;95(3):784-7. doi: 10.1111/j.1572-0241.2000.01860.x. PMID: 10710075.

Dzimianski JV, Scholte FEM, Bergeron É, Pegan SD. ISG15: It's Complicated. J Mol Biol. 2019 Oct 4;431(21):4203-4216. doi: 10.1016/j.jmb.2019.03.013. Epub 2019 Mar 16. PMID: 30890331; PMCID: PMC6746611.

Elmore S. Apoptosis: a review of programmed cell death. Toxicol Pathol. 2007 Jun;35(4):495-516. doi: 10.1080/01926230701320337. PMID: 17562483; PMCID: PMC2117903.

El-Asmi F, McManus FP, Brantis-de-Carvalho CE, Valle-Casuso JC, Thibault P, Chelbi-Alix MK. Cross-talk between SUMOylation and ISGylation in response to interferon. Cytokine. 2020 May;129:155025. doi: 10.1016/j.cyto.2020.155025. Epub 2020 Feb 7. PMID: 32044670.

Efroni S, Duttagupta R, Cheng J, Dehghani H, Hoeppner DJ, Dash C, Bazett-Jones DP, Le Grice S, McKay RD, Buetow KH, Gingeras TR, Misteli T, Meshorer E. Global

transcription in pluripotent embryonic stem cells. Cell Stem Cell. 2008 May 8;2(5):437-47. doi: 10.1016/j.stem.2008.03.021. PMID: 18462694; PMCID: PMC2435228.

El Ghazaly M, Collins MO, Ibler AEM, Humphreys D. Typhoid toxin hijacks Wnt5a to establish host senescence and Salmonella infection. Cell Rep. 2023 Oct 31;42(10):113181. doi: 10.1016/j.celrep.2023.113181. Epub 2023 Oct 4. PMID: 37792529.

Elwell CA, Dreyfus LA. DNase I homologous residues in CdtB are critical for cytolethal distending toxin-mediated cell cycle arrest. Mol Microbiol. 2000 Aug;37(4):952-63. doi: 10.1046/j.1365-2958.2000.02070.x. PMID: 10972814.

Eng, S. K., Pusparajah, P., Ab Mutalib, N. S., Ser, H. L., Chan, K. G., & Lee, L. H. (2015). *Salmonella*: A review on pathogenesis, epidemiology and antibiotic resistance. *Frontiers in Life Science*, *8*(3), 284–293. https://doi.org/10.1080/21553769.2015.105124

Ensminger M, Löbrich M. One end to rule them all: Non-homologous end-joining and homologous recombination at DNA double-strand breaks. Br J Radiol. 2020 Nov 1;93(1115):20191054. doi: 10.1259/bjr.20191054. Epub 2020 Feb 28. PMID: 32105514; PMCID: PMC8519636.

Fàbrega A, Vila J. Salmonella enterica serovar Typhimurium skills to succeed in the host: virulence and regulation. Clin Microbiol Rev. 2013 Apr;26(2):308-41. doi: 10.1128/CMR.00066-12. PMID: 23554419; PMCID: PMC3623383.

Feasey NA, Dougan G, Kingsley RA, Heyderman RS, Gordon MA. Invasive non-typhoidal salmonella disease: an emerging and neglected tropical disease in Africa. Lancet. 2012 Jun 30;379(9835):2489-2499. doi: 10.1016/S0140-6736(11)61752-2. Epub 2012 May 14. PMID: 22587967; PMCID: PMC3402672.

Fedor Y, Vignard J, Nicolau-Travers ML, Boutet-Robinet E, Watrin C, Salles B, Mirey G. From single-strand breaks to double-strand breaks during S-phase: a new mode of action of the Escherichia coli Cytolethal Distending Toxin. Cell Microbiol. 2013 Jan;15(1):1-15. doi: 10.1111/cmi.12028. Epub 2012 Oct 9. PMID: 22978660.

Fowler CC, Chang SJ, Gao X, Geiger T, Stack G, Galán JE. Emerging insights into the biology of typhoid toxin. Curr Opin Microbiol. 2017 Feb;35:70-77. doi: 10.1016/j.mib.2017.01.012. Epub 2017 Feb 16. PMID: 28213043; PMCID: PMC5484737.

Freitas BT, Scholte FEM, Bergeron É, Pegan SD. How ISG15 combats viral infection. Virus Res. 2020 Sep;286:198036. doi: 10.1016/j.virusres.2020.198036. Epub 2020 May 31. PMID: 32492472; PMCID: PMC7483349.

Frisan T. Bacterial genotoxins: The long journey to the nucleus of mammalian cells. Biochim Biophys Acta. 2016 Mar;1858(3):567-75. doi: 10.1016/j.bbamem.2015.08.016. Epub 2015 Aug 20. PMID: 26299818.

Frisan T, Cortes-Bratti X, Thelestam M. Cytolethal distending toxins and activation of DNA damage-dependent checkpoint responses. Int J Med Microbiol. 2002 Feb;291(6-7):495-9. doi: 10.1078/1438-4221-00158. PMID: 11890549.

Frisan T, Cortes-Bratti X, Chaves-Olarte E, Stenerlöw B, Thelestam M. The Haemophilus ducreyi cytolethal distending toxin induces DNA double-strand breaks and promotes ATM-dependent activation of RhoA. Cell Microbiol. 2003 Oct;5(10):695-707. doi: 10.1046/j.1462-5822.2003.00311.x. PMID: 12969375.

Galán JE. Typhoid toxin provides a window into typhoid fever and the biology of Salmonella Typhi. Proc Natl Acad Sci U S A. 2016 Jun 7;113(23):6338-44. doi: 10.1073/pnas.1606335113. Epub 2016 May 24. PMID: 27222578; PMCID: PMC4988619.

Galkin VE, Orlova A, VanLoock MS, Zhou D, Galán JE, Egelman EH. The bacterial protein SipA polymerizes G-actin and mimics muscle nebulin. Nat Struct Biol. 2002 Jul;9(7):518-21. doi: 10.1038/nsb811. PMID: 12055622.

Gal-Mor O, Boyle EC, Grassl GA. Same species, different diseases: how and why typhoidal and non-typhoidal Salmonella enterica serovars differ. Front Microbiol. 2014 Aug 4;5:391. doi: 10.3389/fmicb.2014.00391. PMID: 25136336; PMCID: PMC4120697.

Gal-Mor O. Persistent Infection and Long-Term Carriage of Typhoidal and Nontyphoidal Salmonellae. Clin Microbiol Rev. 2018 Nov 28;32(1):e00088-18. doi: 10.1128/CMR.00088-18. PMID: 30487167; PMCID: PMC6302356.

Ganesan M, Poluektova LY, Tuma DJ, Kharbanda KK, Osna NA. Acetaldehyde Disrupts Interferon Alpha Signaling in Hepatitis C Virus-Infected Liver Cells by Up-Regulating USP18. Alcohol Clin Exp Res. 2016 Nov;40(11):2329-2338. doi: 10.1111/acer.13226. Epub 2016 Sep 26. PMID: 27716962; PMCID: PMC6800117.

Gargan S, Ahmed S, Mahony R, Bannan C, Napoletano S, O'Farrelly C, Borrow P, Bergin C, Stevenson NJ. HIV-1 Promotes the Degradation of Components of the Type 1 IFN JAK/STAT Pathway and Blocks Anti-viral ISG Induction. EBioMedicine. 2018 Apr;30:203-216. doi: 10.1016/j.ebiom.2018.03.006. Epub 2018 Mar 9. PMID: 29580840; PMCID: PMC5952252.

Geiger T, Lara-Tejero M, Xiong Y, Galán JE. Mechanisms of substrate recognition by a typhoid toxin secretion-associated muramidase. Elife. 2020 Jan 20;9:e53473. doi: 10.7554/eLife.53473. PMID: 31958059; PMCID: PMC6996933.

Geiss-Friedlander R, Melchior F. Concepts in sumoylation: a decade on. Nat Rev Mol Cell Biol. 2007 Dec;8(12):947-56. doi: 10.1038/nrm2293. PMID: 18000527.

Ghasemi M, Turnbull T, Sebastian S, Kempson I. The MTT Assay: Utility, Limitations, Pitfalls, and Interpretation in Bulk and Single-Cell Analysis. Int J Mol Sci. 2021 Nov 26;22(23):12827. doi: 10.3390/ijms222312827. PMID: 34884632; PMCID: PMC8657538.

Gloeck NR, Leong T, Iwu-Jaja CJ, Katoto PDM, Kredo T, Wiysonge CS. Typhoid conjugate vaccines for preventing typhoid fever (enteric fever). Cochrane Database Syst Rev. 2023 Jun 14;2023(6):CD015746. doi: 10.1002/14651858.CD015746. PMCID: PMC10266125.

Gonzalez-Escobedo G, Marshall JM, Gunn JS. Chronic and acute infection of the gall bladder by Salmonella Typhi: understanding the carrier state. Nat Rev Microbiol. 2011 Jan;9(1):9-14. doi: 10.1038/nrmicro2490. Epub 2010 Nov 29. PMID: 21113180; PMCID: PMC3255095.

Gonzalez-Meljem JM, Apps JR, Fraser HC, Martinez-Barbera JP. Paracrine roles of cellular senescence in promoting tumourigenesis. Br J Cancer. 2018 May;118(10):1283-1288. doi: 10.1038/s41416-018-0066-1. Epub 2018 Apr 19. PMID: 29670296; PMCID: PMC5959857.

González-Sanz R, Mata M, Bermejo-Martín J, Álvarez A, Cortijo J, Melero JA, Martínez I. ISG15 Is Upregulated in Respiratory Syncytial Virus Infection and Reduces Virus Growth through Protein ISGylation. J Virol. 2016 Jan 13;90(7):3428-38. doi: 10.1128/JVI.02695-15. PMID: 26763998; PMCID: PMC4794669.

Granada AE, Jiménez A, Stewart-Ornstein J, Blüthgen N, Reber S, Jambhekar A, Lahav G. The effects of proliferation status and cell cycle phase on the responses of single cells to chemotherapy. Mol Biol Cell. 2020 Apr 1;31(8):845-857. doi: 10.1091/mbc.E19-09-0515. Epub 2020 Feb 12. PMID: 32049575; PMCID: PMC7185964.

Grasso F, Frisan T. Bacterial Genotoxins: Merging the DNA Damage Response into Infection Biology. Biomolecules. 2015 Aug 11;5(3):1762-82. doi: 10.3390/biom5031762. PMID: 26270677; PMCID: PMC4598774.

Guerra L, Cortes-Bratti X, Guidi R, Frisan T. The biology of the cytolethal distending toxins. Toxins (Basel). 2011 Mar;3(3):172-90. doi: 10.3390/toxins3030172. Epub 2011 Mar 7. PMID: 22069704; PMCID: PMC3202825.
Guerra S, Cáceres A, Knobeloch KP, Horak I, Esteban M. Vaccinia virus E3 protein prevents the antiviral action of ISG15. PLoS Pathog. 2008 Jul 4;4(7):e1000096. doi: 10.1371/journal.ppat.1000096. PMID: 18604270; PMCID: PMC2434199.

Guidi R, Guerra L, Levi L, Stenerlöw B, Fox JG, Josenhans C, Masucci MG, Frisan T. Chronic exposure to the cytolethal distending toxins of Gram-negative bacteria promotes genomic instability and altered DNA damage response. Cell Microbiol. 2013 Jan;15(1):98-113. doi: 10.1111/cmi.12034. Epub 2012 Nov 1. PMID: 22998585; PMCID: PMC4136655.

Haghjoo E, Galán JE. Identification of a transcriptional regulator that controls intracellular gene expression in Salmonella Typhi. Mol Microbiol. 2007 Jun;64(6):1549-61. doi: 10.1111/j.1365-2958.2007.05754.x. PMID: 17555437.
Hakem R. DNA-damage repair; the good, the bad, and the ugly. EMBO J. 2008 Feb 20;27(4):589-605. doi: 10.1038/emboj.2008.15. PMID: 18285820; PMCID: PMC2262034.

Hancuh M, Walldorf J, Minta AA, Tevi-Benissan C, Christian KA, Nedelec Y, Heitzinger K, Mikoleit M, Tiffany A, Bentsi-Enchill AD, Breakwell L. Typhoid Fever Surveillance, Incidence Estimates, and Progress Toward Typhoid Conjugate Vaccine Introduction - Worldwide, 2018-2022. MMWR Morb Mortal Wkly Rep. 2023 Feb 17;72(7):171-176. doi: 10.15585/mmwr.mm7207a2. PMID: 36795626; PMCID: PMC9949843.

Haselbeck AH, Panzner U, Im J, Baker S, Meyer CG, Marks F. Current perspectives on invasive nontyphoidal Salmonella disease. Curr Opin Infect Dis. 2017 Oct;30(5):498-503. doi: 10.1097/QCO.0000000000000398. PMID: 28731899; PMCID: PMC7680934.

Hautefort I, Thompson A, Eriksson-Ygberg S, Parker ML, Lucchini S, Danino V, Bongaerts RJ, Ahmad N, Rhen M, Hinton JC. During infection of epithelial cells Salmonella enterica serovar Typhimurium undergoes a time-dependent transcriptional adaptation that results in simultaneous expression of three type 3 secretion systems. Cell Microbiol. 2008 Apr;10(4):958-84. doi: 10.1111/j.1462-5822.2007.01099.x. Epub 2007 Nov 20. PMID: 18031307; PMCID: PMC2343689.

He S, Sharpless NE. Senescence in Health and Disease. Cell. 2017 Jun 1;169(6):1000-1011. doi: 10.1016/j.cell.2017.05.015. PMID: 28575665; PMCID: PMC5643029.

Helbig KJ, Teh MY, Crosse KM, Monson EA, Smith M, Tran EN, Standish AJ, Morona R, Beard MR. The interferon stimulated gene viperin, restricts Shigella. flexneri in vitro. Sci Rep. 2019 Oct 30;9(1):15598. doi: 10.1038/s41598-019-52130-8. PMID: 31666594; PMCID: PMC6821890.

Herranz N, Gil J. Mechanisms and functions of cellular senescence. J Clin Invest. 2018 Apr 2;128(4):1238-1246. doi: 10.1172/JCI95148. Epub 2018 Apr 2. PMID: 29608137; PMCID: PMC5873888.

Hirose K, Ezaki T, Miyake M, Li T, Khan AQ, Kawamura Y, Yokoyama H, Takami T. Survival of Vi-capsulated and Vi-deleted Salmonella typhi strains in cultured macrophage expressing different levels of CD14 antigen. FEMS Microbiol Lett. 1997 Feb 15;147(2):259-65. doi: 10.1111/j.1574-6968.1997.tb10251.x. PMID: 9119202.

Hoffmann S, Batz MB, Morris JG Jr. Annual cost of illness and quality-adjusted life year losses in the United States due to 14 foodborne pathogens. J Food Prot. 2012 Jul;75(7):1292-302. doi: 10.4315/0362-028X.JFP-11-417. PMID: 22980013.

Holthaus D, Vasou A, Bamford CGG, Andrejeva J, Paulus C, Randall RE, McLauchlan J, Hughes DJ. Direct Antiviral Activity of IFN-Stimulated Genes Is Responsible for Resistance to Paramyxoviruses in ISG15-Deficient Cells. J Immunol. 2020 Jul 1;205(1):261-271. doi: 10.4049/jimmunol.1901472. Epub 2020 May 18. PMID: 32423918; PMCID: PMC7311202.

Hone DM, Attridge SR, Forrest B, Morona R, Daniels D, LaBrooy JT, Bartholomeusz RC, Shearman DJ, Hackett J. A galE via (Vi antigen-negative) mutant of Salmonella typhi Ty2 retains virulence in humans. Infect Immun. 1988 May;56(5):1326-33. doi: 10.1128/iai.56.5.1326-1333.1988. PMID: 3356467; PMCID: PMC259821.

Honke N, Shaabani N, Zhang DE, Hardt C, Lang KS. Multiple functions of USP18. Cell Death Dis. 2016 Nov 3;7(11):e2444. doi: 10.1038/cddis.2016.326. PMID: 27809302; PMCID: PMC5260889.

Hossain MA, Lin Y, Yan S. Single-Strand Break End Resection in Genome Integrity: Mechanism and Regulation by APE2. Int J Mol Sci. 2018 Aug 14;19(8):2389. doi: 10.3390/ijms19082389. PMID: 30110897; PMCID: PMC6122073.

Hu W, Chan H, Lu L, Wong KT, Wong SH, Li MX, Xiao ZG, Cho CH, Gin T, Chan MTV, Wu WKK, Zhang L. Autophagy in intracellular bacterial infection. Semin Cell Dev Biol. 2020 May;101:41-50. doi: 10.1016/j.semcdb.2019.07.014. Epub 2019 Sep 10. PMID: 31408699.

Huang YF, Wee S, Gunaratne J, Lane DP, Bulavin DV. Isg15 controls p53 stability and functions. Cell Cycle. 2014;13(14):2200-10. doi: 10.4161/cc.29209. Epub 2014 May 20. PMID: 24844324; PMCID: PMC4111675.

Hume PJ, Singh V, Davidson AC, Koronakis V. Swiss Army Pathogen: The *Salmonella* Entry Toolkit. Front Cell Infect Microbiol. 2017 Aug 9;7:348. doi: 10.3389/fcimb.2017.00348. PMID: 28848711; PMCID: PMC5552672.

Humphreys D, ElGhazaly M, Frisan T. Senescence and Host-Pathogen Interactions. Cells. 2020 Jul 21;9(7):1747. doi: 10.3390/cells9071747. PMID: 32708331; PMCID: PMC7409240.

Ibler AEM, ElGhazaly M, Naylor KL, Bulgakova NA, F El-Khamisy S, Humphreys D. Typhoid toxin exhausts the RPA response to DNA replication stress driving senescence and Salmonella infection. Nat Commun. 2019 Sep 6;10(1):4040. doi: 10.1038/s41467-019-12064-1. PMID: 31492859; PMCID: PMC6731267.

Isaacs A, Lindemann J. Virus interference. I. The interferon. Proc R Soc Lond B Biol Sci. 1957 Sep 12;147(927):258-67. doi: 10.1098/rspb.1957.0048. PMID: 13465720.

Islam MT, Im J, Ahmmed F, Kim DR, Khan AI, Zaman K, Ali M, Marks F, Qadri F, Kim JH, Clemens JD. Use of Typhoid Vi-Polysaccharide Vaccine as a Vaccine Probe to Delineate Clinical Criteria for Typhoid Fever. Am J Trop Med Hyg. 2020

Aug;103(2):665-671. doi: 10.4269/ajtmh.19-0968. Epub 2020 Jun 18. PMID: 32588803; PMCID: PMC7410438.

Jackson SP, Bartek J. The DNA-damage response in human biology and disease. Nature. 2009 Oct 22;461(7267):1071-8. doi: 10.1038/nature08467. PMID: 19847258; PMCID: PMC2906700.

Jacquet S, Pontier D, Etienne L. Rapid Evolution of HERC6 and Duplication of a Chimeric HERC5/6 Gene in Rodents and Bats Suggest an Overlooked Role of HERCs in Mammalian Immunity. Front Immunol. 2020 Dec 18;11:605270. doi: 10.3389/fimmu.2020.605270. PMID: 33391270; PMCID: PMC7775381.

Jan R, Chaudhry GE. Understanding Apoptosis and Apoptotic Pathways Targeted Cancer Therapeutics. Adv Pharm Bull. 2019 Jun;9(2):205-218. doi: 10.15171/apb.2019.024. Epub 2019 Jun 1. PMID: 31380246; PMCID: PMC6664112.

Jahan F, Chinni SV, Samuggam S, Reddy LV, Solayappan M, Su Yin L. The Complex Mechanism of the Salmonella typhi Biofilm Formation That Facilitates Pathogenicity: A Review. Int J Mol Sci. 2022 Jun 9;23(12):6462. doi: 10.3390/ijms23126462. PMID: 35742906; PMCID: PMC9223757.

Jang HD, Chung YM, Baik JH, Choi YG, Park IS, Jung YK, Lee SY. Caspase-cleaved TRAF1 negatively regulates the antiapoptotic signals of TRAF2 during TNF-induced cell death. Biochem Biophys Res Commun. 2001 Feb 23;281(2):499-505. doi: 10.1006/bbrc.2001.4369. PMID: 11181075.

Jasin M, Rothstein R. Repair of strand breaks by homologous recombination. Cold Spring Harb Perspect Biol. 2013 Nov 1;5(11):a012740. doi: 10.1101/cshperspect.a012740. PMID: 24097900; PMCID: PMC3809576.

Jeon SJ, Chung KC. Covalent conjugation of ubiquitin-like ISG15 to apoptosis-inducing factor exacerbates toxic stimuli-induced apoptotic cell death. J Biol Chem. 2022 Oct;298(10):102464. doi: 10.1016/j.jbc.2022.102464. Epub 2022 Sep 6. PMID: 36075291; PMCID: PMC9547223.

Jeon YJ, Yoo HM, Chung CH. ISG15 and immune diseases. Biochim Biophys Acta. 2010 May;1802(5):485-96. doi: 10.1016/j.bbadis.2010.02.006. Epub 2010 Feb 12. PMID: 20153823; PMCID: PMC7127291.

Jin C, Gibani MM, Moore M, Juel HB, Jones E, Meiring J, Harris V, Gardner J, Nebykova A, Kerridge SA, Hill J, Thomaides-Brears H, Blohmke CJ, Yu LM, Angus B, Pollard AJ. Efficacy and immunogenicity of a Vi-tetanus toxoid conjugate vaccine in the prevention of typhoid fever using a controlled human infection model of Salmonella Typhi: a randomised controlled, phase 2b trial. Lancet. 2017 Dec 2;390(10111):2472-2480. doi: 10.1016/S0140-6736(17)32149-9. Epub 2017 Sep 28. PMID: 28965718; PMCID: PMC5720597.

Jinadasa RN, Bloom SE, Weiss RS, Duhamel GE. Cytolethal distending toxin: a conserved bacterial genotoxin that blocks cell cycle progression, leading to apoptosis of a broad range of mammalian cell lineages. Microbiology (Reading). 2011 Jul;157(Pt 7):1851-1875. doi: 10.1099/mic.0.049536-0. Epub 2011 May 12. PMID: 21565933; PMCID: PMC3167888.

Johnson R, Mylona E, Frankel G. Typhoidal Salmonella: Distinctive virulence factors and pathogenesis. Cell Microbiol. 2018 Sep;20(9):e12939. doi: 10.1111/cmi.12939. Epub 2018 Aug 9. PMID: 30030897.

Jun JI, Lau LF. Cellular senescence controls fibrosis in wound healing. Aging (Albany NY). 2010 Sep;2(9):627-31. doi: 10.18632/aging.100201. PMID: 20930261; PMCID: PMC2984611.

Jurėnas D, Fraikin N, Goormaghtigh F, Van Melderen L. Biology and evolution of bacterial toxin-antitoxin systems. Nat Rev Microbiol. 2022 Jun;20(6):335-350. doi: 10.1038/s41579-021-00661-1. Epub 2022 Jan 2. PMID: 34975154.

Kale A, Sharma A, Stolzing A, Desprez PY, Campisi J. Role of immune cells in the removal of deleterious senescent cells. Immun Ageing. 2020 Jun 3;17:16. doi: 10.1186/s12979-020-00187-9. PMID: 32518575; PMCID: PMC7271494.

Kanehisa M, Goto S. KEGG: kyoto encyclopedia of genes and genomes. Nucleic Acids Res. 2000 Jan 1;28(1):27-30. doi: 10.1093/nar/28.1.27. PMID: 10592173; PMCID: PMC102409.

Kang JA, Kim YJ, Jeon YJ. The diverse repertoire of ISG15: more intricate than initially thought. Exp Mol Med. 2022 Nov;54(11):1779-1792. doi: 10.1038/s12276-022-00872-3. Epub 2022 Nov 1. PMID: 36319753; PMCID: PMC9722776.

Karpinich NO, Tafani M, Rothman RJ, Russo MA, Farber JL. The course of etoposide-induced apoptosis from damage to DNA and p53 activation to mitochondrial release of cytochrome c. J Biol Chem. 2002 May 10;277(19):16547-52. doi: 10.1074/jbc.M110629200. Epub 2002 Feb 25. PMID: 11864976.

Kespohl M, Bredow C, Klingel K, Voß M, Paeschke A, Zickler M, Poller W, Kaya Z, Eckstein J, Fechner H, Spranger J, Fähling M, Wirth EK, Radoshevich L, Thery F, Impens F, Berndt N, Knobeloch KP, Beling A. Protein modification with ISG15 blocks coxsackievirus pathology by antiviral and metabolic reprogramming. Sci Adv. 2020 Mar 11;6(11):eaay1109. doi: 10.1126/sciadv.aay1109. PMID: 32195343; PMCID: PMC7065878.

Ketscher L, Hannß R, Morales DJ, Basters A, Guerra S, Goldmann T, Hausmann A, Prinz M, Naumann R, Pekosz A, Utermöhlen O, Lenschow DJ, Knobeloch KP. Selective inactivation of USP18 isopeptidase activity in vivo enhances ISG15 conjugation and viral resistance. Proc Natl Acad Sci U S A. 2015 Feb 3;112(5):1577-82. doi: 10.1073/pnas.1412881112. Epub 2015 Jan 20. PMID: 25605921; PMCID: PMC4321242.

Kim KI, Yan M, Malakhova O, Luo JK, Shen MF, Zou W, de la Torre JC, Zhang DE. Ube1L and protein ISGylation are not essential for alpha/beta interferon signaling. Mol Cell Biol. 2006 Jan;26(2):472-9. doi: 10.1128/MCB.26.2.472-479.2006. PMID: 16382139; PMCID: PMC1346917.

Kimmey JM, Stallings CL. Bacterial Pathogens versus Autophagy: Implications for Therapeutic Interventions. Trends Mol Med. 2016 Dec;22(12):1060-1076. doi: 10.1016/j.molmed.2016.10.008. Epub 2016 Nov 17. PMID: 27866924; PMCID: PMC5215815.

Knodler LA, Winfree S, Drecktrah D, Ireland R, Steele-Mortimer O. Ubiquitination of the bacterial inositol phosphatase, SopB, regulates its biological activity at the plasma membrane. Cell Microbiol. 2009 Nov;11(11):1652-70. doi: 10.1111/j.1462-5822.2009.01356.x. Epub 2009 Jul 13. PMID: 19614667; PMCID: PMC2762020.

Kopitar-Jerala N. The Role of Interferons in Inflammation and Inflammasome Activation. Front Immunol. 2017 Jul 25;8:873. doi: 10.3389/fimmu.2017.00873. PMID: 28791024; PMCID: PMC5525294.

Koshiol J, Wozniak A, Cook P, Adaniel C, Acevedo J, Azócar L, Hsing AW, Roa JC, Pasetti MF, Miquel JF, Levine MM, Ferreccio C; Gallbladder Cancer Chile Working Group. Salmonella enterica serovar Typhi and gallbladder cancer: a case-control study and meta-analysis. Cancer Med. 2016 Nov;5(11):3310-3235. doi: 10.1002/cam4.915. Epub 2016 Oct 11. PMID: 27726295; PMCID: PMC5119987.

Lara-Tejero M, Galán JE. A bacterial toxin that controls cell cycle progression as a deoxyribonuclease I-like protein. Science. 2000 Oct 13;290(5490):354-7. doi: 10.1126/science.290.5490.354. PMID: 11030657.

Lee S, Yang YA, Milano SK, Nguyen T, Ahn C, Sim JH, Thompson AJ, Hillpot EC, Yoo G, Paulson JC, Song J. Salmonella Typhoid Toxin PltB Subunit and Its Non-typhoidal Salmonella Ortholog Confer Differential Host Adaptation and Virulence. Cell Host Microbe. 2020 Jun 10;27(6):937-949.e6. doi: 10.1016/j.chom.2020.04.005. Epub 2020 May 11. PMID: 32396840; PMCID: PMC7292776.

Lecca P, Ihekwaba-Ndibe AEC. Dynamic Modelling of DNA Repair Pathway at the Molecular Level: A New Perspective. Front Mol Biosci. 2022 Sep 13;9:878148. doi: 10.3389/fmolb.2022.878148. PMID: 36177351; PMCID: PMC9513183.

LeMessurier KS, Häcker H, Chi L, Tuomanen E, Redecke V. Type I interferon protects against pneumococcal invasive disease by inhibiting bacterial transmigration across the lung. PLoS Pathog. 2013;9(11):e1003727. doi: 10.1371/journal.ppat.1003727. Epub 2013 Nov 7. PMID: 24244159; PMCID: PMC3820719.

Lenschow DJ, Lai C, Frias-Staheli N, Giannakopoulos NV, Lutz A, Wolff T, Osiak A, Levine B, Schmidt RE, García-Sastre A, Leib DA, Pekosz A, Knobeloch KP, Horak I,

Virgin HW 4th. IFN-stimulated gene 15 functions as a critical antiviral molecule against influenza, herpes, and Sindbis viruses. Proc Natl Acad Sci U S A. 2007 Jan 23;104(4):1371-6. doi: 10.1073/pnas.0607038104. Epub 2007 Jan 16. PMID: 17227866; PMCID: PMC1783119.

Leo E, Deveraux QL, Buchholtz C, Welsh K, Matsuzawa S, Stennicke HR, Salvesen GS, Reed JC. TRAF1 is a substrate of caspases activated during tumor necrosis factor receptor-alpha-induced apoptosis. J Biol Chem. 2001 Mar 16;276(11):8087-93. doi: 10.1074/jbc.M009450200. Epub 2000 Nov 29. PMID: 11098060.

Lim PL, Tam FC, Cheong YM, Jegathesan M. One-step 2-minute test to detect typhoid-specific antibodies based on particle separation in tubes. J Clin Microbiol. 1998 Aug;36(8):2271-8. doi: 10.1128/JCM.36.8.2271-2278.1998. PMID: 9666004; PMCID: PMC105030.

Liu H, Li C, He W, Chen J, Yang G, Chen L, Chang H. Free ISG15 inhibits Pseudorabies virus infection by positively regulating type I IFN signaling. PLoS Pathog. 2022 Oct 31;18(10):e1010921. doi: 10.1371/journal.ppat.1010921. PMID: 36315588; PMCID: PMC9648840.

Liu X, Chen Z, Jiao X, Jiang X, Qiu J, You F, Long H, Cao H, Fowler CC, Gao X. Molecular Insights into the Assembly and Functional Diversification of Typhoid Toxin. mBio. 2022 Feb 22;13(1):e0191621. doi: 10.1128/mbio.01916-21. Epub 2022 Jan 11. PMID: 35012347; PMCID: PMC8749428.

Lorkowski M, Felipe-López A, Danzer CA, Hansmeier N, Hensel M. Salmonella enterica invasion of polarized epithelial cells is a highly cooperative effort. Infect Immun. 2014 Jun;82(6):2657-67. doi: 10.1128/IAI.00023-14. Epub 2014 Apr 7. PMID: 24711567; PMCID: PMC4019164.

Machado LFM, Galán JE. Loss of function of metabolic traits in typhoidal *Salmonella* without apparent genome degradation. mBio. 2024 May 8;15(5):e0060724. doi: 10.1128/mbio.00607-24. Epub 2024 Apr 4. PMID: 38572992; PMCID: PMC11077982.

Madaan A, Verma R, Singh AT, Kumar Jain S, Jaggi M. A stepwise procedure for isolation of murine bone marrow and generation of dendritic cells. JBM 2014, 1(1), 1. https://doi.org/10.14440/jbm.2014.12

Madan R, Rastogi R, Parashuraman S, Mukhopadhyay A. Salmonella acquires lysosome-associated membrane protein 1 (LAMP1) on phagosomes from Golgi via SipC protein-mediated recruitment of host Syntaxin6. J Biol Chem. 2012 Feb 17;287(8):5574-87. doi: 10.1074/jbc.M111.286120. Epub 2011 Dec 21. PMID: 22190682; PMCID: PMC3285332.

Mahmoud A, Oluyemisi A, Uwishema O, Sun J, Jobran AW, David S, Wireko AA, Adanur I, Dost B, Onyeaka H. Recent advances in the diagnosis and management of typhoid fever in Africa: A review. Int J Health Plann Manage. 2023 Mar;38(2):317-329. doi: 10.1002/hpm.3599. Epub 2022 Dec 1. PMID: 36457176.

Mak T, Saunders ME, Chaddah MR. The Immune Response: Basic and Clinical Principles. 2005. Academic Press.

Malik MNH, Waqas SF, Zeitvogel J, Cheng J, Geffers R, Gouda ZA, Elsaman AM, Radwan AR, Schefzyk M, Braubach P, Auber B, Olmer R, Müsken M, Roesner LM, Gerold G, Schuchardt S, Merkert S, Martin U, Meissner F, Werfel T, Pessler F. Congenital deficiency reveals critical role of ISG15 in skin homeostasis. J Clin Invest. 2022 Feb 1;132(3):e141573. doi: 10.1172/JCI141573. PMID: 34847081; PMCID: PMC8803340.

Marchello CS, Birkhold M, Crump JA; Vacc-iNTS consortium collaborators. Complications and mortality of non-typhoidal salmonella invasive disease: a global systematic review and meta-analysis. Lancet Infect Dis. 2022 May;22(5):692-705. doi: 10.1016/S1473-3099(21)00615-0. Epub 2022 Feb 1. PMID: 35114140; PMCID: PMC9021030.

Masuet-Aumatell C, Atouguia J. Typhoid fever infection - Antibiotic resistance and vaccination strategies: A narrative review. Travel Med Infect Dis. 2021 Mar-Apr;40:101946. doi: 10.1016/j.tmaid.2020.101946. Epub 2020 Dec 8. PMID: 33301931.

Mathiasen SL, Gall-Mas L, Pateras IS, Theodorou SDP, Namini MRJ, Hansen MB, Martin OCB, Vadivel CK, Ntostoglou K, Butter D, Givskov M, Geisler C, Akbar AN, Gorgoulis VG, Frisan T, Ødum N, Krejsgaard T. Bacterial genotoxins induce T cell senescence. Cell Rep. 2021 Jun 8;35(10):109220. doi: 10.1016/j.celrep.2021.109220. PMID: 34107253.

Mathieu NA, Paparisto E, Barr SD, Spratt DE. HERC5 and the ISGylation Pathway: Critical Modulators of the Antiviral Immune Response. Viruses. 2021 Jun 9;13(6):1102. doi: 10.3390/v13061102. PMID: 34207696; PMCID: PMC8228270.

Marquardt I, Jakob J, Scheibel J, Hofmann JD, Klawonn F, Neumann-Schaal M, Gerhard R, Bruder D, Jänsch L. *Clostridioides difficile* Toxin CDT Induces Cytotoxic Responses in Human Mucosal-Associated Invariant T (MAIT) Cells. Front Microbiol. 2021 Dec 21;12:752549. doi: 10.3389/fmicb.2021.752549. PMID: 34992584; PMCID: PMC8727052.

Marshall JS, Warrington R, Watson W, Kim HL. An introduction to immunology and immunopathology. Allergy Asthma Clin Immunol. 2018 Sep 12;14(Suppl 2):49. doi: 10.1186/s13223-018-0278-1. PMID: 30263032; PMCID: PMC6156898.

McClelland M, Sanderson KE, Clifton SW, Latreille P, Porwollik S, Sabo A, Meyer R, Bieri T, Ozersky P, McLellan M, Harkins CR, Wang C, Nguyen C, Berghoff A, Elliott G, Kohlberg S, Strong C, Du F, Carter J, Kremizki C, Layman D, Leonard S, Sun H, Fulton L, Nash W, Miner T, Minx P, Delehaunty K, Fronick C, Magrini V, Nhan M, Warren W, Florea L, Spieth J, Wilson RK. Comparison of genome degradation in Paratyphi A and Typhi, human-restricted serovars of Salmonella enterica that cause

typhoid. Nat Genet. 2004 Dec;36(12):1268-74. doi: 10.1038/ng1470. Epub 2004 Nov 7. PMID: 15531882.

McGhie EJ, Brawn LC, Hume PJ, Humphreys D, Koronakis V. Salmonella takes control: effector-driven manipulation of the host. Curr Opin Microbiol. 2009 Feb;12(1):117-24. doi: 10.1016/j.mib.2008.12.001. Epub 2009 Jan 20. PMID: 19157959; PMCID: PMC2647982.

McNab F, Mayer-Barber K, Sher A, Wack A, O'Garra A. Type I interferons in infectious disease. Nat Rev Immunol. 2015 Feb;15(2):87-103. doi: 10.1038/nri3787. PMID: 25614319; PMCID: PMC7162685.

Mei C, Lei L, Tan LM, Xu XJ, He BM, Luo C, Yin JY, Li X, Zhang W, Zhou HH, Liu ZQ. The role of single strand break repair pathways in cellular responses to camptothecin induced DNA damage. Biomed Pharmacother. 2020 May;125:109875. doi: 10.1016/j.biopha.2020.109875. Epub 2020 Feb 6. PMID: 32036211.

Mezal EH, Bae D, Khan AA. Detection and functionality of the CdtB, PltA, and PltB from Salmonella enterica serovar Javiana. Pathog Dis. 2014 Nov;72(2):95-103. doi: 10.1111/2049-632X.12191. Epub 2014 Jul 16. PMID: 24891290.

Milano L, Gautam A, Caldecott KW. DNA damage and transcription stress. Mol Cell. 2024 Jan 4;84(1):70-79. doi: 10.1016/j.molcel.2023.11.014. Epub 2023 Dec 15. PMID: 38103560.

Miller RA, Betteken MI, Guo X, Altier C, Duhamel GE, Wiedmann M. The Typhoid Toxin Produced by the Nontyphoidal *Salmonella enterica* Serotype Javiana Is Required for Induction of a DNA Damage Response *In Vitro* and Systemic Spread *In Vivo*. mBio. 2018 Mar 27;9(2):e00467-18. doi: 10.1128/mBio.00467-18. PMID: 29588404; PMCID: PMC5874915.

Misselwitz B, Dilling S, Vonaesch P, Sacher R, Snijder B, Schlumberger M, Rout S, Stark M, von Mering C, Pelkmans L, Hardt WD. RNAi screen of Salmonella invasion shows role of COPI in membrane targeting of cholesterol and Cdc42. Mol Syst Biol. 2011 Mar 15;7:474. doi: 10.1038/msb.2011.7. PMID: 21407211; PMCID: PMC3094068.

Mirzalieva O, Juncker M, Schwartzenburg J, Desai S. ISG15 and ISGylation in Human Diseases. Cells. 2022 Feb 4;11(3):538. doi: 10.3390/cells11030538. PMID: 35159348; PMCID: PMC8834048.

Moeglin E, Desplancq D, Conic S, Oulad-Abdelghani M, Stoessel A, Chiper M, Vigneron M, Didier P, Tora L, Weiss E. Uniform Widespread Nuclear Phosphorylation of Histone H2AX Is an Indicator of Lethal DNA Replication Stress. Cancers (Basel). 2019 Mar 13;11(3):355. doi: 10.3390/cancers11030355. PMID: 30871194; PMCID: PMC6468890.

Nathans JF, Cornwell JA, Afifi MM, Paul D, Cappell SD. Cell cycle inertia underlies a bifurcation in cell fates after DNA damage. Sci Adv. 2021 Jan 13;7(3):eabe3882. doi: 10.1126/sciadv.abe3882. PMID: 33523889; PMCID: PMC7806216.

Nelson G, Wordsworth J, Wang C, Jurk D, Lawless C, Martin-Ruiz C, von Zglinicki T. A senescent cell bystander effect: senescence-induced senescence. Aging Cell. 2012 Apr;11(2):345-9. doi: 10.1111/j.1474-9726.2012.00795.x. Epub 2012 Feb 9. PMID: 22321662; PMCID: PMC3488292.

Nelson BC, Dizdaroglu M. Implications of DNA damage and DNA repair on human diseases. Mutagenesis. 2020 Feb 13;35(1):1-3. doi: 10.1093/mutage/gez048. PMID: 32052057; PMCID: PMC7416834.

Nesić D, Hsu Y, Stebbins CE. Assembly and function of a bacterial genotoxin. Nature. 2004 May 27;429(6990):429-33. doi: 10.1038/nature02532. PMID: 15164065.

Ning S, Pagano JS, Barber GN. IRF7: activation, regulation, modification and function. Genes Immun. 2011 Sep;12(6):399-414. doi: 10.1038/gene.2011.21. Epub 2011 Apr 14. PMID: 21490621; PMCID: PMC4437765.

Nishikubo S, Ohara M, Ueno Y, Ikura M, Kurihara H, Komatsuzawa H, Oswald E, Sugai M. An N-terminal segment of the active component of the bacterial genotoxin cytolethal distending toxin B (CDTB) directs CDTB into the nucleus. J Biol Chem. 2003 Dec 12;278(50):50671-81. doi: 10.1074/jbc.M305062200. Epub 2003 Aug 28. PMID: 12947116.

Nössing C, Ryan KM. 50 years on and still very much alive: 'Apoptosis: a basic biological phenomenon with wide-ranging implications in tissue kinetics'. Br J Cancer. 2023 Feb;128(3):426-431. doi: 10.1038/s41416-022-02020-0. Epub 2022 Nov 11. PMID: 36369364; PMCID: PMC9938139.

Noubissi FK, McBride AA, Leppert HG, Millet LJ, Wang X, Davern SM. Detection and quantification of γ-H2AX using a dissociation enhanced lanthanide fluorescence immunoassay. Sci Rep. 2021 Apr 26;11(1):8945. doi: 10.1038/s41598-021-88296-3. PMID: 33903655; PMCID: PMC8076281.

Ohara M, Hayashi T, Kusunoki Y, Nakachi K, Fujiwara T, Komatsuzawa H, Sugai M. Cytolethal distending toxin induces caspase-dependent and -independent cell death in MOLT-4 cells. Infect Immun. 2008 Oct;76(10):4783-91. doi: 10.1128/IAI.01612-07. Epub 2008 Jul 21. PMID: 18644882; PMCID: PMC2546834.

Okoro CK, Barquist L, Connor TR, Harris SR, Clare S, Stevens MP, Arends MJ, Hale C, Kane L, Pickard DJ, Hill J, Harcourt K, Parkhill J, Dougan G, Kingsley RA. Signatures of adaptation in human invasive Salmonella Typhimurium ST313 populations from sub-Saharan Africa. PLoS Negl Trop Dis. 2015 Mar 24;9(3):e0003611. doi: 10.1371/journal.pntd.0003611. Erratum in: PLoS Negl Trop

Dis. 2015 Jun 15;9(6):e0003848. doi: 10.1371/journal.pntd.0003848. Erratum in: PLoS Negl Trop Dis. 2015 Aug 07;9(8):e0003970. doi: 10.1371/journal.pntd.0003970. PMID: 25803844; PMCID: PMC4372345.

Okumura A, Lu G, Pitha-Rowe I, Pitha PM. Innate antiviral response targets HIV-1 release by the induction of ubiquitin-like protein ISG15. Proc Natl Acad Sci U S A. 2006 Jan 31;103(5):1440-5. doi: 10.1073/pnas.0510518103. Epub 2006 Jan 24. PMID: 16434471; PMCID: PMC1360585.

Oracz G, Feleszko W, Golicka D, Maksymiuk J, Klonowska A, Szajewska H. Rapid diagnosis of acute Salmonella gastrointestinal infection. Clin Infect Dis. 2003 Jan 1;36(1):112-5. doi: 10.1086/344953. Epub 2002 Dec 11. PMID: 12491211.

Osiak A, Utermöhlen O, Niendorf S, Horak I, Knobeloch KP. ISG15, an interferon-stimulated ubiquitin-like protein, is not essential for STAT1 signaling and responses against vesicular stomatitis and lymphocytic choriomeningitis virus. Mol Cell Biol. 2005 Aug;25(15):6338-45. doi: 10.1128/MCB.25.15.6338-6345.2005. PMID: 16024773; PMCID: PMC1190360.

Otten EG, Werner E, Crespillo-Casado A, Boyle KB, Dharamdasani V, Pathe C, Santhanam B, Randow F. Ubiquitylation of lipopolysaccharide by RNF213 during bacterial infection. Nature. 2021 Jun;594(7861):111-116. doi: 10.1038/s41586-021-03566-4. Epub 2021 May 19. PMID: 34012115; PMCID: PMC7610904.

Papagrigorakis MJ, Yapijakis C, Synodinos PN, Baziotopoulou-Valavani E. DNA examination of ancient dental pulp incriminates typhoid fever as a probable cause of the Plague of Athens. Int J Infect Dis. 2006 May;10(3):206-14. doi: 10.1016/j.ijid.2005.09.001. Epub 2006 Jan 18. PMID: 16412683.

Panzenhagen PHN, Paul NC, Conte CA Junior, Costa RG, Rodrigues DP, Shah DH. Genetically distinct lineages of Salmonella Typhimurium ST313 and ST19 are present in Brazil. Int J Med Microbiol. 2018 Mar;308(2):306-316. doi: 10.1016/j.ijmm.2018.01.005. Epub 2018 Jan 31. PMID: 29396155.
Park JH, Zhuang J, Li J, Hwang PM. p53 as guardian of the mitochondrial genome. FEBS Lett. 2016 Apr;590(7):924-34. doi: 10.1002/1873-3468.12061. Epub 2016 Feb 3. PMID: 26780878; PMCID: PMC4833664.

Parry CM, Hien TT, Dougan G, White NJ, Farrar JJ. Typhoid fever. N Engl J Med. 2002 Nov 28;347(22):1770-82. doi: 10.1056/NEJMra020201. PMID: 12456854.

Parry CM, Qamar FN, Rijal S, McCann N, Baker S, Basnyat B. What Should We Be Recommending for the Treatment of Enteric Fever? Open Forum Infect Dis. 2023 Jun 2;10(Suppl 1):S26-S31. doi: 10.1093/ofid/ofad179. PMID: 37274536; PMCID: PMC10236504.

Patel PD, Liang Y, Meiring JE, Chasweka N, Patel P, Misiri T, Mwakiseghile F, Wachepa R, Banda HC, Shumba F, Kawalazira G, Dube Q, Nampota-Nkomba N, Nyirenda OM, Girmay T, Datta S, Jamka LP, Tracy JK, Laurens MB, Heyderman RS,

Neuzil KM, Gordon MA; TyVAC team. Efficacy of typhoid conjugate vaccine: final analysis of a 4-year, phase 3, randomised controlled trial in Malawian children. Lancet. 2024 Feb 3;403(10425):459-468. doi: 10.1016/S0140-6736(23)02031-7. Epub 2024 Jan 25. PMID: 38281499; PMCID: PMC10850983.

Perng YC, Lenschow DJ. ISG15 in antiviral immunity and beyond. Nat Rev Microbiol. 2018 Jul;16(7):423-439. doi: 10.1038/s41579-018-0020-5. PMID: 29769653; PMCID: PMC7097117.

Phu Huong Lan N, Le Thi Phuong T, Nguyen Huu H, Thuy L, Mather AE, Park SE, Marks F, Thwaites GE, Van Vinh Chau N, Thompson CN, Baker S. Invasive Non-typhoidal Salmonella Infections in Asia: Clinical Observations, Disease Outcome and Dominant Serovars from an Infectious Disease Hospital in Vietnam. PLoS Negl Trop Dis. 2016 Aug 11;10(8):e0004857. doi: 10.1371/journal.pntd.0004857. PMID: 27513951; PMCID: PMC4981332.

Pilié PG, Tang C, Mills GB, Yap TA. State-of-the-art strategies for targeting the DNA damage response in cancer. Nat Rev Clin Oncol. 2019 Feb;16(2):81-104. doi: 10.1038/s41571-018-0114-z. PMID: 30356138; PMCID: PMC8327299.

Platanias LC. Mechanisms of type-I- and type-II-interferon-mediated signalling. Nat Rev Immunol. 2005 May;5(5):375-86. doi: 10.1038/nri1604. PMID: 15864272.

Pulford CV, Perez-Sepulveda BM, Canals R, Bevington JA, Bengtsson RJ, Wenner N, Rodwell EV, Kumwenda B, Zhu X, Bennett RJ, Stenhouse GE, Malaka De Silva P, Webster HJ, Bengoechea JA, Dumigan A, Tran-Dien A, Prakash R, Banda HC, Alufandika L, Mautanga MP, Bowers-Barnard A, Beliavskaia AY, Predeus AV, Rowe WPM, Darby AC, Hall N, Weill FX, Gordon MA, Feasey NA, Baker KS, Hinton JCD. Stepwise evolution of Salmonella Typhimurium ST313 causing bloodstream infection in Africa. Nat Microbiol. 2021 Mar;6(3):327-338. doi: 10.1038/s41564-020-00836-1. Epub 2020 Dec 21. PMID: 33349664; PMCID: PMC8018540.

Prabhu KS, Kuttikrishnan S, Ahmad N, Habeeba U, Mariyam Z, Suleman M, Bhat AA, Uddin S. H2AX: A key player in DNA damage response and a promising target for cancer therapy. Biomed Pharmacother. 2024 Jun;175:116663. doi: 10.1016/j.biopha.2024.116663. Epub 2024 Apr 30. PMID: 38688170.

Przanowski P, Loska S, Cysewski D, Dabrowski M, Kaminska B. ISG'ylation increases stability of numerous proteins including Stat1, which prevents premature termination of immune response in LPS-stimulated microglia. Neurochem Int. 2018 Jan;112:227-233. doi: 10.1016/j.neuint.2017.07.013. Epub 2017 Jul 31. PMID: 28774718.

Qin Y, Meng X, Wang M, Liang W, Xu R, Chen J, Song H, Fu Y, Li J, Gao C, Jia M, Zhao C, Zhao W. Posttranslational ISGylation of NLRP3 by HERC enzymes facilitates inflammasome activation in models of inflammation. J Clin Invest. 2023 Oct 16;133(20):e161935. doi: 10.1172/JCI161935. PMID: 37651190; PMCID: PMC10575725.

Rabbani MA, Ribaudo M, Guo JT, Barik S. Identification of Interferon-Stimulated Gene Proteins That Inhibit Human Parainfluenza Virus Type 3. J Virol. 2016 Nov 28;90(24):11145-11156. doi: 10.1128/JVI.01551-16. PMID: 27707917; PMCID: PMC5126372.

Radoshevich L, Impens F, Ribet D, Quereda JJ, Nam Tham T, Nahori MA, Bierne H, Dussurget O, Pizarro-Cerdá J, Knobeloch KP, Cossart P. ISG15 counteracts Listeria monocytogenes infection. Elife. 2015 Aug 11;4:e06848. doi: 10.7554/eLife.06848. PMID: 26259872; PMCID: PMC4530601.

Radoshevich L, Cossart P. Listeria monocytogenes: towards a complete picture of its physiology and pathogenesis. Nat Rev Microbiol. 2018 Jan;16(1):32-46. doi: 10.1038/nrmicro.2017.126. Epub 2017 Nov 27. PMID: 29176582.

Ray P, Guha D, Chakraborty J, Banerjee S, Adhikary A, Chakraborty S, Das T, Sa G. Crocetin exploits p53-induced death domain (PIDD) and FAS-associated death domain (FADD) proteins to induce apoptosis in colorectal cancer. Sci Rep. 2016 Sep 13;6:32979. doi: 10.1038/srep32979. PMID: 27622714; PMCID: PMC5020693.

Rec, Lond Med. "THE BACILLUS OF TYPHOID FEVER." *The Sanitarian (1873-1904)* 11.156 (1883): 614.

Reed JC. Mechanisms of apoptosis. Am J Pathol. 2000 Nov;157(5):1415-30. doi: 10.1016/S0002-9440(10)64779-7. PMID: 11073801; PMCID: PMC1885741.

Reyna DE, Gavathiotis E. Self-regulation of BAX-induced cell death. Oncotarget. 2016 Oct 11;7(41):66326-66327. doi: 10.18632/oncotarget.11948. PMID: 27626173; PMCID: PMC5341806.

Rodriguez-Rivera LD, Bowen BM, den Bakker HC, Duhamel GE, Wiedmann M. Characterization of the cytolethal distending toxin (typhoid toxin) in non-typhoidal Salmonella serovars. Gut Pathog. 2015 Jul 24;7:19. doi: 10.1186/s13099-015-0065-1. PMID: 26207144; PMCID: PMC4511993.

Sabbagh SC, Forest CG, Lepage C, Leclerc JM, Daigle F. So similar, yet so different: uncovering distinctive features in the genomes of Salmonella enterica serovars Typhimurium and Typhi. FEMS Microbiol Lett. 2010 Apr;305(1):1-13. doi: 10.1111/j.1574-6968.2010.01904.x. Epub 2010 Jan 20. PMID: 20146749.

Sadler AJ, Williams BR. Interferon-inducible antiviral effectors. Nat Rev Immunol. 2008 Jul;8(7):559-68. doi: 10.1038/nri2314. PMID: 18575461; PMCID: PMC2522268.

Sandy Z, da Costa IC, Schmidt CK. More than Meets the ISG15: Emerging Roles in the DNA Damage Response and Beyond. Biomolecules. 2020 Nov 15;10(11):1557. doi: 10.3390/biom10111557. PMID: 33203188; PMCID: PMC7698331.

Sapkota J, Roberts T, Basnyat B, Baker S, Hampton LM, Dittrich S. Diagnostics for Typhoid Fever: Current Perspectives and Future Outlooks for Product Development and Access. Open Forum Infect Dis. 2023 Jun 2;10(Suppl 1):S17-S20. doi: 10.1093/ofid/ofad120. PMID: 37274534; PMCID: PMC10236505.

Sarkar L, Liu G, Gack MU. ISG15: its roles in SARS-CoV-2 and other viral infections. Trends Microbiol. 2023 Dec;31(12):1262-1275. doi: 10.1016/j.tim.2023.07.006. Epub 2023 Aug 10. PMID: 37573184; PMCID: PMC10840963.

Schultz BM, Melo-Gonzalez F, Salazar GA, Porto BN, Riedel CA, Kalergis AM, Bueno SM. New Insights on the Early Interaction Between Typhoid and Non-typhoid *Salmonella* Serovars and the Host Cells. Front Microbiol. 2021 Jul 1;12:647044. doi: 10.3389/fmicb.2021.647044. PMID: 34276584; PMCID: PMC8282409.

Serrano M, Lee H, Chin L, Cordon-Cardo C, Beach D, DePinho RA. Role of the INK4a locus in tumor suppression and cell mortality. Cell. 1996 Apr 5;85(1):27-37. doi: 10.1016/s0092-8674(00)81079-x. PMID: 8620534.

Shahangian A, Chow EK, Tian X, Kang JR, Ghaffari A, Liu SY, Belperio JA, Cheng G, Deng JC. Type I IFNs mediate development of postinfluenza bacterial pneumonia in mice. J Clin Invest. 2009 Jul;119(7):1910-20. doi: 10.1172/JCI35412. PMID: 19487810; PMCID: PMC2701856.

Shapiro B, Rambaut A, Gilbert MT. No proof that typhoid caused the Plague of Athens (a reply to Papagrigorakis et al.). Int J Infect Dis. 2006 Jul;10(4):334-5; author reply 335-6. doi: 10.1016/j.ijid.2006.02.006. Epub 2006 May 26. PMID: 16730469.

Shao RG, Cao CX, Zhang H, Kohn KW, Wold MS, Pommier Y. Replication-mediated DNA damage by camptothecin induces phosphorylation of RPA by DNA-dependent protein kinase and dissociates RPA:DNA-PK complexes. EMBO J. 1999 Mar 1;18(5):1397-406. doi: 10.1093/emboj/18.5.1397. PMID: 10064605; PMCID: PMC1171229.

Shi HX, Yang K, Liu X, Liu XY, Wei B, Shan YF, Zhu LH, Wang C. Positive regulation of interferon regulatory factor 3 activation by Herc5 via ISG15 modification. Mol Cell Biol. 2010 May;30(10):2424-36. doi: 10.1128/MCB.01466-09. Epub 2010 Mar 22. PMID: 20308324; PMCID: PMC2863703.

Shrivastav M, De Haro LP, Nickoloff JA. Regulation of DNA double-strand break repair pathway choice. Cell Res. 2008 Jan;18(1):134-47. doi: 10.1038/cr.2007.111. PMID: 18157161.

Shukla R, Shukla P, Behari A, Khetan D, Chaudhary RK, Tsuchiya Y, Ikoma T, Asai T, Nakamura K, Kapoor VK. Roles of Salmonella typhi and Salmonella paratyphi in

Gallbladder Cancer Development. Asian Pac J Cancer Prev. 2021 Feb 1;22(2):509-516. doi: 10.31557/APJCP.2021.22.2.509. PMID: 33639667; PMCID: PMC8190372.

Sibinelli-Sousa S, de Araújo-Silva AL, Hespanhol JT, Bayer-Santos E. Revisiting the steps of Salmonella gut infection with a focus on antagonistic interbacterial interactions. FEBS J. 2022 Jul;289(14):4192-4211. doi: 10.1111/febs.16211. Epub 2021 Oct 18. PMID: 34546626.

Simanjuntak CH, Paleologo FP, Punjabi NH, Darmowigoto R, Soeprawoto, Totosudirjo H, Haryanto P, Suprijanto E, Witham ND, Hoffman SL. Oral immunisation against typhoid fever in Indonesia with Ty21a vaccine. Lancet. 1991 Oct 26;338(8774):1055-9. doi: 10.1016/0140-6736(91)91910-m. PMID: 1681365.

Sinha RP, Häder DP. UV-induced DNA damage and repair: a review. Photochem Photobiol Sci. 2002 Apr;1(4):225-36. doi: 10.1039/b201230h. PMID: 12661961.

Snyder RD, Regan JD. Aphidicolin inhibits repair of DNA in UV-irradiated human fibroblasts. Biochem Biophys Res Commun. 1981 Apr 30;99(4):1088-94. doi: 10.1016/0006-291x(81)90730-0. PMID: 6789826.

Song J, Gao X, Galán JE. Structure and function of the Salmonella Typhi chimaeric A(2)B(5) typhoid toxin. Nature. 2013 Jul 18;499(7458):350-4. doi: 10.1038/nature12377. Epub 2013 Jul 10. PMID: 23842500; PMCID: PMC4144355.

Spanò S, Ugalde JE, Galán JE. Delivery of a Salmonella Typhi exotoxin from a host intracellular compartment. Cell Host Microbe. 2008 Jan 17;3(1):30-8. doi: 10.1016/j.chom.2007.11.001. PMID: 18191792.

Speer SD, Li Z, Buta S, Payelle-Brogard B, Qian L, Vigant F, Rubino E, Gardner TJ, Wedeking T, Hermann M, Duehr J, Sanal O, Tezcan I, Mansouri N, Tabarsi P, Mansouri D, Francois-Newton V, Daussy CF, Rodriguez MR, Lenschow DJ, Freiberg AN, Tortorella D, Piehler J, Lee B, García-Sastre A, Pellegrini S, Bogunovic D. ISG15 deficiency and increased viral resistance in humans but not mice. Nat Commun. 2016 May 19;7:11496. doi: 10.1038/ncomms11496. PMID: 27193971; PMCID: PMC4873964.

Stanaway/ GBD 2017 Non-Typhoidal Salmonella Invasive Disease Collaborators. The global burden of non-typhoidal salmonella invasive disease: a systematic analysis for the Global Burden of Disease Study 2017. Lancet Infect Dis. 2019 Dec;19(12):1312-1324. doi: 10.1016/S1473-3099(19)30418-9. Epub 2019 Sep 24. PMID: 31562022; PMCID: PMC6892270.

Stinson BM, Loparo JJ. Repair of DNA Double-Strand Breaks by the Nonhomologous End Joining Pathway. Annu Rev Biochem. 2021 Jun 20;90:137-164. doi: 10.1146/annurev-biochem-080320-110356. Epub 2021 Feb 8. PMID: 33556282; PMCID: PMC8899865.

Sun J, Yan J, Qiao HY, Zhao FY, Li C, Jiang JY, Liu BQ, Meng XN, Wang HQ. Loss of TRIM29 suppresses cancer stem cell-like characteristics of PDACs via accelerating ISG15 degradation. Oncogene. 2020 Jan;39(3):546-559. doi: 10.1038/s41388-019-0992-2. Epub 2019 Sep 9. PMID: 31501523.

Sur D, Ochiai RL, Bhattacharya SK, Ganguly NK, Ali M, Manna B, Dutta S, Donner A, Kanungo S, Park JK, Puri MK, Kim DR, Dutta D, Bhaduri B, Acosta CJ, Clemens JD. A cluster-randomized effectiveness trial of Vi typhoid vaccine in India. N Engl J Med. 2009 Jul 23;361(4):335-44. doi: 10.1056/NEJMoa0807521. PMID: 19625715.

Swatek KN, Aumayr M, Pruneda JN, Visser LJ, Berryman S, Kueck AF, Geurink PP, Ovaa H, van Kuppeveld FJM, Tuthill TJ, Skern T, Komander D. Irreversible inactivation of ISG15 by a viral leader protease enables alternative infection detection strategies. Proc Natl Acad Sci U S A. 2018 Mar 6;115(10):2371-2376. doi: 10.1073/pnas.1710617115. Epub 2018 Feb 20. PMID: 29463763; PMCID: PMC5877979.

Tang D, Kang R, Coyne CB, Zeh HJ, Lotze MT. PAMPs and DAMPs: signal 0s that spur autophagy and immunity. Immunol Rev. 2012 Sep;249(1):158-75. doi: 10.1111/j.1600-065X.2012.01146.x. PMID: 22889221; PMCID: PMC3662247.

Tao W, Chu C, Zhou W, Huang Z, Zhai K, Fang X, Huang Q, Zhang A, Wang X, Yu X, Huang H, Wu Q, Sloan AE, Yu JS, Li X, Stark GR, Rich JN, Bao S. Dual Role of WISP1 in maintaining glioma stem cells and tumor-supportive macrophages in glioblastoma. Nat Commun. 2020 Jun 15;11(1):3015. doi: 10.1038/s41467-020-16827-z. PMID: 32541784; PMCID: PMC7295765.

Tecalco-Cruz AC, Zepeda-Cervantes J. Protein ISGylation: a posttranslational modification with implications for malignant neoplasms. Explor Target Antitumor Ther. 2023;4(4):699-715. doi: 10.37349/etat.2023.00162. Epub 2023 Aug 31. PMID: 37711589; PMCID: PMC10497404.

Tewari M, Mishra RR, Shukla HS. Salmonella typhi and gallbladder cancer: report from an endemic region. Hepatobiliary Pancreat Dis Int. 2010 Oct;9(5):524-30. PMID: 20943463.

Thakur R, Suri CR, Rishi P. Contribution of typhoid toxin in the pathogenesis of Salmonella Typhi. Microb Pathog. 2022 Mar;164:105444. doi: 10.1016/j.micpath.2022.105444. Epub 2022 Feb 9. PMID: 35149176.

Thery F, Martina L, Asselman C, Zhang Y, Vessely M, Repo H, Sedeyn K, Moschonas GD, Bredow C, Teo QW, Zhang J, Leandro K, Eggermont D, De Sutter D, Boucher K, Hochepied T, Festjens N, Callewaert N, Saelens X, Dermaut B, Knobeloch KP, Beling A, Sanyal S, Radoshevich L, Eyckerman S, Impens F. Ring finger protein 213 assembles into a sensor for ISGylated proteins with antimicrobial activity. Nat Commun. 2021 Oct 1;12(1):5772. doi: 10.1038/s41467-021-26061-w. PMID: 34599178; PMCID: PMC8486878.

Tischler AD, McKinney JD. Contrasting persistence strategies in Salmonella and Mycobacterium. Curr Opin Microbiol. 2010 Feb;13(1):93-9. doi: 10.1016/j.mib.2009.12.007. Epub 2010 Jan 6. PMID: 20056478; PMCID: PMC2822150.

Tolomeo M, Cavalli A, Cascio A. STAT1 and Its Crucial Role in the Control of Viral Infections. Int J Mol Sci. 2022 Apr 7;23(8):4095. doi: 10.3390/ijms23084095. PMID: 35456913; PMCID: PMC9028532.

Tosi MF. Innate immune responses to infection. J Allergy Clin Immunol. 2005 Aug;116(2):241-9; quiz 250. doi: 10.1016/j.jaci.2005.05.036. PMID: 16083775.

Tremblay W, Mompart F, Lopez E, Quaranta M, Bergoglio V, Hashim S, Bonnet D, Alric L, Mas E, Trouche D, Vignard J, Ferrand A, Mirey G, Fernandez-Vidal A. Cytolethal Distending Toxin Promotes Replicative Stress Leading to Genetic Instability Transmitted to Daughter Cells. Front Cell Dev Biol. 2021 May 7;9:656795. doi: 10.3389/fcell.2021.656795. PMID: 34026755; PMCID: PMC8138442.

Van Puyvelde S, Pickard D, Vandelannoote K, Heinz E, Barbé B, de Block T, Clare S, Coomber EL, Harcourt K, Sridhar S, Lees EA, Wheeler NE, Klemm EJ, Kuijpers L, Mbuyi Kalonji L, Phoba MF, Falay D, Ngbonda D, Lunguya O, Jacobs J, Dougan G, Deborggraeve S. An African Salmonella Typhimurium ST313 sublineage with extensive drug-resistance and signatures of host adaptation. Nat Commun. 2019 Sep 19;10(1):4280. doi: 10.1038/s41467-019-11844-z. PMID: 31537784; PMCID: PMC6753159.

Valieva Y, Ivanova E, Fayzullin A, Kurkov A, Igrunkova A. Senescence-Associated β-Galactosidase Detection in Pathology. Diagnostics (Basel). 2022 Sep 25;12(10):2309. doi: 10.3390/diagnostics12102309. PMID: 36291998; PMCID: PMC9599972.

Vernì F. DNA Damage Response (DDR) and DNA Repair. Int J Mol Sci. 2022 Jun 29;23(13):7204. doi: 10.3390/ijms23137204. PMID: 35806207; PMCID: PMC9266642.

Vesela E, Chroma K, Turi Z, Mistrik M.
Common Chemical Inductors of Replication Stress: Focus on Cell-Based Studies. Biomolecules. 2017 Feb 21;7(1):19. doi: 10.3390/biom7010019. PMID: 28230817; PMCID: PMC5372731.

Villarroya-Beltri C, Guerra S, Sánchez-Madrid F. ISGylation - a key to lock the cell gates for preventing the spread of threats. J Cell Sci. 2017 Sep 15;130(18):2961-2969. doi: 10.1242/jcs.205468. Epub 2017 Aug 25. PMID: 28842471.

Visser H, Thomas AD. MicroRNAs and the DNA damage response: How is cell fate determined? DNA Repair (Amst). 2021 Dec;108:103245. doi: 10.1016/j.dnarep.2021.103245. Epub 2021 Nov 2. PMID: 34773895.

Waqas SF, Sohail A, Nguyen AHH, Usman A, Ludwig T, Wegner A, Malik MNH, Schuchardt S, Geffers R, Winterhoff M, Merkert S, Martin U, Olmer R, Lachmann N, Pessler F. ISG15 deficiency features a complex cellular phenotype that responds to treatment with itaconate and derivatives. Clin Transl Med. 2022 Jul;12(7):e931. doi: 10.1002/ctm2.931. PMID: 35842904; PMCID: PMC9288839.

Wei L, Nakajima S, Hsieh CL, Kanno S, Masutani M, Levine AS, Yasui A, Lan L. Damage response of XRCC1 at sites of DNA single strand breaks is regulated by phosphorylation and ubiquitylation after degradation of poly(ADP-ribose). J Cell Sci. 2013 Oct 1;126(Pt 19):4414-23. doi: 10.1242/jcs.128272. Epub 2013 Jul 18. PMID: 23868975; PMCID: PMC3784821.

Wiest DB, Cochran JB, Tecklenburg FW. Chloramphenicol toxicity revisited: a 12-year-old patient with a brain abscess. J Pediatr Pharmacol Ther. 2012 Apr;17(2):182-8. doi: 10.5863/1551-6776-17.2.182. PMID: 23118672; PMCID: PMC3470440.

Willers H, Pfäffle H, Zou L. DNA Repair in Cancer Therapy. Ch7 -Targeting Homologous Repair in Cancer. 2012. 119-160. Academic Press.

Williams AB, Schumacher B. p53 in the DNA-Damage-Repair Process. Cold Spring Harb Perspect Med. 2016 May 2;6(5):a026070. doi: 10.1101/cshperspect.a026070. PMID: 27048304; PMCID: PMC4852800.

Wong RS. Apoptosis in cancer: from pathogenesis to treatment. J Exp Clin Cancer Res. 2011 Sep 26;30(1):87. doi: 10.1186/1756-9966-30-87. PMID: 21943236; PMCID: PMC3197541.

World Health Organization = Organisation mondiale de la Santé. (2018). Weekly Epidemiological Record, 2018, vol. 93, 13 [full issue]. *Weekly Epidemiological Record = Relevé épidémiologique hebdomadaire, 93* (13), 153 - 172. World Health Organization = Organisation mondiale de la Santé

Wu Y, Liu C, Tang C, Niragire B, Levy-Zauberman Y, Adapen C, Vernay T, Hugueny J, Baud V, Subtil A. *Chlamydia*-driven ISG15 expression dampens the immune response of epithelial cells independently of ISGylation. mBio. 2024 Sep 30:e0240124. doi: 10.1128/mbio.02401-24. Epub ahead of print. PMID: 39345209.

Xue W, Zender L, Miething C, Dickins RA, Hernando E, Krizhanovsky V, Cordon-Cardo C, Lowe SW. Senescence and tumour clearance is triggered by p53 restoration in murine liver carcinomas. Nature. 2007 Feb 8;445(7128):656-60. doi: 10.1038/nature05529. Epub 2007 Jan 24. Erratum in: Nature. 2011 May 26;473(7348):544. PMID: 17251933; PMCID: PMC4601097.

Yang J, Zhang L, Yu C, Yang XF, Wang H. Monocyte and macrophage differentiation: circulation inflammatory monocyte as biomarker for inflammatory diseases. Biomark Res. 2014 Jan 7;2(1):1. doi: 10.1186/2050-7771-2-1. PMID: 24398220; PMCID: PMC3892095.

Yu J, Zhang L. PUMA, a potent killer with or without p53. Oncogene. 2008 Dec;27 Suppl 1(Suppl 1):S71-83. doi: 10.1038/onc.2009.45. PMID: 19641508; PMCID: PMC2860432.

Yuan Y, Qin H, Li H, Shi W, Bao L, Xu S, Yin J, Zheng L. The Functional Roles of ISG15/ISGylation in Cancer. Molecules. 2023 Jan 31;28(3):1337. doi: 10.3390/molecules28031337. PMID: 36771004; PMCID: PMC9918931.

Zhang X, Bogunovic D, Payelle-Brogard B, Francois-Newton V, Speer SD, Yuan C, Volpi S, Li Z, Sanal O, Mansouri D, Tezcan I, Rice GI, Chen C, Mansouri N, Mahdaviani SA, Itan Y, Boisson B, Okada S, Zeng L, Wang X, Jiang H, Liu W, Han T, Liu D, Ma T, Wang B, Liu M, Liu JY, Wang QK, Yalnizoglu D, Radoshevich L, Uzé G, Gros P, Rozenberg F, Zhang SY, Jouanguy E, Bustamante J, García-Sastre A, Abel L, Lebon P, Notarangelo LD, Crow YJ, Boisson-Dupuis S, Casanova JL, Pellegrini S. Human intracellular ISG15 prevents interferon-α/β over-amplification and auto-inflammation. Nature. 2015 Jan 1;517(7532):89-93. doi: 10.1038/nature13801. Epub 2014 Oct 12. PMID: 25307056; PMCID: PMC4303590.

Zhang Y, Thery F, Wu NC, Luhmann EK, Dussurget O, Foecke M, Bredow C, Jiménez-Fernández D, Leandro K, Beling A, Knobeloch KP, Impens F, Cossart P, Radoshevich L. The in vivo ISGylome links ISG15 to metabolic pathways and autophagy upon Listeria monocytogenes infection. Nat Commun. 2019 Nov 26;10(1):5383. doi: 10.1038/s41467-019-13393-x. PMID: 31772204; PMCID: PMC6879477.

Zhang M, Li J, Yan H, Huang J, Wang F, Liu T, Zeng L, Zhou F. ISGylation in Innate Antiviral Immunity and Pathogen Defense Responses: A Review. Front Cell Dev Biol. 2021 Nov 25;9:788410. doi: 10.3389/fcell.2021.788410. PMID: 34901029; PMCID: PMC8662993.

Zhang L, Tang R, Liang D, Wang W, Min K, Luo T, Li X. Uncovering the Interaction between TRAF1 and MAVS in the RIG-I Pathway to Enhance the Upregulation of IRF1/ISG15 during Classical Swine Fever Virus Infection. Cells. 2024 Jul 8;13(13):1165. doi: 10.3390/cells13131165. PMID: 38995016; PMCID: PMC11240745

Zhao C, Hsiang TY, Kuo RL, Krug RM. ISG15 conjugation system targets the viral NS1 protein in influenza A virus-infected cells. Proc Natl Acad Sci U S A. 2010 Feb 2;107(5):2253-8. doi: 10.1073/pnas.0909144107. Epub 2010 Jan 19. PMID: 20133869; PMCID: PMC2836655

Zhao C, Sridharan H, Chen R, Baker DP, Wang S, Krug RM. Influenza B virus non-structural protein 1 counteracts ISG15 antiviral activity by sequestering ISGylated viral proteins. Nat Commun. 2016 Sep 2;7:12754. doi: 10.1038/ncomms12754. PMID: 27587337; PMCID: PMC5025834.

Zhao B, Rothenberg E, Ramsden DA, Lieber MR. The molecular basis and disease relevance of non-homologous DNA end joining. Nat Rev Mol Cell Biol. 2020 Dec;21(12):765-781. doi: 10.1038/s41580-020-00297-8. Epub 2020 Oct 19. PMID: 33077885; PMCID: PMC8063501.

Zuo C, Sheng X, Ma M, Xia M, Ouyang L. ISG15 in the tumorigenesis and treatment of cancer: An emerging role in malignancies of the digestive system. Oncotarget. 2016 Nov 8;7(45):74393-74409. doi: 10.18632/oncotarget.11911. PMID: 27626310; PMCID: PMC5342061.